UNIVERSITY OF BIRMINGHAM

# DEVELOPING METABOLOMICS APPROACHES FOR CHEMICAL RISK ASSESSMENT


By

Hanna Gruszczynska


A thesis submitted to the University of Birmingham for the degree of

DOCTOR OF PHILOSOPHY


Supervisor: Prof. Mark Viant

Co-supervisor: Prof. John Colbourne

School of Biosciences

College of Environmental and Life Sciences

University of Birmingham


31 December 2022

# COVID-19 STATEMENT

The Covid pandemic restrictions that came into place in March 2020 (second year of my PhD studies) caused multiple disruptions to my planned PhD projects.

My original PhD plan comprised four projects, each to constitute a separate results chapter of my thesis: 1) a multi-omics grouping study, 2) an analytical study/internship with my industrial CASE partners, Thermo Fisher Scientific (San Jose, USA); 3) metabolomics study; and 4) a human metabolic fate study. However, due to Covid-19 restrictions, my research plan was subsequently adapted by splitting the multi-omics grouping project (study 1) conducted during the 1st year and beginning of my 2nd year into two thesis chapters (now chapters 3 and 4, respectively). Chapter 4 (azo dye ADME/TK) was implemented as a computational chapter to focus on more in-depth analysis of existing datasets and minimise time lost due to the laboratory closure at the University of Birmingham for six months.

Two planned analytical chemistry chapters (study 2, originally planned for summer 2020, and study 3) were not performed due to Covid-19 restrictions (including travel restrictions to the USA) and the availability of laboratory time for data collection. The planned (for approx. 6 months) human metabolic fate study with Fisher Thermo Scientific (study 4, described in section 6.4 in chapter 6) was not conducted as my industrial CASE partners unexpectedly withdrew from the project in 2022 due to post-Covid implications. Consequently, the final research project was rescoped to account for the lost time and utilise existing rat plasma samples from the US National Toxicology Program project at Phenome Centre Birmingham (chapter 5). The

selection of samples and chemicals for this final project was driven largely by Covid-19 practicalities and project timeline due to disruption to research.

# ABSTRACT

Chemical use is highly dynamic and the chemical industry is projected to grow four-fold over the next four decades, according to the Organisation for Economic Co-operation and Development (OECD)[1]. However, complete toxicity data are often lacking for many chemicals and their potential harmful impacts on human and environmental health remain poorly characterised. It is widely recognised that traditional toxicity testing methods are no longer fit for purpose to address the huge backlog of untested substances worldwide. Therefore, there is a rapid demand for novel mechanistic approaches to fill information gaps for more robust chemical safety assessment. Among all omics, metabolomics is particularly well placed to address this knowledge gap as it captures the dynamics of molecular perturbations in a biological system, in response to xenobiotic exposure.

The overarching aim of this thesis was to develop and implement untargeted metabolomics approaches suited for safety assessment of chemicals in regulatory toxicology, exploring both toxicodynamics (TD; i.e. endogenous biochemistry) and toxicokinetics (TK; primarily xenobiotic metabolism). Specifically, two applications of toxicometabolomics were explored: 1) a regulatory scenario of chemical grouping for subsequent read-across (G/RAx), and 2) characterisation of xenobiotic metabolism through untargeted metabolomics. Firstly, a novel G/RAx workflow was developed to conduct biology-based grouping of seven data-poor azo dyes, whereby mechanistic multi-omics data (i.e. metabolic, lipid and transcriptional responses in *Daphnia magna*) were considered along conventional *in silico* structure-based approaches. These proof-of-principle investigations demonstrated the potential of metabolomics for more

robust chemical grouping to facilitate future toxicity prediction (i.e. read-across), simultaneously addressing the relative lack of similar regulatory-relevant case studies.

Additionally, untargeted (specifically, nESI-DIMS and UHPLC-MS/MS) metabolomics, principally designed to probe the endogenous toxicity responses, unravelled promising insights into the metabolism of xenobiotics, thus demonstrating the 'added value' of this approach. Specifically, the TK/ADME (absorption, distribution, metabolism, elimination) information was successfully extracted from untargeted $MS^1$ nESI-DIMS metabolomics datasets for the seven azo dyes from the multi-omics grouping study. Building upon this work, untargeted UHPLC-MS/MS metabolomics was applied to characterise ADME/TK properties of five industrial chemicals in rat plasma, revealing rich biotransformation patterns for these xenobiotics.

Although further research is warranted to address the existing knowledge gaps (e.g. annotation and identification of xenobiotic biotransformation products), this power to simultaneously characterise TK and TD properties (all within a single toxicometabolomics assay) holds a promising potential for deeper characterisation of chemical toxicity (i.e. via discovery of mode(s) of action, MoAs), ultimately empowering future chemical safety assessment.

# ACKNOWLEDGEMENTS

First and foremost, I would like to extend my gratitude to my supervisor Prof. Mark Viant and co-supervisor Prof. John Colbourne for giving me the opportunity to pursue this exciting project, and for all the guidance and feedback provided throughout my PhD journey. Your insights, encouragement and unwavering enthusiasm continued to steer me through this research.

I thank my funders, the National Environment Research Council and Thermo Fisher Scientific for funding this PhD project.

I also extend my thanks to all members of the Viant research group (also known as 'ECHA elves') for the collaborative efforts and all your input into the large multi-omics grouping study conducted during the first year of my PhD. Particularly, to Dr Rose Barnett for all the help and support with *Daphnia magna* culturing, toxicity exposures; for sharing your transcriptomics knowledge and conducting transcriptomics data analyses on this project.

Special thanks go to Dr Martin Jones for providing analytical chemistry expertise on 'all things Orbitrap'; and Dr Gavin Lloyd for much needed advice on 'all things statistics', always clearly explaining complex concepts and helping to troubleshoot my scripts.

I also thank (soon-to-be Dr) Tara Bowden, my great 'office buddy', for our laughs (Valencia was amazing!), metabolomics (and non-metabolomics) related chats and rants; and for bringing me up to speed on the Orbitrap ID-X and AcquireX when I was running out of time in the lab.

Finally, I thank my dearest Family and Friends (you know who you are!) for your unconditional love, support and absolute belief in me during these intense four years and three months of my PhD journey in such tumultuous Covid-19 times. I simply could not have done it without you!

# TABLE OF CONTENTS

# LIST OF FIGURES

# LIST OF TABLES

# LIST OF ACRONYMS AND ABBREVIATIONS

| Acronym | Full form |
|---|---|
| AA | Acetic acid |
| ACN | acetonitrile |
| ADME | Absorption, distribution, metabolism and elimination |
| AGC | Automatic gain control |
| ANOVA | Analysis of variance |
| AOP | Adverse outcome pathway |
| APCI | Atmospheric pressure chemical ionisation |
| BPAF | Bisphenol F |
| BEAMS | Birmingham mEtabolite Annotation for Mass Spectrometry |
| BMC | Benchmark concentration |
| BMCL | Benchmark concentration at lower confidence limit |
| BMR | Benchmark response |
| BMCU | Benchmark concentration upper confidence limit |
| BMD | Benchmark dose |
| CID | Collision-induced dissociation |
| CD | Compound Discoverer software |
| C-trap | Curved linear ion trap |
| DDA | Data-dependent analysis |
| DEHP | Di(2-ethylhexyl) phthalate |
| DIMS | Direct infusion mass spectrometry |
| DL | Deep learning |
| DMSO | Dimethyl sulfoxide |
| DO25 | Disperse orange 25 azo dye |
| DO61 | Disperse orange 61 azo dye |
| DR1 | Disperse red 1 azo dye |
| DR13 | Disperse red 13 azo dye |
| DY3 | Disperse yellow 3 azo dye |
| ECHA | European Chemicals Agency |
| EC | European Commission |
| EFSA | European Food Safety Authority |
| EIC | Extracted ion chromatogram |
| EPA | US Environmental Protection Agency |
| FA | Formic acid |
| FDR | False discovery rate |
| FISh | Fragment ion search |
| FT | Fourier transform |
| FT-ICR | Fourier transform ion cyclotron resonance |
| FWHM | Full width at half maximum |
| GA | Genetic algorithm |
| G/RAx | Grouping and read-across |
| HCA | Hierarchical cluster analysis |
| HCD | Higher-energy collision dissociation |
| HILIC | Hydrophilic interaction liquid chromatography |
| HMDB | Human Metabolome Database |
| HPLC | High-performance liquid chromatography |
| HRMS | High-resolution mass spectrometry |

| Acronym | Full form |
|---|---|
| IPA | Isopropanol |
| KIE | Key initiating event |
| LOEC | Lowest observed effect concentration |
| MAD | Median absolute deviation |
| MALDI | Matrix-assisted laser desorption ionisation |
| MetID | Metabolite identification |
| MERIT | MEtabolomics standaRds Initiative in Toxicology |
| MoA | Mode of action |
| MIE | Molecular initiating event |
| MP | Mobile phase |
| mQACC | Metabolomics Quality Assurance and Quality Control Consortium |
| MRF | Metabolomics Reporting Framework |
| MS | Mass spectrometry |
| $MS^1$ | Full-scan MS |
| $MS^n$ | MS/MS |
| MSI | Metabolomics Standards Initiative |
| mRSD | Median relative standard deviation (expressed in %) |
| *m/z* | Mass-to-charge ratio |
| NAMs | New Approach Methodologies |
| NCE | Normalised collision energy |
| NEC | New emerging contaminants |
| nESI | Nanoelectrospray ionisation |
| NN | Neutral network |
| NOAEL | No observed adverse effect level |
| NRC | US National Research Council |
| NTP | National Toxicology Program |
| OECD | Organisation for Economic Co-operation and Development |
| Orbitrap | Orbital ion trapping |
| PBTK | Physiologically-based toxicokinetics |
| PCA | Principal Component Analysis |
| PLS-DA | Partial least-squares discriminant analysis |
| POD | Point-of-departure |
| ppm | Parts per million |
| PQN | Probabilistic quotient normalisation |
| Q | Quadrupole |
| QA | Quality assurance |
| QC | Quality control |
| RAAF | Read-across Framework |
| REACH | Registration, Evaluation, Authorisation and Restriction of Chemicals |
| RP | Reverse phase chromatography |
| RSD | Relative standard deviation (expressed in %) |
| RT | Retention time |
| S/N | Signal-to-noise ratio |
| SD | Standard deviation |
| SIM | Selected ion monitoring |
| SMILE | Simplified molecular-input line-entry system |
| SRG | Sudan red G azo dye |
| SRM | Standard reference materials |
| S1 | Sudan 1 azo dye |
| TBBPA | Tetrabromobisphenol |

| Acronym | Full form |
|---|---|
| TCCP | Tris(2-chloroisopropyl) phosphate |
| TD | Toxicodynamics |
| TG | Triglyceride |
| TK | Toxicokinetics |
| ToF | Time of flight |
| TCS | Triclosan |
| UHPLC-MS | Ultra-high performance liquid chromatography mass spectrometry |

# CHAPTER 1 – GENERAL INTRODUCTION

## 1.1 Challenges and opportunities in regulatory toxicology and chemical safety science

Chemical pollution is a global problem affecting human and environmental health. There are approximately 140,000 chemicals in commercial use in Europe alone[13]. Until recently the numbers of chemicals in production and use have been grossly underestimated; an estimated 350,000 chemicals are registered worldwide, of which approximately 14% are reported as 'confidential' and a further 20% are 'ambiguously described[14]. The chemical industry is projected to grow four-fold between 2018 and 2060, according to the Organisation for Economic Co-operation and Development (OECD)[1]. This upward trend in chemical production is only set to accelerate in the future due to the changing demographics of a globally rising human population, technological development, and a general increase in consumption worldwide. The intensification of human activities has resulted in many unregulated substances rapidly 'emerging' in the environment (termed as 'contaminants of emerging concern'[15]) due to substantial growth in the number of newly synthesized compounds, recent advances in analytical techniques allowing for lower limits of detection (LODs) and more efficient monitoring programmes[16].

High-quality and scientifically robust toxicity data are often lacking for many substances currently in use and their potential harmful impacts on human and environmental health remain poorly understood. The EU REACH (Registration,

Evaluation, Authorisation and Restriction of Chemicals) regulation attempted to improve the protection of human and environmental health in Europe by introducing a risk-based chemical control programme and shifting the burden of proof to demonstrate the safety of chemicals from public authorities to industry[17]. However, many registration dossiers are rejected by the European Chemicals Agency (ECHA) due to insufficient quality. The REACH chemical database contains approximately 18% of all substances used in Europe, resulting in a huge backlog of chemicals awaiting safety reviews[18].

The current chemical landscape is highly dynamic, posing new human and environmental health risks. This is in contrast with the lack of major methodological advances in the field of traditional toxicology, whose experimental foundations date back to 1920 and have not changed considerably over the past half-century[19]. A transformative new vision of toxicity testing in the 21$^{st}$ century outlined by the US National Research Council one and a half decades ago marks a significant paradigm shift in modern toxicology[20]. This vision is built around the notion of 'toxicity pathways', originally defined as cellular response pathways that, when sufficiently perturbed by exposure chemicals are expected to result in adverse health effects in a biological system[21]. However, my thesis goes one step beyond this original definition, i.e. a molecular-level response pathway that can provide data on toxicological mechanisms of action and adverse metabolic outcomes. Central to molecular mechanistic toxicology is the concept of the adverse outcome pathway (AOP), i.e. a cascade of causally linked molecular events across increasing levels of biological organisation. The first step, a 'molecular initiating event' (MIEs) is triggered by xenobiotic interaction with a biological macromolecule (e.g such as receptor/ligand interaction). This is

followed by a series of measurable 'key events' (KEs) that occur from the cellular (e.g. gene activation or altered cell signalling) through to the tissue and organ level (e.g. disrupted homeostatis), leading to adverse outcomes (AOs), such as lethality or reproductive impairment at the organism or population level[22]. The AOP framework is a knowledge management system that facilitates the use of experimental data (i.e. measurements of KEs) for regulatory purposes ('apical endpoints') to support chemical safety assessment based on mechanistic reasoning[23].

Consequently, it is widely recognised that the traditional empirical toxicity testing methods that are woefully reliant on treating animals with test substances and observing adverse outcomes (or 'apical endpoints') are no longer fit for future scientific and regulatory purposes due to their high cost, lack of mechanistic insights and ethical considerations[24–26]. Therefore, other 'alternative' and higher-throughput non-animal testing approaches must be explored to address the huge backlog of untested substances worldwide[13,14,27] and to ensure a more robust chemical safety assessment. One initiative aiming to address this challenge is the US 'Toxicology in the 21st century' or Tox21 Programme. It is a collaborative venture led by the US National Toxicology Program (NTP) to further the field of mechanistic toxicology and improve the quality and pace of toxicological assessment by implementing high-throughput screening cellular bioassays and building the ToxCast/Tox21 database, which currently covers >9000 environmental chemicals and can be used to inform chemical prioritisation and toxicity prediction strategies[25,28]. Another example is the PrecisionTox project (https://precisiontox.org/), which uses a suite of biomedical model organisms including the ecotoxicological model species *Daphnia*, human cell lines and artificial intelligence

(AI) to unravel molecular toxicity pathways shared among species to improve confidence in chemical toxicity predictions.

Recent changes in chemical regulations worldwide drive the rapid demand for novel, high-quality experimental data to fill information gaps relating to chemical safety and exposure. This has spurred the active interest of the scientific community and regulators in so-called new approach methodologies (NAMs) that also include high-content multi-omics methods, such as metabolomics or transcriptomics[29,30]. The ongoing challenge remains how to facilitate the timely uptake of these 'alternative' approaches globally in toxicology and chemical safety science to protect human and environmental health which is part of a continuous dialogue between regulators, industry and academia[5,30,31].

## 1.2 Introduction to metabolomics and its applications

Metabolomics is a powerful analytical approach aiming to reproducibly measure the endogenous metabolome (i.e., the complement of metabolites) of low-molecular weight molecules (typically, <1.5kDa) in complex biological samples (cells, tissues or biofluids) to study molecular perturbations in response to environmental stress, disease or toxicity[32,33]. The metabolome is time-dependent and highly dynamic. The Human Metabome Database (HMDB Version 5.0; www.hmdb.ca), the world's largest, organism-specific metabolomic database currently contains 220,945 entries, highlighting the complexity of metabolite measurements[34]. Metabolites cover a broad dynamic range (i.e. their concentrations span several orders of magnitude) and are chemically very diverse (in terms of polarity, solubility, stability, pKa, charge, reactivity,

etc.). Consequently, no single sample preparation protocol and analytical platform can capture and measure the entire complement of the metabolome at once. Therefore, multiple analytical techniques and methods are often utilised to maximise metabolite coverage[35,36].

Three types of metabolomics-based experiments can be conducted, depending on specific research questions[32,37–39].

1. Untargeted (or 'discovery-driven'), global large-scale hypothesis-generating assays aim to provide unbiased semi-quantitative measurements of the global metabolome in a biological sample without *a priori* knowledge of the metabolome. Peak areas or relative (not absolute) concentrations are reported for (typically, hundreds and up to low thousands of) metabolites detected when applying multiple information-rich mass spectrometry platforms. The chemical identities of metabolites are unknown prior to data acquisition and identification is typically performed using full scan $MS^1$ and $MS^n$ fragmentation data collected during the experiment. Untargeted metabolomics is a powerful approach for biomarker discovery to reveal metabolites indicative of a particular disease or toxicity phenotype[38,40].

2. Targeted (or 'hypothesis-driven'), typically hypothesis-testing (validation) assays offer higher accuracy, sensitivity and selectivity compared to untargeted metabolomics. This approach provides precise quantitative measurements of a small subset of pre-defined specific biologically relevant metabolites (typically, <50) whose chemical identities are known prior to data acquisition. Absolute

concentrations of metabolites are derived by the addition of isotopically labelled internal standards or using the external standard calibration method with a single calibration curve for each metabolite. Targeted metabolomics provides targeted analytical validation of biomarkers required for the translation of findings into clinical practice[39].

3. Semi-targeted (hybrid) hypothesis generating or hypothesis-testing assays represent an intermediate strategy between untargeted and targeted approaches and offer a good compromise of metabolite coverage, quantification, and identification[4,41]. This approach provides semi-quantitative measurements of a selected subset of known, biologically important metabolites (typically, hundreds are measured). Approximate metabolite concentrations are defined by applying one calibration curve and internal standard to a class of structurally similar metabolites or lipids.

Metabolic phenotyping experiments frequently apply both untargeted metabolic profiling followed by targeted (or semi-targeted) approaches, whereby untargeted biomarker discovery and identification precedes targeted validation and precise quantification of the specific biomarkers identified from either the untargeted study or hypothesis-driven from literature[39].

The metabolome is most closely related to the functional phenotype of an organism and, therefore, offers a unique opportunity to study the relationship between the genotype and phenotype in response to genetic or environmental changes, utiltising the systems biology approach[42]. Recent technology advancements (e.g. HRAM mass

spectrometry) have paved the way for the increasing use of metabolomics in mainstream biomedical applications, such as drug discovery, precision medicine[43] and human exposome studies. For example, metabolomics is now widely applied during the early stages of drug discovery to identify drug candidate targets and elucidate their mode of action (MoA)[44]. In clinical applications, metabolomics studies focus on the discovery and quantification of diagnostic biomarkers of disease, such as rheumatological conditions, neurological disorders or cardiovascular disease. In the context of human exposome studies, metabolomic holds a promising potential in unravelling the causal links between environmental exposure and human health[45,46]. The concept of human exposome describes the complex interactions of a biological system with its environment defined as the sum of environmental exposures and biomolecular responses to these exposures[47–49].

One advantage of metabolomics, compared to other omics, is that the endogenous metabolome is the most 'downstream' expression of biochemical pathways. Therefore, it most closely represents the molecular phenotype of an organism's genome in response to disease or changes occurring in the environment, including chemical exposure[50,51]. As such, toxicological metabolomics (or toxicometabolomics), a subfield of metabolomics, offers a unique opportunity to provide insights into toxicity mechanisms and derive chemical modes of action (MoAs), discover new molecular biomarkers and build toxicity prediction models for improved chemical safety assessment [19,52].

In the context of toxicological metabolomics, hypothesis-generating studies provide a more holistic understanding of effects inducted by xenobiotic exposure in a biological

test system[53]. Therefore, in this thesis, I explore the applications of untargeted 'discovery-driven' metabolomics assays to study both endogenous (biological effects) and exogenous (xenobiotic metabolism) responses to chemical toxicity in two *in vivo* model organisms: *Daphnia magna* (water flea) and *Rattus* (rat).

## 1.3 Environmental metabolomics

Environmental metabolomics (also sometimes termed xenometabolomics in literature) can be considered a subdiscipline of metabolomics, which aims to characterise the interactions of biological systems with their environment and aims to study the impact of environmental stress and pollution on living organisms[54,55].

Regarded as the 'end-point' of omics cascade, metabolomics is the closest reflection of the phenotype, making it a valuable tool in predictive toxicology, chemical risk assessment and exposome studies[56]. Environmental metabolomics has been widely applied in the field of aquatic (eco)toxicology to gain insights into the mechanisms associated with xenobiotic-induced perturbations in a range of sentinel model organisms, including *Daphnia magna*[57–59], zebra fish (*Danio rerio)*[60,61], microalgae *Chlamydomonas reinhardtii*[62], green algae *Raphidocelis subcapitata*[63] or marine mussels *Mytilus galloprovincialis* and *Mytilus edulis* [64,65]. Xenobiotic exposure results in the detection of both the endometabolome (endogenous organism biochemistry) and xenometabolome or exposome (exogenous xenobiotics) in biological systems[66] and both these dimensions of toxicity are of the focus of the thesis.

A significant contribution of the thesis to the field of environmental metabolomics is made by investigating molecular acute toxicity responses in *Daphnia magna*, an established model organism in aquatic toxicology (as described in chapter 3).

## 1.4 Applications of metabolomics in regulatory toxicology

The development of approaches enabling more accurate mechanism-based risk assessment remains the key challenge of modern toxicology to address the paradigm shift from purely observing 'apical endpoints' (or adverse outcomes, e.g. growth, reproductive impairment) in a whole organism towards understanding modes of action (MoAs) of new industrial chemicals and constructing adverse outcome pathways[44]. Hence, over recent years there has been a growing focus from regulatory scientists on high-content and high-throughput omics technologies (i.e. transcriptomics, metabolomics, proteomics, genomics, epigenomics) and their applications in the context of the adverse outcome pathway (AOP) framework[22,26,67]. For instance, the Organisation for Economic Cooperation and Development (OECD) actively promotes the benefits of using state-of-the art omics approaches and their applications in chemical safety evaluations which is reflected in the recently published comprehensive guidance documents and the dedicated 'Omics technologies in chemical testing' website (https://www.oecd.org/chemicalsafety/testing/omics.htm)[68,69].

As the endogenous metabolome best reflects the molecular phenotype most 'downstream' from xenobiotic exposure, it follows that hazard (or adverse outcome) and MoAs can likely be determined from the observable quantitative changes in metabolite levels[70]. Consequently, data-driven metabolomics is well placed to discover

toxicological pathways and molecular initiating events (MIEs, defined as the initial direct toxicant-induced chemical-biological interaction in a biological system) within adverse outcome pathways (AOPs) and has the potential to emerge as a solution to the global chemical safety crisis[22,67,71]. The potential of NMR-based metabolomics was previously successfully demonstrated for preclinical toxicological screening to predict liver and kidney toxicity of candidate drugs based on >100 *in vivo* rodent studies as part of the COMET (Consortium for Metabonomic Toxicology) project two decades ago[72,73].

The four main applications of metabolomics that could benefit regulatory toxicology and advance safety assessment of industrial chemicals include: 1) chemical grouping (or category formation) to enable biologically-driven read-across; 2) elucidating modes of actions (MoAs) of chemicals and contributing to existing or identifying novel adverse outcome pathways (AOPs) to better understand mechanisms of toxicity; 3) deriving molecular points-of-departure (PODs) using the benchmark dosing approach (BMD) and 4) improving knowledge of cross-species extrapolation of toxicity (or 'biological read-across') through an understanding of mechanistic/pathway-based processes and biological conservation between species[3,68,74–76]. In chapter 3 of this thesis, I investigate how untargeted metabolomics (integrated with transcriptomics) can support chemical grouping and read-cross of data-poor chemicals, which is perhaps the most immediate application of this approach in the context of regulatory toxicology.

Another relatively unexplored area in regulatory toxicology is untargeted toxicokinetics (TK) or the measurement of ADME (absorption, distribution, metabolic transformation and elimination) properties (as a function of dose and time) as part of an untargeted

toxicometabolomics study[3]. This approach offers promising insights into the metabolism and metabolic fate of exposure chemicals in a biological system within the same untargeted metabolomics measurements already used for the investigation of toxicant-induced endogenous molecular responses[3,6,66,77]. Knowledge of ADME/TK taken together with toxicodynamics has the potential to contribute to regulatory toxicology applications by enhancing the understanding of chemical MoAs, supporting chemical grouping and advancing cross-species extrapolation of toxicity[3,78].

ADME/TK information could, in theory, be collected as part of a standard toxicological study[79,80]. However, *in vivo* metabolic fate studies are often costly, technically challenging and time-consuming. Therefore, in practice, they are rarely conducted outside of pharmaceutical and agrochemical industries. Consequently, many industrial chemicals lack ADME/TK data necessary for safety assessment which often relies on purely theoretical *in silico* predicted biotransformation products[81]. In this thesis, I address this knowledge gap by investigating how untargeted metabolomics can be applied to simultaneously study toxicodynamics and ADME/TK properties, without the need for additional metabolism studies.

Despite being widely used in academic research, the implementation of metabolomics in regulatory toxicology has been largely hindered by the relative lack of robust, regulatory relevant case studies[3,33] combined with the lack of standardisation and transparency in conducting and reporting metabolomics studies[82]. Additional challenges are associated with validation and interpretation of datasets in the context of risk assessment[26,29,67]. Some of these challenges are being addressed by the Metabolomics standaRds Initative in Toxicology (MERIT)[3]. The recently published

OECD *Metabolomics Reporting Framework* aims to provide best practice guidance on conducting and reporting metabolomics studies, ultimately improving consistency and transparency of these approaches which is vital for accelerating their regulatory uptake and acceptance[82,83].

## 1.5 Transcriptomics in (eco)toxicology and chemical risk assessment

Transcriptomics (or gene expression profiling) is a study of the transcriptome, i.e. the complete set of RNA transcripts (both coding and non-coding) within a biological system[84]. The transcriptome (RNA) provides a 'snapshot in time' of all the genes actively expressed in an organism (upregulated or downregulated) in response to toxicity or reflective of an adverse outcome (e.g. induced by chemical exposure)[85]. Although this thesis is essentially devoted to the use of metabolomics as a NAM, multi-omics data integration was achieved to explore the value of integrating metabolomics and transcriptomics data streams for chemical grouping and read-across (introduced in section 1.7). Therefore, for the purpose of the thesis, example transcriptomics applications to (eco)toxicology are discussed below.

Toxicological investigations using transcriptomcs data (toxicogenomics) are highly abundant. For instance, *in vivo* toxicogenomics data from rodent studies was previously successfully utilised to derive modes of actions (MoAs) and points of departure (PODs), using benchmark modelling (BMD), for a well-studied carcinogen, benzo(*a*)pyrene, demonstrating the value of this approach in supporting safety assessment of data-poor chemicals in the absence of apical endpoints[86]. Another study on uncoupling of oxidative phosphorylation (OXPOS) chemicals shows that

MoA-specific gene expression profiles derived from *in vitro* cell assays can be used to group these chemicals and can distinguish them from polar narcotics. Additionally this study revealed that the same chemical can reveal multiple MoAs, thereby complementing chemical classification based solely on structure[87]. Recently, Nakagawa *et al*. (2021) demonstrated the value of *in vitro* toxicogenomics for elucidating MoA of chemicals for grouping and read-across of naphthalene and its three analogues based on oxidative stress responses in rat primary hepatocytes[88].

Lately, genome-wide investigations of the transcriptome based on whole-genome sequencing (WGS) data have been replaced by lowered-cost “reduced-representation transcriptomics” including platforms designed specifically for toxicogenomics (S1500+ platform designed by the Tox21 Working Group of the US National Toxicology Program). A custom platform that contains probes of homologous *Daphnia* genes to those of the human S1500+ is used for my investigations. This thesis builds upon the earlier progress using gene expression data to explore the complementarity of both data types (specifically, untargeted metabolomics integrated with targeted transcriptomics) to optimally improve these two applications to benefit regulatory toxicology in the context of chemical grouping and read-across case study on seven dyes, as described in research chapter 3. This thesis is focused on utilising gene expression data only in support of metabolomics under the notion of systems toxicology.

## 1.6 *Daphnia magna* as a model organism for (eco)toxicology and chemical risk assessment

*Daphnia magna* (or water flea) is a well characterised freshwater sentinel species indicative of environmental stress. Due to their short lifecycle, high fecundity and parthenogenic reproduction (i.e. asexual production of genetically identical female offspring, thereby reducing confounding biological variability) and ease of culturing water fleas are particularly well suited for laboratory-controlled experiments of environmental stress and chemical exposure[89,90].

*D. magna* a long-established model organism in aquatic toxicity testing and one of the recommended OECD test species (alongside algae and fish) utilised in widely employed toxicity assays, such as the OECD Test No. 202: *Daphnia sp., acute immobilisation test*[91] and the OECD Test No. 211: *Daphnia magna Reproduction Test*[92]. More recently, the significance of *Daphnia* ssp. in ecotoxicology and chemical risk assessment was consolidated by the mapping of the ecoresponsive genomes of *D. pulex* [93] and *D. magna*[94]. Noteworthily, *Daphnia* genome consists of 30,907 genes the majority of which are shared with humans further highlighting the relevance of this species to human toxicology[93]. In addition, the *Daphnia* genus is recognised as a model organism for basic biomedical research (i.e. human health) in the US National Institute of Health (NIH)[95]. Finally, *Daphnia* is an invertebrate species and therefore falls outside of current testing regulations which allows compatibility with the 3Rs principles (the replacement, reduction and refinement of animal research) and supports the underlying goal of REACH to minimise animal use in chemical risk assessment[29].

*Daphnia magna* is a major focus of this thesis and was selected as a model organism for the azo dye grouping study presented in chapter 3. In addition, *Daphnia* biotransformation capabilities of azo dyes were discussed in chapter 4.

*Rattus* (rat) is an important model species in traditional toxicology studies (such as drug metabolism and pharmacodynamic studies; both acute and (sub)chronic studies) to predict human health toxicity outcomes[96]. It is also widely utilised in OECD toxicity assays for testing new industrial chemicals, including OECD Test No. 407: *Repeated-dose 28-day oral toxicity study in rodents*[97] and Test No. 408: *Repeated-dose 90-day oral toxicity study in rodents*[98].

The selection of the model species for the work presented in chapter 5 was dictated purely by Covid-19 practicalities (as explained in Covid-19 Statement). The existing rat plasma samples from the US National Toxicology Program (NTP) primarily designed to study the endogenous metabolism in response to five industrial chemicals were utilised to simultaneously characterise xenobiotic metabolism within the same toxicity assay.

## 1.7 Chemical grouping and read-across for inferring the toxicity of data-poor chemicals

Grouping and read-across (G/RAx) is one of the approaches frequently applied in regulatory toxicology for data gap filling. The first step is to group (or form categories) of substances to formulate the original 'grouping hypothesis'. This is followed by gap-filling or 'reading across' the known endpoint toxicity from an analogous (tested) 'source' substance to an unknown (untested) 'target' substance(s) within the same group/category[80,99]. Figure 1.1 illustrates the grouping and read-across concept.

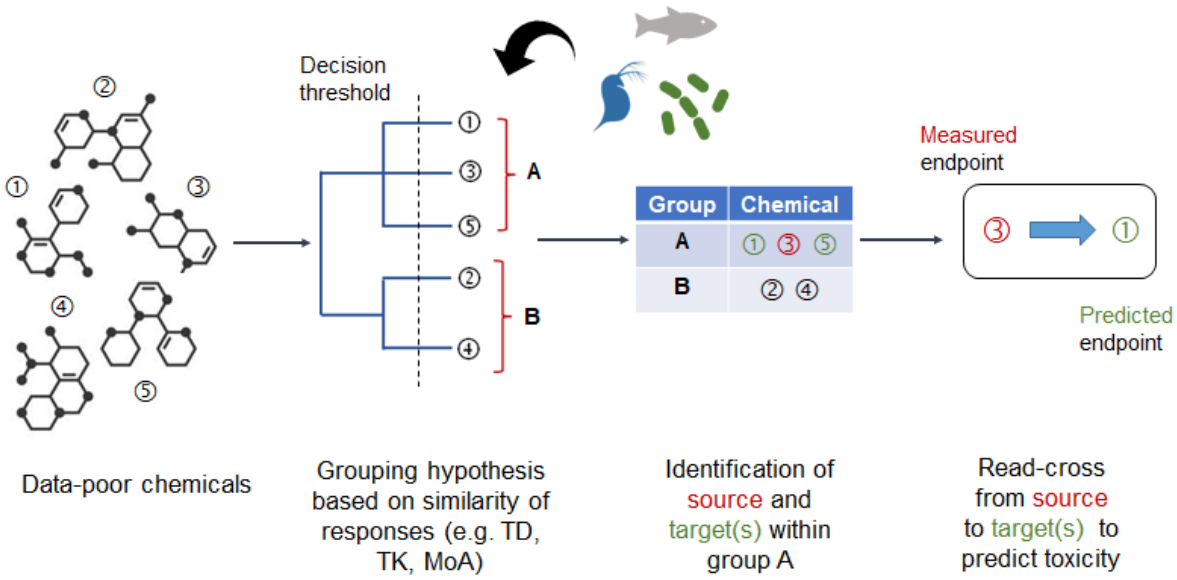


**Figure 1.1** Grouping and read-across approach used to predict the toxicity of untested, data-poor chemicals under the ECHA's Read-across Framework (RAAF; ECHA, 2017). The first step is grouping chemicals to generate the initial grouping hypothesis based on similarity of chemical structure and / or responses . This is followed by 'reading-across' toxicity for a given endpoint to another group member.

The traditional grouping and read-across approach heavily relies on chemical similarity (and related physicochemical properties) for toxicity prediction of data-poor chemicals, hypothesising that structurally similar substances will induce a similar toxicological response. This assumption is inherently flawed and does not consider the complex nature of toxicity mechanisms[100–102]. One example of two structurally-related chemicals that induce completely different toxicological effects are 2-acetylaminofluorene (2-AAF) and 4-acetylaminofluorene (4-AAF), where by 2-AAF is a liver carcinogen and 4-AAF is non-carcinogenic[103]. Various software tools have been developed to date to facilitate grouping approaches and associated gap filling. For example, the ECHA OECD Toolbox (https://www.oecd.org/chemicalsafety/risk-

assessment/oecd-qsar-toolbox.htm) is considered the most comprehensive (and most advanced in terms of its functionality to address regulatory questions) read-across tool currently available. It closely mimics the regulatory workflow and begins to incorporate adverse outcome pathways (AOPs) into its structure[102,104]. The workflow follows the OECD grouping guidance[80], whereby the chemical of interest is characterised using predefined profiles linked to databases or inventories prior to collecting multiple endpoint data. However, the mechanistic profilers in the Toolbox are often purely theoretical in nature collections of *in silico* structural alerts, which have not been supported by any relevant experimental data[102].

Grouping and read-across (G/RAx) have been used to predict at least one toxicological endpoint (ecotoxological or higher tier human) in up to 75% of chemical registration dossiers submitted to the European Chemicals Agency (ECHA)[105,106]. Extensive guidance documents and frameworks exist to support constructing and reporting G/RAx cases, for instance, the OECD *Guidance on Grouping of Chemicals*[80] and ECHA's *Read-Across Assessment Framework* (RAAF)[99]. The two key aspects of any G/Rax argument are assessing similarity and conducting uncertainty analysis[107,108]. The prerequisite for regulatory acceptance of a toxicological G/Rax prediction is establishing and suitable justification of similarity (or dissimilarity) between the 'source' and 'target' substance(s) in terms of three broadly defined criteria 1) structural/physicochemical similarity, 2) similar (bio)transformation (toxicokinetics, metabolism and/or abiotic transformation processes), and 3) similarity in *in vivo* toxicological responses and toxicodynamics within the group/category[107].

However, while ECHA strongly advocates the applications of grouping and read-across, it also rejects most read-across cases, largely due to a lack of scientific rigour in defining the grouping hypothesis and insufficient supporting evidence to demonstrate toxicokinetic and toxicodynamic similarities between compounds[103,109]. Consequently, the general consensus in the scientific community is that the quality of the grouping and read-across evaluation needs to improve to increase confidence in category formation, ultimately leading to more accurate and biologically relevant predictions of toxicity for data-poor chemicals[3,109,110].

Several studies demonstrated the value of metabolomics in supporting biologically driven grouping and read-across. For instance, endogenous metabolomics responses obtained during a 28-day rat toxicity test improved the quality of read-across conducted on three phenoxy herbicides (MCPP, MCP and 2-4 DP), demonstrating the higher applicability of biological data compared to the data related to chemical structure alone[111] . Specifically, the authors concluded that the 90-day rat toxicity study on MCPP ('target' substance) could be waived for 2-4-DP ('source') based on the similarities identified for these chemicals from a 28-day metabolomics study. Another proof-of-principle study by Sperber *et al.* (2019) concluded that mechanistic metabolomics data (i.e. 274-biomarker panel derived from the rat metabolome) can validate a read-across case for 3-aminopropanol and 2-aminoethanol, initially based on structural similarity of these two compounds. In this approach metabolic patterns associated with a specific MoA for the two chemicals of interest were compared against a proprietary database (MetaMap® Tox library[112]) to identify an appropriate 'source' (2-aminoethanol) for subsequent read-across to the 'target' (3-aminopropanol), demonstrating how metabolomic similarity can reduce inherent uncertainties

associated with grouping based solely on structure[113]. Recently, the metabolomics data obtained from a (14-day oral dosing) toxicity study in rats substantiated another structure-based read-across case for >1200 'Unknown or Variable Composition, complex reaction products or Biological materials' (UVCBs)[114]. Over 60,000 metabolic profiles and >120 specific metabolite patterns discovered in rat plasma were screened against the BASF MetaMap® Tox library[112] as indicators for toxicological MoAs (*Conference presentation and abstract*)[114].

While the applications of metabolomics for G/RAx are gaining a steady momentum, knowledge gaps remain on how to apply it in a regulatory context to predict toxicity of many untested chemicals. One challenge is the relative lack of relevant proof-of concept case studies demonstrating the potential of this approach for biologically-based grouping, which is addressed by this thesis.

## 1.8 Untargeted mass spectrometry-based workflow

Mass spectrometry is an extensively used technology in the field of metabolomics, owing to its excellent sensitivity and increased selectivity, combined with high-throughput capabilities and relative depth of coverage in comparison with nuclear magnetic resonance (NMR)[115]. As discussed in section 1.2, untargeted metabolomics aims to profile the entire metabolome present in a biological sample and is a discovery-driven approach that is particularly beneficial if there is no initial hypothesis (e.g. derived from literature) for the study[116]. In the context of toxicology and safety science, untargeted metabolomics has the potential to discover toxicological MoAs or metabolic key events in AOPs[3]. The sections below discuss the typical steps and considerations

in an untargeted metabolomics workflow as the basis for improvements presented in the thesis.

### 1.8.1 Experimental design, sample preparation, quality control (QC) and quality assurance (QA)

Robust experimental design is a key contributing factor for a successful metabolomics study. It enables addressing specific research questions by producing biologically meaningful results, while reducing non-biological confounding factors or biases (i.e. minimising analytical/technical variance) and therefore numbers of false positives. The key components of an experimental design include: 1) sample considerations (e.g. biological and technical replication, randomisation); 2) treatment and sampling (e.g. selection of treatment groups, dose and time point selection, choice of sampling and quenching methods); 3) sample preparation (e.g. appropriate sample storage and pooling methods, selection of extraction protocols); 4) analytical workflow (e.g. choice of a suitable analytical platform and method, QC strategies) and 5) data processing and analysis (e.g. choice of univariate and multivariate statistical methods, parametric or non-parametric tests). An example experimental workflow is shown in Figure 1.2.

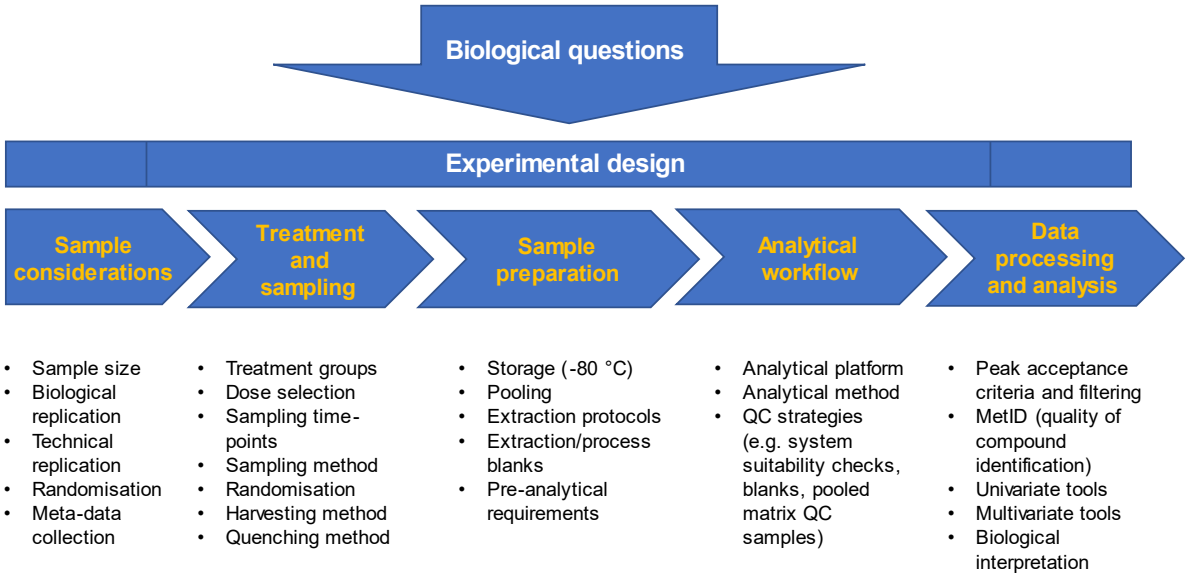


**Figure 1.2** Study design considerations and experimental workflow in untargeted nESI-DIMS and LC-MS-based metabolomics (adapted and updated from Rodrigues *et al*.,2019[2]).

The appropriate level of replication is important to assess the biological variability associated with subjects within a study as it can affect the downstream data analysis and interpretation. The number of biological replicates selected for a study will be determined by a biological system used. Studies based on carefully selected, well-characterised cells or model organisms in controlled environments typically require a lower level of replication compared to human subjects. The level of replication varies from study to study but most metabolomics studies in eco(toxicology) using model organisms typically report between six[117] to eight[58] replicates for *Daphnia magna*. Ten biological replicates were previously included to allow for highly replicated omics-driven discovery of molecular MoAs using algal toxicity testing[62]. The general recommendation is to include six replicates (n=6) per treatment group; however, biological replicate number will depend on the specific scientific questions and

statistical power calculations[2,10,68]. The need for a higher level of biological (or technical) replication can be determined by conducting a preliminary study to estimate the variance associated with analytical or pre-analytical workflows used within the main study[60]. Technical replication allows an assessment of analytical variance, such as sample preparation bias (i.e. any deviations in sample collection, storage or extraction that can affect the measured analytes), sample complexity bias (the impact of mixture effects in a sample on analyte measurements) or analytical bias (caused by changes in analytical conditions during measurements or due to matrix effects i.e. enhancement or suppression of ionisation) and should also be considered in experimental design[118].

Randomisation (e.g. during toxicity exposures, sample collection, sample processing and data acquisition) is important for making causal inferences and helps to eliminate any uncontrolled factors which may vary over the course of the experiment. Various strategies can be employed, such as complete randomisation (i.e. the order of all samples is randomised across all treatment and control groups within a batch) or more structured “blocking” randomisation. In this technique “block 1” is generated by randomly selecting a sample from each biological class to ensure each treatment group is proportionally represented. The process is subsequently repeated to generate “block 2”, “block 3”, “block *n*” until all samples are assigned to “blocks”. Both the order of the samples within each block and the order of the “blocks” are randomised[119].

The choice of a sampling (harvesting) method and sample preparation method is often dictated by the type of biological sample (e.g. biofluids, tissue or whole organisms) as well as the analytical technique employed in the study. Crucially, sample handling and processing should be minimal to limit metabolite loss while ensuring high

reproducibility and yield of metabolites and lipids[120]. Sample preparation methods include protein precipitation (performed by addition of organic solvents to biofluids, e.g. plasma, serum or urine), liquid-liquid extractions and solid-phase extractions. Solvent-based extraction methods (used for tissues, cells or whole organisms, e.g. *Daphnia magna*) can be further divided into biphasic or mono-phasic metabolite extractions using different organic solvent systems. Southam *et al*. (2021) compared various solvent-based extraction methods and concluded that monophasic extractions offer at least the same magnitude of detection responses as more time-consuming biphasic methods, rendering them suitable for future sample processing automation[121]. For *Daphnia magna*, typically biphasic extractions of metabolites and lipids are performed on whole-organism homogenates, using the standard Bligh and Dyer or (modified or unmodified) Matyash methods[122].

Appropriate quality assurance (QA) and quality control (QC) strategies should also be implemented at each step of the experimental workflow (from sample collection and preparation through to data acquisition, and subsequent data processing and analysis) to ensure integrity of the data, whilst limiting technical bias and confounding factors. In terms of suitable QC strategies, the inclusion of up to four different types of QC samples within an LC-MS-based metabolomics study is recommended by the MEtabolomics standaRds Initiative in Toxicology (MERIT) and the Metabolomics Quality Assurance and Quality Control Consortium (mQACC)[3,37,123]. These can include the following: 1) intra-study (or pooled matrix) QC samples (used for the assessment of analytical drift and technical variation); 2) intra- and 3) inter-laboratory QC samples (used for the evaluation of data reproducibility within the same laboratory or across laboratories); and 4) up to three types of blank samples, such as process (or extraction)

blanks, system suitability (or solvent blanks) with standards, or solvent blanks (without standard addition). The last two types of blanks are used to ensure optimal performance of the analytical instrument prior to data acquisition, typically via multiple injections of test samples at the beginning of an analytical sequence.

Other general good laboratory practices include the use of isotopically-labelled (or other compounds that are not present in biological samples under study) internal standards to assess data quality, use of technical replicates of experimental samples (i.e repeat analysis using either 'injection replicates' or 'extraction replicates'), run order randomisation and balancing for high-throughput multi-batch analyses. Recommended post-analysis quality management procedures involve ensuring the highest possible quality of compound annotation or identification (MetID to MSI standards) and conducting data quality reviews at regular intervals (e.g. using retention time window tolerance to assess analytical data quality)[123].

### 1.8.2 Ionisation

Mass spectrometry detects mass-to-charge ratios (*m/z* values of ions) and can provide both qualitative (structure) and quantitative (molecular mass or concentration) information on the analyte molecules. The first step of the analysis is ionisation and conversion of ions into the gas phase[124].

Electrospray ionisation (ESI) and atmospheric pressure ionisation (APCI) are the two common ionisation methods of choice in LC-MS-based metabolomics. ESI and APCI are considered soft ionisation techniques i.e. significantly fewer fragment ions are produced in the source compared to the number of intact molecular ion species.

In both methods ionisation takes place at atmospheric pressure and includes nebulisation and desolvation, but the ionisation mechanism itself is very different. In ESI protonation of the analyte occurs in the liquid phase and this method is more suitable for semi-polar and polar, non-volatile molecules. The formation of charged droplets is obtained by spraying the sample through an electrospray needle or nozzle in a strong electric field. Solvent evaporation leads to droplet shrinkage until the surface tension can no longer sustain the charge (the Rayleigh limit), fission occurs, and the highly charged droplet disintegrates (via 'Coulombic explosion'). This generates smaller droplets that subsequently undergo the same process as well as naked charged analyte molecules, which can be either singly or doubly charged. The positively or negatively charged ions in the gas phase are subsequently sampled in a skimmer cone and accelerated into the mass analyser[124–126].

In APCI a protonated solvent molecule donates a proton to the analyte in the gas phase and this method of ionisation is better suited for neutral or non-polar, volatile low molecular weight analytes. While ESI is well suited for the analysis of the majority of metabolites, APCI has been shown to be more effective in ionisation of weakly polar and non-polar metabolites that do not ionise in solution[127]. ESI and APCI can be considered complementary techniques to increase metabolite coverage in large-scale untargeted metabolomics experiments[126].

A further advancement of electrospray ionisation technology, performed at lower flow rates (typically, 200-1000 nL $min^{-1}$) is nano-ESI. It delivers better ionisation efficiency, higher sensitivity and reduced ion suppression and matrix effects compared to conventional ESI due to producing smaller droplets[128,129]. Chip-based nano-ESI

technology has been implemented into a TriVersa NanoMate ion source (Advion) that can be coupled with direct infusion mass spectrometry (DIMS) or LC-MS applications. This chip-based nano-ESI technology enables high throughput analysis using low sample volume (typically few µL), decreased carryover (a clean nano-ESI nozzle is used per injection), better spray stability and reduced ion source contamination when coupled with DIMS[9,130].

The third most common ionisation techniques used in mass spectrometry is atmospheric pressure photoionisation (APPI). (Kauppila Syage, 2015, APPI). Analytes amendable to APPI include metabolites not easily ionised by other two techniques (ESI and APCI), e.g. non-polar molecules, weak acids and halogenated organic compounds. For instance, APPI has been shown to outperform ESI and APCI in the analysis of lipids resulting in higher sensitivity, better signal-to-noise (S/N) ratio and cleaner mass spectra with less ion suppression[131].

Matrix-assisted laser desorption ionisaton (MALDI) and desorption ESI (DESI) are the two techniques commonly applied in spatial metabolomics which utlises imaging mass spectrometry (IMS) technology to probe the spatial distribution of metabolites within tissues and organs[132,133]. Compared to ESI, MALDI predominantly produces easier to interpret singly charged ions (except for very high mass molecules), therefore allowing simple molecular mass determinations for most compounds and is frequently used for analysing macromolecules (e.g. proteins or nucleic acids) with less sample consumption[9,134,135]. The main advantage of DESI imaging is that it can provide a wealth of spatial information particularly on small molecule metabolites (e.g. lipids or aminoacids) with minimum sample preparation required[136].

### 1.8.3 Mass spectrometry analysis

As mentioned in the previous section, mass analysers used in mass spectrometry measure mass-to-charge ratios (*m/z*) of ions. High-resolution accurate-mass mass spectrometry (HRAM or HRMS) is characterised by high precision of these *m/z* measurements. Mass accuracy (expressed in root-mean-square (RMS) ppm) is the difference between measured and exact mass (i.e. based on elemental composition) and requires high mass resolution to ensure that each peak corresponds to a single elemental composition in a given experimental mass measurement[137].

Mass resolution and mass resolving power (often used interchangeably) are the two terms used to characterise instrument and method related performance in HRAM mass spectrometry[138]. Mass resolution in mass spectrometry describes the ability to distinguish between two peaks of equal height and weight[139]. Mass resolving power is used as a performance indicator of HRMS instruments (values > 10,000) using the 'full width at half maximum' (FWHM) method, whereby mass ($m$) is divided by the peak width at 50% of the maximum peak height in Orbitrap technology (50% $m/\Delta m_{50\%}$)[140]. Mass resolving power depends on mass spectral signal-to-noise (S/N) values, specific dynamic range, digital resolution, *m/z* ratio and isotopic fine structure[137].

There are three main types of mass analysers applied in HRMS, namely time of flight mass analysers (ToF), fourier transform ion cyclotrone resonance (FT-ICR) and Orbitrap mass analysers.

ToF mass spectrometers obtain the lower end of mass resolving power for HRMS (~40, 000 FWHM at 386 *m/z*), but their main advantage are faster scanning speeds (up to 50 Hz, i.e. 50 spectra per second), rendering them suitable for high speed analysis[141]. Both ICR and Orbitrap mass analysers use fourier transform (FT) to yield a spectrum of ion cyclotron frequencies subsequently converted to *m/z* spectra. In ICR the ions are confined and oscillated by a strong magnetic field in a Penning trap, whereas in an Orbitrap the ions oscillate around a central electrode and in between two external electrodes, whereby the frequency of axial oscillations depends on ion mass-to-charge rations[142].

Both types of mass analysers detect the image current as a function of time and the resulting signal, called a free induction decay (FID) or transient, is converted by FT from the time domain (frequency of oscillations) to the frequency domain followed by mass calibration to yield *m/z* spectra of measured ions[143]. ICR outperforms any other types of HRMS mass analysers and can achieve over 2,000,000 resolving power[144,145]. Orbitrap mass analysers offer high and ultra-high resolution, achieving a nominal resolving power of up to 1,000,000 (at 200 *m/z*) and a sub ±1 ppm mass accuracy, all within a single benchtop instrument. This allows to discriminate and resolve analytes of interest from interfering ions resulting in higher confidence in the determination of elemental composition and, therefore, makes Orbitrap technology particularly suitable for the analysis of endogenous metabolites, lipids, xenobiotics and related fragment ions at low *m/z* ranges (<200 *m/z*)[146].

Orbitrap systems are well suited for untargeted metabolomics owing to their high mass resolving power, the capability to provide accurate mass measurements and acquire

full scan $MS^1$ data over a wide *m/z* range in a single scan. High-resolution $MS^n$ data aids database annotations (e.g. using HMDB, MassBank) and can also improve annotation attempts using *in silico* fragmentation tools (e.g. MetFrag, SIRIUS, MS-FINDER) where no direct spectral match is available. Tandem MS ($MS^n$) capabilities and interfacing with ion mobility technology further facilitate metabolite identification[147]. In addition, hyphenated techniques, such as connecting Orbitrap-based platforms to ultra-high-performance liquid chromatography (UHPLC) or gas chromatography (GC) have been shown to enhance separation of isobaric and isomeric molecular species, allow high-throughput workflows[148], and increase sensitivity and metabolic coverage[149].

### 1.8.4 Data processing, statistical analysis and biological interpretation

Untargeted metabolomics raw data files typically contain thousands of features of both biological and non-biological origin (such as isotopes, adducts, dimers or neutral loss fragments), including xenobiotic-related features and other artifact peaks resulting from contamination or impurities. Therefore, complex and streamlined data processing analysis and interpretation is required to achieve the following: 1) remove random noise features and retain only high-quality metabolic features for statistical analyses (termed peak picking and blank filtering), 2) correct for any systematic errors especially in high throughput studies, such as instrumental ppm mass drift or batch effects (signal drift and batch effect correction), 3) ensure that all samples within the dataset are comparable, i.e. they mostly contain the same features (sample filtering)[8,150].

A typical metabolomics processing workflow is shown in Figure 1.3 and the steps in the workflow are described in detail below.

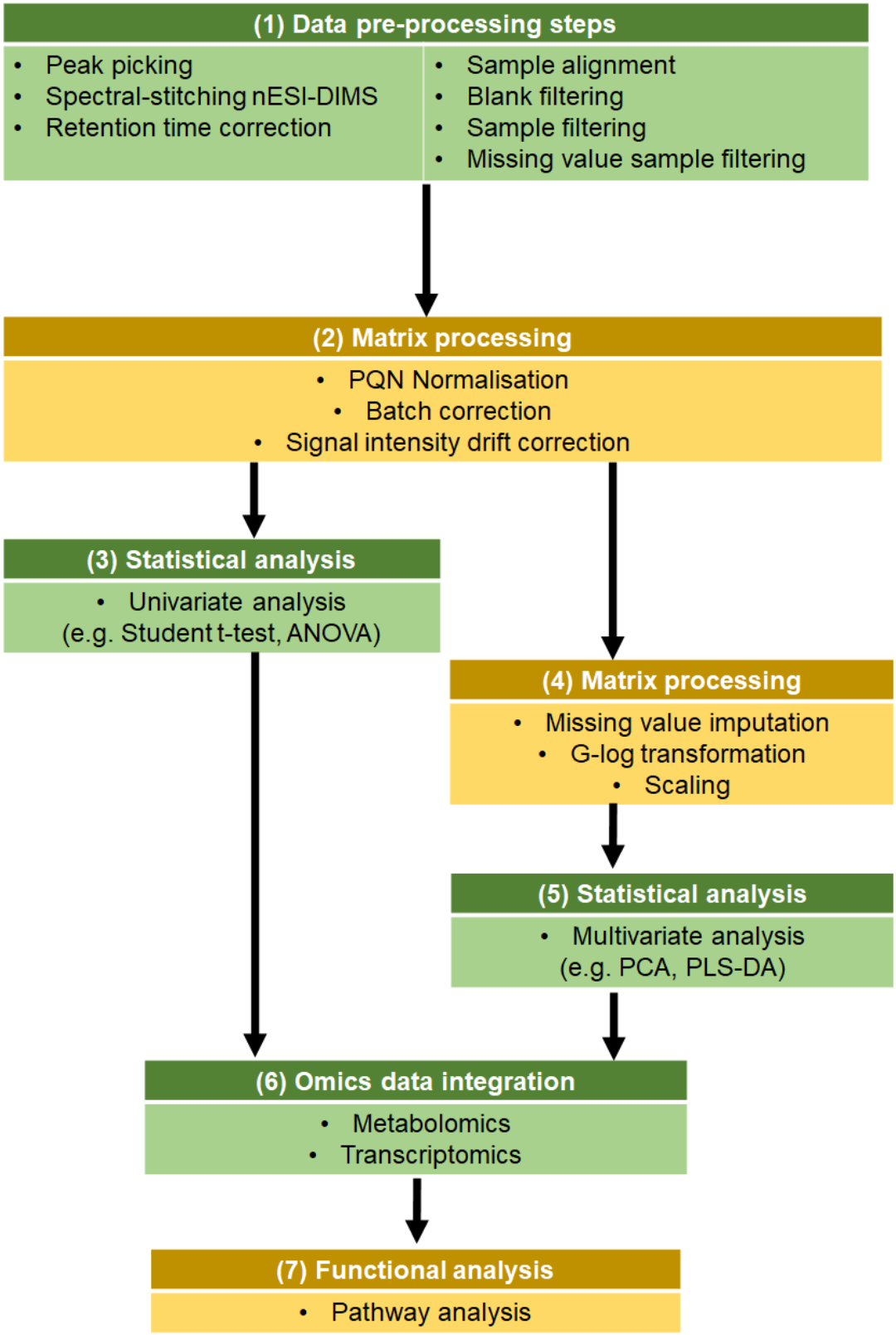


**Figure 1.3** Metabolomics data processing and analysis workflow (adapted from Viant *et al.* 2019[3], and Chen *et al*., 2022[4]).

### i. Data pre-processing

The first step in data pre-processing (1) is peak picking (or peak detection) which removes random noise features and retains features of interest determined by a specified signal-to-noise ratio (typically, S/N ≥ 3). For nESI-DIMS, this step also includes spectral-stitching i.e. merging a series of overlapping *m/z* SIM spectral windows into a single spectrum[8].

This is followed by alignment of *m/z* values to generate a peak intensity matrix and ensure that a specific metabolite is accurately defined across all the samples. For LC-MS data, retention time (RT) correction is performed to align *m/z* values and retention times across all the samples, and subsequently group them by spectral peaks corresponding to different isotopes and adduct species generated from the same metabolite.

The resulting peak intensity matrix is subjected to two-step filtering. First, any artifact peaks detected in process (extraction) blanks are excluded from the matrix (blank filter). Secondly, only features of biological origin that are present in a defined percentage of samples (typically, 80%) are retained (sample filter) to ensure optimal sample filtering and reduce the number of features with missing values[8]. An additional user-defined missing value sample filter (e.g. >50% threshold) removes from the matrix

### ii. Matrix processing

The next step in the workflow is matrix processing (2**)**. The filtered peak intensity matrix undergoes normalisation to account for any slight variations in concentration between the samples originating from sample processing (e.g. measurement errors) or slight

biomass differences. The ‘gold standard’ normalisation approach in metabolomics is probabilistic quotient normalisation (PQN) which scales the feature intensity matrix to the most probable dilution factor for each sample (PQN coefficient). Normalisation coefficient is calculated as the median fold change of intensities between each experimental sample and a representative pre-defined reference, typically a median spectrum from pooled intra-study QC samples or all study samples[151]. Compared to other normalisation methods, PQN preserves biological differences and prevents bias from high intensity features that may dominate the mass spectra. Additional signal intensity drift and batch effect correction step can also be applied to the dataset (using QC samples) to assess and/or correct for any technical variation relating to intra-batch signal drift and inter-batch effects for multiple-batch studies[8,150]. The PQN-normalised feature intensity matrix can now be subjected to univariate statistical analysis (3). However, no missing value imputation (MVI), scaling or transformation are not appropriate for univariate tests and can result in false positives[152].

### iii. Additional matrix processing prior to multivariate statistical analysis

Three additional matrix processing (4) steps can be applied to render the data suitable for subsequent multivariate statistical analysis (Figure 1.3), namely: missing value imputation, transformation and scaling [8,152].

Missing values arising from biological (e.g. features are not present in samples) or technical reasons (e.g. values are below the LOD or missed during reprocessing) are addressed as they can be problematic for multivariate statistical analysis and lead to biased results or impact statistical power. Various methods can be used for handling missing values, for instance by applying the mean (mean replacement method), or

median (median replacement method) of intensities. The *k*-nearest neighbour (KNN) imputation algorithm is considered the most robust approach used for approximating missing metabolite abundances in DIMS[153] and LC-MS[152] datasets. The assumption behind KNN for missing values is that samples with similar features have similar intensity distributions across the entire dataset. A weighted average of pre-defined (e.g. $k = 5$, where $k$ is the number of nearest neighbours considered) closest elements (samples) is used to impute a unique missing intensity value for every metabolite feature (in terms of *m/z* values) in specific samples[152,153].

Scaling is an optional step that may be performed (e.g. for variables spanning different ranges) using various methods, including autoscaling (standard deviation is used as scaling factor) or Pareto scaling (square root of standard deviation is used as a scaling factor) that can be influenced by outliers or extreme values. This step may be applied to adjust fold change variations between metabolites[152,154].

The PQN-normalised peak matrix is subsequently transformed to remove any systematic bias (i.e. overestimation of small values and underestimation of large values) and stabilise the measurement variance in the dataset by rescaling the data or reducing batch effects, while preserving biological information[155]. For nESI-DIMS variance-stabilising generalised (G-log) transformation is recommended, whereby the transformation parameter $\lambda$ (lambda) is optimised using the pooled QC samples in the dataset[8] The G-log transformation of metabolomics data is more suited for measurement errors that are stable at low intensities and increases at higher intensity; it also improves multivariate statistical analysis[156].

### iv. Statistical analysis

Statistical analysis (3 and 5) is the next step in the untargeted metabolomics workflow. Complementary univariate and multivariate methods are applied to metabolomics data to reveal information pertaining to the biological problem studied. For univariate methods only one variable is analysed at a time and correlations between metabolites are not considered. Multivariate methods include all variables and consider simultaneous relationships among these variables, revealing metabolites that discriminate between different sample groups[8,157,158].

Univariate methods enable to identify significant changes in the metabolite abundances between samples and they can be parametric (assuming a normal data distribution) or non-parametric. If it is assumed that the data follows a normal distribution, two-sample t-test (compares two groups of samples) or ANOVA (compares multiple groups of normally distributed samples) may be applied. Non-parametric tests, for example the Wilcoxon signed-rank test (for two sample groups) and the Kruskal-Wallis Mood's median test (for multiple groups) can be applied when data is not normally distributed but they are generally less powerful (i.e. require a larger sample size) than parametric tests[158].

The overall aim of statistical analysis of metabolomics data is to reveal statistically significant relationships between the measured metabolome and the observed effects, free from observational bias. Due to the complexity and high-dimensional nature of metabolomics datasets, univariate analyses with multiple testing corrections are performed to reduce the number of false positives resulting from the measurements of repeated variables (termed the multiple testing or multi comparisons problem). The

Bonferroni and Benjamini-Hochberg methods are frequently applied to this end. The Bonferroni correction is the simplest adjustment method (performed by multiplying the raw *p*-values by the number of tests) but it is known to be overly conservative and may lead to missing metabolites of potential interest[159].

An alternative and more powerful method was proposed by Benjamini and Hochberg, 1995[160]. The Benjamini–Hochberg false-discovery rate (FDR) procedure controls the number of false positives among the variables where a significant difference was found in multiple hypothesis testing. For example, if 200 features are found to be significant after FDR correction, then up to 5% of those could be false positive. Therefore, by accepting a small proportion of false positives, enough significant features can be reported. This is a less conservative *p*-value adjustment procedure well suited for exploratory data analysis. In contrast, when applying the Boniferroni method in order to keep the probability of false positives low, the number of false negatives is so high that it leaves very few features to draw conclusions from[161,162].

Two multivariate statistical methods are typically applied in metabolomics: principal component analysis (PCA) and partial least squares discriminant analysis (PLS-DA). PCA is an unsupervised dimension-reduction method that ignores the class labels (groups) of the samples and is used for explorative analysis (e.g., to assess data reproducibility, identify outliers and visualise the variation in multi-variable datasets). PLS-DA is a supervised method that fully considers the class labels. The first principal component in PCA captures maximum variance in the original data, while in PLS-DA captures maximum covariance between the original data and its labels. PLS-DA can be used for dimension reduction, feature classification and feature selection in

metabolomics studies[163]. However, as supervised methods are prone to overfitting (e.g. as a result of assigning importance to 'noise' or irrelevant information within the model), PLS-DA outcomes require validation to determine statistical significance of the observed group separation[164]. This can be achieved by using e.g. double cross-validation – a statistical method to evaluate the performance of the model, whereby the data is divided into two subsets: the training dataset (used for model building and model selection) and test dataset (used for model assessment). First, the model with the lowest prediction errors is selected (validation set) and then then the predictive performance of the model is evaluated. Another method is permutation testing, which is used to determine the statistical significance of the model by rearranging the data in multiple ways to estimate the sampling distribution[165].

In this thesis, both multivariate classification methods and FDR-corrected univariate statistical methods were implemented.

The final step in the workflow (6) involves deriving biological knowledge from metabolomics measurements by unravelling associations between metabolites and the biological processes or observed adverse effects[55]. This step may be followed by integrating metabolomics with another omics, such as transcriptomics, for more robust characterisation of the complex nature of a biological system under study[166,167] (7). Biological interpretation of the results typically requires some level of feature annotation or identification. Pathway enrichment analysis (PEA; also termed functional enrichment analysis or overrepresentation analysis) is a knowledge-driven bioinformatics approach that combines information from existing pathway databases (e.g. KEGG, MetaCyc, the Ingenuity Pathway Analysis, MetaboAnalyst) with

experimental findings to facilitate functional interpretation of metabolomics data, by identifying important groups of metabolites (biological pathways)[168,169].

Pathway enrichment (or over-representation) analysis, commonly applied in metabolomics and transcriptomics, seeks to determine if features (metabolites or genes) from pre-defined sets (i.e. belonging to a specific pathway) are present more than would be expected by chance ('over-represented') in a subset of the data in question[32,168]. Probability of observing significantly changing metabolites (for a pathway of interest) is calculated applying Fisher's Exact test and a set of significantly changing features is used to derive a smaller subset of perturbed biological pathways and/or processes[170]. One limitation of this approach is that it is requires unambiguous metabolite annotation. Any level of inaccuracy in metabolite annotation (e.g. 4% metabolite 'misidentification rate' by molecular weight or formula) is likely to enhance inherent biological 'noise' in the data and, therefore, result in simplifying or not detecting significantly enriched pathways[168,171]. An alternative approach is the *Mummichog* algorithm (www.mummichog.org) which can be applied directly to unannotated untargeted LC-MS metabolomics data to perform both pathway analysis and network module analysis[172]. The algorithm uses a combined list of all possible candidate metabolites detected in the dataset to search pathways and compute an enrichment *p*-value for each candidate (or a combination), per pathway. The probability of inferring correct pathways and metabolites is quantified by comparing the results obtained for statistically significant features with random data[172].

### 1.8.5 Direct infusion mass spectrometry (DIMS) and ultra-high performance liquid chromatography-mass spectrometry (UHPLC-MS) in untargeted metabolomics

This thesis explores the applications of mass spectrometry-based untargeted metabolomics in toxicology to probe endogenous (toxicodynamics) and exogenous (toxicokinetics) responses to selected industrial chemicals. Specifically, two platforms were applied: nano-electrospray direct infusion mass spectrometry (nESI-DIMS) and ultra-high performance liquid chromatography-mass spectrometry (UHPLC-MS).

While nESI-DIMS offers excellent high-throughput capabilities combined with lower sample biomass requirements, UHPLC-MS represents the 'gold standard' technique in metabolite detection and identification, accounting for 80% of untargeted metabolomics experiments, according to the MetaboLights repository (https://www.ebi.ac.uk/metabolights/)[173]. The strength of UHPLC-MS/MS lies in its separation power of liquid chromatography combined with the multi-stage mass analysis capability of Orbitrap-based HRMS. Depending on the analytes of interest, reversed-phase (RP) chromatographic columns can be used for lipidomics assays (e.g. C18 or C30 alkyl bonded stationary phases), while hydrophilic interaction chromatography (HILC) is more suited for polar metabolomics assays and provides a broad metabolome coverage including metabolite classes not typically analysed using RP (e.g. amino acids, small organic acids)[174]. HILIC and RP-based methods are considered complementary as early eluting analytes in RP are usually well retained in HILIC stationary phases. However, the latter often suffers from inferior separation efficiency compared to RPLC-MS, poorer retention time reproducibility and requires longer column equilibration times[9,174]. Optimal separation of analytes can be achieved

by the appropriate choice of a chromatographic column to increase LC selectivity and the separation power of the HRMS instrument and, therefore, aid annotation or identification of isobaric and isomeric species in untargeted metabolomics analysis. For example, Jankevics *et al*. (2021) developed an improved data dependent acquisition (DDA) approach, whereby only selected ions are fragmented based upon their intensities in the full scan $MS^1$ data[175]. This modified 'scheduled MS/MS' strategy (using narrower *m/z* windows for different lipid classes) on an electrospray Q Exactive Plus mass spectrometer coupled to $C_{30}$ RP chromatography improved coverage and identification of lipid species in complex matrices at highly reduced instrument time[176]. Another study demonstrated the capabilities of UHLPC-HRMS (on an electrospray Vion travelling wave ion mobility, TWIMS-QToF mass spectrometer, with and without ion chromatography, IC) for metabolite annotation, and also concluded that a novel polymeric zwitterionic stationary phase (zHILIC) was complementary to RP and HILIC-based applications with the highest metabolome coverage. A total of 338 metabolites were annotated in human plasma, 109 of which were found to be uniquely detected by zHILC[177].

The implementation of the spectral-stitching method (SIM-stitch nESI-DIMS) significantly improved sensitivity and dynamic range of nESI-DIMS measurements while maintaining high mass accuracy and accelerated sample throughput[8,58]. This approach was successfully applied to probe the *Daphnia magna* metabolome following 21-day exposures to three chemicals (cadmium, 2,4-dinitrophenol or propranolol) and resulted in the discovery of 49 early-response biomarkers predictive of reproductive fitness[58], only 11 of which were also putatively annotated or identified. Another example is the characterisation of the metabolic profiles of microalgae

*Chlamydomonas reinhardtii* cultures in a novel algae-based toxicity testing assay with chlorobenzene[62]. Both studies demonstrated the capability of nESI-DIMS metabolomics to discover toxicant-induced perturbations, highlighting the value of this approach in chemical risk assessment (e.g. via providing molecular evidence indicative of a chemical MoA). However, the main limitation remains metabolite annotation and identification, which could be addressed, for example, by large-scale comprehensive untargeted characterisation of model organism metabolomes (via a large suite of bioanalytical and computational methods), such as the Deep Metabolome Annotation (DMA) workflow for the *Daphnia magna* metabolome[58,178].

The advantages and challenges associated with both analytical platforms are summarised in Table 1.1 below. While both untargeted metabolomics approaches have their merits, UHPLC-MS/MS experiments often collect orthogonal analytical data (i.e. chromatographic retention time, full scan accurate *m/z*, isotopic pattern, $MS^n$ fragmentation data) and therefore enhance confidence in metabolite and lipid annotations, as described in the previous section.

**Table 1.1** Comparison of MS-based untargeted metabolomics platforms (based on Southam *et al*., 2017[8] and Ren *et al*., 2018[9]).

| | **Advantages** | **Challenges** |
|---|---|---|
| **nESI-DIMS** | • High-throughput technique<br>• High sensitivity<br>• Low sample biomass required (1 mg biomass or 5 µL)<br>• Reduced ion suppression by implementing nESI ion source and SIM-stitching approach<br>• No bias introduced by chromatographic separation<br>• Minimal analytical carryover due to no chromatography<br>• Simplified data processing due to no RT information | • Isomers cannot be distinguished<br>• No separation of analytes<br>• Ion suppression or ion enhancement for complex samples |
| **UHPLC-MS/MS** | • High coverage of detected metabolites<br>• High sensitivity and selectivity<br>• Separation of complex samples and less complex mass spectra<br>• RT information aids metabolite annotation | • Higher sample biomass required<br>• Longer analytical run |

## 1.9 Current challenges in metabolomics

The rapid development of new methods and techniques in metabolomics over the last decade has been largely driven by technological (e.g. a wide adoption of HRAM mass spectrometry) and bioinformatics advancements (e.g. implementation of tools for high-throughput metabolite profiling and annotation) in the field[179,180]. Although metabolomics is a mature science in academia, with over two decades of research and development, unambiguous metabolite identification and assigning biological interpretation are often considered the main limitations of untargeted metabolomics. This is attributed to the sheer complexity of metabolomics datasets (often containing thousands of small chemically diverse biomolecules) in contrast with a relatively large number of uncharacterised metabolites of interest for which entries are not available in standard libraries and databases, such as ChemSpider, the Human Metabolome Database (HMDB), MetLin or mzCloud (https://www.mzcloud.org/). It is postulated that the human metabolome comprises over 1,000,000 of (both endogenous and exogenous) compounds representing over 3,000 chemical classes while only approximately 114,000 metabolites and lipids have been identified to date[51]. This is reflected in a relatively low proportion of annotations whereby on average ca. <10% (and up to 30%) of features are annotated in a typical human untargeted metabolomics experiment[181,182]. Consequently, new experimental and computational strategies are being continually developed to improve metabolite coverage and identification[33,183].

Multiple frameworks exist to define different levels of confidence in metabolite annotation and identification (MetID), using orthogonal data derived from HRMS experiments (specifically, chromatographic peak RT, accurate *m/z* full scan $MS^1$ data

and $MS^n$ fragmentation data) to enhance metabolite annotation and identification[11,184,185]. The main reference document for MetID in the metabolomics community is the Metabolomics Standards Initiative (MSI) classification system[10,184] which defines four distinct categories of confidence based on the level of analytical evidence obtained for a feature of interest, as described in Table 1.2.

However, the metabolomics community recognises that the current classification system lacks the capability to clearly distinguish compounds with similar (yet not unique) level of identification, such as isomers. Constitutional isomers have the same molecular formula but different bonding arrangements (e.g. fatty acid positional isomers, such as phosphocholines PC (16:0/18:1) vs. PC (18:1/16:0)), whereas stereoisomers differ in spatial arrangement of atoms. [186] The addition of a quantitative scoring system was also postulated to improve the current classification.[187].

An alternative 5-tier scale was proposed by Schymansky *et al.* (2014) for xenobiotics and their biotransformation products as a more data-dependent approach that differentiates between different levels of structural annotation (i.e. confirmed structure, probable structure, etc.) and also provides sublevels (2a and 2b). Both confidence level scales require $MS^n$ fragmentation data to achieve the highest two levels of identification or annotation[11].

**Table 1.2** Confidence scale for metabolite annotations based on analytical evidence obtained from HRMS measurements (adapted from Sumner *et al*., 2007[10] and Schymansky *et al*., 2014[11]).

| MSI Level | Confidence level | Analytical evidence required | Corresponding Schymansky *et al*., 2014 confidence level |
|---|---|---|---|
| 1 | **Identified/ confirmed** compounds | Confirmed by ≥2 appropriate orthogonal data types* with authentic reference standards injected in the same analytical sequence. | Level 1: Confirmed structure |
| 2 | **Putatively annotated** compounds | Physico-chemical properties and/or mass spectra of compounds match databases/ spectral libraries / literature sources. | Level 2: Probable structure<br>2a: Library/ literature spectrum match; or<br>2b: Diagnostic evidence |
| 3 | **Putatively annotated** compounds / classes | Physico-chemical properties and/or mass spectra of compounds representative of a distinct compound class. | Level 3: Tentative candidate(s) |
| 4 | **Unknown** compounds | Unidentified and unclassified metabolites/ compounds which can be differentiated and quantified based on spectral data (e.g. full scan $MS^1$ data). | Level 4: Unequivocal molecular formula (isotope/adduct)<br><br>Level 5: Exact mass (without unequivocal formula assignment) |

*Chromatography and HRMS data types: RT, accurate *m/z* full scan $MS^1$ data, $MS^n$ fragmentation data (i.e. $MS^2$ and/or $MS^3$). Examples of appropriate orthogonal data include accurate mass with RT, or accurate mass and fragmentation data or isotopic pattern.

The highest level of identification is inherently challenging to achieve due to the lack of (authentic, high-purity) reference standards to confirm identities of many unknown compounds. However, the diverse orthogonal information collected within HMRS measurements enables the identification of unknown features with relatively high confidence[185]. $MS^n$ fragmentation data is particularly useful as it provides a molecular fingerprint by revealing rich structural information on the selected precursor ion and allows to discover and annotate substructures or chemical moieties of unknown compounds in a biological sample. The choice of a specific fragmentation technique is largely based on the nature of the analyte of interest. In Orbitrap-based instruments, Collision-induced dissociation (CID; occurs in the ion trap) is commonly used along with a complementary Orbitrap-specific technique, higher-energy collision dissociation (HCD; occurs in a collision cell behind the C-trap) which is more suitable for low *m/z* fragment ions[188]. CID $MS^n$ is the main strategy used in spectral library matching and interpreting fragmentation patterns for structure elucidation of metabolites of interest[189]. The experimental fragment ions are matched with a reference spectrum which can be derived from publicly available experimental mass spectral libraries (e.g. PubChem, Metlin, Massbank or mzCloud) or *in silico* fragmentation libraries for unknown compounds (e.g. commercial tools include Mass Frontier, MS-Fragmenter, Molecular Structure Correlator). The latter is often the case for xenobiotics and their biotransformation products for which experimental mass spectral data frequently does not exist or is limited and, therefore, (sub)structure annotations are based on theoretical *in silico* predicted fragments generated using chemical fragmentation rules[189]. Another challenge with spectral matching and searching large chemical repositories is a high rate of false positive matches resulting from the multiple testing

problem (FDR; described in section 1.7.4) as well as the lack of organism-specific curated metabolome databases, many of which are often biased towards human metabolism[65,190].

Although the lack of robust metabolite identification can be considered as one of the barriers for the successful uptake and applications of metabolomics in regulatory safety science, the level of required annotation is often dictated by the specific regulatory scenario. For instance, in the context of biologically-driven grouping and read-across, reporting metabolites to Level 4 MSI (unidentified compounds) is often considered sufficient[191]. This approach is successfully demonstrated by the research within this thesis, whereby the grouping of substances is based solely on the similarity of the endogenous responses to azo dye toxicity in *Daphnia magna* (presented in chapter 3)

The challenges of metabolite annotation and identification are being actively addressed by the metabolomics community via implementing various computational and analytical strategies. Some examples include the development of new statistical methods for estimating and limiting FDR of annotations based on library matching using similarity scores and decoy databases[192], retention time prediction for metabolites where no reference standard is available[183,193] or the use of fragmentation trees and multi-stage mass spectrometry ($MS^n$) trees to improve metabolite structural characterisation[189,194].

Recent technological developments have also emerged to address the MetID 'identity crisis' in metabolomics. This includes the implementation of novel analytical instrumentation (e.g. the Orbitrap ID-X Tribrid mass spectrometer for small molecule characterisation) and commercial software packages such as the AquireX Intelligent

Data Acquisition software (designed to generate high-quality fragmentation data on relevant biomolecules)[195,196]. Another example is Compound Discoverer, a comprehensive data-mining tool for *in silico* prediction, identification, and structural elucidation of compounds, using information-rich HRMS datasets from Orbitrap-based instruments[197]. This recent state-of-the art technology was implemented to characterise metabolism and metabolic fate of xenobiotics (five industrial chemicals) in untargeted metabolomics experiments, as described in chapter 5.

Another knowledge gap is how to develop efficient and comprehensive approaches for integrating metabolomics data with other omics platforms (genomics, transcriptomics and proteomics) to enhance mechanistic understanding of biological functions and unravel correlations between omics data streams, ultimately enhancing confidence in identifying molecular toxicity pathways[198,199]. To date, successful integration of more than two high-throughput omics datasets is infrequent and poses a significant challenge due to differences in data mining and statistical analysis methods, different feature identification strategies and biological contextualisation of individual omics datasets[200]. This thesis partially addresses this challenge by exploring the application of multi-omics approaches for biology-based chemical grouping in a regulatory context, integrating metabolomics and transcriptomics data streams.

Other challenges present at every level of the metabolomics experiment include the selection of appropriate standard operating procedures (SOP) and separation methods (e.g. reverse phase vs. normal phase approaches, two-dimensional chromatographic separations), and combinations of multiple analytical platforms to increase metabolite coverage and aid identification[201]. Despite the development and recent advancements

in bioinformatics tools for metabolomics data processing and analysis, the significant 'big data' challenges in the field remain data acquisition, feature extraction, precise quantification and robust statistical analysis of the results[202]. Recent software tools that utilise spectral and compound databases (e.g. the Metabolite Annotation Workflow; MAW) hold a promising potential to facilitate automated metabolite identification based on experimental tandem mass spectrometry data ($MS^2$) or *in silico* predictions[203].

Aside from the study of toxicodynamics (biological effects), untargeted toxicometabolomics can also potentially provide relevant insights into absorption, distribution, metabolism and excretion (ADME) processes and toxicokinetics rates (TK) in a biological test system. This information could be explored to characterise metabolism and metabolic fate of xenobiotics, as demonstrated in chapters 4 and 5 of the thesis. However, while *in silico* prediction of xenobiotic metabolism is an active area of research, a major limitation in the study of xenobiotic metabolism is the scarcity of open-source databases containing high-quality experimental biotransformation data on xenobiotics. One example of an open access xenobiotic metabolism database for drug discovery and toxicology applications is XMetDB (https://pharmb.io/tool/xmetdb/)[204].

## 1.10 Exploring metabolism and metabolic fate of xenobiotics through untargeted metabolomics

Characterisation of ADME and TK (also termed pharmacokinetics, PK) properties relating to the absorption, distribution, metabolism and excretion of a candidate chemical in a biological system forms an integral part of the pre-clinical and clinical

phases of drug development and pharmaceutical safety assessment process. Conventional chemical disposition (ADME) and toxicokinetics (TK) studies usually employ liquid chromatography-tandem mass spectrometry (LC-MS/MS) or radiolabelled compounds (e.g. $^{14}C$ or $^{3}H$) to identify and quantify the parent xenobiotic (and its metabolites) within the systemic circulation and target tissue as a function of dose and time. Typically, multiple sampling points (i.e. sample collection at fixed defined time points or across a timed interval) are used to derive rates of absorption and clearance, and estimate the bioavailability of a new molecular entity[205,206]. ADME/TK characterisation of xenobiotics can in principle enable to understand systemic exposure and establish correlations between the internal concentration/dose levels and observed toxicity responses. This information may be used to benefit chemical risk assessment in a number of ways: 1) guiding more robust dose selection (and setting exposure limits) for subsequent toxicity studies, 2) cross-species extrapolation of toxicity (considering both TD and TK data) or 3) developing physiologically-based toxicokinetic (PBK) models[78,207–210].

To date, ADME/TK studies have been less frequently applied in non-pharmaceutical contexts and, as mentioned in section 1.4, this area remains relatively unexplored in regulatory toxicology[3] mainly due to associated time and cost constraints. Rather promisingly, the value of this approach is being increasingly recognised by regulators (e.g. in a MoA analysis or cross-species extrapolation), as reflected in existing and more recent OECD guidelines[79,80,83]. In the context of grouping and read-across, ADME/TK similarity can be used when information on metabolism and metabolic fate is available for a class of compounds that also share common biotransformation products (BTPs)[5,107].

While the AOP framework does not take into account ADME/TK processes, the separation of TD and xenobiotic metabolism appears arbitrary from the systems toxicology point of view as both are key in understanding chemical mechanisms of action[211]. The importance of incorporating ADME/TK dimension within chemical risk assessment was also recently highlighted by the European Foods Standards Agency (EFSA)[5] in the proposed extension of the AOP framework[23], whereby the combined knowledge of both toxicodynamics (TD) and toxicokinetics (TK) is central to understanding a chemical MoA (Figure 1.4). Despite demonstrating its merit in characterising TD (biological effects), fewer applications of 'alternative' mechanistic toxicology approaches (or NAMs) to study ADME/TK exist to date[103].

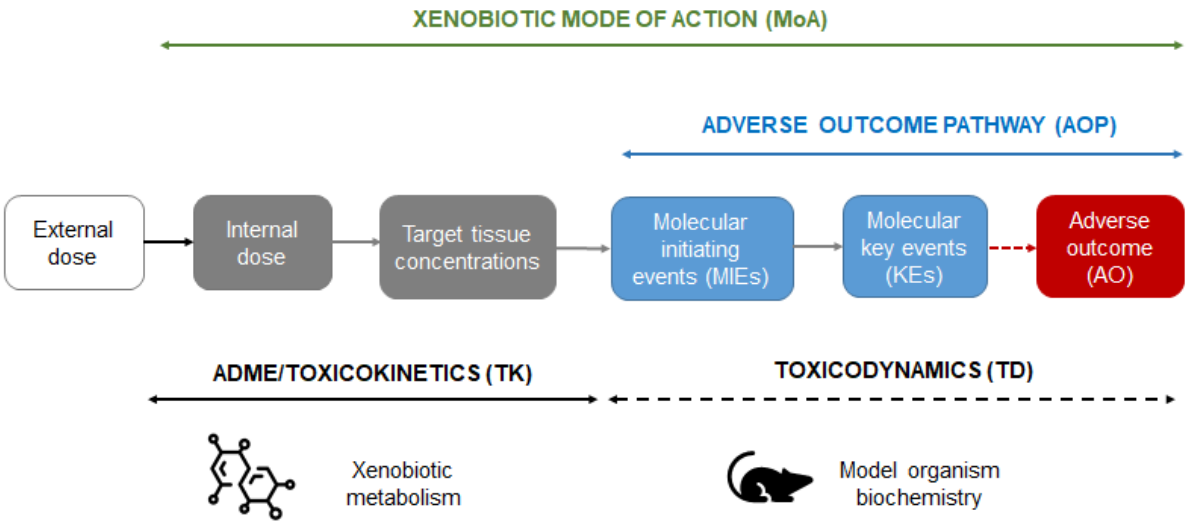


**Figure 1.4** Value of ADME/TK information in the context of mode of action (MoA) and adverse outcome (AOP) frameworks (adapted from EFSA, 2021[5]). MoA considers both toxicodynamics and xenobiotic metabolism and, as such, is better placed to predict risks associated with chemical exposure (Leist *et al*., 2017[211]).

Experimental ADME/TK data required for chemical risk assessment is not available for the majority of chemicals currently in production and use[81]. This lack of data is regarded as a vast impediment to the applications of predictive toxicology e.g. in grouping and read-across[103,212]. While ADME/TK is considered a significant part in assessing uncertainty of a read-across case, "*metabolism is often seen as the most contentious of the toxicokinetic similarity justification"*[75] which emphasizes the importance of obtaining robust TK/ADME information on xenobiotics to facilitate future regulatory acceptance.

Untargeted metabolomics has a powerful potential to address this knowledge gap by obtaining both toxicodynamics (biochemical effects) and toxicokinetics (xenobiotics metabolism) information, all within a single toxicometabolomics assay. For instance, two studies by Southam *et al*.[66,77] previously demonstrated the value of untargeted DIMS metabolomics in detecting both endogenous toxicity responses and xenobiotic-related features (also termed xenometabolome or exogenous metabolome) in common roach (*Rutilus rutilus*) following chemical exposures to fenitrothion, triclosan, chloroxylenol and chlorophene. More recently, ADME/TK information was successfully extracted from untargeted metabolomics UHPLC-MS/MS datasets using a novel computational xenobiotic processing workflow. This provided insights into the metabolism and metabolic fate of two model cardiotoxins (sunitinib and KU60648) in rat (plasma and cardiac tissue) resulting in the discovery of 9 novel previously unreported BTPs for sunitib[6]. Another study applied the same workflow to reveal 11 metabolites of triphenyl in rat liver (Sostare *et al.*, 2022: *manuscript in preparation*). Of note, both studies used $MS^n$ fragmentation data to increase confidence in annotation and identification of xenobiotic-related features (to MSI Levels 1-3) in untargeted

toxicometabolomics datasets, highlighting the capability of this approach in revealing novel insights into xenobiotic metabolism under study.

This thesis explores this under-researched potential of untargeted metabolomics experiments (nESI-DIMS and UHPLC-MS/MS, respectively) to simultaneously measure the metabolism and biochemical effects of xenobiotics in a biological test system within a single toxicity assay.

## 1.11 Aims and objectives of the thesis

Untargeted metabolomics is a powerful 'alternative' approach to chemical safety testing that ought to significantly advance the field of mechanistic toxicology and contribute to more robust 21st century risk assessment of many untested chemicals. However, as introduced in previous sections, one impediment to accelerating the implementation and regulatory acceptance of metabolomics data for modernising regulatory toxicology is the relative lack of transparent, regulatory-relevant studies demonstrating the value of this approach. This thesis addresses this impediment by overcoming technical and methodological challenges of an untargeted metabolomics workflow for chemical risk assessment that simultaneously integrates both toxicodynamics (i.e. biological effects induced by xenobiotics) with toxicokinetics by the untargeted ADME/TK (i.e. chemical effects, xenobiotic metabolism) characterisation of xenobiotics (presented in chapter 4 and chapter 5 of this thesis). The work of exploring metabolomics to achieve greater certainty in the grouping (or category formation) of chemicals (investigated in chapter 3 of the thesis) based on their modes of action is important for the realisation of a vision and strategy proposed around elucidating pathways to toxicity.

The overarching aim of this thesis was to develop and implement untargeted metabolomics approaches suited for hazard assessment of chemicals in regulatory toxicology, exploring both toxicodynamics and toxicokinetics.

Three principal objectives (corresponding to three research chapters) were defined in order to address the above aim:

1. Demonstrate the value of metabolomics measurements (collected as part of a multi-omics workflow) to improve confidence in grouping of data-poor chemicals for subsequent read-across prediction of toxicity. Chapter 3 describes a proof-of-principle case study conducted with seven structurally similar azo dyes in an invertebrate model, *Daphnia magna*. This research project seeks to implement multi-omics (specifically, untargeted nESI-DIMS metabolomics and targeted Temp-O-Seq transcriptomics) to a regulatory-relevant scenario to evaluate the potential of this approach for biology-based grouping. Transcriptomics is not the primary focus of this thesis, however.

2. Assess the capacity of untargeted $MS^1$ nESI-DIMS metabolomics measurements to simultaneously provide information on toxicokinetics (xenobiotic metabolism) as well as toxicodynamics (*D. magna* biochemistry, already studied in chapter 3) processes. This investigation focuses on implementing a novel untargeted xenobiotic processing workflow to the same untargeted nESI-DIMS datasets (from chapter 3) to seek evidence of internal xenobiotic exposure (i.e. detection of the azo dye parent chemicals) and reveal insights into the azo dye metabolism via the attempted discovery of metabolic biotransformation products (BTPs) within the exposed *D. magna*. This ADME/TK work is detailed in chapter 4 along with the series of criteria developed to improve confidence in the quality of annotations of azo dye-related xenobiotic features.

3. Evaluate the capacity of untargeted UHPLC-MS/MS-based metabolomics for more in-depth ADME/TK characterisation of xenobiotics, with added confidence from experimental $MS^n$ fragmentation data. Specifically, chapter 4 builds upon the discoveries made in chapter 3 by incorporating relatively new state-of-the art analytical and computational technology (i.e. Thermo Fisher Scientific Orbitrap ID-X tribrid mass spectrometer and Compound Discoverer software) to detect and identify parent chemicals and any metabolic biotransformation products of five structurally-different xenobiotics (industrial chemicals) in existing rat plasma samples provided by the US National Toxicology Program (NTP).

The incorporation of untargeted metabolomics approaches in chemical risk assessment, providing both TD and ADME/TK knowledge on xenobiotics is expected to offer a deeper understanding of chemical toxicity.

# CHAPTER 2 – METHODS AND MATERIALS

## 2.1. Selection of exposure chemicals

Azo dyes (described in more detail in section 3.2) are diverse, ubiquitous yet data-poor industrial chemicals that pose many environmental issues due their toxicity and persistence in the environment[213]. Therefore, they were of particular interest to the project funders, the European Chemicals Agency (ECHA). A series of specific criteria were developed to guide the selection of specific exposure chemicals for the multi-omics grouping study, considering both regulatory (ECHA) and practical experimental perspectives (Table 1.1). ECHA prioritised azo dyes registered under REACH (Registration, Evaluation, authorization and Restriction of Chemicals) i.e. manufactured or imported at more than one tonne per year. However, commercial availability (at highest available purity) was the deciding factor in the final chemical selection. Seven structurally-related dyes (i.e. two sudan dyes and five disperse dyes) were selected for the study described in chapter 3.

Sudan red G (SRG), sudan 1 (S1), disperse orange 61 (DO61), disperse red 1 (DR1), disperse red 13 (DR13) and disperse yellow 3 (DY3), were purchased from LGC Standards (UK), and disperse orange 25 (DO25) was purchased from Sigma-Aldrich (UK). All chemicals (certified reference materials) had purity between 95% (DO25 only) and 99.2% (confirmed by the manufacturer's certificate of analysis) to ensure that toxicity was induced by the azo dye, and not by other additives or impurities in the material. Identifiers are provided in Table 2.1, the structures are shown in Figure 2.1 for the seven azo dyes selected for the study.

**Table 2.1** Summary of the criteria guiding the selection of azo dyes for the grouping study.

| **Regulatory (ECHA) considerations** | **Experimental considerations** |
|---|---|
| 1. Structure: a specific core and different functional groups (no homologous series)<br><br>2. Log $K_{ow}$ (n-octanol/water partition coefficient): approx. 4-7 (some water solubility)<br><br>3. *Daphnia* acute toxicity data (OECD Test Guideline 202): available or predicted<br><br>4. *Daphnia* chronic toxicity data (OECD Test Guideline 211): available<br><br>5. Include REACH registered substances | 1. Available to purchase<br><br>2. Available at high purity (95%-99.2%, depending on azo dye)<br><br>3. At least partial water solubility with low volatility<br><br>*4.* Known, reported in literature toxicity to *Daphnia* |

**Table 2.2** Azo dye identifiers: Chemical Abstracts Services (CAS) registry number, European Community (EC) number, and Simplified Molecular-Input Line-Entry System (SMILES) notation; and commercial suppliers with purity.

| Azo dye | Abbr. | CAS-RN | EC | SMILES | Supplier (Batch no.) | Purity |
|---|---|---|---|---|---|---|
| Sudan 1 | S1 | 842-07-9 | 212-668-2 | Oc(ccc(c1ccc2)c2)c1N=Nc(cccc3)c3 | LGC Standards (G170606) | 99.6% |
| Sudan red G | SRG | 1229-55-6 | 214-968-9 | O(c(c(N=Nc(c(c(ccc1)cc2)c1)c2O)ccc3)c3)C | LGC Standards (G165933) | 97.1% |
| Disperse orange 25 | DO25 | 31482-56-1 | 250-654-8 | N(=O)(=O)c(ccc(N=Nc(ccc(N(CCC(#N))CC)c1)c1)c2)c2 | Sigma-Aldrich (12106HB) | 95% |
| Disperse orange 1 | DO61 | 55281-26-0 | 259-563-8 | N(=O)(=O)c(cc(c(N=Nc(ccc(N(CCC(#N))CC)c1)c1)c2Br)Br)c2 | LGC Standards (G167394) | 98.7% |

| Azo dye | Abbr. | CAS-RN | EC | SMILES | Supplier (Batch no.) | Purity |
|---|---|---|---|---|---|---|
| Disperse red 1 | DR1 | 2872-52-8 | 220-704-3 | O=N(=O)c(ccc(N=Nc(ccc(N(CCO)CC)c1)c1)c2)c2 | LGC Standards (G132128) | 98.3% |
| Disperse red 13 | DR13 | 3180-81-2 | 221-688-1 | O=N(=O)c(ccc(N=Nc(ccc(N(CCO)CC)c1)c1)c2Cl)c2 | LGC Standards (737819) | 99.2% |
| Disperse yellow 3 | DY3 | 2832-40-8 | 220-600-8 | O=C(Nc(ccc(N=Nc(c(O)ccc1C)c1)c2)c2)C | LGC Standards (G122504) | 98.8% |

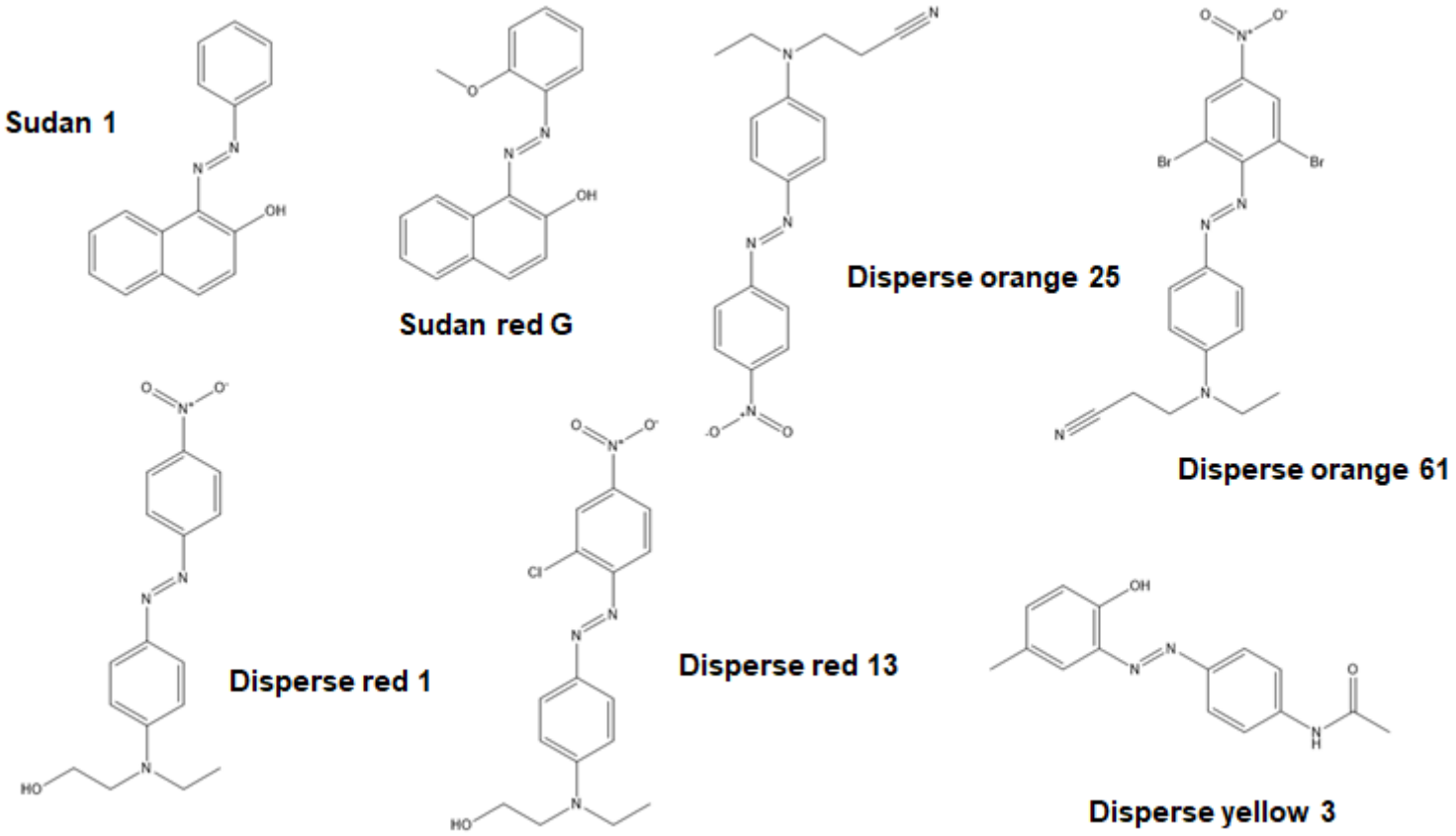


**Figure 2.1** Azo dye chemical structures: Sudan 1 (S1), Sudan red G (SRG), Disperse orange 25 (DO25), Disperse orange 61 (DO61), Disperse red 1 (DR1), Disperse Red 13 (DR13) and Disperse Yellow 3 (DY3).

## 2. 2 *Daphnia magna* acute (48 h) exposure studies

### 2.2.1 Culturing of *Daphnia magna*

Cultures of *D. magna* were maintained as previously reported[57,58]. Briefly, all *D. magna* were maintained at a density of 20 Daphnia per 1 L in water drawn from a borehole at the University of Birmingham. Semi-static culturing conditions at a constant temperature of 20 °C with a fixed photoperiod of 16h light:8h dark were consistently applied. Culturing medium was renewed three times weekly and all stocks were fed daily with increasing volumes of green freshwater algal suspension of *Chlorella vulgaris* depending on age of daphnids (days 1-2: 1mL of algae per 20 Daphnia, days 3-7: 1.5 mL, days 8 onwards: 2 mL), corresponding to 0.08 mgC per *Daphnia*. Individuals (young daphniids, i.e. <24-h old neonates) used for exposures were obtained from cultures after daily filtration (using the third brood or later), in accordance with standardised toxicity tests developed by the OECD[91].

The overall workflow for the acute *D. magna* toxicity studies is presented in Figure 2.2. The workflow comprised 1) acute dose range-finding studies, 2) benchmark dose (BMD) modelling and final dose selection for multi-omics exposures 3) further acute exposures to generate samples for multi-omics measurements. All acute (48 h) exposures were conducted as per OECD Test Guideline 202 (*Daphnia sp. Acute Immobilisation Test*)[91]using dimethyl sulfoxide (DMSO; Fisher Chemical, UK; >99% purity) as a carrier solvent (at a final concentration of 0.1%) to aid azo dye solubility, in line with recent toxicity studies[214].

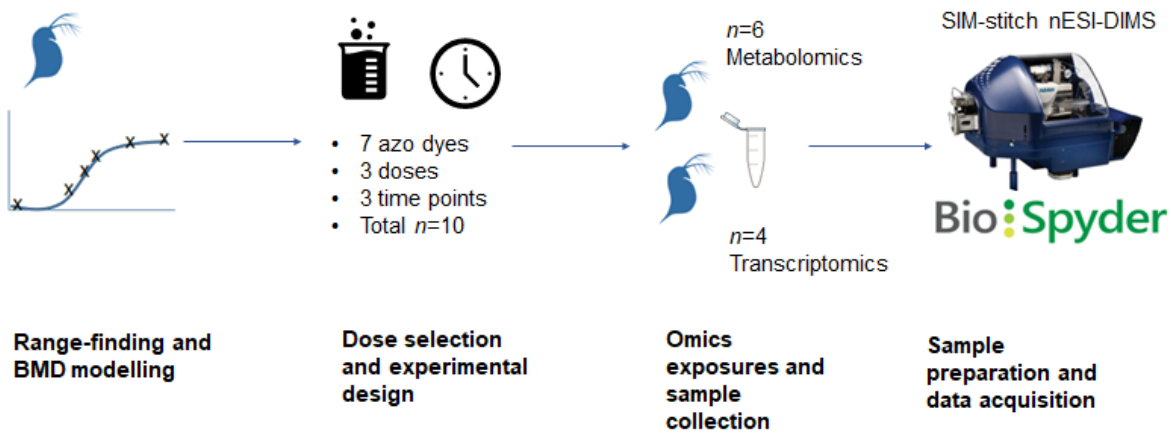


**Figure 2.2** Overall workflow for the acute *Daphnia magna* toxicity studies to generate samples for the multi-omics measurements. First, range-finding studies and benchmark dose (BMD) modelling were conducted to guide dose selection and overall experimental design for the omics studies. This was followed by omics exposures and sample collection. Polar metabolites and lipids were extracted and subsequently analysed using nESI-DIMS, RNA extracts were sent for analyses to BioSpyder (US).

### 2.2.2 Range-finding studies and benchmark dose (BMD) modelling

First, published aquatic toxicity data (Table 3.1 in chapter 3) was consulted prior to conducting the initial crude dose-range finding studies (data not shown). Next, seven extensive dose range-finding studies were conducted to establish azo dye toxicity and guide the dose selection for the acute multi-omics study. Five *D. magna* neonates (<24-h old neonates, 3rd brood or later) in 200 mL borehole water were exposed for 48 h to a range of nominal concentrations (≥5) of each azo dye tested (*n*=3 exposure vessels per concentration). DMSO concentration was maintained at 0.1% across all chemical treatments and untreated controls. Daphniids were not fed for the duration of the 48 h exposures and observations of any immobilisation were recorded after 24 h and 48 h. The test conditions for the acute dose selection studies are summarised in

Table 2.3, highlighting the challenge of low solubilities of some of the azo dyes in aqueous (0.1% DMSO) solution.

**Table 2.3** Summary of test conditions and experimental observations from the acute range-finding studies.

| Azo dye | Nominal exposure concentrations (mg $L^{-1}$) | Experimental observations (dye) |
|---|---|---|
| **S1** | 0.025,0.05, 0.1, 0.25, 0.5, 1.0 | Dye particles visible in solutions at 0.25 mg $L^{-1}$and above |
| **SRG** | 0.5, 1.0, 2.5, 5.0, 10.0 | Dye particles visible in solutions at 0.5 mg $L^{-1}$and above |
| **DO25** | 0.26, 0.52, 1.04, 2.08, 4.15, 8.3 | Dye particles visible in solutions at 2 mg $L^{-1}$and above |
| **DO61** | 0.0005, 0.001, 0.005, 0.01, 0.025, 0.05, 0.1, 0.25, 0.5 | No precipitation at any test concentration |
| **DR1** | 0.025, 0.05, 0.1, 0.25, 0.5, 1.0 | No precipitation at any test concentration |
| **DR13** | 0.01, 0.025, 0.05, 0.1, 0.25, 0.5 | No precipitation at any test concentration |
| **DY3** | 0.025, 0.05, 0.1, 0.25, 0.5, 1.0 | No precipitation at any test concentration |

Benchmark dose (BMD) modelling was subsequently conducted on the *Daphnia* immobilisation data from the seven acute dose-selection studies, using the PROCAST webtool (https://proastweb.rivm.nl/, version 66.39). Data were analysed as quantal at a benchmark response (BMR) of 0.1 (that induces approximately 10% Daphnia immobilisation). The best-fit models were selected using the lowest Akaike Information Criterion (AIC = 2). Two-sided 90% confidence intervals to the BMD value were generated per model: the lower estimate of BMD (BMDL) and upper estimate of BMD

(BMDU). Model-averaging (*n*=200 bootstrap runs) was applied to derive the estimated BMDL and BMDU values for each dye.

### 2.2.3. Experimental design and dose selection strategy for acute multi-omics study

The multi-omics experimental design included three sampling time points (2 h, 24 h and 48 h) and three dose groups (and untreated controls containing 0.1% DMSO only). Exposures were conducted in six batches, with each dye having a matched control group (Table 3.7, chapter 3).

The strategy for dose selection was based on the concept of 'phenotypic anchoring'[215,216], whereby the highest dose for each azo dye induced an equivalent adverse outcome i.e. approximately 10% immobilisation of the exposed *Daphnia.* The underlying driver for this approach was to provide confidence that metabolic responses and gene expression changes would be detectable in *Daphnia*. The selected dose range represented approximately one order of magnitude change, where a medium dose was set at one-third of the highest dose, and a low dose was equal to one-third of the medium dose for each dye.

Benchmark dose modelling (BMD) results of the *Daphnia* immobilisation data from the seven acute range-finding studies are summarised in Table 2.4. The estimated BMDL and BMDU values were derived for the six dyes except for DO25 that did not induce any immobilisation at any of the investigated test concentrations.

**Table 2.4** Outputs of the benchmark dose (BMD) modelling of the *Daphnia* immobilisation data following the seven azo dye exposures to test concentrations summarised in Table **2.3**. These results were used to select exposure doses for the omics exposure study. Lower and upper estimates of BMD (BMDL and BMDU, respectively) were calculated using PROAST.

| Azo dye | BMDL (mg $L^{-1}$) | BMDU (mg $L^{-1}$) | Mean of BMDL & BMDU (mg $L^{-1}$) |
|---|---|---|---|
| S1 | 0.069 | 0.087 | 0.078 |
| SRG | 1.5 | 5.2 | 3.35 |
| DO25 | - | - | - |
| DO61* | 0.0018 | 0.0066 | 0.0042 |
| DR1* | 0.048 | 0.15 | 0.099 |
| DR13 | 0.013 | 0.024 | 0.018 |
| DY3 | 0.86 | 0.97 | 0.91 |

*Highest dose removed from BMD modelling.

Based on the steepness of the experimentally measured dose-response curves for these dyes, the dose range selected was approximately one order of magnitude for each dye to ensure the optimal coverage of the concentration range to capture molecular effects at each of the sampling time points. The highest dose (inducing approx. 10% immobilisation of *Daphnia*) was set to the mean of the BMDL and BMDU values for the six azo dyes (Table 2.4). A medium dose was set to one-third of the highest dose, and a low dose was equal to one-third of the medium dose.

The selected high doses for all seven dyes spanned almost three orders of magnitude, with DO61 causing ca. 10% *Daphnia* immobilisation at 0.004 mg $L^{-1}$ and SRG inducing the same adverse outcome at 3.35 mg $L^{-1}$. BMD modelling was not possible for DO25 as it did not induce any *Daphnia* immobilisation at any of the concentrations tested, even at levels far exceeding water solubility. Therefore, the highest dose for DO25 was

set to 3 mg L-1 to approximately reflect the highest dose used across the other six azo dyes.

### 2.2.4 Omics exposure study and sample collection

The acute (48 h) exposures and subsequent preparation of the biological samples for the multi-omics study were conducted using experimental batches. This design was chosen so that new data generated in the future, for additional chemicals, could in principle be added to the data from the azo dye study. Specifically, *Daphnia* were exposed to each azo dye alongside a set of dedicated dye-specific *Daphnia* control samples, forming one experimental batch. Each experimental batch of samples was extracted at the same time (with randomisation of the order of sample extractions within each batch), and subsequently each experimental batch was measured using an omics technology at the same time (again, with re-randomisation of the order of omics analyses within each batch to reduce any batch effects). This design was used as the scale of the study was so large it was impossible to conduct all exposures on a single day, nor to extract all samples on a single day, nor to measure all samples on a single day. The one exception to this design was the use of a shared set of control samples for azo dyes SRG and DR1 (as SRG, DR1 and one set of control samples were collected on one day, extracted on another, and analysed together on another day).

Nominal exposure concentrations selected for acute (48 h) exposures to generate samples for the omics measurements (i.e. polar metabolomics, lipidomics and transcriptomics) and the final experimental batch design are summarised in Table 3.7.

Seven acute (48 h) toxicity studies were conducted in accordance with OECD Test Guideline 202 (OECD, 2004) to generate samples for multi-omics measurements (i.e. polar metabolomics, lipidomics and transcriptomics). All acute exposures were conducted using the same conditions as for the dose range-finding and dose selection studies described earlier in section 2.2.2. Acute tests were conducted in a static system with no feeding at three exposure concentrations (see Table 3.7, chapter 3) and unexposed controls (containing 0.1 % DMSO only), with sampling at three time points (2 h, 24 h and 48 h). Each dose/time group had 6 replicates (*n*=6 separate exposure vessel) with *Daphnia* exposed in 200mL borehole water. Exposures were initiated with <24-h old *Daphnia* neonates (10-12 animals per 200mL replicate exposure vessel) to obtain sufficient biomass and number of experimental replicates for the omics measurements. At each time point, the 10-12 neonates per vessel were sampled and divided into two replicates, one used for metabolomics analysis (5-6 animals per biological replicate, *n*=6 replicates per treatment) and the other for transcriptomics analysis (5-6 animals per biological replicate, *n*=4 replicates per treatment).

Following exposures, daphnids were harvested at the three different time points for each azo dye and quickly transferred into 2 mL Precellys tubes (CK14; Stretton Scientific Ltd., UK) with a fine-tipped pipette and immediately flash-frozen in liquid nitrogen to quench metabolism and prevent RNA degradation. Collection of all samples was randomised within each exposure batch. Resulting samples were stored at –80°C prior to metabolite and lipid, and RNA extractions. Additional untreated *Daphnia* neonates were collected at different life stages (2 h, 24 h and 48 h) from the same stock cultures for intra-study quality control (QC) samples. Two 48 h dose groups were

discarded for S1 (high and medium doses) and one for DO61 (high dose) due to high *Daphnia* immobilisation during the acute exposures.

## 2.3. Polar metabolomics and lipidomics: sample extraction and nESI-DIMS data acquisition

The MEtabolomics standaRds Initiative in Toxicology (MERIT) best practice guidelines[3] were followed in all steps of the omics workflow, including use of a system suitability QC (ssQC), intra-study QC and process (extraction) blank QC samples. Prior to omics analyses, a nESI-DIMS biomass optimisation study was conducted to determine an optimal number of *Daphnia* neonates per sample for subsequent polar metabolomics and lipidomics measurements (see section 3.3 in chapter 3).

Analytical grade reagents (>98% purity) and LCMS grade solvents (Honeywell, Merck, UK) were used in all experiments. Solvents were precooled on wet ice. Extraction (process) blanks were prepared with each sample batch to identify and eliminate any possible sources of contamination that arise from sample processing. Due to the scale of the study, samples were batched and randomised within and across batches for extractions and nESI-DIMS analyses to prevent batch effects.

Metabolites were extracted manually from *Daphnia* neonates using well-established bead-based homogenisation followed by the modified two-step biphasic Blight and Dyer (1959) method (chloroform:methanol:water, the final ratio: 2:2:1.8), as previously reported[8,57,58,217]. Briefly, frozen *Daphnia* samples (assumed biological sample mass ≤ 10 mg) were homogenised in pre-cooled methanol (32 µL of methanol for each mg of frozen biological sample mass; 32 µL/mg) and water (10.6 µL/mg), using the Precellys-24 homogeniser (Bertin, France; homogenisation at 2 x 10 s bursts at 6400

rpm with a 5 s gap between the cycles). The homogenates were then removed from the Precellys tubes and transferred to clear 1.8 mL glass vials for extraction. Pre-cooled chloroform (16 µL/mg) was added to each vial, followed by brief vortex-mixing for 30 s and incubating on ice for 10 mins. Following this, an additional aliquot of ice-cold chloroform (16 µL/mg) and water (18.2 µL/mg) were added to the solution, vortex-mixed (30 s) and left on wet ice for 10 min to induce phase separation. The vials were then incubated at room temperature for 5 mins to allow the biphasic separation to begin to partition. After centrifugation (4000 rpm, 10 mins at 18°C) to remove precipitated proteins, both polar metabolomics (2 x 200 µL into 1.5 mL Eppendorf tubes) and lipidomics (2 x 100 µL into 1.8 mL glass vials) fractions were removed using a 250 µL Hamilton syringe and transferred to 2 mL Eppendorf tubes (polar metabolomics extracts) or 1.8 mL glass vials (lipidomics extracts). Polar metabolomics aliquots were dried down overnight in a SPD11V SpeedVac concentrator (Thermo Fisher Scientific). Lipidomics aliquots were dried under a gentle stream of nitrogen for ca. 10 min. All extracts were stored at -80°C prior to analytical measurements.

Dried *Daphnia* extracts were reconstituted in 25 µL of 4:1 methanol:water (v/v, Honeywell, Merck) containing a total of 0.1% formic acid (v/v, Merck) for polar metabolomics analyses and 40 µL of 2:1 7.5 mM methanolic ammonium acetate:chloroform (v/v, Merck) for lipidomics analyses. Both types of extracts were centrifuged to remove any suspended particulates and debris prior to being plated onto a 384-well Eppendorf plate (15 µL for polar metabolomics and 24 µL for lipdomics extracts). Due to the high number of samples, resuspended extracts were distributed across three 384-well plates with samples from up to two exposure batches per plate.

Pooled intra-study QC samples (prepared from untreated *Daphnia* collected from the same cultures at different life stages to mirror the biomass of samples generated for the multi-omics study) were distributed every 7$^{th}$ experimental sample. All biological and intra-study QC samples were placed in a random order across the 384-well plate to reduce potential bias resulting from analysis order.

All *Daphnia* extracts were analysed using the well-established spectral-stitching nanoelectrospray (nESI) direct infusion mass spectrometry (DIMS) method[8] with slight modifications for low biomass samples (i.e. 'internal scan replication' method) to yield higher sensitivity. This optimised selected-ion-monitoring (SIM)-stitching method acquires MS data as a series of overlapping mass-to-charge (*m/z* ratio) windows that are subsequently stitched together to obtain a complete spectrum. In comparison with the traditional wide range scan method, this mass spectral stitching approach shows higher detection sensitivity and metabolome coverage[8,150]. The analyses were conducted on a Thermo Scientific Orbitrap Elite Hybrid Ion Trap-Orbitrap mass spectrometer coupled with an automated chip-based nESI sample ionisation platform (Advion Triversa NanoMate), controlled by ChipSoft software (Advion, v8.1.0), as previously described[8]. The data were acquired by Xalibur software (Thermo Scientific, v2.0) in two ion modes: positive (to profile polar metabolites and lipids) and negative (to measure polar metabolites).

All analytical procedures adhered to the MEtabolomics standaRds Initiative in Toxicology (MERIT) best practice guidelines[3]. Therefore, data were collected for three types of QC samples: 1) system suitability QC samples (analysed in triplicates at the beginning and end of each analytical sequence) to ensure that the mass spectrometer was operating within specification prior to data acquisition of the experimental samples;

an intra-study QC sample to measure the analytical reproducibility and allow to assess and correct for any intra- and inter-batch variation[8,150]; and a process (extraction) blank QC samples to measure the background signals (approx. 6-8 per analytical batch).

## 2.4. Polar metabolomics and lipidomics data processing and metabolite annotation

For each metabolomics data set corresponding to the seven azo dyes studied (i.e. 3 assays per each dye), nESI-DIMS mass-spectra were subsequently processed using DIMSPy package implemented in Galaxy (https://github.com/computational-metabolomics/dimspy-galaxy). This included the application of three stages of feature (or peak) picking and noise filtering, as previously reported[8,150] with slight modifications. First, features in the process blanks were excluded from the data matrix unless they were >10-fold more intense in the biological samples. This 'blank-filtered' feature intensity matrix was later used as the input data for the untargeted ADME/TK workflow (described in chapter 4 of this thesis).

Secondly, the sample filter was set to retain features present in >80% of all biological samples, which removed any azo dye related (exogenous) features from this endogenous feature matrix. Thirdly, samples with >50% missing values were excluded from further analysis to ensure only the highest quality of m/z features are retained for the final statistical analyses (see section 2.5).

This filtered feature intensity matrix was probabilistic quotient normalised (PQN) on a dye-by-dye basis, due to variation in feature counts across dyes. Missing values were imputed using the k-nearest neighbour approach ($k$=5), producing a data matrix for univariate statistical analysis. This matrix was generalised log (glog) transformed prior

to any multivariate analyses. The described data processing workflow resulted in seven endogenous data matrices (one per dye), per nESI-DIMS assay.

The *m/z* features were putatively annotated using the the Python package, BEAMSPy (Birmingham mEtabolite Annotation for Mass Spectrometry Python package, v0.1.0; https://more.bham.ac.uk/beams/) pipeline operated in Galaxy. The mass error was set to ±5 ppm. This threshold was determined by examining the system suitability QC data. Subsequently, following inspection of mass error distributions, the error tolerance was reduced to 2 ppm for lipids (+0.5 to -1.5 ppm) polar metabolites (+1.0 to -1.0 ppm)

The list of adducts and isotopes selected to annotate peak patterns was set to default. The databases used for the annotation were ChEBI (Chemical Entities of Biological Interest), HMDB (Human Metabolome Database), KEGG (Kyoto Encyclopaedia of Genes and Genomes) for *Daphnia pulex* and Lipid Maps.

All RNA sample extractions and subsequent data processing of BioSpyder TempO-Seq gene expression data (BioSpyder, US) were conducted by Dr Rosemary Barnett, using the DESeq2 package in the R programming language (version 1.30.0)[218]. However, transcriptomics workflow is not within the scope of this thesis and therefore it is not described in detail.

## 2.5. Statistical analyses to group azo dyes using single and multi-omics data

The overall workflow for statistical analyses and grouping of the multi-omics data is shown in Figure 2.3. The three data streams (nESI-DIMS polar metabolomics and lipidomics, and the BioSpyder transcriptomics) were processed using technique-specific standard methods, as described in section 2.4. This step was followed by

statistical analyses of all three datasets. All statistical analyses were conducted in the R environment (version R-4.0.3), using the structToolbox (version 1.3.1) and *pvclust* packages (version 2.2-0)[219]. First, principal component analysis (PCA) was applied to identify any outlying samples in each omics dataset, for each dye. Samples lying outside a 95% confidence interval (CI) limit were excluded from further analyses.

Next, independent two-sample t-tests (adjusted for a false discovery rate; $q < 0.05$) were applied across all molecular features (i.e. polar metabolomics and lipidomics *m/z* features, and genes), comparing dye-specific untreated controls with each of nine treated dose/time groups (per dye), to give an indication of the extent of the molecular perturbations induced by each azo dye in the exposed *Daphnia*. These analyses were performed on treated and control samples for each dye separately, considering each dose/time combination as a separate sample type.

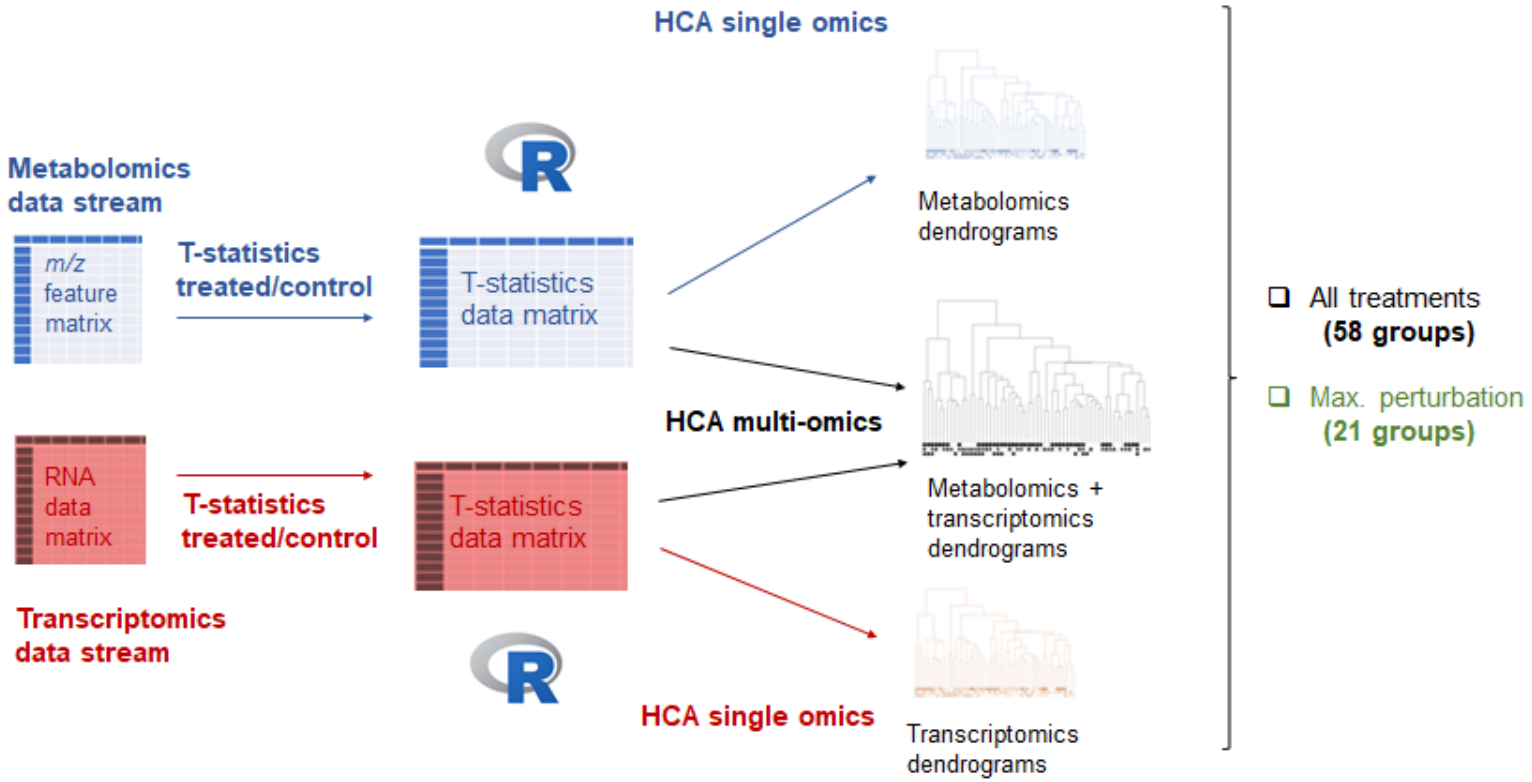


**Figure 2.3** Overall workflow for the analysis and grouping of the multi-omics data. Each data stream was analysed separately as described in section 2.4. T-statistics formed the input data for hierarchical clustering analyses (HCA) using single versus multi-omics approaches for 'all treatments' (58 groups) and 'max. approach' (21 groups). The resulting dendrograms were examined visually to derive grouping patterns for the seven azo dyes based on molecular responses in the *Daphnia*.

In addition, the t-statistics derived from these independent two-sample t-tests served as the basis for one-mode clustering (i.e. either experiment or metabolite clusters are created[220]), utilising unsupervised hierarchical cluster analyses (HCA). Cluster (or clustering) analyses were employed to group sample dose/time treatment groups (based on their similarities or dissimilarities) and create visual representations of the ecotoxicological similarities between treatments. HCA and PCA are two common cluster analysis methods that can be applied to mine multi-dimensional metabolomics data to identify patterns among biological samples[221]. Here, HCA was performed on the vector normalised t-statistics (*n*=10,000 bootstrap replications), utilising Euclidean distance and Ward's linkage method ("ward.D2" method in R, implementing Ward2 algorithm)[222]. HCA was applied to three combinations of input data, considering both single omics and multi-omics approaches: 1) t-statistics derived from combined most 'downstream' polar metabolomics and lipidomics responses only; 2) a fusion of the t-statistics from all three omics data streams; and 3) t-statistics derived from transcriptomics responses only.

In addition, for each of these above-described combinations of input data, two further approaches were applied. First, HCA of all (typically 9) dose/time groups per dye, for all 7 dyes (i.e. considering all possible 58 groups in the dataset, referred to as the 'all treatments' approach). Secondly, HCA of 3 dose groups per dye, for all 7 dyes (i.e. considering 21 dose/time groups). This reduced the three time points to a single point by selecting only the largest metabolic and lipid, and the largest transcriptional perturbations (by using the highest absolute t-statistic across the three time points), referred to as the 'maximum perturbation' approach.

Taken together, this combination of HCA analyses enabled a comparison of single versus multi-omics based grouping, providing an overview of the effects of dose and time per dye. The first 58-group ‘all treatments’ approach yielded a relatively complex dendrogram. A more interpretable clustering pattern of the seven dyes at three doses (low, medium and high) was derived using the ‘maximum perturbation’ 21-group HCA analyses.

# CHAPTER 3 – ENHANCING GROUPING OF AZO DYES WITH OMICS-BASED EVIDENCE FROM *DAPHNIA MAGNA* TOXICITY STUDIES. A PROOF-OF-PRINCIPLE STUDY

## 3.1 Introduction

The concept of grouping and read-across (G/RAx) under ECHA's Read-across Assessment Framework (ECHA, 2017) was introduced in section 1.6 (chapter 1). It is frequently used in regulatory toxicology (up to 75% of ECHA chemical registration dossiers)[105,106] to predict toxicity of data-poor chemicals and reduce unnecessary animal testing[105,106]. The first step is to group (or form categories) of chemicals and then 'read-across' a specific toxicity endpoint (e.g. no observed effect concentration, NOEC) from a 'source' to (single or multiple) 'target(s), thereby reducing the need to perform additional *in vivo* toxicity studies for each individual group member (Figure 1.1). Formation of categories is based on chemical similarity (e.g. common functional groups and shared biotransformation products) and physico-chemical properties, and does not consider toxicity mechanisms. Consequently, many G/RAx cases are rejected by ECHA and, to date, only a relatively small number of scientifically rigorous cases contributed to minimising animal testing in repeated dose toxicity studies commonly conducted in chemical risk assessment[103]. Thus, it is widely recognised that current G/RAx practices are not fit for purpose and the quality of this approach needs to improve by incorporating robust experimental data to accurately predict toxicity of the ever-increasing numbers of chemicals on the market[103,107,223]. Several studies to date revealed the potential of untargeted metabolomics to strengthen read-across cases for

a range of chemicals (e.g. for phenoxy herbicides, amino alcohols and complex petrochemical mixtures), particularly in the context of BASF's MetaMap® Tox database[111–114], thereby reducing the inherent weakness of conventional structure-based grouping. Another study demonstrated the capability of metabolic profiling to differentiate between toxicological MoAs between diethylhexylphthalate (DEHP) and Hexamoll® DINCH and, therefore, disproved the original hypothesis by Campioli *et al*. (2015) suggesting similar lipid accumulation perturbations *in vivo* for both plasticisers[224]. However, despite these read-across improvements, further case studies are required to demonstrate the proof of principle of this approach (ideally, combined with another omics tool), and supported by relevant, robust experimental evidence to increase confidence that group members share the same or a similar mode of action (MoA)[103].

In light of the above considerations, the investigations presented in this chapter conducted with the project funders, the European Chemicals Agency (ECHA), sought to demonstrate concepts of biology-based grouping using high-throughput omics technologies. The overarching aim of the work was to evaluate the capabilities of high-throughput multi-omics (specifically, polar metabolomics, lipidomics and transcriptomics) for chemical grouping and subsequent read-across of seven azo dyes in a single OECD test species, *Daphnia magna*.

In order to appropriately address this aim, a number of critical objectives were formulated, as listed below:

1) Determine the optimal biomass of *D. magna* extracts for high-throughput nESI-DIMS (SIM-stitch 'internal scan replication' method) analyses to ensure high

technical reproducibility of the results, while minimising metabolic variability across biological samples.

2) Develop and implement a grouping workflow (analytical and computational) which allows omics-derived molecular mechanistic data (i.e. metabolic, lipid and transcriptional responses in *Daphnia magna*) to be considered alongside conventional (i.e. structural and physico-chemical) data when forming chemical groups of azo dyes.

3) Apply conventional grouping approaches (e.g. (Q)SAR and ClassyFire) to form an initial grouping hypothesis for the seven azo dyes.

4) Substantiate (or test) this initial hypothesis using multi-omics approaches, specifically to group substances based on molecular toxicity responses, using untargeted metabolomics and transcriptomics data.

It is envisioned that addressing the above-mentioned objectives will enable to draw conclusions on the capability of high-throughput omics with regard to supporting biologically-driven grouping and read-across (G/RAx) cases as well as identifying areas for further work and development to increase the applicability of this approach in chemical risk assessment.

## 3.2 Azo dye toxicity

Azo dyes constitute a large heterogenous group (4103 listed in US EPA CompTox Dashboard online database: https://comptox.epa.gov/dashboard/chemical-lists/AZODYES) of synthetic colorants, and account for approx. 60-70% of all dyes used for industrial purposes, primarily in textile and food industries. They typically contain between one (monoazo dyes) or three (di- or triazo dyes) functional azo group(s) (-N=N-) that may be bonded to aromatic (benzene or heterocyclic) rings, naphthalenes or aliphatic chains[225]. Some azo dyes are reported to form one or more of the regulated 22 carcinogenic aromatic amines (via reductive cleavage) in humans and for this reason they are restricted under REACH[226]. However, recent studies suggest that azo dyes may release further 36 mutagenic non-regulated aromatic amines[227]. Human and environmental concerns associated with azo dye exposure have spurred a significant interest around these chemicals from regulators in Europe and beyond[228–230].

As a result of their large-scale production (> 1 million tons annually) and widespread application, many azo dyes are continuously released into the aquatic environment in huge quantities (ca. 200 billion litters), mainly from the textile industry effluents[231]. Due to their ubiquity in the freshwater ecosystems at low concentrations (from $ngL^{-1}$ to $\mu gL^{-1}$), azo dyes are now considered micropollutants and their toxic effects on the aquatic organisms such as *Daphnia magna*, green microalgae (*Raphidocelis subcapitata*) or zebrafish (*Danio rerio*) are well known but remain poorly characterised and understood[231–233].

Many azo dyes are classified as mutagenic (show cytotoxicity and genotoxicity), but their molecular mechanism of action is unknown. Therefore, a greater understanding of their toxicity is required for improved chemical risk assessment[234–236].

The published aquatic toxicity data (mainly from literature and ECHA chemical registration dossiers) for the seven dyes under study is summarised in Table 3.1. This data was used to guide earlier acute (48 h) toxicity range-finding studies described in section 2.2.2.

**Table 3.1** Aquatic toxicity data for azo dyes studied along with information on the REACH registration status.

| **Azo dye** | **Aquatic toxicity data** | **REACH registered** | **Notes on registration** |
|---|---|---|---|
| **S1** | *D. magna* 48-hr EC50 > 100 mg/L (ECHA dossier) | Yes | REACH (0-10 tonnes pa)<br><br>Notified classification: Aquatic Chronic 4 for chronic toxicity according to the CLP Regulation (EC 1272/2008) |
| **DY3** | Aquatic toxicity 96-h PNEC = 0.0023 mg/L from read-across of acute toxicity data for Solvent Yellow 1 (CAS RN 60-09-3) (Environment Canada); Fathead minnow LC50 > 180 mg/L (Little and Lamb 1973) | No | Prohibited in textile materials under EU 2002/371/EC<br>EU Cosmetics Regulation (1223/2009), Annex II - Prohibited Substances; classification: Carc. 2 |
| **SRG** | Larval fathead minnows LC50 = 16.7 µg/L (Parrott *et al*., 2016) | Yes | REACH (0-10 tonnes pa)<br><br>Justification for waiving the test information in the REACH registration dossier: In accordance with Annex VIII |

| Azo dye | Aquatic toxicity data | REACH registered | Notes on registration |
|---|---|---|---|
| | | | (REACH), testing for aquatic toxicity endpoints is considered scientifically unjustified since there are mitigating factors indicating that aquatic toxicity is unlikely to occur as the substance is highly insoluble (solubility: 0.00033 mg/L at 25° C) in water |
| **DO61** | *D. magna* 48-h EC50 = 18.6 mg/L (ECHA dossier) | Yes | REACH (10-100 tonnes pa)<br><br>Notified classification: Aquatic Chronic Toxicity 3 for chronic toxicity according to the CLP Regulation (EC 1272/2008) |
| **DO25** | *D. magna* LC50 = 110 mg/L (Brown 1992); zebrafish IC50 = 268 mg/L; *Scenedesmus subspicatus* EC50 = 54 mg/L; Bacteria EC50 > 100 mg/L<br>*D. magna* 48-h EC50 > 100 mg/L (ECHA dossier) | Yes | REACH (10-100 tonnes pa)<br><br>Not classified |
| **DR1** | *D. similis* EC50 = 0.12 mg/L (de Luna, 2014); *D. magna* LC50 = 0.58 mg/L, *D. similis* NOEC 14 days = 0.003 mg/L (Vacchi *et al*., 2016); *D. similis* EC50 = 0.13 mg/L (Vacchi *et al*., 2016); *D. similis* EC50 = 0.127 mg/L, NOEC = 0.01 mg/L (Ferraz *et al*., 2011) | No | Not classified for environment |

| Azo dye | Aquatic toxicity data | REACH registered | Notes on registration |
|---|---|---|---|
| **DR13** | *D. similis* EC50 = 0.18 mg/L (de Luna, 2014); *D. similis* EC50 = 0.0187 mg/L | No | Not classified for environment |

## 3.3 Biomass optimisation study for nESI-DIMS analyses

First, a biomass optimisation study was conducted (using the methods described in detail in chapter 2) to determine an optimal number of *Daphnia* neonates per experimental sample to ensure reproducibility of the subsequent metabolomics analyses, using nESI-DIMS SIM-stitch 'internal scan replication' method[8]. The aim was to minimise the number of neonates per sample (from pooled *n=30* neonates at 72 h) for metabolomics and lipidomics nESI-DIMS analyses (in a single ion mode), while keeping metabolic variability across samples sufficiently low. Two objectives were defined to appropriately address this aim:

1) Assess sensitivity (i.e. feature or peak count) and technical variability of a dilution series of *Daphnia* samples.

2) Assess reproducibility and total (i.e. biological and technical) variability of a dilution series of *Daphnia* samples.

The first specific objective was formulated to test the instrument performance at extremely low sensitivity (using pooled extracts), while the second objective sought to identify any variability issues associated with pooling extremely low number of *Daphnia*

neonates (e.g. *n*=1), whereby the high biological variability across (*n*=6) biological replicates can potentially mask the toxicological effects from azo dye exposures. Therefore, the findings from this initial biomass optimisation study were used to guide the final omics experimental design to ensure robustness of this approach. The biomass optimisation study comprised 1, 2, 4, 8 and 15 dilution series of *Daphnia* neonates plus 30 neonates for comparisons (number of *Daphnia* historically used for nESI-DIMS analyses). All *Daphnia* were collected at 72 h (*n*=6 per dilution series) and prepared using identical methods as the omics samples (as described in section 2.3).

Figure 3.1 shows the total peak count for each group size (dilution series of 1-30 neonates, plotted on a continuous x-axis) and the measure of spectral reproducibility (reported as the median relative standard deviation of peak intensities, mRSD.

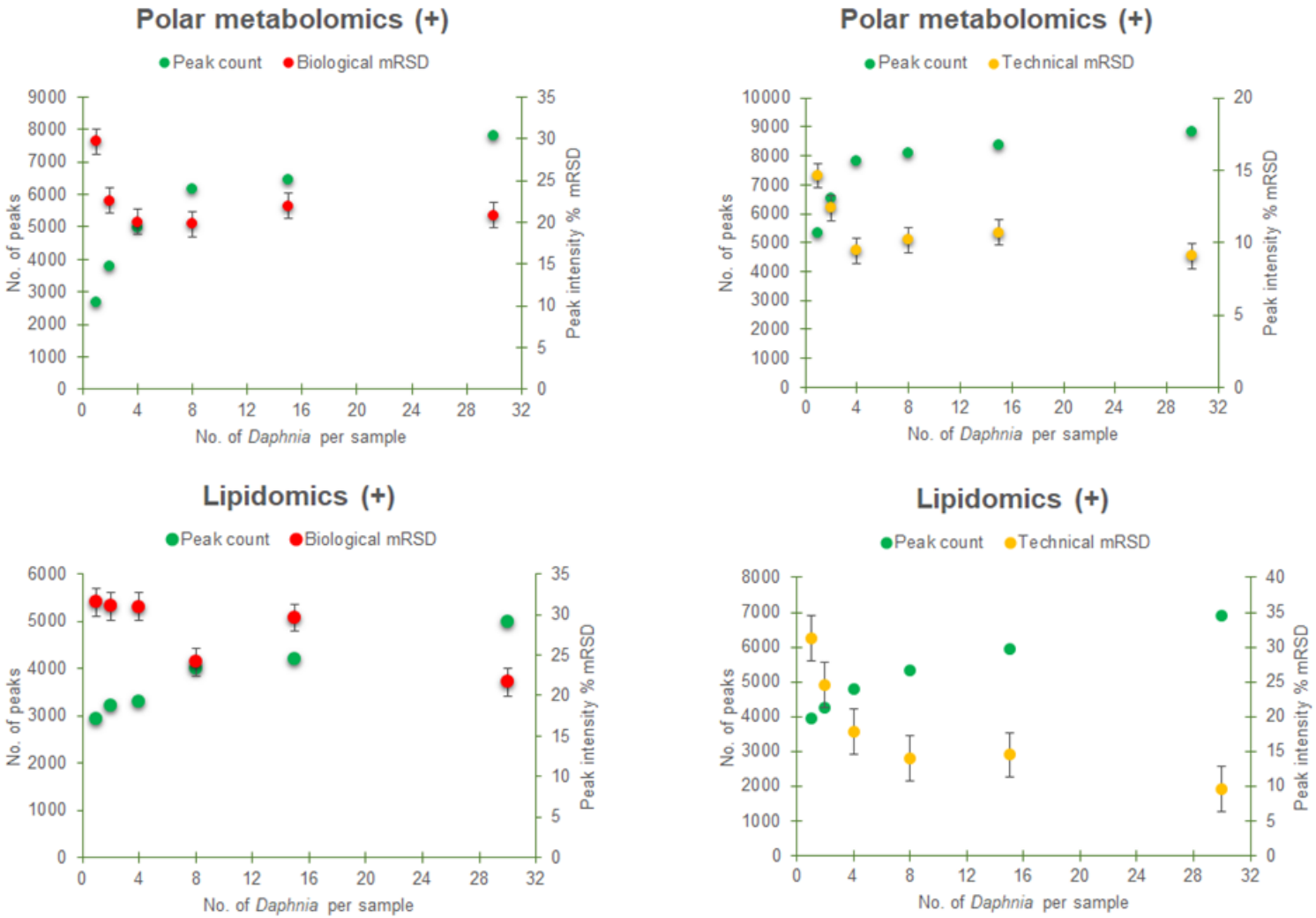


**Figure 3.1** Scatter plots demonstrating technical and biological variability of metabolic and lipid features measured in positive ion nESI-DIMS mass spectra of *D. magna* extracts in the biomass optimisation study (*n=6* per dilution series). Error bars represent standard error.

Acceptable technical variability (approx.10-15% mRSD) and biological variability (< 30% mRSD) was observed in both nESI-DIMS assays for a sample size between 4 and 8 *Daphnia* neonates, as shown in Figure 3.2. Therefore, it was concluded that an average value of *n=6* was an optimal number of neonates per sample to ensure high reproducibility during nESI-DIMS analyses, whilst keeping metabolic (biological) variability resulting from pooling *Daphnia* neonates sufficiently low. This finding guided the future omics experimental design and the numbers of neonates collected per experimental sample over the course of 48 h exposures with *Daphnia magna* (as described in section 3.5).

**Technical variability**

| | Polar metabolomics (+) nESI-DIMS | | | Lipidomics (+) nESI-DIMS | | |
|---|---|---|---|---|---|---|
| **No. of *Daphnia*** | **4** | **8** | **30** | **4** | **8** | **30** |
| Peak count | 7845 | 8109 | 8853 | 4781 | 5349 | 6891 |
| Peak intensity % mRSD | 9 | 10 | 9 | 18 | 14 | 10 |
| | 89% | 92% | | 69% | 78% | |

**Biological variability**

| | Polar metabolomics (+) nESI-DIMS | | | Lipidomics (+) nESI-DIMS | | |
|---|---|---|---|---|---|---|
| **No. of *Daphnia*** | **4** | **8** | **30** | **4** | **8** | **30** |
| Peak count | 4971 | 6166 | 7808 | 3306 | 4006 | 4986 |
| Peak intensity % mRSD | 20 | 20 | 21 | 31 | 24 | 22 |
| | 63% | 79% | | 66% | 80% | |

**Table 3.2** Technical and biological variability of metabolic and lipid features measured in positive ion nESI-DIMS mass spectra of *D. magna* extracts in the biomass optimisation study, reported as the median spectral RSD (%). Percentage values (in blue) indicate % of features detected in each 'dilution series' (i.e. *n*=4 or *n*=6 neonates) relative to *n*=30 pooled neonates used. These findings indicate that a sample size between >4 and <8 *Daphnia* neonates (at 72 h) provide optimal biomass for a sufficient recovery of biological material and analytical reproducibility.

## 3.4 Conventional grouping hypothesis based on physico-chemical properties and structural similarity

This section describes how the initial grouping pattern of the seven dyes was derived using various predictive *in silico* tools. A conventional grouping hypothesis was formed by manually examining physico-chemical properties, ClassyFire chemical classification (http://classyfire.wishartlab.com/)[237] and (Q)SAR alerts (conducted by ECHA project partners).

First, physico-chemical properties of the seven azo dyes were considered to formulate the initial grouping hypothesis. Available experimental and predicted physico-chemical properties of the dyes are summarised in Table 3.3. Crucially, these chemicals are poorly characterised and limited measured data for log $K_{ow}$ and water solubility exists. Log $K_{ow}$ and water solubility were additionally predicted by ECHA using various (Q)SAR tools, namely EPISUITE models WSKOW (log Kow based), and WaterNT (fragment based), and Percepta (ACD/Labs Release 2016.2) for logP. There are some discrepancies between the experimental and predicted values for log $K_{ow}$, and even greater discrepancies for water solubility for the seven dyes.

Overall, the seven azo dyes are characterised by rather low water solubility. Water solubility predicted with WSKOW appears to be closer to the experimentally-derived values. The WSKOW predictions suggest that five out of seven dyes are relatively moderately soluble in water, i.e. between 0.1 and 1 $mgL^{-1}$ for both sudan dyes (S1 and SRG), for both disperse red dyes (DR1 and DR13), and for DO25. Water solubility is very low for DO61 (0.00056 $mgL^{-1}$), and DY3 is the most soluble of the dyes with more than 10 $mgL^{-1}$.

If it is the case that these azo dyes have no specific mode of action (i.e. exhibit baseline toxicity or narcosis), then their toxicities could be related to log $K_{ow}$. Therefore, the sudan dyes (S1 and SRG) should exhibit higher toxicity compared to DY3, DR1, DR13 and DO25. For DO61 there is conflicting information between experimental data and predicted log $K_{ow}$, the latter suggesting the highest log $K_{ow}$ and hence the highest narcotic toxicity of all of the dyes.

In addition, the sudan dyes and DY3 give an alert for tautomerisation in the QSAR Toolbox (v4.3). Tautomers could have different physico-chemical properties. However, azo-hydrazone tautomerisation (i.e. migration of a hydrogen atom from an -OH group *ortho* or *para* to the azo group, and a shift in the location of a double bond) can only occur under specific experimental conditions (e.g. temperature, pH of media, solvents used)[225]. It is unclear if, in practice, azo dye tautomers would be observed during toxicity exposures with *Daphnia magna*, therefore, this information is likely redundant in the context of this study.

**Table 3.3** Overview of physico-chemical properties and organic functional groups of the seven dyes investigated. Available experimental data is highlighted in grey.

| **Azo dye** | **Organic functional groups (nested) – QSAR Toolbox** | **Log $K_{ow}$** | | | **Water solubility ($mgL^{-1}$)** | | |
|---|---|---|---|---|---|---|---|
| | | **Experimental** | **KOWWIN v1.68** | **ACD/Labs Percepta logP** | **Experimental** | **EPI Suite - WaterNT** | **EPI Suite - WSKOW** |
| **S1** | Azo;<br>Fused carbocyclic aromatic;<br>Aryl;<br>Phenol;<br>Naphtalene | - | 5.51 | 4.46 | 0.018 (ECHA CHEM) | 4.39 | 0.67 |
| **S1 tautomer (stable form)** | Aryl;<br>Hydrazone;<br>Quinoid compounds | - | 3.312 | 3.81 | - | 4.0 | 36 |

| Azo dye | Organic functional groups (nested) – QSAR Toolbox | Log $K_{ow}$ | | | Water solubility ($mgL^{-1}$) | | |
|---|---|---|---|---|---|---|---|
| | | **Experimental** | **KOWWIN v1.68** | **ACD/Labs Percepta logP** | **Experimental** | **EPI Suite - WaterNT** | **EPI Suite - WSKOW** |
| **DY3** | Azo;<br>Aryl;<br>Phenol;<br>Organic amide and thioamide;<br>Alkyl (hetero)arenes;<br>Alkyl-, alkenyl- and alkynyl (hetero)arenes | - | 3.98 | 3.27 | 0.00033<br><br>1.18 (QSAR TB) | 257 | 10.25 |
| **DY3** tautomer | Allyl;<br>Aryl;<br>Hydrazone;<br>Quinoid compounds;<br>Organic amide and thioamide | - | 1.97 | 1.41 | - | 53 | 386 |

| Azo dye | Organic functional groups (nested) – QSAR Toolbox | Log $K_{ow}$ | | | Water solubility ($mgL^{-1}$) | | |
|---|---|---|---|---|---|---|---|
| | | **Experimental** | **KOWWIN v1.68** | **ACD/Labs Percepta logP** | **Experimental** | **EPI Suite - WaterNT** | **EPI Suite - WSKOW** |
| **SRG** | Azo;<br>Ether;<br>Fused carbocyclic aromatic;<br>Aryl;<br>Phenol;<br>Naphtalene;<br>Alkoxy | 7.5 (ECHA CHEM) | 5.59 | 4.69 | 0 (ECHA CHEM)<br>0.00033 (QSAR TB) | 2.3 | 0.38 (0.009 using exp log $K_{ow}$) |
| **SRG** tautomer (stable form) | Ether;<br>Aryl;<br>Hydrazone;<br>Quinoid compounds;<br>Alkoxy | - | 3.39 | - | - | 2.1 | 20 |
| **DO61** | Azo;<br>Aryl halide;<br>Nitrile; | 2.132 (ECHA CHEM) | 6.47 | 5.48 | < 20 | 0.17 | 0.00056 |

| Azo dye | Organic functional groups (nested) – QSAR Toolbox | Log $K_{ow}$ | | | Water solubility ($mgL^{-1}$) | | |
|---|---|---|---|---|---|---|---|
| | | **Experimental** | **KOWWIN v1.68** | **ACD/Labs Percepta logP** | **Experimental** | **EPI Suite - WaterNT** | **EPI Suite - WSKOW** |
| | Aromatic amine;<br>Nitrobenzene | | | | | | (2.8 using exp log $K_{ow}$) |
| **DO25** | Azo;<br>Nitrile;<br>Aromatic amine;<br>Nitrobenzene | 4.38 (ECHA CHEM) | 4.69 | 4.46 | <0.02 (ECHA CHEM)<br><br>40000 (QSAR TB) | 4.02 | 0.17<br><br>(0.33 using exp log $K_{ow}$) |
| **DR1** | Alcohol;<br>Azo;<br>Aromatic amine;<br>Nitrobenzene | 4.3 (QSAR TB) | 4.2 | 4.1 | 0.16 (QSAR TB) | 58 | 0.79 |
| **DR13** | Alcohol;<br>Azo;<br>Aryl halide;<br>Aromatic amine; | - | 4.85 | 4.68 | 0.012 (QSAR TB) | 13 | 0.16 |

| Azo dye | Organic functional groups (nested) – QSAR Toolbox | Log $K_{ow}$ | | | Water solubility ($mgL^{-1}$) | | |
|---|---|---|---|---|---|---|---|
| | | Experimental | KOWWIN v1.68 | ACD/Labs Percepta logP | Experimental | EPI Suite - WaterNT | EPI Suite - WSKOW |
| | Nitrobenzene | | | | | | |

Next, the seven dyes were grouped based on their chemical structures and chemical features using two independent approaches: ClassyFire (a web-based tool extensively used in the metabolomics community to associate biological activity with molecular structure)[237] and (Q)SAR profiling (conducted by Doris Hermann, ECHA). The grouping patterns that emerged from the application of these approaches are summarised in Table 3.4 and Table 3.5, respectively. ClassyFire categorised the seven azo dyes into two distinct groups separating the two sudan dyes from the remaining five disperse dyes.

**Table 3.4** ClassyFire taxonomic classification of the seven azo dyes.

| Azo dye | ClassyFire taxonomic classification |
|---|---|
| S1, SRG | Kingdom: Organic compounds<br>Superclass: Benzenoids<br>Class: Naphthalenes<br>Subclass: Naphthols and derivatives |
| DY3, DO61, DO25, DR1, DR13 | Kingdom: Organic compounds<br>Superclass: Organoheterocyclic compounds<br>Class: Azobenzenes |

In contrast, based on the (Q)SAR profiling results, the seven azo dyes can be categorised into three subgroups: 1) group 1 – sudan dyes, 2) group 2 – disperse orange and red dyes and 3) group 3 – disperse yellow 3 dye. In theory, the aquatic toxicity (on a molar basis) should correlate with the log $K_{ow}$ within these sub-groups.

One observation from this grouping pattern is that three dyes: both sudan dyes (S1 and SRG, group 1) and DY3 (group 3) were all classified as phenols, indicating there are some similarities among these three dyes.

**Table 3.5** Conventional grouping hypothesis based on (Q)SAR profiling (conducted by ECHA), highlighting some similarities between the sudan dyes and disperse yellow 3 dye (grey shading).

| (Q)SAR tool output | **Group 1 - sudan dyes** | **Group 2 - disperse orange and red dyes** | **Group 3 - disperse yellow dye** |
|---|---|---|---|
| | SRG, S1 (polar narcotics) | DO61, DR13, DO25, DR1 (non-polar narcotics) | DY3 (polar narcotic) |
| ECOSAR 2.0 (Ecological Structure Activity Relationships) | Belong to **Phenols** | Belong to Neutral organics | Belongs to **Phenols**, Amides, Phenol amines |
| OASIS (QSAR Toolbox) | Reactive unspecified alert by acute aquatic toxicity MoA | Reactive unspecified alert by acute aquatic toxicity MoA | Reactive unspecified alert by acute aquatic toxicity MoA |
| US-EPA New Chemical Categories | | Only DR13 and DO61 are identified as Neutral organics | Identified as Phenols (Acute toxicity) |
| OECD HPV Chemical Categories | | | Belongs to m,p-Cresols |

### Summary of conventional grouping hypotheses and conclusions

The conventional grouping hypotheses derived from predictive *in silico* tools and the assessment of physico-chemical properties are summarised in Table 3.6. It can be concluded from these findings that there is no single grouping hypothesis that arises

from considering physico-chemical properties, chemical structure (ClassyFire) and by applying (Q)SAR analyses. These findings revealed some similarities among three azo dyes (all classified as polar narcotics and phenols): DY3, SRG and S1. DY3 forms its own group but it is most structurally similar to the other two sudan dyes.

Of note, this initial azo dye grouping hypothesis is based on purely theoretical in nature *in silico* predictions that are used as an alternative approach to fill experimental data gaps and aid chemical prioritisation for further assessment[238]. However, many *in silico* tools for aquatic toxicity show decreased prediction accuracy for ionisable and poorly soluble chemicals (classified as narcotics)[239]. Therefore, there is an inherent uncertainty associated with how these azo dyes will act in practice within the exposed *Daphnia magna*.

**Table 3.6** Summary of the grouping hypotheses prior to molecular mechanistic studies.

| **Approach** | **Grouping hypothesis** |
|---|---|
| ClassyFire taxonomic classification | **Group 1** - S1, SRG<br>**Group 2** - DO25, DO61, DR1, DR13, DY3 |
| Physico-chemical properties (ECHA) | No clear groups are formed, instead predicted gradients of toxicity inferred from log $K_{ow}$ and water solubilities (assuming a narcotic MoA): e.g., relative toxicities based on predicted log $K_{ow}$ only DO61 > SRG > S1 > DR13 > DO25 > DR1 > DY3 |
| (Q)SAR (ECHA) | **Group 1** - SRG, S1 (polar narcotics)<br>**Group 2** - DO61, DR13, DO25, DR1 (non-polar narcotics)<br>**Group 3** - DY3 (polar narcotic) |

## 3.5 *Daphnia magna* acute toxicity exposures for omics study

The findings obtained from the acute (48 h) range-finding experiments and benchmark dose (BMD) modelling (as described in section 2.2.2 in chapter 2) were used to determine the final test doses for the omics exposures. A series of 48 h exposure studies (as per OECD guidelines[91]) were subsequently conducted to generate *Daphnia* samples for multi-omics analyses. Each experimental sample comprised *n*=6 neonates, as concluded from the biomass optimisation study described in the previous section (3.4).

The final omics experimental design comprised seven azo dyes (S1, DY3, SRG, DO61, DO25, DR1, DR13) three doses (treated low, medium and high, and untreated control samples containing 0.1% DMSO) and three sampling points (2 h, 24 h and 48 h). Therefore, for a single azo dye, there were nine possible dose/time treatment groups and a total of 63 possible groups in this seven-substance grouping study.

The exposure concentrations for each dye, number of samples collected for each of the omics assays (i.e. metabolomics + lipidomics, and transcriptomics) and experimental observations following the acute exposures are summarised in Table 3.7. Due to considerable differences in azo dye toxicity, the high doses for the seven dyes spanned nearly three orders of magnitude: DO61 caused ca. 10% *Daphnia* immobilisation at 0.004 mg $L^{-1}$ while SRG induced the same adverse outcome at 3.35 mg $L^{-1}$ (see section 2.2.3).

For clarity, the total numbers of theoretical samples per dye were calculated as follows:

1) For polar metabolomics + lipidomics analyses: *n*=6 biological replicates × (3 treated doses +1 untreated controls) exposure concentrations × 3 time points = 72 samples per dye.
2) For transcriptomics analyses: *n*=4 biological replicates × (3 treated doses +1 untreated controls) exposure concentrations × 3 time points = 48 samples per dye.

The actual numbers of samples collected were slightly lower due to sample loss during the omics exposures. Specifically, five treatment groups were removed from the study due to *Daphnia* immobilisation (i.e. 48 h medium and high dose for S1, 48 h high dose for DO61).

Azo dye concentrations used in all toxicity studies were nominal concentrations and, therefore, the actual exposure may be slightly lower due to limited solubility and partial adherence of dye particles to the glass exposure vessels and animals. Therefore, any future azo dye exposures should incorporate the analysis of media samples to determine the actual test concentrations.

Figure 3.2 shows a light microscope image of *Daphnia magna* exposed to SRG, highlighting the 'real-world' challenges associated with complex physico-chemical properties of these azo dyes. Due to hydrophobic nature of the azo dyes, every effort was made to set testing concentrations at or below solubility levels to avoid any complications associated with physical toxicity induced by undissolved particles rather than the inherent toxicity of the dyes.

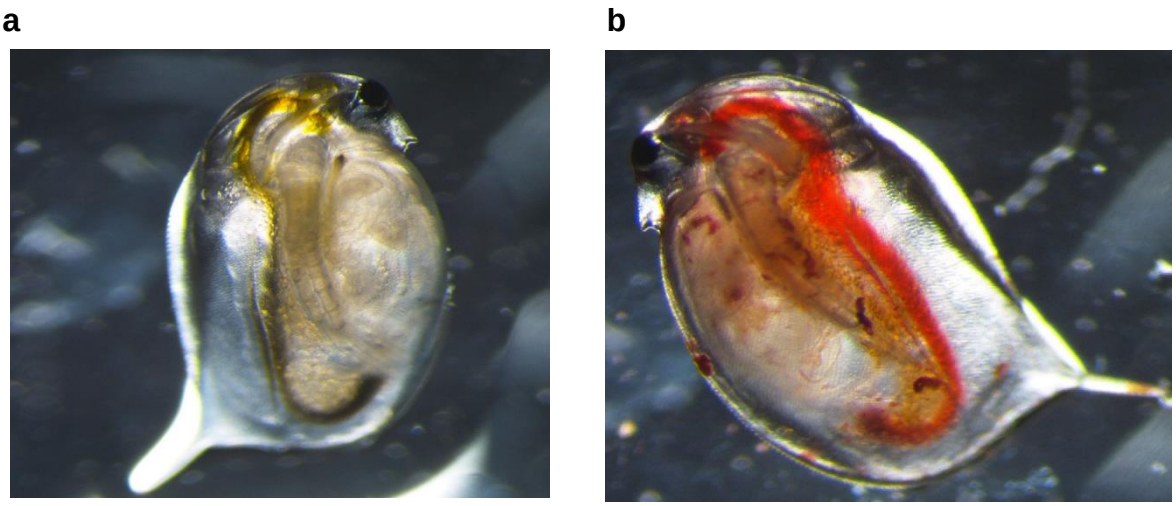


**Figure 3.2** Light microscope images of (a) *Daphnia* control and (b) *Daphnia* exposed to 1 mg $L^{-1}$ SRG for 24 h. Pigmentation and dye particles appear to be present on the antennae, carapace and in high concentration in the gut suggesting that dye particles adhere to the exposed animal (approximately 100× magnification).

**Table 3.7**. Summary of test conditions, experimental observations and experimental batch design for the *Daphnia* acute (48 h) multi-omics study.

| Azo dye | Nominal exposure concentrations for acute multi-omics study (mg $L^{-1}$) | Exposure batch (A-F) | Metabolite + lipid and RNA extraction batch (1-6) | Experimental observations (dye) | No. of samples collected for polar metabolomics + lipidomics and transcriptomics analyses |
|---|---|---|---|---|---|
| S1 | 0.0087, 0.026, 0.078 | Batch E | Batch 5 | No precipitation | 59 + 40* |
| SRG | 0.3, 1.0, 3.35 | Batch B | Batch 2 | Dye particles visible ≥ 0.3 mg $L^{-1}$ | 72 + 48 (controls shared with DR1) |
| DY3 | 0.1, 0.3, 0.91 | Batch D | Batch 4 | No precipitation | 72 + 48 |
| DO25 | 0.3, 1.0, 3.0 | Batch A | Batch 1 | Dye particles visible = 3 mg $L^{-1}$ | 72 + 48 |
| DO61 | 0.0004, 0.0013, 0.004 | Batch C | Batch 3 | No precipitation | 69 + 44* |
| DR1 | 0.01, 0.03, 0.1 | Batch B | Batch 2 | No precipitation | 72 + 48 (controls shared with SRG) |
| DR13 | 0.002, 0.006, 0.018 | Batch F | Batch 6 | No precipitation | 72 + 48 |

*Samples discarded due to *Daphnia* immobilisation at 48h.

In addition, 339 samples were analysed externally by BioSpyder Templated Oligo-Sequencing (TempO-Seq) transcriptomics (BioSpyder, US). The overall QC/QA assessment of gene expression data and subsequent analyses were conducted by the co-authors on the study: Prof. John Colbourne, Dr Rosemary Barnett and Dr Jiauri Zhou. However, the analysis of transcriptomics datasets is not within the scope of this thesis, thus it is not discussed in detail.

## 3.6 Quality control (QC) assessment of nESI-DIMS untargeted metabolomics

The scale of untargeted nESI-DIMS raw data collection for this high-throughput omics study is presented in Table 3.8. For each extracted sample, three nESI-DIMS assays (i.e. polar metabolomics in positive and negative ion modes, and lipidomics in negative ion mode only) were applied to maximise the detection of endogenous metabolites and lipids in the *Daphnia*.

**Table 3.8** Summary of nESI-DIMS analyses of *D. magna* extracts following acute (48 h) exposures to the seven azo dyes.

| Study name | No. of samples | Total of $MS^1$ nESI-DIMS analyses |
|---|---|---|
| Biomass optimisation study | 76 | 152 |
| Acute azo dye study | 603 | 1,809 |
| Total | 679 | 1,961 |

As described in section 2.3, QC strategies applied within this study align with MERIT best practice guidelines[3]. Therefore, three types of QC control samples were included, namely: 1) system suitability QC samples (ssQC), 2) pooled intra-study QC samples and 3) process (extraction) blanks.

System suitability QC data collected with each analytical batch were examined to derive mass error tolerance for lipidomics and polar metabolomics datasets at ±5 ppm and ±10 ppm, respectively.

The overall technical quality of the polar metabolomics and lipidomics datasets was reported using the median of the relative standard deviations over all pooled intra-study QC peak measurements ($mRSD^{QC}$). The $mRSD^{QC}$ values for each assay are listed in Table 3.6, describing the analytical reproducibility for each of the three assay types across all of the experimental batches of samples (Exposure batches A-F combined, see Table 3.7).

**Table 3.9** Analytical precision of the three nESI-DIMS metabolomics assay types following extensive DIMSPy data processing (as detailed in section 2.4).

| **nESI-DIMS assay** | **$mRSD^{QC}$ (%)** | **No. of peaks in extensively processed dataset** |
|---|---|---|
| Polar metabolomics (+) | 26.6 | 245 |
| Lipidomics (-) | 21.8 | 177 |
| Polar metabolomics (-) | 31.1 | 94 |

Based on these findings, the nESI-DIMS polar negative metabolomics dataset was deemed as poor quality due to relatively low feature count and high $mRSD^{QC}$ values, and therefore excluded from further omics analyses and hierarchical clustering analyses (HCA) for grouping of the seven azo dyes.

The initial assessment of data quality for the remaining two assays (polar metabolomics and lipidomics, both measured in positive ion mode) was conducted by applying principal component analysis (PCA) to the glog-transformed peak matrix for each dye. Figure 3.3 shows separation of QC samples from experimental dye samples. The clustering of QC samples indicates good reproducibility and robustness of nESI-DIMS analyses.

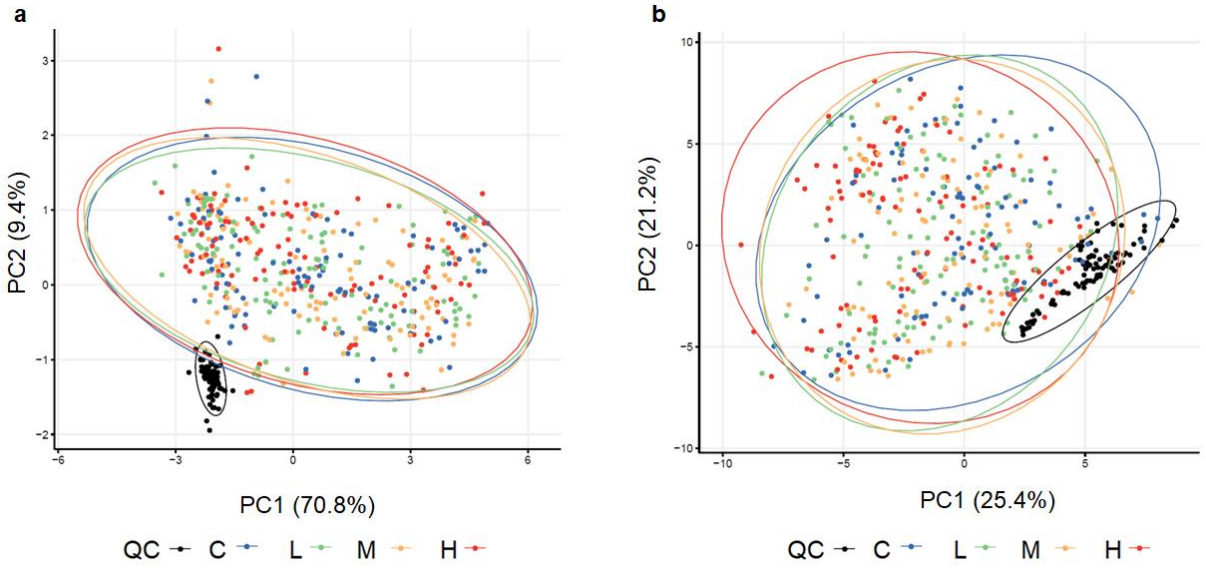


**Figure 3.3** PCA scores plots showing clear separation of QC samples (black) from all biological dye samples (C, L, M, H) in nESI-DIMS lipidomics (left) and polar metabolomics (right). PC1 captures 25.4% and 70.8% of variance in the data for polar metabolomics and lipidomics, respectively. Abbreviations: C – controls, L – low dose, M – medium dose, H – high dose.

Any outlying samples (i.e. lying outside of the 95% CI ellipse in PCA) were subsequently removed from each dataset (13 samples from polar metabolomics and 20 samples from lipidomics) prior to conducting HCA analyses. The numbers of samples taken for further omics analyses are summarised in table 3.10.

In addition, both datasets were assessed for instrumental drift and any batch effects in this multi-batch study. It was concluded that no correction was required.

**Table 3.10** Summary of sample numbers for HCA analyses following the removal of outliers identified via PCA analyses.

| Azo dye | nESI-DIMS metabolomics (+) | nESI-DIMS lipidomics (+) |
|---|---|---|
| **S1** | 50 | 54 |
| **DY3** | 69 | 69 |
| **SRG** | 66 | 65 |
| **DO61** | 66 | 65 |
| **DO25** | 45 | 63 |
| **DR1** | 67 | 68 |
| **DR13** | 69 | 67 |
| Total no. of samples for HCA analyses | 432 | 451 |

Further assessment of QC samples concluded that they were not representative of the experimental samples, hence normalisation was conducted using all dye-specific biological samples for a given dye due to the unique experimental design of the study, whereby each dye was analysed with a specific set of control samples (as previously described in section 2.2.4). Using biological samples for normalisation yielded a more

consistent distribution of PQN coefficients across all the doses and time points (per dye) compared to the standard normalisation method using intra-study QC samples.

## 3.7 Omics-based grouping approaches

As described in section 3.5, based on the experimental design for the *D. magna* omics exposures (incorporating three treated doses and three sampling time points), there were nine possible dose/time groups for a single dye, resulting in 63 possible groups in this seven-dye study. Five groups were subsequently removed from the study due to *Daphnia* immobilisation (i.e. 48 h medium and high dose for S1, 48 h high dose for DO61) and/or sample loss during the initial data processing and PCA (i.e. 2 h low dose and medium dose for DO25 outside 95% confidence intervals; CI), leaving 58 dose/time treatment groups in total for statistical analyses (using methods described in section 2.5). For consistency, any dose/time groups missing for one omics data stream were also excluded from further analyses.

Prior to multivariate (i.e. PCA) and univariate (i.e. independent two-sample t-test) statistical analyses, omics data were processed separately, using established methods, as described in section 2.4.

First, PCA was employed to mine the datasets and reveal any underlying patterns for individual dyes. For example, typical PCA scores plots for SRG azo dye show partial separation of treatment groups (C, L, M, H) and time-course (2 h, 24 h, 48 h) in nESI-DIMS lipidomics, suggesting that dose and time-dependent metabolic perturbations occurred in the *Daphnia* during acute exposures (Figure 3.4). PC1 captures 58.4 % of the total variance in this dataset.

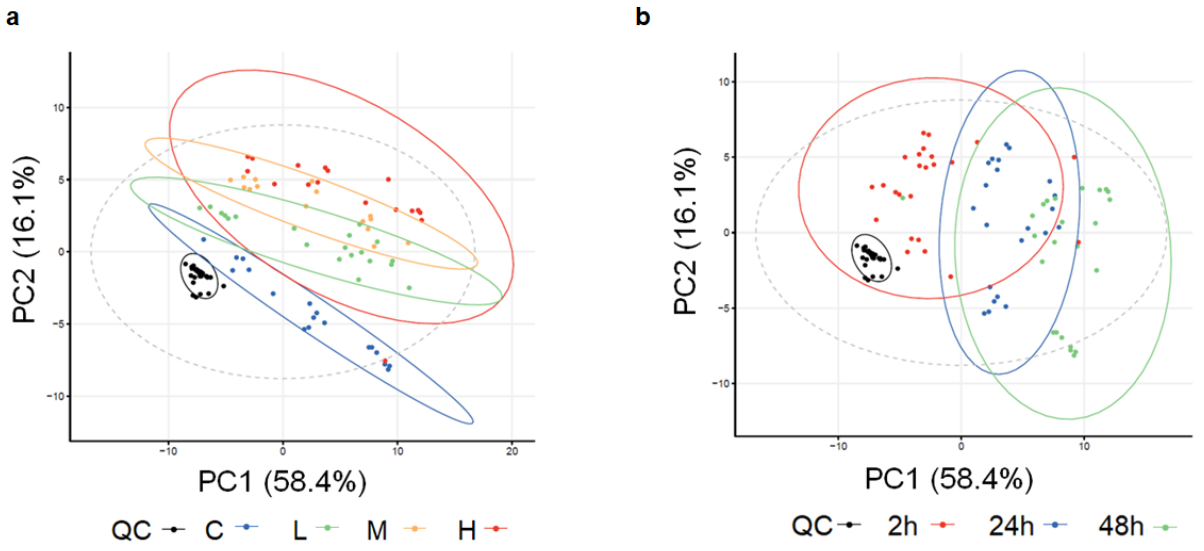


**Figure 3.4** PCA scores showing separation of (**a**) treatment groups and (**b**) sampling time points in *D. magna* nESI-DIMS lipidomics following acute (48 h) exposure to SRG azo dye. QC samples are separated from experimental samples and cluster together, indicating high reproducibility. Abbreviations: C – controls, L – low dose, M – medium dose, H – high dose.

Next, the t-statistics derived from univariate analyses of all molecular features (i.e. *m/z* metabolomics and lipidomics features, and genes) were used to conduct unsupervised hierarchical cluster analyses (HCA; as described in section 2.5) to reveal a grouping pattern (dendrogram) for the dyes based on the toxicological similarities (or dissimilarities) of molecular responses in *Daphnia magna*. Various feature selection and group selection approaches were considered to ensure the robustness of the cluster analyses performed on the omics datasets.

Specifically, three different feature selection strategies were explored to derive an optimal grouping strategy based on the number of distinct low, medium and high (L+M+H) dose clusters formed in a dendrogram for each dye (relative to the maximum number of 18 possible clusters, given the missing dose/time groups), and stability of

those clusters, expressed as approximately unbiased (AU) probability values (*p*-values) calculated for each cluster using the *pvclust* R-package[219]. The three strategies (considering all molecular features, or significant features only, i.e. non FDR-corrected $p<0.05$ and FDR-corrected $q<0.1$) and the corresponding numbers of molecular features used for clustering analyses are summarised in Table 3.11. The final approach (i.e. using all detected molecular responses in *D. magna*) applied in the azo dye omics grouping is highlighted in blue.

Polar metabolomics and lipidomics features were considered together as the most 'downstream' reflection of a phenotype, and, therefore merged into a 428-feature matrix for subsequent HCA analyses. The resulting data matrix for cluster analyses contained a total of 2317 features (including 245 polar metabolic and 193 lipid *m/z* features, and 1889 genes) for 58 dose/time treatment groups. This defined the strategy for the first type of HCA analyses conducted on this dataset.

**Table 3.11** Feature selection approaches for the azo dye grouping using HCA. Blue shading indicates features considered for the subsequent omics analyses (all detected features), yellow shading indicates significant features ($p$<0.05) that were used for the pre-assessment of molecular responses (illustrated in **Figure 3.5** and explained further in the text below).

| Features | Polar metabolomics | Lipidomics | Transcriptomics | All omics |
|---|---|---|---|---|
| All features considered | 245 | 183 | 1889 | 2317 |
| $p$<0.05 (non-FDR-corrected) | 233 | 178 | 1792 | 2203 |
| $q$<0.1 (FDR-corrected) | 93 | 119 | 918 | 1130 |

Feature selection was followed by an initial assessment of the molecular responses across all omics to guide specific dose/time group selection for each of the seven dyes for another type of final HCA analyses conducted on a smaller subset of treatment groups. Specifically, Figure 3.5 summarises the results from univariate analyses, illustrating the percentage of significant features (non FDR-corrected $p$<0.05) at each dose group for the three sampling time points. The bar charts clearly show the effects of time, dose, for each dye, for each type of omics assay. These findings were used to select a single dose with the largest overall molecular effect occurring within each time point (i.e. the largest absolute t-values across the 2h, 24 h and 48 h time-series, per dose, per dye), reducing the overall number of treatment groups from 58 (when all possible groups were considered) to 21 (i.e. 3 groups per dye). The rationale for this approach was to capture the highest level of molecular perturbations that occurred in the *Daphnia* over the time-course of azo dye exposures.

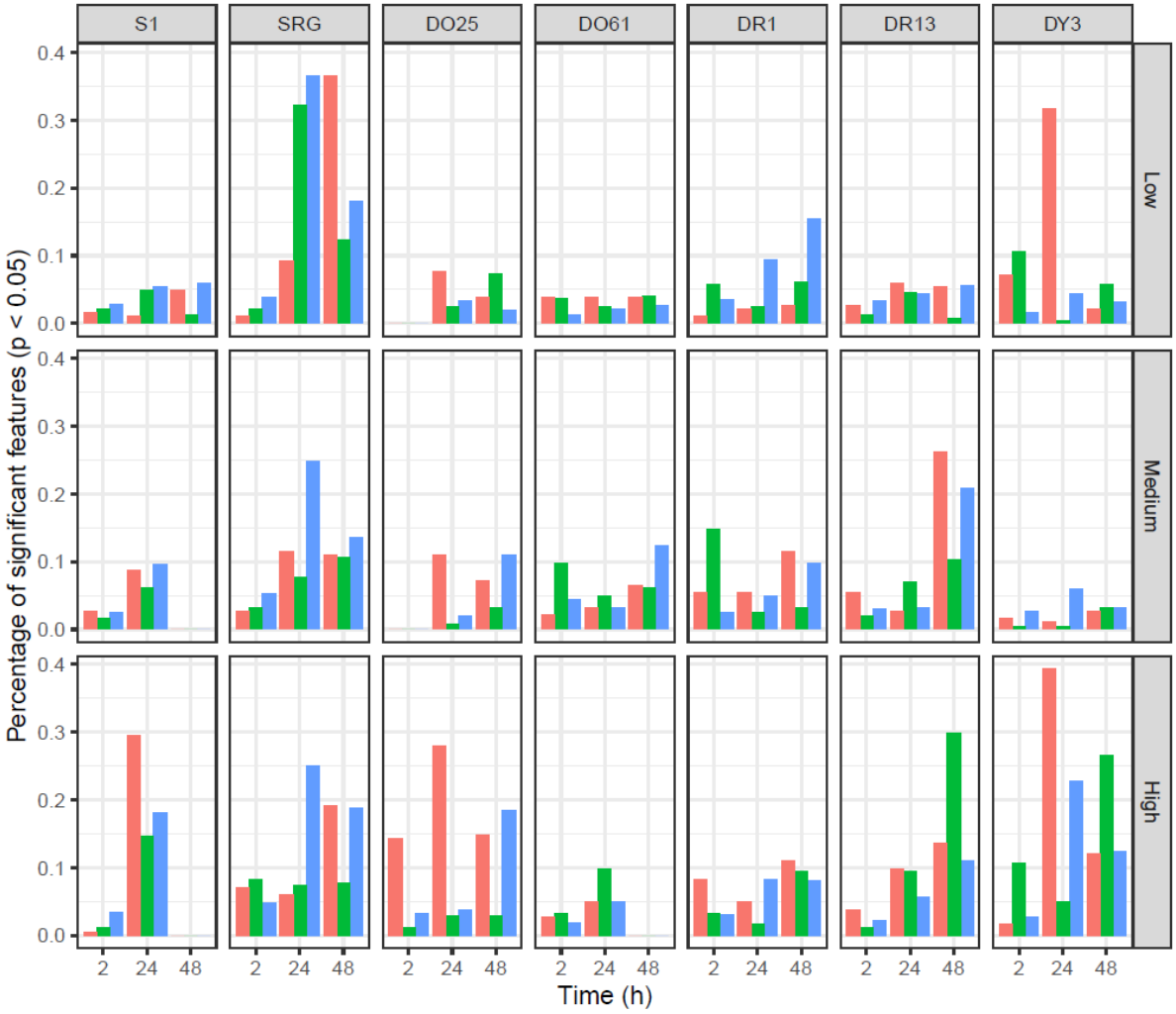


**Figure 3.5** Bar charts showing percentage of significant features (non FDR-corrected $p$<0.05) per dye, per dose (low, medium, high) and per sampling time point (2 h, 24 h, 48 h) for each type of omics assay: red – nESI-DIMS lipidomics, green – nESI-DIMS polar metabolomics, blue – transcriptomics. Significant feature numbers (per omics assay) behind the bar charts are detailed in **Table 3.11** above (figure produced by Dr Rosemary Barnett).

The azo dye dendrograms resulting from the two approaches: 1) 'all treatments' (considering all possible 58 dose/time treatment groups across the three timepoints) approach and 2) 'maximum perturbation' approach (considering 21 dose/time treatment groups for a single time point) are presented and discussed below. HCA was

applied to examine clustering patterns for the seven azo dyes emerging from multi-omics (i.e. metabolomics + lipidomics + transcriptomics) and single omics (i.e. metabolomics + lipidomics, or transcriptomics only) analyses, using both of the above approaches. Both types of analyses were conducted on a total of 2317 features for multi-omics: specifically, 428 combined polar metabolomics and lipidomics *m/z* features, and 1889 genes.

### 3.7.1 Azo dye grouping patterns revealed by the HCA 'all treatments' approach

Figures 3.6-8 show relatively complex dendrograms (with calculated AU *p*-values) that resulted from the hierarchical cluster analyses of the acute omics datasets containing all 58 possible treatment groups. The key observation from these results is that low (L), medium (M) and high (H) doses of each dye cluster together at each time point. This indicates that relatively subtle changes of dose levels (i.e. 3-fold higher and 3-fold lower than the mid-dose) induce relatively consistent molecular responses for any one dye, compared to the differences in the biological effects induced across time and across the different azo dyes. The highest number of distinct clusters (16 out of 18 possible clusters reduced from 21 due to sample loss) emerge in the dendrogram obtained from the HCA analyses considering all 2317 features from three omics data streams, whereby only two dose/time groups (DO25 48 h high dose and DY3 48 h low dose) do not follow this pattern (Figure 3.7). In contrast, single omics analyses result in the formation of 11 (tending towards 13) and 10 (tending towards 15) separate L+M+H dose clusters for polar metabolomics and lipidomics (Figure 3.6), and transcriptomics (Figure 3.8), respectively. The higher number of clusters observed when considering all three omics data streams suggests that multi-omics indeed has

the power to more comprehensively characterise toxicological similarities among the dyes, compared to single omics interrogations. This is further supported by the highest overall *p*-values (approaching 100) and, therefore, higher stability of these L+M+H dose clusters observed in the multi-omics dendrograms, compared to single omics analyses.

The clustering pattern for the three dyes of interest (S1, DY3, SRG) that starts to emerge in all three dendrograms (highlighted in yellow) is further explored in the next section (3.7.2). In addition, 20 significantly changing shared metabolites ($q < 0.1$) representing six lipid classes were putatively annotated for the three dyes in the nESI-DIMS lipidomics dataset (Appendix B, Figure B-1).

Another observation is that the time of observation of the molecular changes occurring in the exposed *Daphnia* has a significant impact on the grouping pattern, i.e. the three time points (2 h, 24 h, 48 h) for each dye rarely cluster together within the dendrograms. This highlights the dynamic nature of the molecular changes within the *Daphnia* following exposure to the seven dyes azo dyes.

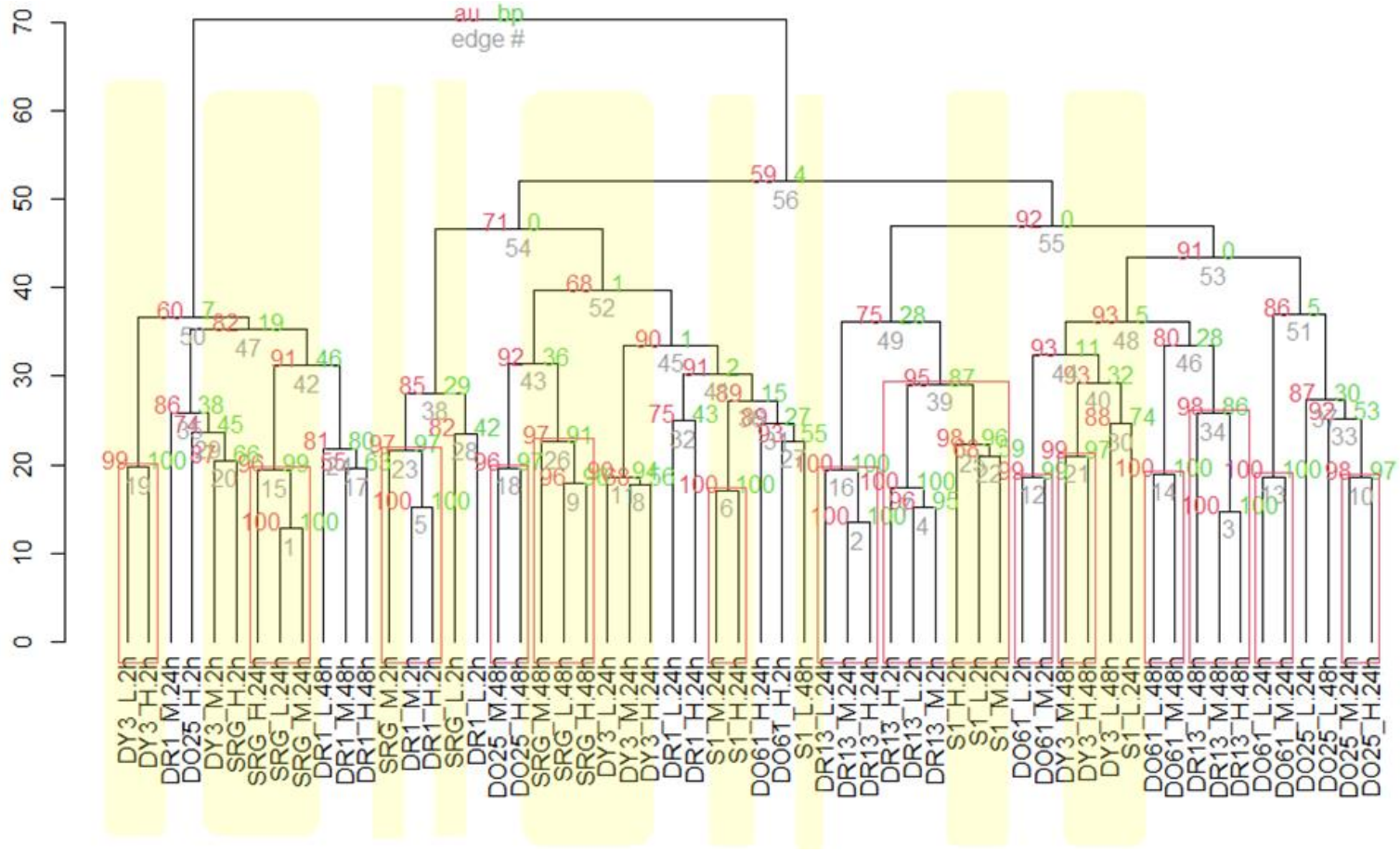


**Figure 3.6** Dendrogram resulting from the 'all results' approach for all 58 groups (i.e. maximum of 9 dose/time treatment groups per dye) comparison of polar metabolomics and lipidomics. At least 11 and up to 13 L+M+H dose clusters are observed for all 428 features. Example L+M+H (low, medium, high) dose clusters for S1, DY3 and SRG are highlighted (yellow shading). AU (approximately unbiased) *p*-values are shown in red and BP (bootstrap probability) values for each cluster are shown in green.

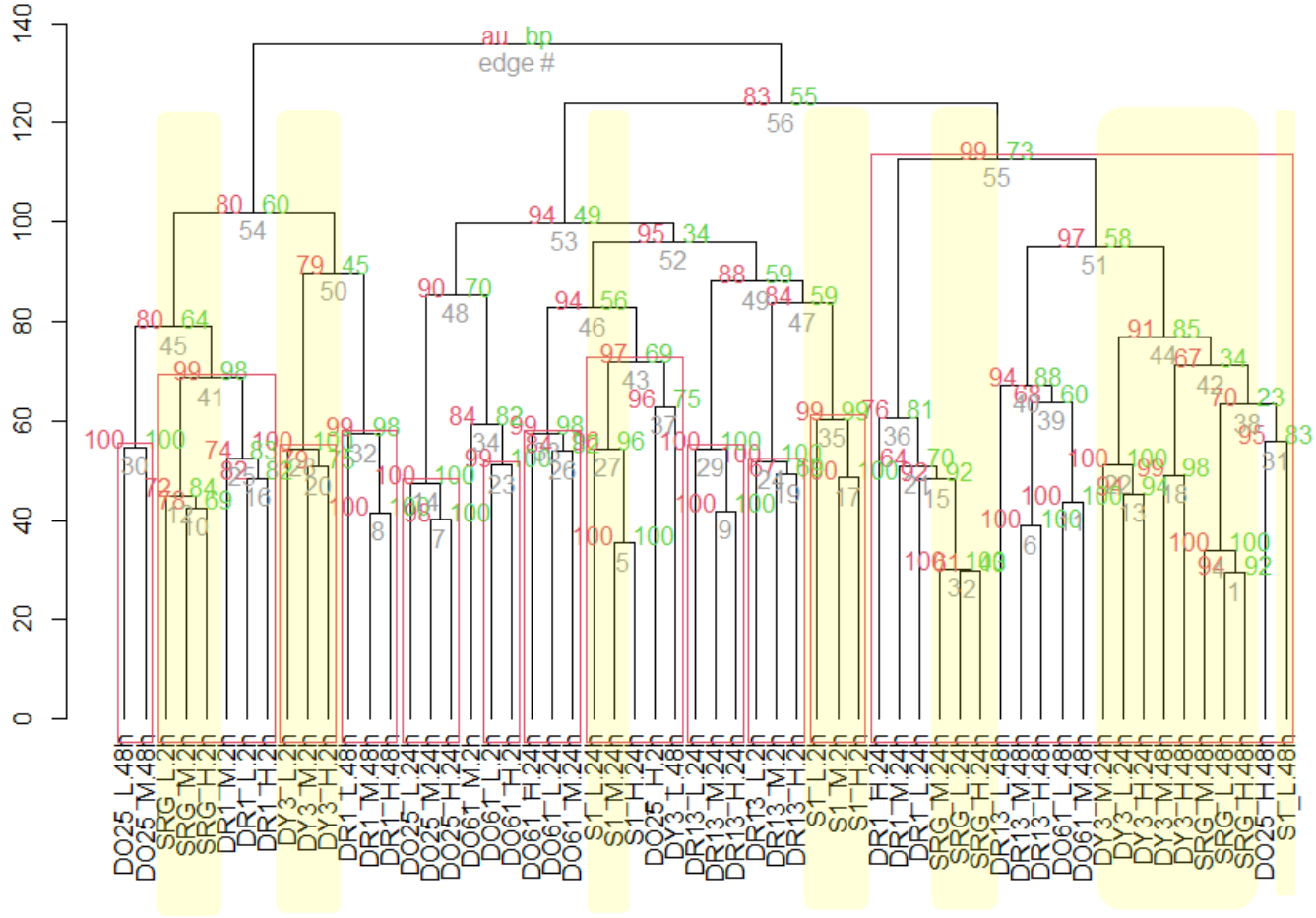


**Figure 3.7** Dendrogram resulting from the 'all results' approach for all 58 groups (i.e. maximum of 9 dose/time treatment groups per dye) comparison of all omics features (polar metabolomics, lipidomics and transcriptomics). 16 of L+M+H dose clusters are observed for all 2317 features. Example L+M+H (low, medium, high) dose clusters are highlighted for S1, DY3 and SRG (yellow shading). AU (approximately unbiased) *p*-values are shown in red and BP (bootstrap probability) values for each cluster are shown in green.

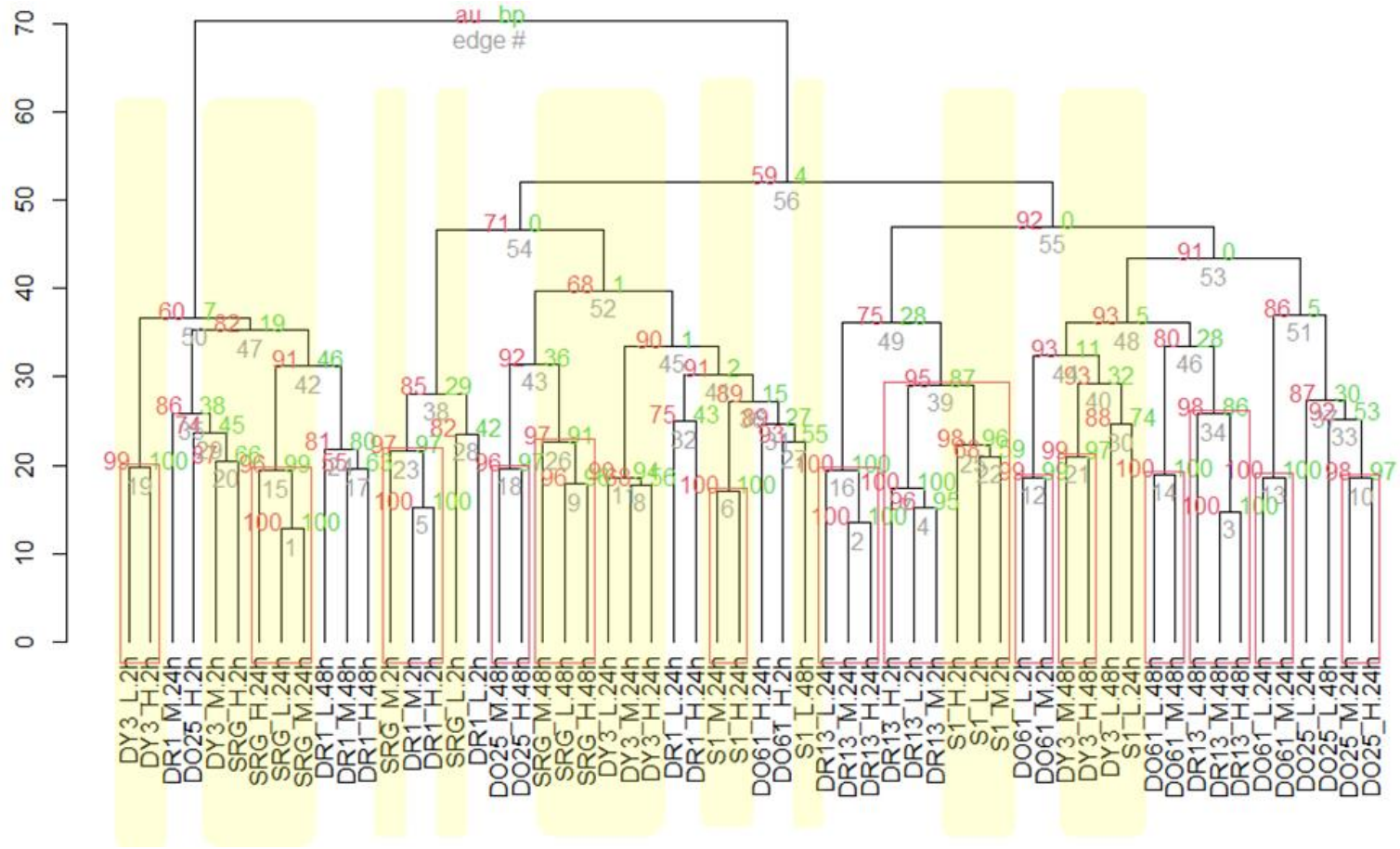


**Figure 3.8** Dendrogram resulting from the 'all results' approach for all 58 groups (i.e. maximum of 9 dose/time treatment groups per dye) comparison of transcriptomics. At least 10 and up to 15 possible L+M+H dose clusters are observed for all 1889 genes. Example L+M+H (low, medium, high) dose clusters are highlighted (yellow shading). AU (approximately unbiased) *p*-values are shown in red and BP (bootstrap probability) values for each cluster are shown in green.

### 3.7.2 Azo dye grouping patterns revealed by the HCA 'max. perturbation' approach

Figures 3.9-11 illustrate more interpretable dendrograms (with AU *p*-values) resulting from the hierarchical cluster analyses of the acute omics datasets based on the largest observed molecular effect in the exposed *Daphnia*. The first observation from these 21-group analyses is that L+M+H (low, medium, high) dose clusters are formed for any given dye, providing evidence of similarity in omics responses that are consistent with responses observed when all 58 treatment groups are considered (as discussed section 3.7.1). Also, the highest overall number of these distinct clusters are again observed for multi-omics analyses integrating all three data streams (polar metabolomics, lipidomics and transcriptomics).

The second observation is that while three major clusters form in all three dendrograms, the clearest pattern consistently emerges from multi-omics analyses, as illustrated in Figure 3.10. There are two distinct groups of disperse red and orange dyes, and the third cluster contains the three dyes of interest (S1, DY3, SRG) that were identified as similar in the initial grouping hypothesis using conventional approaches (see section 3.4). The stability of this cluster is evidenced by high AU *p*-values that increase from 72% for polar metabolomics + lipidomics (Figure 3.9) to 94% for multi-omics derived grouping (Figure 3.10).

Individual omics produce similar results, but with lower confidence (Figures 3.9 and 3.11, respectively). This is consistent with the results revealed by the 58-group HCA analyses presented in the previous section.

These findings clearly demonstrate that polar metabolomics and lipidomics responses are capable of revealing deep grouping patterns for the dyes as part of a multi-omics approach. While conventional approaches suggest that the two sudan dyes and DYR3 azo dye are similar, the inclusion of mechanistic omics-derived data in the G/RAx workflow allows to fine tune the approach and confidently identify a possible ‘source’ and ‘target’ (S1 and DY3) for subsequent read-across within the SRG-S1-DY3 cluster, as shown in Figure 3.11. Given the similarity of molecular responses between S1 and DY3, a specific toxicity endpoint (e.g. for NOEC or LOEC, no and lowest observed effect concentrations, respectively) could be ‘read-across’ (or predicted) for one of the dyes (e.g. from S1 ‘source’ to DY3 ‘target’). However, this hypothesis would require further validation with experimental data, e.g. by conducting 21-day reproductive toxicity studies for both dyes, applying benchmark dose (BMD) modelling and comparing the derived NOEC/LOEC values for S1 and SRG.

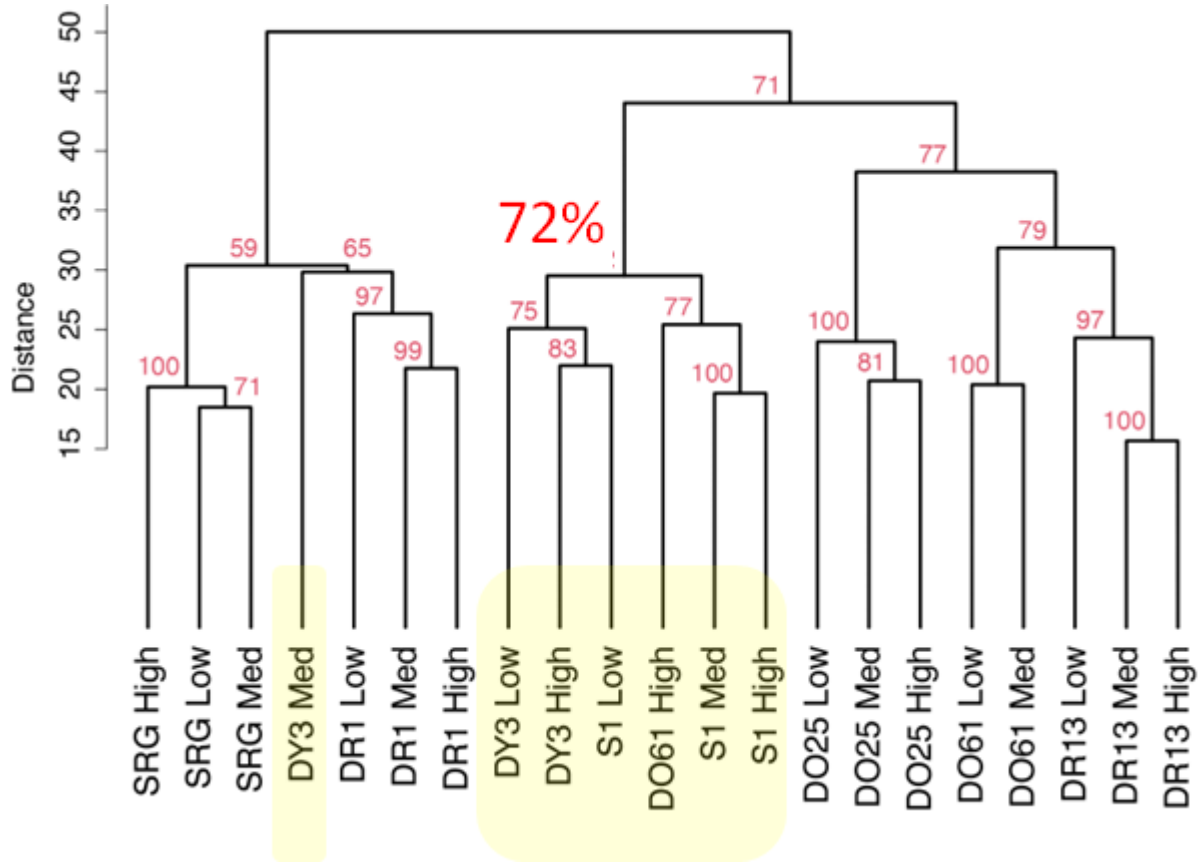


**Figure 3.9** Dendrogram resulting from the 'maximum perturbation' approach for 21 groups (single time point) comparison of polar metabolomics and lipidomics. Four L+M+H (low, medium, high) dose clusters are observed for all 428 features. The cluster containing SRG, S1, DY3 (yellow shading) shows 72% AU values.

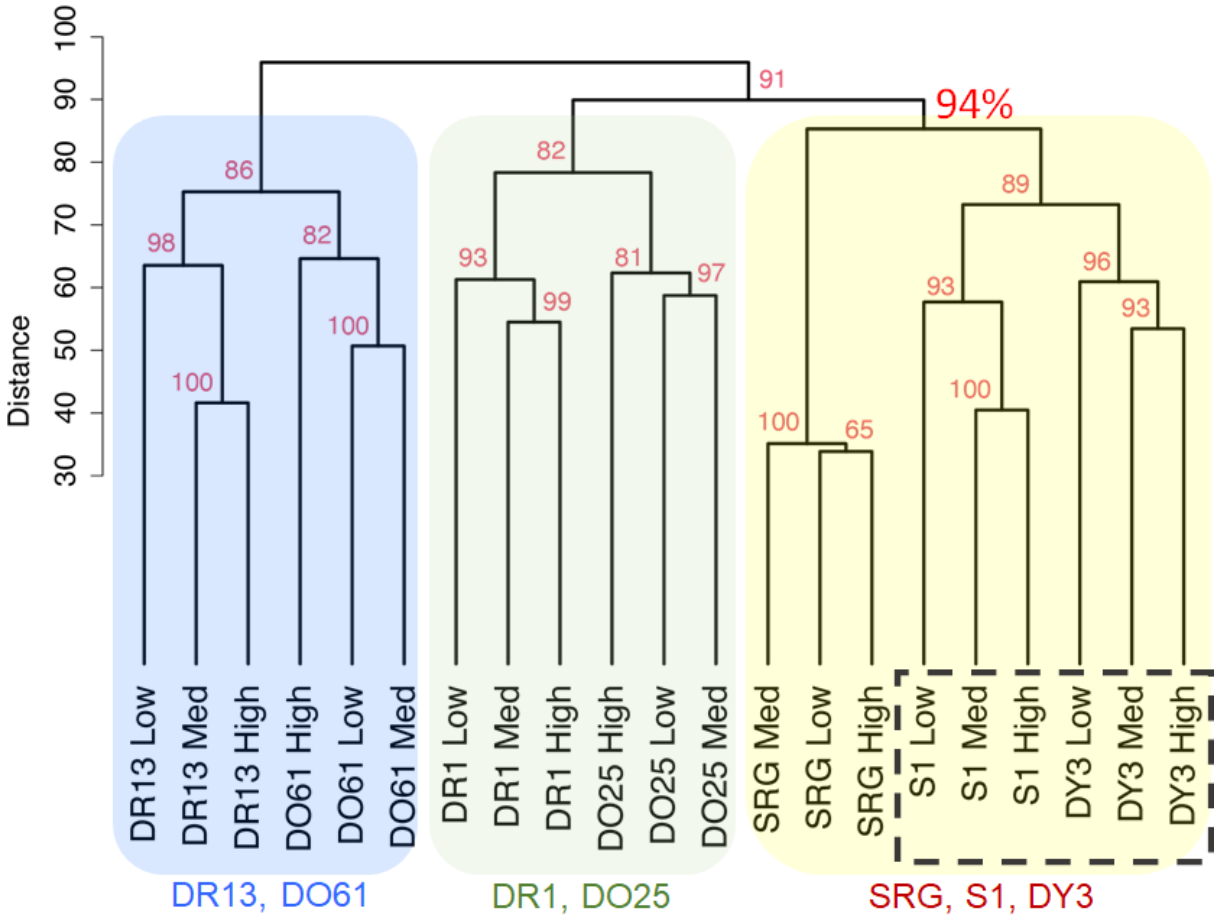


**Figure 3.10** Dendrogram resulting from the 'maximum perturbation' approach for 21 groups (single time point) comparison of all omics features (polar metabolomics, lipidomics and transcriptomics). Seven of L+M+H (low, medium, high) dose clusters are observed for all 2317 features. Three major clusters are formed, the cluster containing SRG, S1, DY3 (yellow shading) shows high confidence 94% AU values. Dashed line indicates that S1 and DY3 azo dyes are most similar, allowing to select a potential 'source' and 'target' for subsequent read-across.

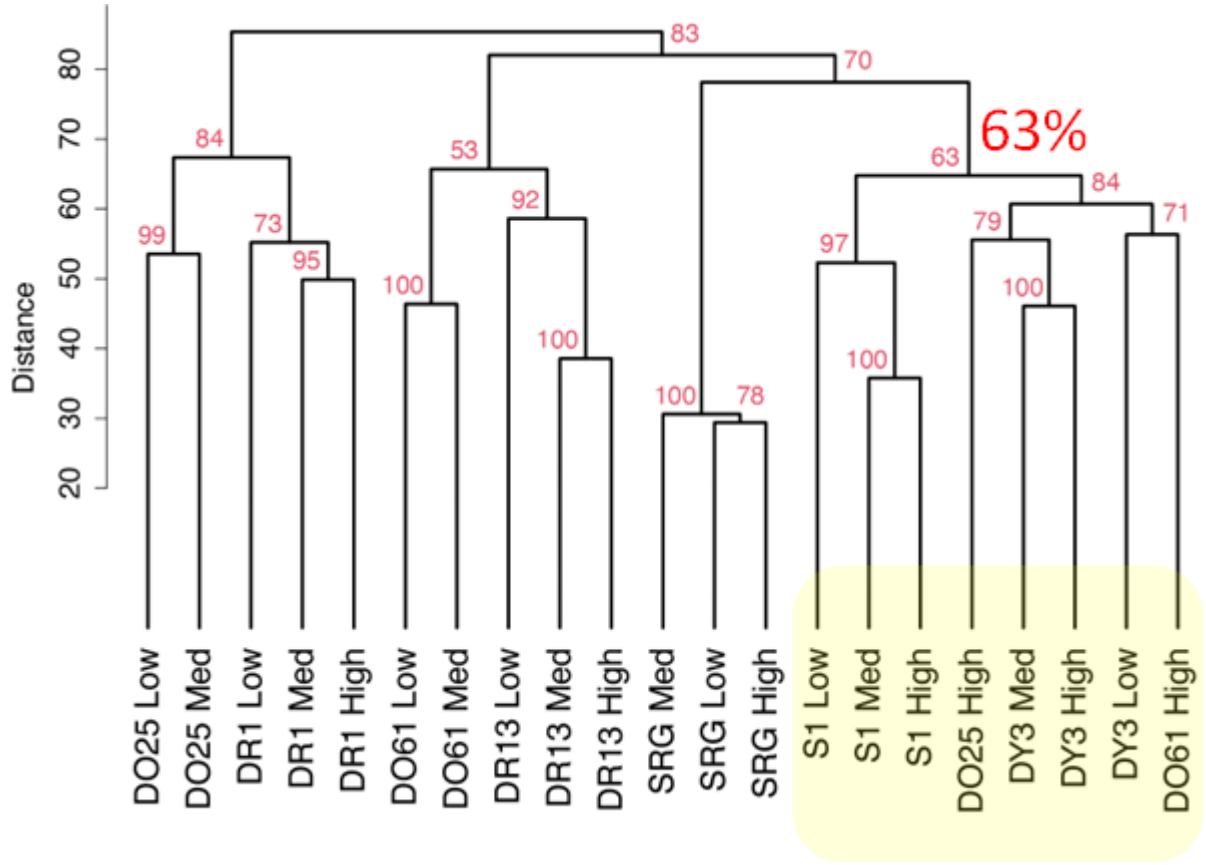


**Figure 3.11** Dendrogram resulting from the 'maximum perturbation' approach for 21 groups (single time point) comparison of transcriptomics. Five L+M+H (low, medium, high) dose clusters are observed for all 1889 genes. The cluster containing SRG, S1, DY3 (yellow shading) shows 63% AU values.

## 3.8 Conclusions and further work

The aim of the work presented in this chapter was to assess the capabilities of multi-omics (specifically, polar metabolomics, lipidomics integrated with transcriptomics) to form categories of seven azo dyes based on the molecular perturbations induced in *Daphnia magna* following acute (48 h) exposures. With the above in mind, the first objective was achieved by developing and implementing a grouping workflow that integrated high-throughput untargeted nESI-DIMS (1,961 analyses) and targeted

BioSpyder transcriptomics analyses (further 339 analyses). The experimental design incorporating three doses and three sampling time points across three omics assays was implemented to maximise the chance of detecting molecular-level perturbations in the *Daphnia*.

The initial grouping hypothesis (mainly based on structure) revealed some similarities between three dyes of interest: S1, SRG and DY3. Specifically, all three dyes were classified as non-polar narcotics (i.e. exhibiting no specific MoA) and phenols, applying conventional *in silico* approaches (various (QS)AR tools and ClassyFire) that are frequently utilised in regulatory toxicology to predict toxicity in the absence of experimental data. However, it should be noted that accuracy of (Q)SAR predictions for aquatic toxicity for non-specific acting chemicals, such as azo dyes, is inherently limited[240].

This initial structure-based grouping hypothesis was substantiated and refined by incorporating omics data in the workflow to unravel a deeper biology-driven grouping pattern among the dyes, considering both 58 possible groups ('all treatments' approach) and the 'maximum perturbation' approach (21 groups). Untargeted metabolomics clearly demonstrates its capability to form categories of the seven azo dyes based on the unidentified (MSI Level 4) *m/z* features and a grouping pattern emerges, particularly when considering the largest azo dye-related molecular perturbations in *D. magna* (21 groups). However, the confidence in the observed cluster for the three dyes of interest (S1, DY3 and SRG) is further strengthened by applying the combination of all three omics data streams (increasing from 72% to 94%, respectively), suggesting that multi-omics indeed increases sensitivity of this approach.

This allows to identify similarities (or dissimilarities) among the two sudan dyes and DY3 with higher precision and confidence (compared to the conventional methods presented in section 3.4), in order to guide selection of possible chemicals for subsequent read-across (here, proposed S1 and DY3 dyes), ultimately leading to more accurate toxicity predictions.

The study also highlighted a number of challenges for deeper examination. First, while the selection of data-poor chemicals attempted to address the knowledge gap in toxicity and chemical risk assessment of azo dyes, it is important to note that there is no 'gold standard' method available to validate the grouping results. Secondly, given the dynamic nature of molecular responses in *D. magna*, the proposed G/RAx workflow would further benefit from a strategy that considers the changes in the grouping pattern as a function of exposure time, e.g. similarity could be based on a molecular trajectory (over a time interval), rather than for a specific time point. In addition, the experimental design for future grouping studies could be improved by incorporating positive and negative control chemicals (i.e. artificial outgroups in hierarchical cluster analysis) to provide additional confidence in grouping patterns that emerge from molecular responses in a biological system. For HCA analyses, deriving decision thresholds on the dendrogram in a robust manner requires attention. One way to address this challenge is e.g. by employing a dynamic tree cutting algorithm using the R programming language[241].

In addition, alternative methods could be explored for discriminating groups of azo dyes, such as two-mode clustering (to simultaneously obtain similar groups of experiments and metabolites) based on a genetic algorithm (GA)[220,242]. GA-based

clustering is a multivariate approach that can reveal biologically meaningful clusters in the untargeted mass spectrometry-based metabolomics data and has been successfully applied for pattern recognition and pathway analysis, also in combination with a neutral network (NN), a deep learning (DL) tool[243,244]. The advantage of the extensive GA validation approaches is the identification of metabolites with unstable clustering and gaining information on the homogeneity of the clusters[220]. Also, other DL approaches increasingly applied in drug discovery and drug development to establish e.g. drug-drug similarity could in principle provide further insights into azo dye similarity predictions. [245]

As extension of the work presented in this chapter, pathway-based metabolite enrichment analysis could be implemented to provide information on the perturbed toxicity pathways and potentially reveal biomarkers of toxicity in response to azo dye exposure, particularly for the three dyes of interest in the study (S1, SRG, DY3) that share similarities in molecular responses. One caveat in this approach is that it usually requires high level of feature annotation and identification, which presents a formidable challenge if only $MS^1$ level nESI-DIMS data are collected, which is a consistent limitation for most untargeted metabolomics studies.

This chapter investigated azo grouping patterns that emerged from endogenous molecular responses in the exposed *Daphnia.* Another aspect of G/RAx worth exploring is ADME/TK (mainly xenobiotic metabolism). This information could, in principle, complement the azo dye toxicodynamics and add further confidence to the omics-derived grouping presented in this chapter (i.e. by identifying shared biotransformation products), thus contributing to an even deeper understanding of

chemical toxicity. The potential added value of untargeted metabolomics in ADME/TK characterisation of xenobiotics is discussed in chapter 4 of the thesis.

Overall, this proof-of-principle study successfully demonstrated that untargeted metabolomics data can and should be considered, along conventional approaches, to enhance confidence in grouping of the seven azo dyes. While transcriptomics is not the primary focus of this thesis, this study reiterates the benefits of integrating metabolomics with another omics data stream for a more sensitive and comprehensive toxicological evaluation. To the best of my knowledge, the investigations presented in this chapter represent a first multi-omics grouping project of this scale conducted on data-poor chemicals to demonstrate concepts of biology-based G/RAx in the context of regulatory toxicology. As such, despite its certain limitations, this study is an early but important step towards building more solid grouping and read-across cases, ultimately accelerating regulatory acceptance of untargeted metabolomics approaches.

# CHAPTER 4 – REVEALING ADME/TK INFORMATION EXISTING WITHIN UNTARGETED nESI-DIMS METABOLOMICS OF *DAPHNIA MAGNA* EXTRACTS FROM ACUTE AZO DYE TOXICITY STUDIES

## 4.1 Introduction

As previously highlighted, untargeted metabolomics is a promising approach that can potentially be applied in various regulatory contexts, including chemical grouping to enable biologically-driven read-across, hazard (or adverse outcome) identification and deriving molecular points-of-departure (PODs) via benchmark dosing[3,68,76]. There is a growing interest of the regulatory toxicology community in exploring and promoting acceptance of new predictive toxicology approaches to accelerate the applications of metabolomics in chemical safety assessment[3,83,246]. In particular, the integration of toxicokinetics and toxicodynamics information in NAMs for chemical safety assessment remains an active area of development[5,247,248].

Untargeted toxicokinetics (TK) and the measurement of the absorption, distribution, metabolic biotransformation and/or elimination (ADME) of a xenobiotic, specifically within an untargeted metabolomics experiment, is a relatively under-researched area in toxicology and industrial chemical safety[3,29]. As internal concentration of a xenobiotic largely drives the magnitude of the final adverse effect, TK/ADME properties are an important consideration alongside mechanistic evidence in the development of quantitative AOP, bridging the gap between descriptive knowledge and the prediction of the adverse outcome[46,249]. Consequently, information on xenobiotic metabolism and

disposition can in principle play a key part in evaluating the systemic exposure and its relationship to temporal dose-toxicity responses induced by the xenobiotic (and its metabolites) thus improving the quality of hazard assessment strategies[250].

Regulatory agencies increasingly recognise that robust ADME/TK data has the potential to not only substantiate grouping and read-across cases in the chemical safety evaluation, but also reduce the uncertainty in such assessments[79,80,251]. However, the associated costs, time delays and technical challenges of conducting separate ADME/TK studies call for a more practical approach of collecting relevant TK data within the same toxicity testing assay[80,208].

Information on xenobiotic disposition and metabolism can strengthen the biological evidence[107,109], particularly for negative read-across (i.e., for chemicals with low or no toxicity) and can also be utilised for justification of conflicting experimental endpoints of structurally similar substances[252] . However, toxicokinetic similarity of substances is often associated with high uncertainty due to inadequacy of experimental ADME/TK data that can hinder its application in grouping and read-across[103,108]. Also, the lack of ADME data for many industrial chemicals and poor understanding of their diverse metabolic behaviour that covers a very broad chemical space poses a significant challenge for accelerating the inclusion of ADME/TK information in chemical risk assessment[109,253,254].

The recent work of Bowden *et al*.[6] (*manuscript under review*) demonstrated that information on the relationships between the toxicokinetics and toxicodynamics can indeed be obtained from the same untargeted toxicometabolomics data that were collected to investigate the molecular toxicity responses to xenobiotics. A newly

developed multi-step data processing and analysis ADME/TK computational workflow was previously successfully applied to $MS^2$ data from UHPLC-MS (ultrahigh performance liquid chromatography mass spectrometry) untargeted metabolomics experiments to explore drug metabolism of two model cardiotoxins in rat plasma and cardiac tissue[6].

In light of the above-described considerations, the overarching aim of the work presented in this chapter was to demonstrate that the untargeted ADME/TK workflow (after Bowden *et al*.[6]), with slight modifications, can be successfully applied to untargeted $MS^1$ nESI-DIMS metabolomics data to extract xenobiotic (i.e. exogenous) azo dye-related features from the same metabolomics experiment that was principally designed to probe the endogenous toxicity responses to azo dye exposure in the *D. magna* grouping study (see chapter 3). The first objective of the research was to apply the multi-step ADME/TK workflow to three $MS^1$ nESI-DIMS datasets (specifically, lipidomics in positive ion mode only and polar metabolomics in both positive and negative ion modes) to provide confirmation of internal chemical exposure in the acute (48 h) study for each of the seven azo dyes and relate these findings to external dosing. Secondly, the ADME/TK information contained in all three nESI-DIMS datasets was explored to gain insights into the metabolism and metabolic fate of the azo dyes under study by revealing the metabolic biotransformation product(s). A series of criteria were derived to gain further confidence in these putative annotations. The third objective was to provide a crude visualisation of the uptake, metabolic biotransformation and clearance rates (i.e., TK measurements) of the azo dye parent chemicals from the biological test system, *D. magna*.

## 4.2 Materials and methods

### 4.2.1 Metabolite extractions and untargeted nESI-DIMS metabolomics of *Daphnia magna* extracts

The same methods were used as previously described in chapter 2 (see section 2.3 – untargeted nESI-DIMS metabolomics). Briefly, metabolites were extracted manually from *Daphnia* neonates (5-6 animals per sample) using a well-established bead-based homogenisation and biphasic extraction (with a final ratio of chloroform:methanol:water of 2:2:1.8) protocol[8,57,58,217]. Extraction (or process) blanks (containing no biological material) were prepared in the same manner with each sample batch to identify and eliminate any possible sources of contamination that arise from sample processing. Immediately prior to analysis, dried *Daphnia* extracts were resuspended in 25 µL of 4:1 methanol:water (v/v, Honeywell, Merck) containing a total of 0.1% formic acid (v/v, Merck) for polar metabolomics samples and 40 µL of 2:1 7.5 mM methanolic ammonium acetate:chloroform (v/v, Merck) for non-polar lipidomics samples. Both polar and non-polar extracts were centrifuged to remove any suspended particulates and debris prior to being plated onto a 384-well Eppendorf plate (15 µL for polar and 24 µL for non-polar extracts).

For clarity, the nESI-DIMS analyses were conducted in the same manner as described in section 2.3. The data acquisition parameters were as previously detailed[8] with minor modifications to optimise the sample biomass required in order to yield higher analytical sensitivity of nESI- DIMS measurements of low biomass *D. magna* neonate samples (see section 3.3 – *Daphnia* biomass optimisation study). The data were

acquired in two ion modes: positive (to profile polar and lipid metabolites) and negative (to measure polar metabolites).

For each metabolomics dataset corresponding to the seven azo dyes studied (3 assays per each dye), nESI-DIMS mass spectra were subsequently pre-processed using DIMSPy package implemented in Galaxy (https://github.com/computational-metabolomics/dimspy-galaxy)[8]. Peak picking, spectral SIM-stitch, sample alignment and blank filter (to remove contaminant peak arising from the extraction process) were applied as previously reported (see section 2.4)[8,150]. The resulting three data matrices containing both endogenous and exogenous features for all seven azo dyes were then subjected to dye-specific TK/ADME analyses.

### 4.2.2 Applying the untargeted xenobiotic processing workflow to nESI-DIMS datasets

The objective of this part of the project was to obtain evidence of internal chemical exposure of *D. magna* to each azo dye and gain insights into the absorption, distribution, metabolic transformation and/or elimination (ADME) of the seven azo dyes within the exposed *Daphnia*. This was achieved by interrogating ADME/TK information derived from the untargeted nESI-DIMS measurements obtained from the same biological samples that were used for the investigation of endogenous responses to the seven dyes in the acute (48 h) toxicity study, as detailed in chapter 3.

A new untargeted ADME/TK workflow reported in Bowden *et al*[6] (*manuscript under review*), with slight modifications, was applied to the three nESI-DIMS metabolomics and lipidomics datasets (specifically, $MS^1$ spectra) for each azo dye to reveal any

toxicokinetic/ADME information existing within the untargeted nESI-DIMS measurements. The overall workflow for the extraction and visualisation of TK features detected in the untargeted metabolomics datasets is shown in Figure 4.1 (adapted from Bowen *et al*.[6]). Briefly, the nESI-DIMS datasets were first pre-processed (peak picking and noise filtering, as described above) using the DIMSPy Galaxy platform. The resulting blank-filtered data matrix was subsequently processed in the R environment (version R-4.0.3), using a three-stage filter to retain only features arising from the seven azo dyes and their potential biotransformation products (BTPs). Those filters are: (1) features must be present in >80% of all treated high (H) dose biological samples for each dye; (2) features must be present in <50% of all untreated dye-specific control (C) samples; and (3) a >10 median fold change of peak intensities between high dose and untreated control samples. Subsequent exploratory correlation analysis of the putative azo dye-related features was conducted to reveal any associations among specific dye-related features across the high dose treated samples. Next, the TK-filtered azo dye-related feature intensity was normalised to account for subtle differences in mass spectral intensities using the scaling factor derived from the PQN normalisation of the endogenous features in the same biological samples (see section 2.4).

The resulting azo dye-related feature intensity matrix was putatively annotated to at least MSI Level 3[10,184] using the list of *in silico* predicted metabolic biotransformation products (Systematic Generation of potential Metabolites; SyGMa) for each azo dye (using SyGMa python library operated in Galaxy[255]). The number of phase I and phase II biotransformation steps were set to 3 in SyGMa. Predictions with identical molecular formulae were merged and only predictions with SyGMa probability score ≥0.01% were

retained to provide further confidence that a given theoretical biotransformation product is metabolically generated in a biological system[255]. The SyGMa predicted metabolites for each of the azo dyes were matched against the putative azo dye-related features with mass error tolerance of ±5 ppm for lipidomics, and ±10 ppm for metabolomics (thresholds determined by examining the system suitability quality control data, see section 3.6 in chapter 3).

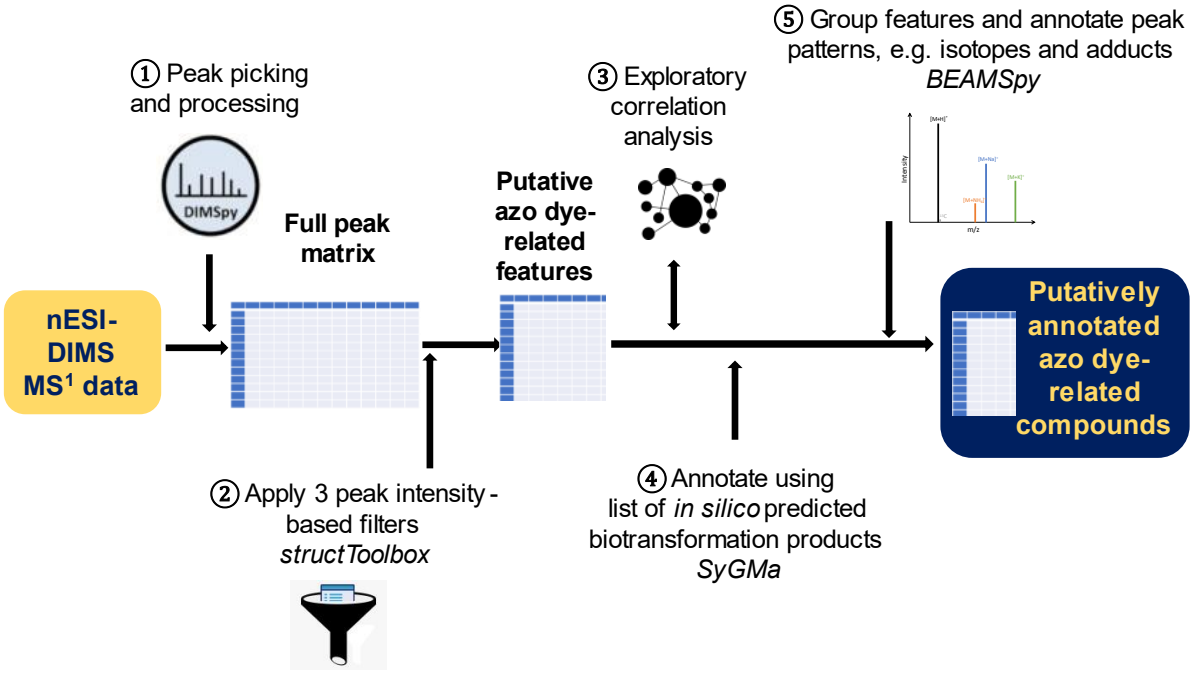


**Figure 4.1** Overview of untargeted xenobiotic processing workflow for the extraction and visualisation of xenobiotics and their biotransformation products applied to untargeted $MS^1$ nESI-DIMS metabolomics data (adapted from Bowen *et al.*[6]). (1) Full scan $MS^1$ data undergoes pick picking and processing using DIMSpy to generate a 'full peak matrix', (2) a series of 3 intensity-based filters are applied to produce a list of 'putative azo dye-related features' which is further explored by (3) correlation analysis to reveal any relationships between features. (4) Annotation of compounds using a list of expected biotransformation products generates a list of annotated azo dye-related compounds. (5) Grouping of features and annotations of peak patterns.

In addition, normalised relative *m/z* intensities (associated with internal relative concentrations) of all putatively annotated azo dye-related features (i.e., the parent chemical and any metabolic biotransformation products detected) were examined to identify any dose-response relationships as a function of time, which provided further indirect evidence for the putative annotations. Finally, the putatively annotated azo dye BTPs were assigned Markush structures[256] (as explicit metabolite structures and precise sites of metabolism could not be predicted solely from nESI-DIMS $MS^1$ data) to determine if a given feature could be explained by common phase I and phase II modifications predicted by SyGMa.

Further confidence was achieved by conducting ion form annotation and correlation-based grouping (to MSI Level 3) of the putative SyGMa annotations by the application of the the Python package, BEAMSPy (Birmingham mEtabolite Annotation for Mass Spectrometry Python package, v0.1.0; https://more.bham.ac.uk/beams/) pipeline operated in Galaxy to identify multiple metabolic features (isotope or adduct patterns) common to a single azo dye, using a ±5 ppm mass error window. The list of adducts and isotopes selected to annotate peak patterns was set to default.

A series of criteria derived to putatively annotate the azo dye parent chemicals and their potential biotransformation product(s) are summarised in Figure 4.2.

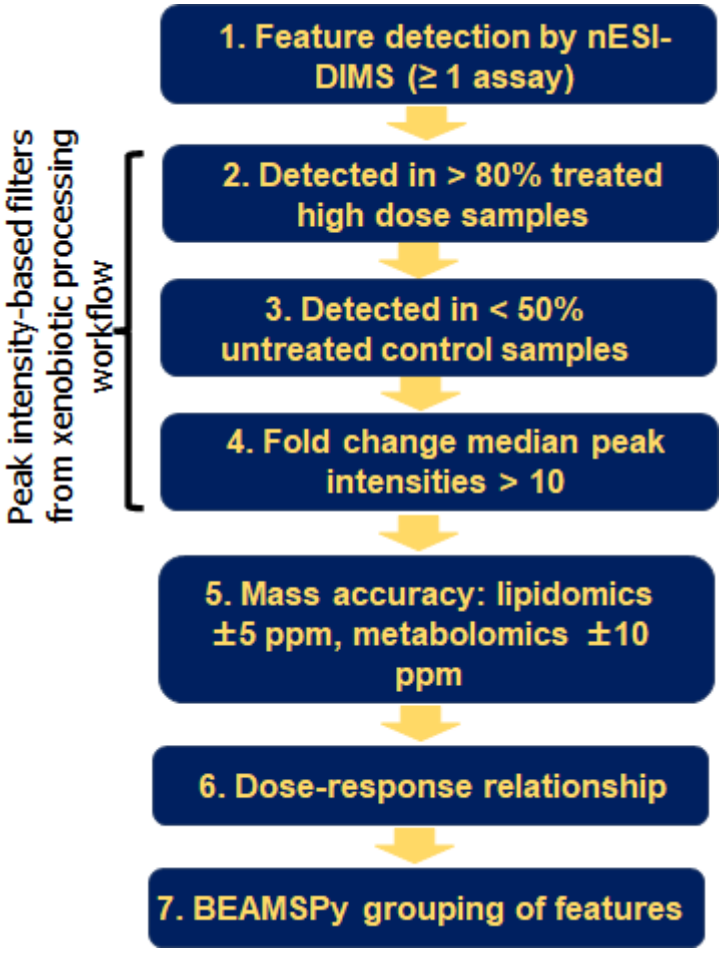


**Figure 4.2** Summary of data-driven and knowledge-driven criteria used for SyGMa-derived putative annotations (at least MSI Level 3) of azo dye-related features in the nESI-DIMS $MS^1$ data.

## 4.3 Results and discussion

The modified untargeted xenobiotic processing workflow was applied to the *D. magna* nESI-DIMS datasets (specifically, $MS^1$ spectra of lipids in a positive ionisation mode, and polar metabolites in both positive and negative ionisation modes) for each dye to obtain evidence of internal chemical exposure, evidence of azo dye metabolism, and to provide crude visualisation of metabolic clearance from the exposed *Daphnia*.

### 4.3.1 Evidence of internal azo dye exposure

The following subsections describe the steps in the workflow and a series of criteria derived to putatively annotate the azo dye parent chemicals in the three nESI-DIMS datasets to obtain estimates of the relative internal concentrations of these chemicals in the *Daphnia*.

#### 4.3.1.1 Discovering azo dye-related features in nESI-DIMS datasets

First, the three intensity-based ADME/TK filters (as described in section 4.2.2) were applied to the full blank-filtered data matrix (containing unannotated endogenous and exogenous features related to the seven dyes) for each of the three nESI-DIMS datasets separately. The application of the TK filters to the full blank-filtered peak matrix from the lipidomics assay yielded different numbers of putative azo dye-related features for each of the seven dyes, ranging from 3 (for S1) to 363 (for SRG). The same filtering was also applied to the polar metabolomics datasets in both positive and negative ionisation modes (each data matrix comprising 114,525 and 28,289 features, respectively), extracting at least two exogenous features for the three dyes of interest (S1, DY3 and SRG). The summary of the numbers of features (detected in the treated high dose samples for each dye) before and after the implementation of the xenobiotics processing workflow filters is presented in Table 4.1.

**Table 4.1** Number of putative azo dye-related features discovered in untargeted nESI-DIMS datasets (per dye, per assay) following the application of the intensity-based ADME/TK filters to the full data matrix. Key: **[1]** No. of unannotated features in the full peak matrix (containing all seven azo dyes); **[2]** No. of features present in 80% treated high (H) dose samples and <50% untreated controls (C); **[3]** No. of putative azo dye-related features with H/C intensity fold change > 10. Abbreviations: L(+) – positive lipidomics, M(+) – polar positive metabolomics, M(-) – polar negative metabolomics.

| **Azo dye** | **nESI-DIMS L(+)** | | | **nESI-DIMS M(+)** | | | **nESI-DIMS M(-)** | | |
|---|---|---|---|---|---|---|---|---|---|
| | **[1]** | **[2]** | **[3]** | **[1]** | **[2]** | **[3]** | **[1]** | **[2]** | **[3]** |
| **S1** | 59,442 | 35 | 3 | 114,525 | 187 | 2 | 28,289 | 10 | 4 |
| **DY3** | | 51 | 43 | | 56 | 27 | | 32 | 17 |
| **SRG** | | 439 | 363 | | 66 | 4 | | 21 | 19 |
| **DO61** | | 20 | 6 | | 10 | 0 | | 5 | 0 |
| **DO25** | | 98 | 12 | | 13 | 1 | | 4 | 0 |
| **DR1** | | 13 | 10 | | 9 | 1 | | 7 | 0 |
| **DR13** | | 15 | 6 | | 32 | 0 | | 41 | 0 |

Following the ADME/TK filtering, seven lists of expected metabolic biotransformation products of the azo dyes (one metabolic profile per dye) were generated using SyGMa *in silico* prediction tool[255]. The original SyGMa outputs were subsequently filtered to SyGMa probability score ≥0.01% and predictions with identical molecular formulae were merged resulting in between 28 and 40 distinct molecular formulae, including the parent chemical for each of the seven azo dyes (Table 4.1). The last step was to putatively annotate the TK-filtered matrix using these filtered SyGMa outputs for each dye.

In addition, grouping of SyGMa-annotated features conducted on BEAMSPy revealed correlations between putatively annotated azo dye-related features across treated high dose samples for S1, DY3 and SRG. This added an additional level of confidence to their predicted origin from the parent chemicals.

The highest number of azo dye biotransformation products was discovered in the nESI-DIMS lipidomics dataset (Table 4.2). Specifically, the parent chemical was putatively annotated against the TK-filtered nESI DIMS lipidomics data for six azo dyes except for DO25, where the parent chemical was present at a lower fold change (FC<10) and therefore did not survive the original TK filtering parameters. In addition, at least one biotransformation product was detected for three azo dyes (S1, DY3 and SRG) in the same dataset.

**Table 4.2** Number of *in silico* predicted biotransformation products for the seven azo dyes (SyGMa score ≥0.01%) and number of SyGMa annotated azo dye-related features in the filtered datasets (per dye, per assay), using the TK-filtering settings summarised in **Figure 4.2**.

| Azo dye | S1 | DY3 | SRG | DO61 | DO25 | DR1 | DR13 |
|---|---|---|---|---|---|---|---|
| No. of SyGMa predicted biotransformation products per dye, inclusive of parent chemical | 28 | 39 | 39 | 30 | 30 | 40 | 40 |
| No. of SyGMa annotated azo dye-related features in **lipidomics positive nESI-DIMS dataset** | 2 | 5 | 3 | 1 | 2[a] | 1 | 1 |
| No. of SyGMa annotated azo dye-related features in **polar positive metabolomics nESI-DIMS dataset** | 1 | 3 | 2[c] | 0 | 1[b] | 1 | 0 |
| No. of SyGMa annotated azo dye-related features in **polar negative metabolomics nESI-DIMS dataset** | 2 | 5[d] | 4 | 0 | 0 | 0 | 1[e] |

[a]Two DO25-related features did not pass the fold change filter (i.e. FC<10 for these features).
[b]Tentative DO25 parent.
[c]Tentative SRG parent (FC<10).
[d]Two DY3-related features (including the parent) were present in <80% high dose samples.
[e]Feature present in <80% high dose samples.

The polar metabolomics dataset (acquired in positive ion mode) reveals the presence of the parent chemical for four out of seven dyes (S1, DY3, SRG and DR1) and additional biotransformation products were also putatively annotated for DY3 and SRG (two and one, respectively). No xenobiotic-related features were discovered for DO61 and DR13 in this dataset, suggesting that the two azo dyes were present below the limit of the detection (LOD) for the nESI-DIMS polar metabolomics assay.

The nESI-DIMS polar metabolomics dataset measured in negative ion mode was also interrogated for the presence of xenobiotic-related features. The assessment of the system suitability data and peak count relative to the other two nESI-DIMS datasets indicates that this is a problematic dataset and was therefore disregarded from the main azo dye grouping study (with endogenous metabolites, see section 3.6 in chapter 3) but was subjected to TK-filtering to offer potential insights into the azo dye internal exposure levels and metabolism, therefore providing additional level of confidence particularly if the same putative annotations were discovered across multiple nESI-DIMS assays. Initially, S1 and SRG parent chemicals and related biotransformation products (one for S1 and three for SRG) were putatively annotated in this dataset (Table 4.3). However, due to the data quality, slightly less stringent TK filters (i.e., feature present <70% high dose samples) were applied to this dataset revealing the presence of an additional three tentative annotations, including DY3 parent chemical, a further DY3 biotransformation product and a DR13 biotransformation product (present in 67%, 72% and 78% high dose samples, respectively; Tables 4.2 and 4.6).

#### 4.3.1.1 Mass accuracy of azo dye-related features discovered in nESI-DIMS datasets

Mass error tolerance of ±5 ppm for the lipid dataset and ±10 ppm for both polar metabolomics datasets was determined based on the assessment of the system suitability quality control (QC) samples analysed in triplicates at the beginning and end of each analytical sequence for all three nESI-DIMS assays (as described in section 2.3).

The azo dye-related putative annotations in the nESI-DIMS lipidomics dataset show sub ±5 ppm mass accuracy for the majority of the features (except for the S1 parent chemical and its biotransformation product, and DR13 parent chemical), thereby increasing confidence in these annotations (Table 4.3). Also, all reported *m/z* errors are positive values and errors for DR1 and DO61 average to an error of about 1.6 ppm suggesting that a slight drift in calibration occurred over the course of the analytical run.

Mass accuracy for the azo dye-related putative annotations in both positive (Table 4.4) and negative ESI-DIMS polar metabolomics datasets (Table 4.5) falls below the ±10 ppm threshold for all the detected features, both parent chemicals and their biotransformation products. In addition, the S1 parent and DY3 parent chemicals were detected with sub ±5 ppm mass error tolerance within the positive metabolite dataset: 2.01 ppm and 4.26 ppm, respectively (Table 4.4). Mass measurement errors are generally higher in the negative metabolite dataset except for the S1 parent chemical which was detected with the mass error of -2.16 ppm. Higher mass errors can be explained by the overall lower quality of this dataset which is reflected in lower peak count and mRSD values compared to the other nESI-DIMS datasets (see section 3.6). Also, the azo dye-related putative annotations measured in the negative metabolite dataset are lower intensity features which can result in lower mass measurement accuracy[257].

**Table 4.3** Mass measurement accuracy comparisons for the azo dye-related features discovered in the lipidomics positive nESI-DIMS dataset.

| Dye biotransformation product (BTP) | BEAMS feature ID | Theoretical SyGMa m/z of $[M+H]^+$ ion | Measured nESI-DIMS m/z of $[M+H]^+$ ion | Mass error (ppm) |
|---|---|---|---|---|
| **S1 parent** | M2376 | 249.10223 | 249.10364 | 5.7 |
| S1 BTP1 | M3121 | 265.09715 | 265.09864 | 5.6 |
| **DY3 parent** | M3310 | 270.12370 | 270.12398 | 1.01 |
| DY3 BTP1 | M1325 | 228.11314 | 228.11378 | 2.8 |
| DY3 BTP2 | M4055 | 284.13935 | 284.13979 | 1.5 |
| DY3 BTP3 | M4171 | 286.11862 | 286.11906 | 1.5 |
| DY3 BTP4 | M5412 | 308.06995 | 308.07129 | 4.3 |
| **SRG parent** | M1980 | 279.11280 | 279.11286 | 0.2 |
| SRG BTP1 | M2387 | 293.12845 | 293.12917 | 2.4 |
| SRG BTP2 | M2434 | 295.10772 | 295.10858 | 2.9 |
| **DO61 parent** | M19475 | 481.96457 | 481.96487 | 0.6 |
| Tentative **DO25 parent*** | M6553 | 324.14550 | 324.14551 | 0.03 |
| Tentative DO25 BTP1* | M7971 | 342.15607 | 342.15681 | 2.2 |
| **DR1 parent** | M5886 | 315.14517 | 315.14595 | 2.5 |
| **DR13 parent** | M8494 | 349.10619 | 349.10807 | 5.4 |

*FC<10.

**Table 4.4** Mass measurement accuracy comparisons for the azo dye-related features discovered in the polar positive nESI-DIMS metabolomics dataset.

| Dye biotransformation bioproduct (BTP) | BEAMS feature ID | Theoretical SyGMa m/z of $[M+H]^+$ ion | Measured nESI-DIMS m/z of $[M+H]^+$ ion | Mass error (ppm) |
|---|---|---|---|---|
| **S1 parent** | M29228 | 249.10223 | 249.10273 | 2.01 |
| **DY3 parent** | M34544 | 270.12370 | 270.12485 | 4.26 |
| DY3 BTP1 | M45239 | 308.06995 | 308.07216 | 7.17 |
| DY3 BTP2 | M23429 | 228.11313 | 228.11466 | 6.70 |
| Tentative **SRG parent*** | M36623 | 279.11280 | 279.11471 | 6.84 |
| SRG BTP1 | M41341 | 295.10771 | 295.10984 | 7.21 |
| DO25 parent | M49992 | 324.14550 | 324.14758 | 6.44 |
| DR1 parent | M47336 | 315.14516 | 315.14770 | 8.06 |

*FC<10.

**Table 4.5** Mass measurement accuracy comparisons for the azo dye-related features discovered in the polar negative nESI-DIMS metabolomics dataset.

| Dye biotransformation bioproduct (BTP) | BEAMS feature ID | Theoretical SyGMa m/z of $[M-H]^-$ ion | Measured nESI-DIMS m/z of $[M-H]^-$ ion | Mass error (ppm) |
|---|---|---|---|---|
| **S1 parent** | M6059 | 247.08769 | 247.08715 | -2.16 |
| **S1 BTP1** | M7037 | 263.08260 | 263.08427 | 6.34 |
| Tentative **DY3 parent*** | M7376 | 268.10915 | 268.10734 | -6.76 |
| DY3 BTP1 | M9922 | 306.05540 | 306.05527 | -0.42 |
| DY3 BTP2 | M8510 | 284.10407 | 284.10393 | -0.46 |
| DY3 BTP3 | M12990 | 348.06597 | 348.06309 | -8.26 |
| Tentative **DY3 BTP4*** | M4751 | 226.09859 | 226.09719 | -6.16 |
| **SRG parent** | M8018 | 277.09826 | 277.09970 | 5.24 |
| SRG BTP1 | M7037 | 263.08260 | 263.08427 | 6.34 |
| SRG BTP2 | M9062 | 293.09317 | 293.09473 | 5.33 |
| SRG BTP3 | M10140 | 309.08808 | 309.08981 | 5.60 |
| Tentative DR13 BTP1* | M19222 | 427.04846 | 427.04566 | -6.54 |

*Present in <80% high dose samples.

#### 4.3.1.2 Dose-response relationship for azo dye parent chemicals

The highest number of azo dye parent chemicals was discovered in the nESI-DIMS $MS^1$ lipidomics dataset, where all seven dyes were putatively annotated, including a tentative DO25 parent. (This dye was also problematic and challenging to work with from lab-based toxicity experiments through to subsequent data processing and analysis due to low water solubility, see chapter 3). These results are consistent with water solubility data, log $K_{ow}$ values and physico-chemical properties of the dyes (see Table 3.3 in chapter 3) that are more likely to partition into the lipids phase during biphasic extractions. Noteworthily, the S1, DY3 and SRG parent chemicals were consistently detected in all three untargeted toxicometabolomics datasets, providing additional confidence in these putative annotations.

The dose-response was explored for the azo dye parent chemicals to provide information on the uptake and relative internal levels of these xenobiotics within the exposed *Daphnia* at three sampling time points (2 h, 24 h and 48 h). The boxplots of normalised relative intensity measurements show a clear dose-response relationship for each of the three azo dye parent chemicals (S1, DY3 and SRG) in at least one sampling time point in the positive lipidomics and polar metabolomics datasets (Figure 4.3a and b), where the parent concentration clearly increases across the three doses (low, medium and high), therefore providing reassurance that the azo dye dosing using the nominal test concentrations was correct during acute (48 h) *Daphnia* toxicity studies. The dose-response trend is less pronounced and more erratic for the negative polar metabolomics dataset (Figure 4.3c) which is a noisier, problematic dataset with generally lower signal intensities for all three dyes of interest and incomplete data for

DY3 as the dye was only detected in 12 (out of 18 originally collected) high dose samples and was not detected at the lower doses (low and medium). Additional boxplots depicting the increase in the normalised intensities (corresponding to internal relative concentrations) as a function of increasing external doses for all azo dye BTPs measured in the nESI-DIMS datasets are included in Appendix B (Figures B-1 to B-4).

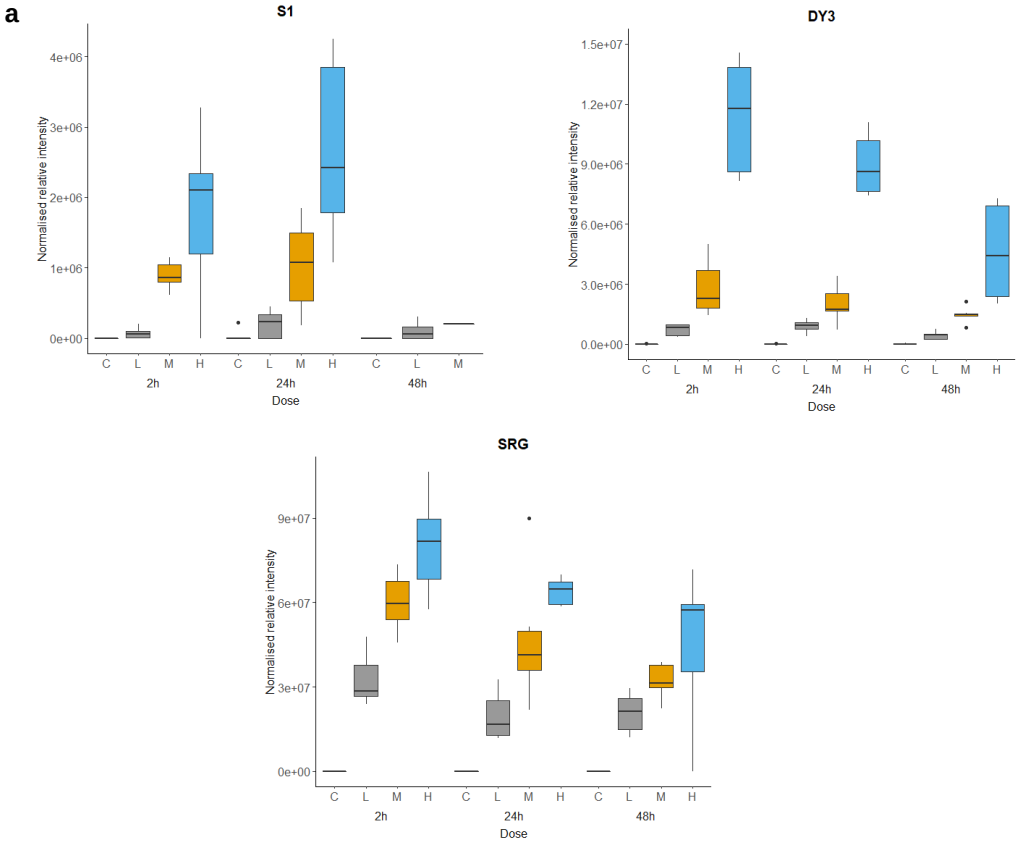
a
S1
DY3
SRG
Normalised relative intensity
Dose
2h
24h
48h
C
L
M
H

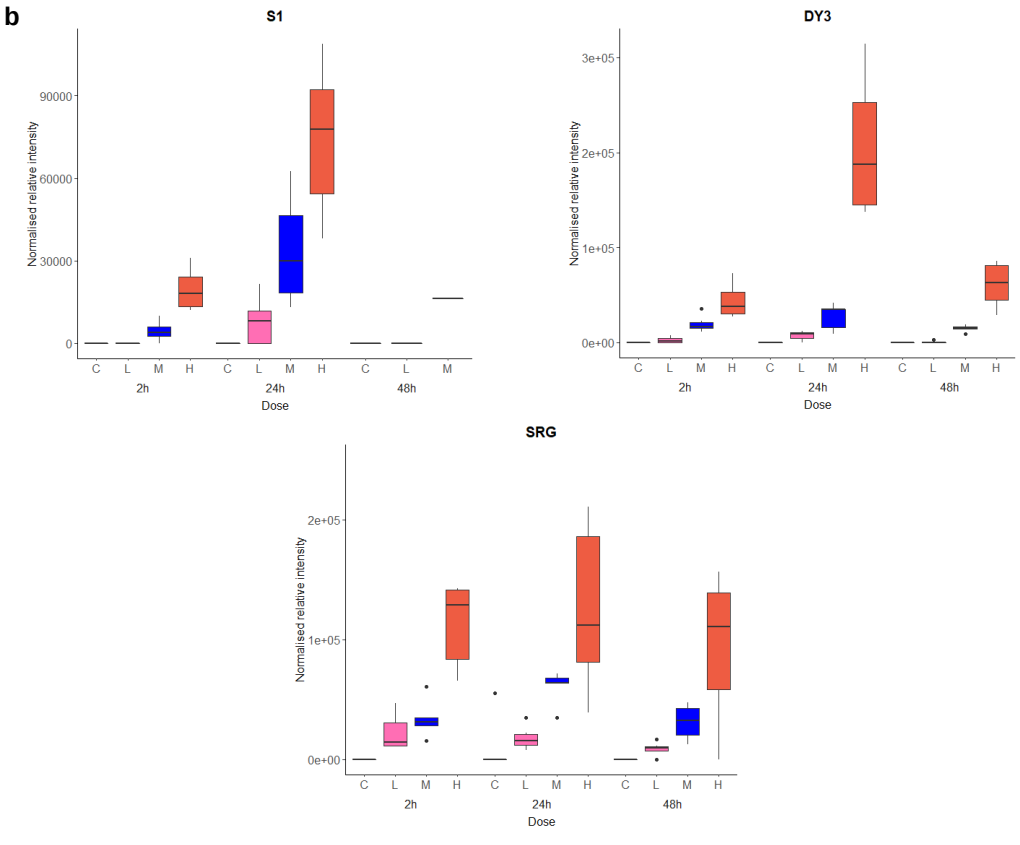
b
S1
DY3
SRG
Normalised relative intensity
Dose
2h
24h
48h
C
L
M
H

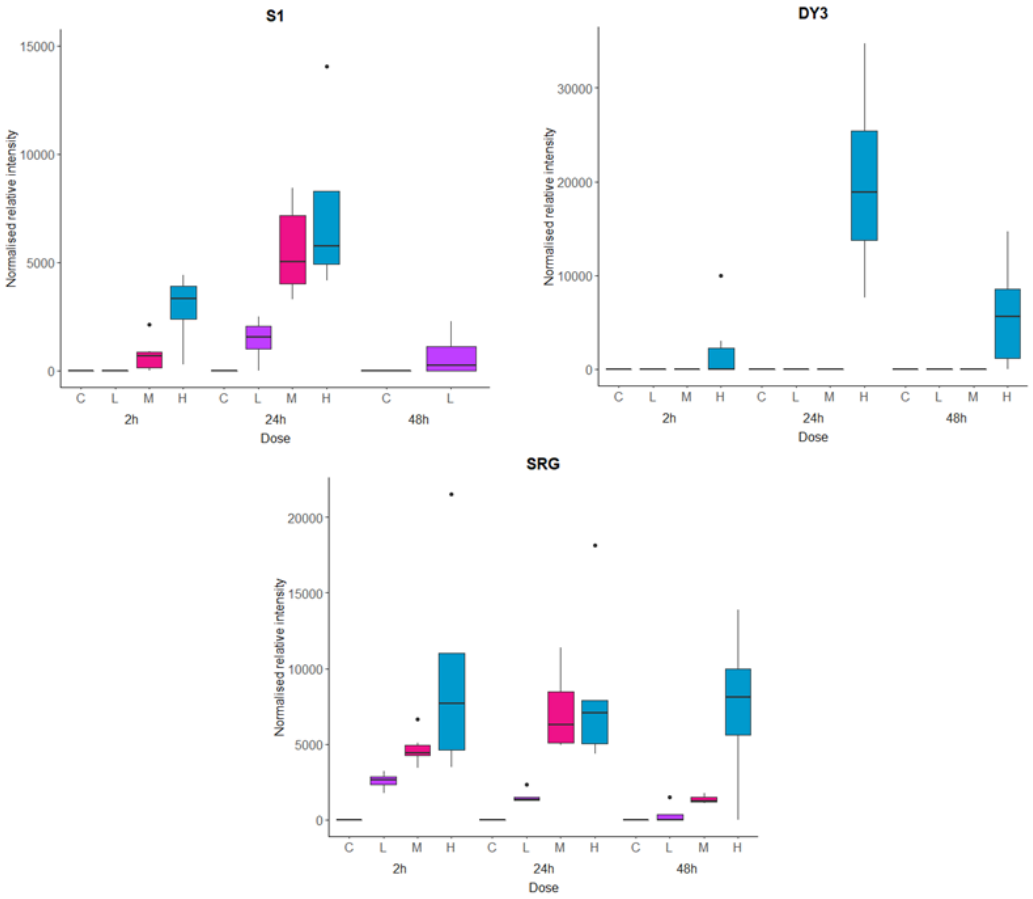


**Figure 4.3** Normalised peak intensities (corresponding to relative internal concentrations) of the azo dye parent chemicals (S1, DY3, SRG) measured across three treatment doses (L – low, M – medium and H – high) and three sampling time points (2 h, 24 h, 48 h) in the three nESI-DIMS datasets: (**a**) lipidomics, (**b**) polar positive metabolomics and (**c**) polar negative metabolomics. Data is missing at 48 h time point for S1.

### 4.3.2 Evidence of azo dye metabolism

In addition to discovering the parent chemicals for all seven dyes, between one and five biotransformation products (BTPs) per dye were detected for S1, DY3 and SRG in at least two nESI-DIMS assays, revealing some differences in azo dye metabolism within the exposed *Daphnia* (Table 4.6, Figure 4.4). The highest number of BTPs was detected for DY3 across multiple nESI-DIMS assays (five BTPs in total), suggesting that DY3 is the most metabolised of the azo dyes. SRG also formed a relatively high number of detectable BTPs across all three assays (four BTPs in total). In contrast, no biotransformations were measured for DO61 in any of the nESI-DIMS assays and one BTP was detected for S1 which may suggest that these dyes are the least metabolised by the *Daphnia*. Also, both dyes have the highest log $K_{ow}$ values (6.47 and 5.51, respectively) indicating higher lipophilicity and therefore potentially higher bioaccumulation potential than DY3.

The majority of biotransformations for all of the azo dyes were detected in the polar negative metabolomics (9 BTPs) and the lipidomics (7 BTPs) assays. These include five phase I modifications: (double) aromatic hydroxylation (S1 BTP1, S1 BTP2, DY3 BTP2, SRG BTP4), *O*-demethylation (SRG BTP3) and six phase II modifications: *N*-deacetylation (DY3 BTP1), methylation (DY3 BTP3, SRG BT1), sulphation (DY3 BTP5), aliphatic sulphation (DR13 BTP1) and *N*-deacetylation followed by sulphation (DY3 BTP4).

Biotransformation maps were proposed for four dyes (S1, DY3, SRG and DR13) showing Markush chemical structures[256] of the BTPs discovered in the nESI-DIMS $MS^1$

datasets, and common biotransformation reactions predicted by SyGMa (Figure 4.4). A common biotransformation product discovered for S1 and SRG may suggest toxicokinetic similarity between the two chemicals that also group together with DY3 in the azo dye grouping study (see chapter 3). In addition, in contrast to the other dyes, S1, SRG and DY3 all have a hydroxyl functional group which might also lead to the formation of some likely 'shared' BTPs among all three dyes, thereby providing further line of evidence to substantiate the grouping pattern derived in chapter 3.

**Table 4.6** Azo dye biotransformation products (putative annotations) discovered in the nESI-DIMS data, per dye and per assay. Abbreviations: L(+) – positive lipidomics, M(+) – polar positive metabolomics, M(-) – polar negative metabolomics.

| | **nESI-DIMS assay** | **S1** | **DY3** | **SRG** | **DO61** | **DO25** | **DR1** | **DR13** |
|---|---|---|---|---|---|---|---|---|
| **Parent chemical detected** | L(+) | ✓ | ✓ | ✓ | ✓ | ✓[a] | ✓ | ✓ |
| | M(+) | ✓ | ✓ | ✓[a] | × | ✓ | ✓ | × |
| | M(-) | ✓ | ✓[b] | ✓ | × | × | × | × |
| **No. of BTPs detected** | L(+) | 1 | 4 | 2 | 0 | 1[a] | 0 | 0 |
| | M(+) | 0 | 2 | 1 | 0 | 0 | 0 | 0 |
| | M(-) | 1 | 4 (incl. 1[b]) | 3 | 0 | 0 | 0 | 1[b] |

[a]Tentative annotation as fold change filtering criteria (FC>10) was not met.
[b]Tentative annotation as high dose filtering criteria (>80%) was not met.

**a**

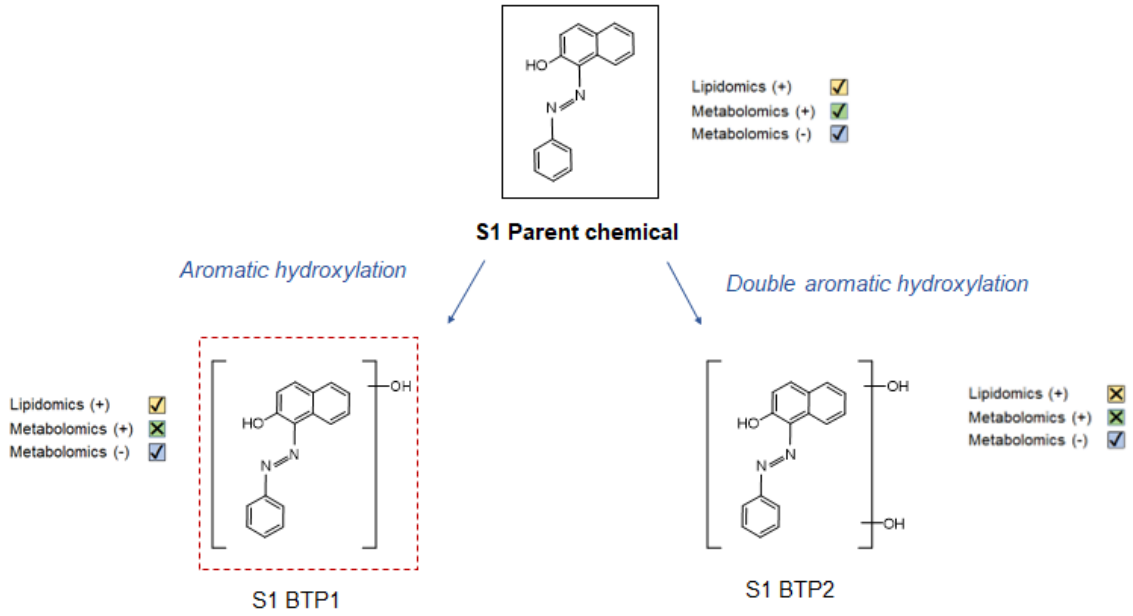
Lipidomics (+)
Metabolomics (+)
Metabolomics (-)
S1 Parent chemical
Aromatic hydroxylation
Double aromatic hydroxylation
Lipidomics (+)
Metabolomics (+)
Metabolomics (-)
S1 BTP1
Lipidomics (+)
Metabolomics (+)
Metabolomics (-)
S1 BTP2

**b**

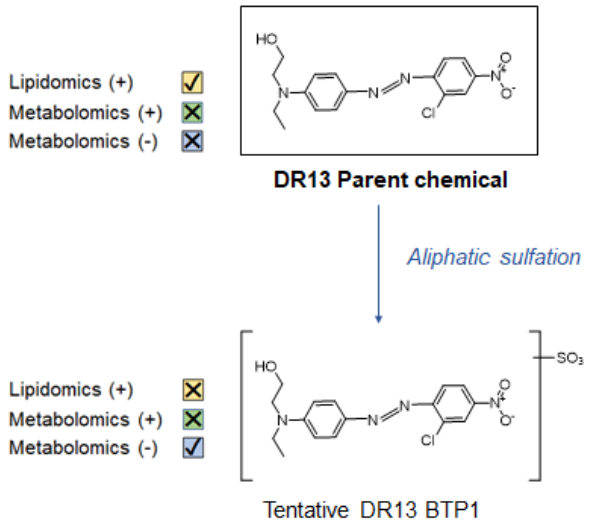
Lipidomics (+)
Metabolomics (+)
Metabolomics (-)
DR13 Parent chemical
Aliphatic sulfation
Lipidomics (+)
Metabolomics (+)
Metabolomics (-)
Tentative DR13 BTP1

**c**

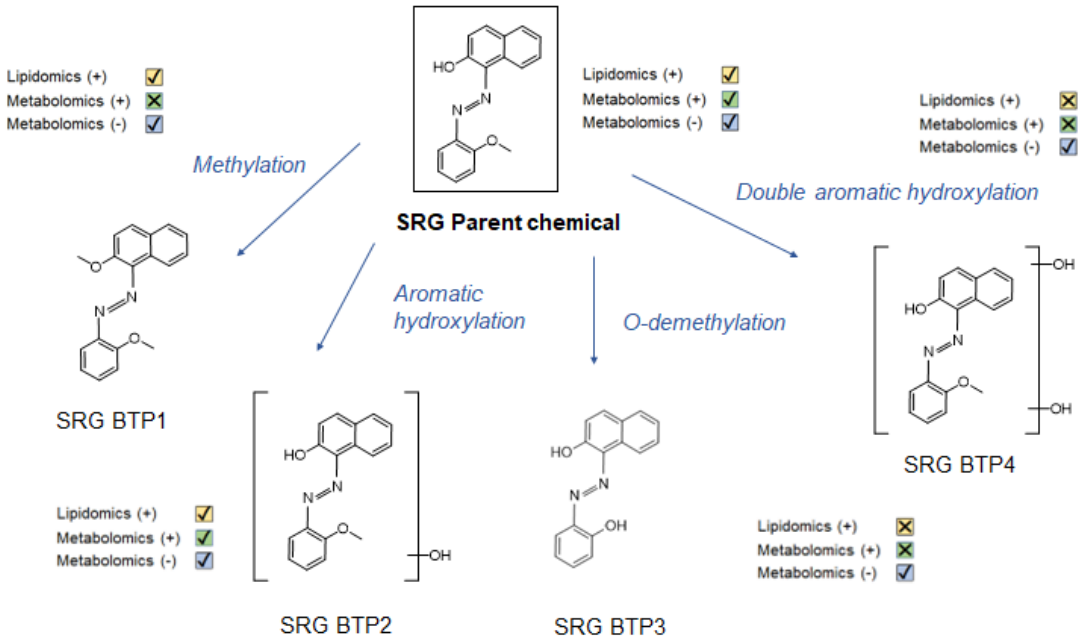


**d**

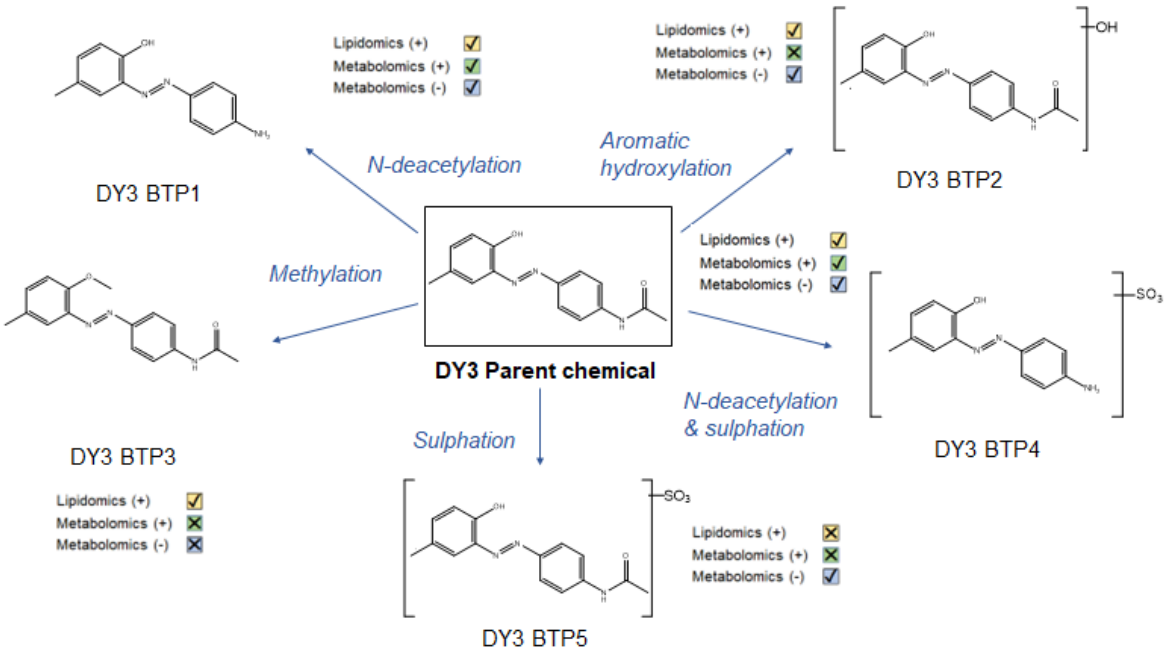


**Figure 4.4** Proposed biotransformation maps of (**a**) S1, (**b**) DR13, (**c**) SRG and (**d**) DY3 azo dyes illustrating the biotransformation products discovered (✓) in the untargeted nESI-DIMS

datasets by xenobiotic processing (per dye, per assay) and common SyGMa-derived biotransformation reactions. The dashed red line indicates the shared biotransformation product between S1 and SRG (at the level of a Markush structure). Chemical structures were generated from canonical SMILES using the ChemDraw Professional software (v22.0.0.22; PerkinElmer).

### 4.3.3 Visualisation of azo dye clearance

The same normalised peak intensities utilised to investigate the dose-response relationship for the azo dye parent chemicals (see section 4.3.1.2) were further plotted as line plots to offer some insights into metabolic uptake and clearance of these xenobiotics from the *Daphnia* over the course of the acute (48 h) toxicity study (Figure 4.4). While TK rates are normally assessed for all components of a biological test system using multiple time points[253] i.e., both the model organism and fresh/spent biological media in which the organism is located, here very crude estimation of uptake and clearance rates were obtained within the exposed *Daphnia* only by measuring the intensities of the parent chemicals (corresponding to the internal azo dye concentrations) at each of the three sampling time points (2 h, 24 h and 48 h).

The relative median intensity measurements of the azo dye parent chemicals provided a very crude estimation of the temporal changes in the uptake (fold changes calculated between 2 h and 24 h, and which is assumed to be solely a period of uptake), biotransformation and metabolic elimination (fold changes calculated between 24 h and 48 h, which is assumed to be solely a period of metabolism and depuration) of these xenobiotics in the biological test system. The kinetics information mined from the untargeted nESI-DIMS toxicometabolomics datasets revealed some differences in

uptake and clearance rates among the dyes as shown in Figure 4.5 and Table 4.7. The clearance plots for the remaining four dyes (DO61, DO25, DR1 and DR13) in the nESI-DIMS lipidomics dataset are included in Figure A-5, Figure A-6 shows clearance plots in the polar negative datsets for S1, DY3 and SRG (Appendix A).

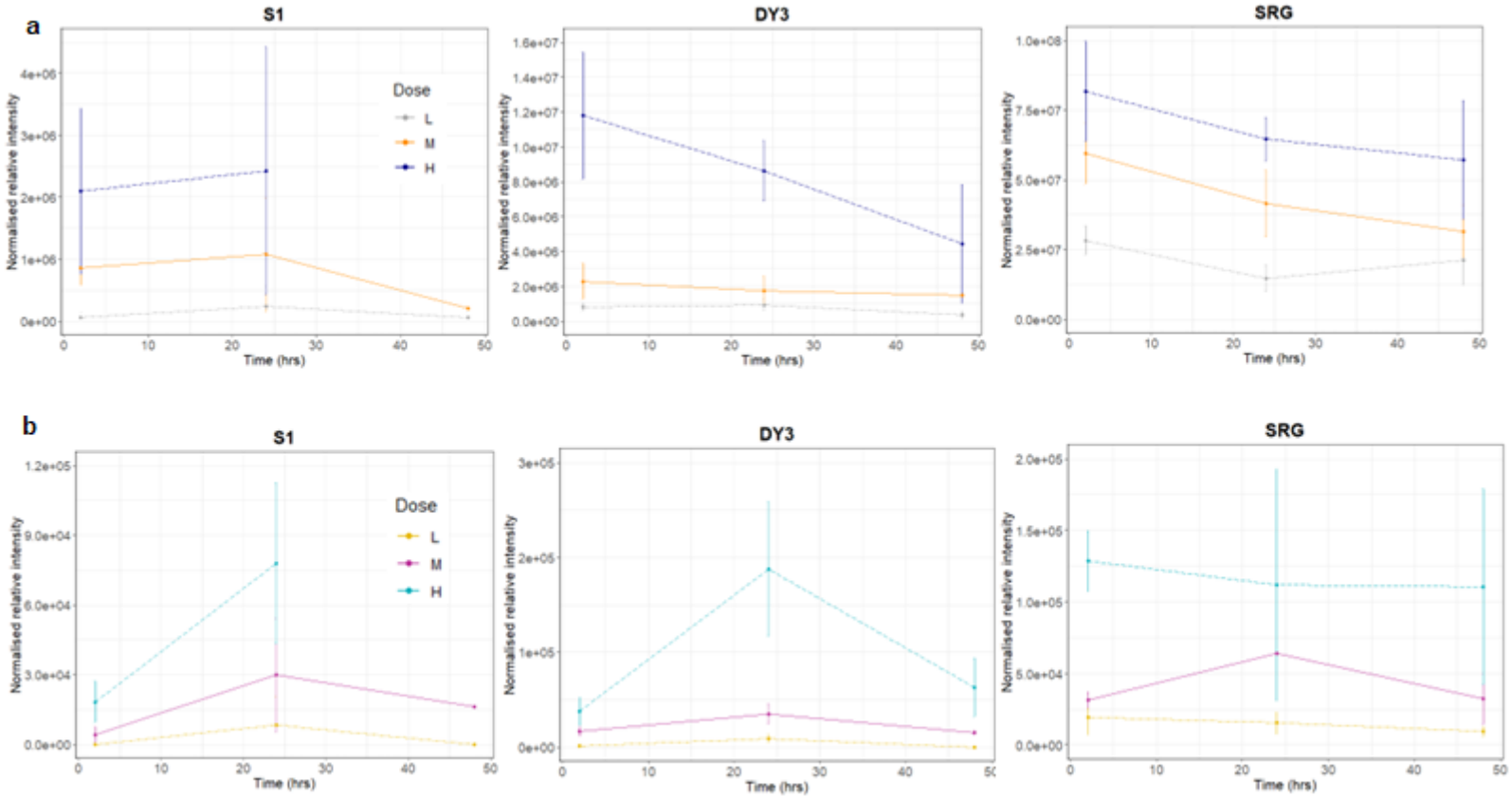


**Figure 4.5** Visualisation of azo dye TK rates. Median relative intensities (corresponding to relative internal concentrations) of the S1, DY3 and SRG azo dye parent chemicals measured over the duration of the 48-h study for the three treatment doses (L – low, M – medium and H – high) in the three nESI-DIMS datasets: (**a**) lipidomics, (**b**) – polar positive metabolomics. Error bars indicate median absolute deviation (MAD). Data is missing at 48 h time point for S1, DY3 only occurs at high dose samples in the negative metabolomics dataset.

**Table 4.7** Estimated kinetic rates of the azo dye parent chemicals detected in the nESI-DIMS lipidomics dataset. Fold-change ratios between sampling time points were calculated by comparing normalised median peak intensities (associated with relative internal concentrations) at a representative medium (M) dose for each dye. This table makes the crude assumption that only uptake occurs during 2-24 h and only metabolism and clearance occurs between 24-48 h.

| Azo dye parent chemical | 2 h M Median peak intensity | 24 h M Median peak intensity | 48 h M Median peak intensity | Fold change | |
|---|---|---|---|---|---|
| | | | | 2 h → 24 h Uptake | 24 h → 48 h Clearance |
| **S1** | 8.58775E+05 | 1.07586E+06 | 2.02953E+05 | 1.3 | 0.2 |
| **DY3** | 2.27758E+06 | 1.74223E+06 | 1.48331E+06 | 0.8 | 0.9 |
| **SRG** | 5.95025E+07 | 4.14363E+07 | 3.14363E+07 | 0.7 | 0.8 |
| **DO61** | 2.31870E+04 | 3.84468E+04 | 2.46884E+04 | 1.7 | 0.6 |
| **DO25*** | 6.66593E+07 | 8.05250E+07 | 6.06869E+07 | 1.2 | 0.8 |
| **DR1** | 4.41984E+05 | 6.25180E+05 | 3.95524E+05 | 1.4 | 0.6 |
| **DR13** | 2.05930E+05 | 2.72900E+05 | 1.95959E+05 | 1.3 | 0.7 |

*Impure feature, tentative annotation only.

DO61 shows the highest uptake between 2 h and 24 h (fold changes 1.7), which correlates with the highest log $K_{ow}$ value for this dye (6.47), while no biotransformations were detected in any of the nESI-DIMS assays and it exhibits a relatively low clearance rate (fold change 0.6).

In contrast, DY3 and SRG are characterised by the lowest uptake values between 2 h and 24 h (fold changes 0.8 and 0.7, respectively) with the highest clearance rates (0.8 and 0.9, respectively) after 48 h exposures. Also, DY3 formed more detectable biotransformation products than any other dye, suggesting that it undergoes most biotransformation in the *Daphnia*. This observation may correlate with the physico-

chemical properties of DY3, including the lowest log $K_{ow}$ value (3.89) of all the seven dyes, indicating the lowest bioaccumulation potential. The relationship between TK/ADME information and physico-chemical properties is less clear for SRG as this dye appears to be rapidly metabolised by the *Daphnia* and forms up to four different BTPs. However, its predicted log $K_{ow}$ value (5.59) is very similar to that of S1 (5.51), despite a very different clearance profile (Figure 4). S1 shows the lowest fold change between 24 h and 48 h (0.2) suggesting low metabolic clearance and the potential to bioaccumulate. This indication is supported by physico-chemical properties of S1, namely its lowest molecular weight of 248.82 g mol $^{-1}$ compared to the other dyes, smaller cross-sectional diameter and log Kow of 5.51[230]. However, the image of the juvenile *Daphnia* exposed to SRG (Figure 3.2 in chapter 3) highlights the complexity of this very crude clearance estimation for the azo dyes based on *m/z* feature intensities measured within the exposed *Daphnia* alone, and also without considering the whole system (i.e., both the *Daphnia* and the fresh/spent media). Also, as discussed in previous sections (see section 2.1 in chapter 2), the azo dyes selected for the study are inherently challenging to work with due to limited water solubility and large particle sizes, particularly for the disperse dyes[258–260] adhering to the animals and thereby potentially causing physical toxicity.

Alternatively, the azo dye may just pass through the *Daphnia* gut without getting absorbed and causing any toxicity on the molecular level (such an assessment would require an imaging experiment). As all the azo dyes under study are rather hydrophobic (moderate to high predicted log $K_{ow}$ ranging from 3.98 for DY3 to 6.47 for DO61) with low solubility in water (< 1 mg $L^{-1}$), their bioavailability is expected to be relatively low and some of the less soluble particles may precipitate from the test solution during the

48 h exposures and exist as solid particles. The uptake from water and toxicity of some of the disperse azo dyes may also be impeded by their large cross-sectional diameters and higher molecular weight (> 360 g mol $^{-1}$)[258,260]. Therefore, to robustly assess the kinetics of the whole system (both the exposed *Daphnia* and fresh/spent test media), other important parameters should be considered, including measuring the dye concentration in the test solution (before and after exposures and at multiple sampling time points), measuring the rate of *Daphnia* feeding, measuring rate of metabolism and rate of elimination of the azo dyes.

## 4.4 Key findings, conclusions and future work

The study demonstrated that the untargeted ADME/TK workflow can be successfully applied to the three untargeted nESI-DIMS $MS^1$ datasets to extract azo dye-related xenobiotic (exogenous) features from the dataset that was collected to probe endogenous toxicity responses (as described in chapter 3). Tables 4.8 – 4.10 below summarise the azo dye parent chemicals and their metabolic biotransformation products discovered in each assay by the xenobiotic processing and annotated using the criteria described in Figure 4.1

**Table 4.8** Summary of azo dye parent chemicals and/or biotransformation products (BTPs) putatively annotated in the lipidomics nESI-DIMS dataset using the criteria described in **Figure 4.1**. Biotransformation steps predicted by SyGMa are shown in italics.

| Azo dye parent and BTPs | Present in >80% high (H) dose samples | Present in <50% controls | Fold change > 10 | Within 5 ppm mass error | Dose-response observed |
|---|---|---|---|---|---|
| **S1 parent** | ✓ 82% | ✓ 6% | ✓ 10.7 | ✕ 5.7 | ✓[a] |
| **BTP1** *Aromatic hydroxylation* | ✓ 82% | ✓ 0% | ✓ ∞ | ✕ 5.6 | ✓[a] |
| **DY3 parent** | ✓ 100% | ✓ 28% | ✓ 198.7 | ✓ 1.0 | ✓ |
| **BTP1** *N-deacetylation* | ✓ 100% | ✓ 0% | ✓ ∞ | ✓ 2.8 | ✓ |
| **BTP2** *Methylation* | ✓ 94% | ✓ 0% | ✓ ∞ | ✓ 1.5 | ✕[b] |
| **BTP3** *Aromatic hydroxylation* | ✓ 100% | ✓ 0% | ✓ ∞ | ✓ 1.5 | ✕[b] |
| **BTP4** *N-deacetylation + sulphation* | ✓ 94% | ✓ 0% | ✓ ∞ | ✓ 4.3 | ✕[b] |
| **SRG parent** | ✓ 89% | ✓ 0% | ✓ ∞ | ✓ 0.2 | ✓ |
| **BTP1** *Methylation* | ✓ 89% | ✓ 0% | ✓ ∞ | ✓ 2.4 | ✓ |
| **BTP2** *Aromatic hydroxylation* | ✓ 89% | ✓ 0% | ✓ ∞ | ✓ 2.9 | ✓ |
| **DO61 parent** | ✓ 100% | ✓ 0% | ✓ ∞ | ✓ 0.6 | ✓[c] |
| Tentative **DO25 parent** | ✓ 100% | ✓ 17% | ✕ 2.3 | ✓ 0.03 | ✓ |
| Tentative **BTP1** *Nitrile to amide* | ✓ 100% | ✓ 17% | ✕ 3.3 | ✓ 2.2 | ✓ |
| **DR1 parent** | ✓ 100% | ✓ 0% | ✓ ∞ | ✓ 2.5 | ✓ |
| **DR13 parent** | ✓ 100% | ✓ 0% | ✓ ∞ | ✕ 5.4 | ✓ |

[a]Data missing for 48 h dose group.

[b]Detected in high dose samples only.

[c]Low intensity feature with high dose and 50% medium dose groups missing at 48h.

**Table 4.9** Summary of azo dye parent chemicals and/or biotransformation products (BTPs) putatively annotated in the polar positive metabolomics nESI-DIMS dataset. Biotransformation steps predicted by SyGMa are shown in italics.

| **Azo dye parent and BTPs** | **Present in >80% high dose samples** | **Present in <50% controls** | **Fold change > 10** | **Within 10 ppm mass error** | **Dose-response observed** |
|---|---|---|---|---|---|
| **S1 parent** | ✓ 100% | ✓ 0% | ✓ ∞ | ✓ 2.01 | ✓[a] |
| **DY3 parent**<br>**BTP1** *N-deacetylation + sulphation*<br>**BTP2** *N-deacetylation* | ✓ 100%<br>✓ 100%<br>✓ 100% | ✓ 0%<br>✓ 0%<br>✓ 11% | ✓ ∞<br>✓ ∞<br>✓ 19.0 | ✓ 4.26<br>✓ 7.17<br>✓ 6.70 | ✓<br>✓<br>✓ |
| Tentative **SRG parent**<br>**BTP1** *Aromatic hydroxylation* | ✓ 94%<br>✓ 94% | ✓ 6%<br>✓ 0% | ✓ 2.34<br>✓ ∞ | ✓ 6.84<br>✓ 7.21 | ✓<br>✓ |
| Tentative **DO25 parent** | ✓ 94% | ✓ 44% | ✓ 48.3 | ✓ 6.44 | × |
| **DR1 parent**[b] | ✓ 94% | ✓ 0% | ✓ ∞ | ✓ 8.06 | × |

[a]Data missing for 48 h dose group.

[b]Low intensity feature.

**Table 4.10** Summary of azo dye parent chemicals and/or biotransformation products (BTPs) putatively annotated in the polar negative metabolomics nESI-DIMS dataset. Biotransformation steps predicted by SyGMa are shown in italics.

| **Azo dye parent and BTPs** | **Present in >80% high dose samples** | **Present in <50% controls** | **Fold change > 10** | **10 ppm mass error** | **Dose-response observed** |
|---|---|---|---|---|---|
| **S1 parent**<br>**S1 BTP1** *Aromatic hydroxylation* | ✓ 91%<br>✓ 91% | ✓ 0%<br>✓ 0% | ✓ ∞<br>✓ ∞ | ✓ -2.16<br>✓ 6.34 | ✓[a]<br>✓[a] |
| Tentative **DY3 parent**<br>**BTP1** *N-deacetylation + sulphation*<br>**BTP2** *Hydroxylation*<br>**BTP3** *Sulphation*<br>Tentative **BTP4** *N-deacetylation* | ✓ 67%<br>✓ 89%<br>✓ 89%<br>✓ 100%<br>✕ 72% | ✓ 0%<br>✓ 0%<br>✓ 0%<br>✓ 5%<br>✓ 0% | ✓ ∞<br>✓ ∞<br>✓ ∞<br>✓ ∞<br>✓ ∞ | ✓ -6.76<br>✓ -0.42<br>✓ -0.46<br>✓ -8.26<br>✓ -6.16 | ✓[b]<br>✓<br>✓<br>✓<br>✓[c] |
| **SRG**[d] **parent**<br>**BTP1** *O-demethylation*<br>**BTP2**[d] *Aromatic hydroxylation*<br>**BTP3**[d] *Double aromatic hydroxylation* | ✓ 83%<br>✓ 89%<br>✓ 89%<br>✓ 89% | ✓ 0%<br>✓ 0%<br>✓ 5%<br>✓ 5% | ✓ ∞<br>✓ ∞<br>✓324.30<br>✓ 28.34 | ✓ 5.24<br>✓ 6.34<br>✓ 5.33<br>✓ 5.60 | ✓<br>✓<br>✕<br>✕ |
| Tentative **DR13 BTP1** *Aliphatic sulphation* | ✕ 78% | ✓ 0% | ✓ ∞ | ✓ -6.54 | ✓ |

[a]Data missing for 48 h dose group.
[b]Feature only detected in high dose samples at all three time points.
[c]Feature not detected in low dose samples and not detected at 2h.
[d]Low intensity feature.

Noteworthily, the parent chemicals for the three dyes of interest (S1, DY3 and SRG) were consistently detected across multiple nESI-DIMS assays, providing confirmation of the relative internal exposure (estimated from normalised peak intensities) of *D. magna* to each azo dye across the three dose groups: low, medium and high (L, M and H) during the acute (48 h) exposures. Confidence in these annotations is further

increased when their normalised intensities clearly correlate with the external doses of the azo dyes in at least one time point.

In addition, up to 5 biotransformation products were discovered for each dye (Table 4.6), highlighting the differences in metabolism and bioaccumulation potential among the dyes due to their different physico-chemical properties (particularly log $K_{ow}$). Three identical biotransformation reactions (i.e., one phase I modification: aromatic hydroxylation, and two phase II modifications: *N*-deacetylation and *N*-deacetylation followed by sulphation) were revealed for all three dyes in at least two nESI-DIMS assays, providing insights into the azo dye metabolism within the *Daphnia*, and providing further evidence for the uptake of the dyes (beyond their passage through the *Daphnia* gut). The discovery of a shared biotransformation product for S1 (following aromatic hydroxylation) and SRG (following *O*-demethylation) suggests some similarity in metabolism between the two dyes and could potentially enhance the S1, SRG and DY3 grouping presented in chapter 3. However, in the absence of MSn fragmentation data for the azo dyes, the available TK/ADME data is not sufficient to establish toxicokinetic similarity with high confidence and, therefore, the uncertainty associated with these findings is relatively high. Also, the comparison of relative intensity measurements over the duration of the 48 h toxicity study revealed some variability in TK properties among the azo dyes (Figure 4.5, Table 4.7). For instance, DY3 shows relatively rapid clearance and undergoes the most metabolic biotransformation (five BTPs discovered) compared to S1 that displays low clearance, least biotransformation (one BTP formed) suggesting that it may begin to accumulate in the *Daphnia* at 48 h. However, it was not possible to fully conclude this due to incomplete 48 h data for this dye.

Ultimately, this work highlights the capability of untargeted nESI-DIMS toxicometabolomics experiments, principally designed to probe the biological responses to chemical exposure, to simultaneously provide valuable insights into the metabolism and metabolic fate of xenobiotics. All this information can be obtained from a single toxicity assay, demonstrating the potential of metabolomics in modern chemical risk assessment. However, the application of nESI-DIMS on *D. magna* extracts for ADME/TK characterisation comes with inherent limitations. Crucially, nESI-DIMS $MS^1$ data alone falls short of identifying xenobiotic-related features with high confidence in a biological test system and therefore collection of $MS^n$ data should be considered to improve xenobiotic feature annotation and identification. Also, this study was not specifically designed to explore the metabolism and metabolic fate of xenobiotics per se. The additional analyses conducted on the untargeted toxicometabolomics datasets highlight the complexity of azo dye ADME/TK characterisation based solely on the time-series measurements (across only three time points) of peak intensities within the *Daphnia*. Next chapter 5 attempts to address these points by employing a more refined analytical and computational approach to conduct a more extensive study aiming to characterise metabolism and metabolic fate of five industrial chemicals using ultra-high performance liquid chromatography-mass spectrometry (UHPLC-MS/MS).

# CHAPTER 5 – EXPLORING THE POSSIBILITY OF IMPLEMENTING UNTARGETED UHLPC-MS/MS METABOLOMICS TO CHARACTERISE ADME PROPERTIES OF INDUSTRIAL CHEMICALS IN RAT PLASMA EXTRACTS

## 5.1 Introduction

As previously mentioned in section 1.9 (chapter 1), ADME (absorption, distribution, metabolism and elimination) and TK (toxicokinetics) studies are routinely used in drug development to understand safety and efficacy of drug candidates, and are essential for regulatory approval. A similar approach can be applied to characterise metabolism and metabolic fate of industrial chemicals through untargeted metabolomics, but it is still relatively under-researched in chemical safety science[3]. While ADME testing in a pharmacological context aims to study properties of compounds with a specific mode of action (MoA) and used in small doses, one challenge of applying this approach in chemical risk assessment is characterisation of a very diverse chemical landscape of xenobiotics, often with non-specific or multiple MoAs, diverse physico-chemical properties, and frequently lacking a complete toxicological profile. One advantage of ADME/TK information is that it allows the correlation of toxicity with corresponding internal levels of xenobiotic exposure. It can also be used to inform study design, provide information on bioavailability and guide dose selection or selection of model species, particularly in early stages of chemical safety assessment[250].

The integration of toxicokinetics with toxicodynamics within a single toxicity assay offers an excellent opportunity to not only complement the endogenous molecular

responses but also enhance understanding of chemical toxicity. Recent studies demonstrated that untargeted LC-MS/MS metabolomics assays can simultaneously measure xenobiotics within a biological sample as well as profiling the endogenous metabolome (Bowen *et al*.[6]: *manuscript under review*; Sostare *et al*.: *manuscript in preparation*).

The work discussed in the previous chapter demonstrates that xenobiotic-related features can be successfully derived from an untargeted metabolomics nESI-DIMS experiment, the main limitation of this approach being low confidence in annotation of the xenobiotics due to only full scan $MS^1$ data being available. This chapter attempts to build on this earlier work by employing a more refined analytical and computational approach, whereby orthogonal data (i.e. full scan $MS^1$ accurate *m/z*, chromatographic peak RT, and $MS^n$ fragmentation data) are collected and considered to aid identification of xenobiotic-related features.

With the above in mind, the aim of the work presented in this chapter was to apply the metabolite identification (Met ID) step of an untargeted metabolomics workflow to study metabolism and metabolic fate of five industrial chemicals in plasma samples from a 5-day rat toxicity study, originally designed to probe the rat metabolome and transcriptome following chemical exposure.

In order to fulfil the above aim, a number of critical objectives were formulated. The first objective was to assess the capability of relatively new technology (specifically, Thermo Fisher Scientific Orbitrap ID-X Tribrid mass spectrometer) and commercial software (Compound Discoverer version 3.3.1.111, Thermo Fisher Scientific, Hemel Hempstead, UK) to obtain measurements of xenobiotics (five industrial chemicals)

within untargeted UHLPC-MS/MS (HILIC and RP $C_{18}$ lipidomics) analyses to discover and confirm identities of their parent chemicals. For added confidence, the parents measured in chemical-specific treated biological samples (rat plasma extracts) were also compared against measurements of authentic analytical standards (reference materials, RF) of the five parent xenobiotics, using identical analytical methods.

The second objective was to examine the same untargeted UHLPC-MS/MS datasets using the computational Compound Discoverer (CD) workflow to reveal and identify any biotransformation products of the five xenobiotics, and to summarise these results using metabolic biotransformation maps for selected xenobiotics under study.

Finally, the third objective was to compare these results with Phenome Centre Birmingham (PCB) findings (blinded study) acquired using an older technology (specifically, Thermo Fisher Scientific Q Exactive Focus Orbitrap UHPLC-MS/MS system) and analysed using an existing in-house xenobiotic processing workflow, to evaluate the potential 'added value' of the newer approach.

## 5.2 Materials and methods

### 5.2.1 Overview of industrial chemicals selected for the study

Chemical selection for the metabolism and metabolic fate study described in this chapter was largely driven by existing plasma samples from a 5-day exposure study of 18 xenobiotics conducted by the National Toxicology Program (NTP)[261], in male Sprague-Dawley rats, that had previously been provided to PCB. These industrial chemicals are considered well-studied as apical toxicity data in rodent models (mice

and/or rats) exists for these xenobiotics from historical NTP (sub)chronic toxicity records[261]. Out of these 18 xenobiotics, ten were subsequently investigated in a parallel ADME/TK study conducted by PCB, and five of these xenobiotics were selected for the current ADME/TK characterisation using an Orbitrap ID-X Tribrid mass spectrometer (Thermo Fisher Scientific, Hemel Hempstead, UK), based on the likelihood of detection of parent chemicals and/or any biotransformation products in at least one UHPLC-MS/MS assay. The key identities and chemical structures of all five xenobiotics under study are summarised in Table 5.1 and Figure 5.1, respectively. Chemical structures were generated from canonical SMILES using the ChemDraw Professional software (v22.0.0.22; PerkinElmer).

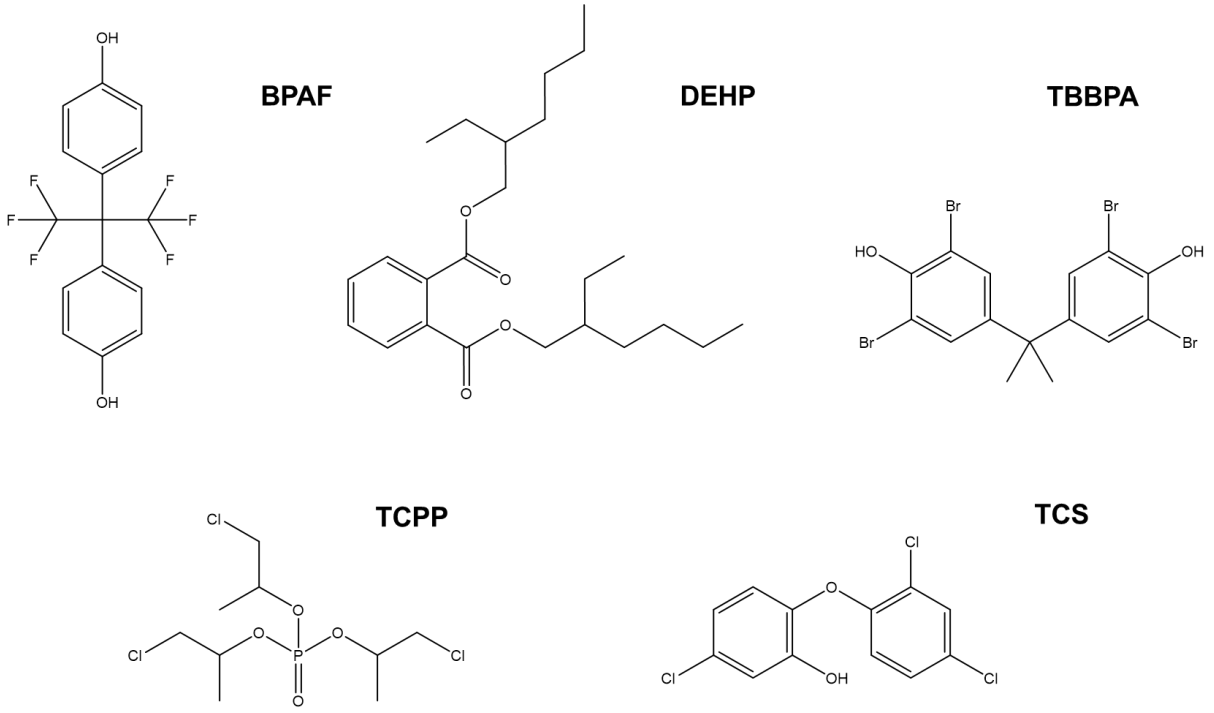


**Figure 5.1** Chemical structures of the five xenobiotics selected for the study. Abbreviations: **BPAF** – bisphenol AF, **DEHP** – di(2-ethylhexyl) phthalate, **TBBPA** – tetrabromobisphenol, **TCCP** – tris(2-chloroisopropyl) phosphate, **TCS** – triclosan. Chemical structures were generated from canonical SMILES using the ChemDraw Professional software (v22.0.0.22; PerkinElmer).

Classification of the xenobiotics into super class level and class level was conducted based on chemical structures and structural features using the web-based application ClassyFire as described elsewhere (http://classyfire.wishartlab.com)[237].

**Table 5.1** Overview of the xenobiotics selected for the study. The xenobiotic identifiers, including the International Union of Pure and Applied Chemistry (IUPAC) name, Chemical Abstract Services registry number (CAS-RN), European Community (EC) number and Simplified Molecular-Input Line-Entry System (SMILES) notation.

| Name (abbr.) | IUPAC Name | CAS-RN | EC | Canonical SMILES | Exact mass (Da) | Applications |
|---|---|---|---|---|---|---|
| Bisphenol AF (**BPAF**) | 4-[1,1,1,3,3,3-hexafluoro-2-(4-hydroxyphenyl)propan-2-yl]phenol | 1478-61-1 | 216-036-7 | C1=CC(=CC=C1C(C2=CC=C(C=C2)O)(C(F)(F)F)C(F)(F)F)O | 336.05850 | Plasticiser |
| Di(2-ethylhexyl) phthalate (**DEHP**) | bis(2-ethylhexyl) benzene-1,2-dicarboxylate | 117-81-7 | 204-211-0 | CCCCC(CC)COC(=O)C1=CC=CC=C1C(=O)OCC(CC)CCCC | 390.27701 | Plasticiser |
| Tetrabromobisphenol (**TBBPA**) | 2,6-dibromo-4-[2-(3,5-dibromo-4-hydroxyphenyl)propan-2-yl]phenol | 79-94-7 | 201-236-9 | CC(C)(C1=CC(=C(C(=C1)Br)O)Br)C2=CC(=C(C(=C2)Br)O)Br | 543.75298 | Flame retardant |
| Tris(2-chloroisopropyl) phosphate (**TCCP**) | bis(2-ethylhexyl) benzene-1,2-dicarboxylate | 13674-84-5 | 237-158-7 | CC(CCl)OP(=O)(OC(C)CCl)OC(C)CCl | 326.00083 | Flame retardant / OP pesticide / plasticiser |

| Name (abbr.) | IUPAC Name | CAS-RN | EC | Canonical SMILES | Exact mass (Da) | Applications |
|---|---|---|---|---|---|---|
| Triclosan (**TCS**) | 5-chloro-2-(2,4-dichlorophenoxy) phenol | 3380-34-5 | 222-182-2 | C1=CC(=C(C=C1Cl)O)OC2=C(C=C(C=C2)Cl)Cl | 287.95116 | Antimicrobial agent |

## 5.2.2 Experimental design

The untargeted ADME/TK (experimental and computational) workflow was applied to existing rat plasma samples from 5-day exposure toxicity assays conducted by the National Toxicology Program (NTP) in male Sprague-Dawley rat models, as described elsewhere[261]. The subset of experimental samples comprised a representative pooled (from *n*=4 biological replicates) treated sample for each xenobiotic (forming five pooled samples in total) and a single untreated control sample per xenobiotic (forming a further five samples in total). Only the highest (or second highest for BPAF due to the missing highest dose group for this chemical) test concentration was selected for UHPLC-MS/MS analyses to increase the probability of discovering parents and biotransformation products in at least one assay. The nominal test concentrations selected for the study are summarised in Table 5.3.

**Table 5.3**. Summary of rat plasma samples selected for the ADME/TK study of five xenobiotics.

| Name (abbr.) | Treatment group | Nominal test concentration (mg kg $^{-1}$) |
|---|---|---|
| **BPAF** | Control | 0 |
| **BPAF** | 2$^{nd}$ Highest dose | 500 |
| **DEHP** | Control | 0 |
| **DEHP** | High dose | 1000 |
| **TBBPA** | Control | 0 |
| **TBBPA** | High dose | 2000 |
| **TCCP** | Control | 0 |
| **TCCP** | High dose | 2000 |
| **TCS** | Control | 0 |
| **TCS** | High dose | 1000 |

Aside from biological samples, five analytical reference standards (one per xenobiotic) at a final nominal concentration of ca. 10 µg $mL^{-1}$ were incorporated into the experimental design and characterised by UHPLC-MS/MS to aid identification of parent chemicals in the rat plasma samples.

### 5.2.3 Chemicals and reagents

High-purity reference materials used for the preparation of analytical standard samples were purchased from Sigma-Aldrich (Gillingham, UK) and LGC Standards (Teddington, UK) and stored as per manufacturers' recommendations (Table 5.4).

**Table 5.4** Commercial suppliers with purity of reference materials used to prepare analytical standards for each xenobiotic studied.

| Name (abbr.) | CAS-RN | Supplier | Batch no. | Purity (%) |
|---|---|---|---|---|
| **BPAF** | 1478-61-1 | LGC Standards | G1075989 | 99.9 |
| **DEHP** | 117-81-7 | Sigma-Aldrich | BCCC8985 | ≥ 98.0 |
| **TBBPA** | 79-94-7 | Sigma-Aldrich | MKCB9769 | 97.0 |
| **TCCP** | 13674-84-5 | Sigma-Aldrich | BCBX4369 | ~66.0 main isomer |
| **TCS** | 3380-34-5 | Sigma-Aldrich | LRAA9132 | 99.7 |

Solvents used in the preparation of mobile phases and needle wash solutions for UHPLC-MS/MS analyses were of LC-MS grade except for propan-2-ol (isopropanol) which was of HPLC grade (Fisher Scientific, Loughborough, UK). Water was purchased from Merck (Feltham, UK) and acetonitrile was obtained from VWR Chemicals (Lutterworth, UK). The same solvents were used in the preparation of biological samples and analytical standards in addition to methanol (LC-MS grade) manufactured by Honeywell Research Chemicals (Charlotte, NC).

The mobile phase modifiers and additives (LC-MS grade) used were as follows: ammonium formate (≥99.0%) and acetic acid (≥99.7%) obtained from Fisher Scientific (Loughborough, UK); ammonium acetate (≥99.99%, trace metal basis) and formic acid (~98.0%) were manufactured by Honeywell Research Chemicals (Charlotte, NC).

## 5.2.4 Sample pooling and extraction of xenobiotics from rat plasma

All rat plasma samples were stored at -80 °C prior to pooling and extractions. Sample pooling was performed to generate a representative high dose sample for each xenobiotic and a homogenous control sample for UHPLC-MS/MS analyses. Plasma preparation followed established protocols for HILIC plasma UHPLC-MS analyses (monophasic 50:50 methanol:water v/v) and RP $C_{18}$ UHPLC-MS plasma lipidomics (monophasic 100% isopropanol v/v), as previously described by Southam *et al*. (2020)[120]. These methods were reported to provide the highest extraction yield of metabolites and lipids combined with high reproducibility[120].

### 5.2.4.1 Preparation of pooled samples

The samples were first thawed on wet ice and briefly (5 s) vortexed. Four identical volumes (5 µL aliquots) from each (*n*=4) biological replicate per xenobiotic were pooled and transferred into a 2 mL Eppendorf branded tube to form a single 20 µL representative treated high dose sample for UHPLC-MS/MS analyses. Two 20 µL aliquots per xenobiotic were prepared, one for HILIC assays and one for RP $C_{18}$ lipids assays.

Three individual pooled control samples (20 µL each) were also prepared for the ADME/TK study by pooling five identical volumes (4 µL aliquots) from *n*=5 biological replicates (i.e., one out of *n=5* randomly selected control sample per xenobiotic) and transferring the pooled aliquot into a 2 mL Eppendorf branded tube. These control samples were later used for the generation of exclusion list in the AcquireX workflow and LC column equilibration prior to each analytical run (see section 5.2.5).

### 5.2.4.2 Extractions of xenobiotics from rat plasma

#### 5.2.4.2.1 HILIC UHPLC-MS ASSAYS

A 60 µL aliquot (3× original sample volume) of ice-cold methanol:acetonitrile (50:50 v/v) was added to each 20 µL aliquot in a 2 mL Eppendorf branded tube. After vortexing (15 s) and centrifugation (20,000-g, 4°C, 20 min), the supernatant (ca. 78 µL) was transferred to a single LC-MS vial with a conical 200 µL glass insert for treated samples and set on an autosampler (at 4°C) for immediate analysis. The three control samples were prepared using the identical method with an additional re-pooling step into a single 2 mL Eppendorf branded tube prior to centrifugation to eliminate any batch effects and yield a homogenous control sample. The supernatant (ca. 228 µL) was removed and split into five LC-MS vials with conical 200 µL glass inserts, one per xenobiotic, for immediate analysis.

#### 5.2.4.2.2 RP $C_{18}$ LIPIDS UHPLC-MS ASSAYS

A 60 µL aliquot (3× original sample volume) of 100% (v) ice-cold propan-2-ol (isopropanol; LC-MS grade) was added to each 20 µL aliquot in a 2 mL Eppendorf

branded tube. After vortexing (15 s) and centrifugation (20,000-g, 4°C, 20 min), the supernatant (ca. 78 µL) was transferred to a single LC-MS vial with a conical 200 µL glass insert for treated samples and set on an autosampler (at 4°C) for immediate analysis. The three control samples were prepared using the identical method with an additional re-pooling step into a single 2 mL Eppendorf branded tube prior to centrifugation to eliminate any batch effects and yield a homogenous control sample. The supernatant (ca. 228 µL) was removed and split into five LC-MS vials with conical 200 µL glass inserts, one per xenobiotic, for immediate analysis.

## 5.2.5 Preparation of chemical standard samples

Stock solutions of analytical standards were prepared in water:acetonitrile:methanol (1:1.5:1.5 v/v/v) for HILIC metabolomics analysis and in propan-2-ol:water (3:1 v/v) for RP $C_{18}$ lipidomics analysis, and stored in the dark at 4°C. Working solutions (final nominal concentration of ca. 10 µg $mL^{-1}$ for each xenobiotic studied) were prepared fresh daily prior to UHPLC-MS/MS analyses using LC-MS grade solvents stored at 4°C.

## 5.2.6 UHPLC-MS/MS data acquisition

### 5.2.6.1 UHPLC-MS instrumentation with AcquireX

Analyses of experimental rat plasma samples were conducted in positive and negative electrospray ionisation (ESI) modes separately using an existing method[6,120,121] with slight modifications on a Vanquish UHPLC system coupled to an Orbitrap ID-X Tribrid

mass spectrometer (Thermo Fisher Scientific, Hemel Hempstead, UK). The Vanquish UHPLC system consisted of a Vanquish binary pump, a Vanquish autosampler and a Vanquish column compartment.

Data were acquired using the Xcalibur software (Thermo Fisher Scientific, Hemel Hempstead, UK; version 4.3) and the AcquireX data acquisition workflow (specifically, 'Deep Scan' mode) was implemented to collect $MS^n$ fragmentation data as described previously[6,196]. Briefly, a DDA (data dependent acquisition) $MS^n$ method for each xenobiotic of interest was first manually updated with an inclusion list of preferred ions corresponding to target features (the protonated $[M+]H^+$ and deprotonated species $[M-H]^-$ and other common adducts in each ion mode) from *in silico* predicted biotransformation products using SyGMa (Systematic Generation of potential Metabolites) software[255] for improved characterisation of xenobiotic-related features. Identification of potential BTPs was not limited to the SyGMa-generated inclusion list, however. For consistency, this study used the final SyGMa inclusion lists produced by PCB (Dr Matthew Smith) for each of the xenobiotics under investigation.

The AcquireX data acquisition feature was subsequently used to automatically generate and modify a background exclusion list (containing endogenous features) and an inclusion list containing xenobiotic (i.e. exogenous) features related to the five xenobiotics under investigation (Figure 5.2).

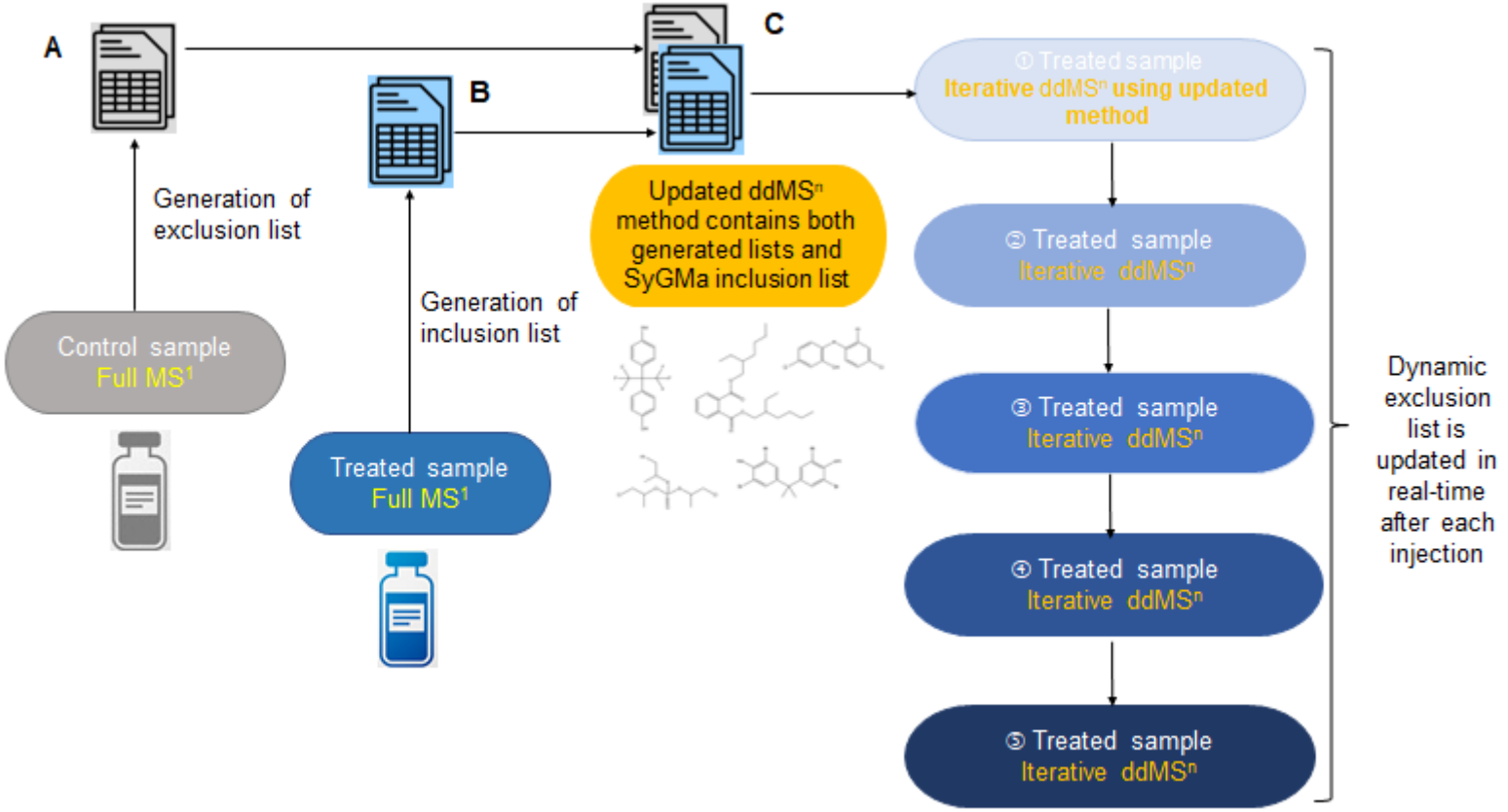


**Figure 5.2** AcquireX data acquisition workflow implemented in the ADME/TK study for UHPLC-MS/MS analyses of xenobiotics (adapted from Souza *et al*., 2018[7]). First, an exclusion list is generated following an injection of a single control sample per xenobiotic (A). Secondly, an inclusion list is generated following an injection of a treated sample (B). The ddMS$^n$ method is subsequently updated to include both lists (C). The inclusion list in the ddMS$^n$ method is iteratively updated in real time after each injection of a treated sample (1-5).

First, an exclusion list was generated from a single injection of a control sample (experimental 'blank') in a full scan $MS^1$ mode. These background matrix ions were automatically excluded from $MS^n$ triggering (Figure 5.2, A). Next, an exclusion list was generated from a single injection of a biological rat plasma (representative chemical-specific treated) sample in a full scan $MS^1$ mode (Figure 5.2, B). The inclusion list contained unique precursor features of interest targeted for $MS^n$ fragmentation for each xenobiotic under study. Both lists were subsequently incorporated into the DDA method ($ddMS^n$) to drive AcquireX intelligent acquisition of $MS^1$ and $MS^n$ data (Figure 5.2, C) [7,196].

This was followed by five iterative injections of a biological sample (iterative $MS^n$) per xenobiotic. After each injection, the inclusion list was automatically updated to move precursors already fragmented to the exclusion list (Figure 5.2, steps 1-5). The updated lists were imported back into the experimental DDA method and the process was repeated for the remaining four iterative injections, or until the inclusion list was exhausted (i.e. all the target precursor ions on the list had been fragmented into product ions)[7].

The analytical sequence for each UHPLC-MS assay comprised five AcquireX sequences (one per xenobiotic). Identical analytical methods (implemented without AcquireX) and instrumentation, as described in detail below, were applied to obtain measurements (specifically, $MS^1$ spectra, retention time and $MS^n$ fragmentation data) of all five xenobiotics from analytical standards. In addition, two process extraction blanks were analysed at the beginning and end of each analytical run to identify and eliminate any sources of contamination arising from solvents used and the extraction

process. A total of ten untreated rat plasma equilibration samples (pooled control samples) were analysed to allow system equilibration and assess the instrument performance prior to each analytical sequence.

#### 5.2.6.2 HILIC UHLPC-MS/MS analyses

Metabolomics UHLPC-MS/MS analyses of rat plasma extracts were conducted using an existing method employing hydrophilic interaction chromatography (HILIC), as previously described[6,120,121,262], with slight modifications. Separation of xenobiotics in the HILIC assays was obtained with an Accucore 150 Amide HILIC column (2.1 x 100 mm, particle size 2.6 µm; Thermo Fisher Scientific), maintained at 35 °C for both positive and negative ionisation modes. Mobile phase A was composed of 95% acetonitrile:water (10 mM ammonium formate, 0.1% formic acid), and mobile phase B was composed of 50% acetonitrile:water (10 mM ammonium formate, 0.1% formic acid) for the positive ionisation mode. In the negative ionisation mode, the mobile phase modifiers and additives were replaced with 10 mM ammonium acetate and 0.1% acetic acid in mobile in phase A and mobile phase B, respectively. The linear (curve = 5) gradient elution (15 min) was as follows: t = 0.0–4.1 min, 1% B; t = 4.1–7.1 min, 15% B; t = 7.1–10.1 min, 50% B; t = 10.1–11.0 min, 95% B; t = 11.0–11.5 min, 95% B; t = 11.5–15.0 min, 1% B. The flow rate of mobile phase was 0.4 mL $min^{-1}$. Samples were maintained at 4 °C and sample injection volume was 2 µL.

High resolution full scan $MS^1$ and $MS^n$ data were acquired in a data-dependent (DDA) fashion, as described above. $MS^1$ data in full scan mode were collected using an Orbitrap mass analyser over a 70-1050 *m/z* scan range at a resolution of 120,000 (at

*m/z* 200 FWHM), a normalised AGC (automatic gain control) target of 25% and a maximum injection time of 75 ms. Ion source parameters for all four assays are summarised in Table 5.5.

The collection of $MS^2$ fragmentation data was performed with an Orbitrap mass analyser in a quadrupole isolation mode (with an isolation window of 3 *m/z*) at a resolution 30,000 (at 200 *m/z* FWHM), a normalised AGC target of 20% and a maximum injection time of 50 ms. Stepped normalised HCD collision energies (NCEs) of 20, 40 and 100 % were used for positive ion mode and 20, 40 and 130% for negative ion mode to produce a large number of fragments.

$MS^3$ data were obtained using an ion trap (with three scan filters set to: 1) 5.0e3 intensity threshold, 2) dynamic exclusion of 2.5 s and mass tolerance of 5 ppm; and 3) targeted mass inclusion and exclusion filter) at a normalised AGC target of 20%, CID collision energy set to 35% and 15,000 Orbitrap resolution (at 200 *m/z* FWHM).

**Table 5.5** Ion source parameters for UHLPC-MS/MS data acquisition using Thermo Fisher Orbitrap ID-X Tribrid mass spectrometer.

| **H-ESI ion source parameters** | **HILIC** | **RP $C_{18}$ lipidomics** |
|---|---|---|
| **Sheath gas (Arb)** | 40 | 40 |
| **Auxiliary gas (Arb)** | 8 | 8 |
| **Sweep gas (Arb)** | 1 | 1 |
| **Spray voltage (kV), positive ion mode** | 3200 | 3200 |
| **Spray voltage (kV), negative ion mode** | 2700 | 2700 |
| **Ion transfer tube temp. (°C)** | 300 | 300 |
| **Vaporiser temp. (°C)** | 350 | 350 |
| **S-Lens RF level** | 30 | 60 |

The instrument was calibrated in positive and negative ion modes prior to each analytical run, using the recommended by manufacturer Pierce FlexMix™ calibration solution (P/N A39239). Also, the Orbitrap ID-X EASY-IC™ ion source with internal lock-mass calibration was used in all the instrument methods in order to improve *m/z* assignment accuracy to sub 1 ppm (up to 1500 *m/z*)[195,263].

### 5.2.6.3 RP $C_{18}$ UHPLC-MS/MS lipidomics

UHLPC-MS/MS lipidomics analyses of rat plasma extracts were based upon an established method for plasma liquids using RP $C_{18}$ chromatography, as previously described[120,121,176,262], with slight modifications. Chromatography in both $C_{18}$ RP lipidomics assays was achieved using a reversed-phase Hypersil GOLD C18 column (100 × 2.1 mm, 1.9 µm; Thermo Fisher Scientific), maintained at 55 °C for both positive and negative ionisation modes. Mobile phase A was composed of 60% acetonitrile:water (10 mM ammonium formate, 0.1% formic acid), and mobile phase B was composed of 85.5:9.5:5 v/v/v propan-2-ol:acetonitrile:water (10 mM ammonium formate, 0.1% formic acid) for both positive and negative ionisation modes. The gradient elution (15 min) was as follows: t = 0.0–9.4 min, 20% B; t = 9.4–12.6 min, 100% B; t = 12.6–15.0 min, 20% B. The flow rate of mobile phase was 0.4 mL $min^{-1}$. Samples were maintained at 4 °C and sample injection volume was 2 µL.

High resolution full scan $MS^1$ and $MS^n$ data were acquired in a data-dependent (DDA) fashion, as described above. $MS^1$ data in full scan mode were collected using an Orbitrap mass analyser over a 150-2000 *m/z* scan range at a resolution of 120,000 (at *m/z* 200 FWHM), a standard AGC target and a maximum injection time mode set to

'automatic'. Ion source settings for HILIC and RP $C_{18}$ methods are summarised in Table 5.5.

The $MS^n$ fragmentation data were collected in the same manner as described in the previous section 5.2.5.2 for the HILIC assays.

## 5.2.7 Untargeted xenobiotic data processing of UHPLC-MS/MS data

### 5.2.7.1 *In silico* prediction of xenobiotic metabolism

The five xenobiotics under study were profiled by the PCB (Dr Matthew Smith) using SyGMa Python library for the Systematic Generation of Metabolites, a knowledge-based *in silico* prediction tool (https://sygma.readthedocs.io/en/latest/)[255]. It comprises 144 reaction rules (approximately 70% of metabolic reactions observed in humans) combining expert knowledge and statistical analysis of phase I and phase II human metabolic reactions. Each prediction is assigned a probability score (SyGMa score), representing the accuracy of each biotransformation rule applied.

The number of both phase I and phase II transformation steps was set to three and the most common ion forms and natural abundance isotopes that can be detected in LC-ESI-MS based metabolomics were considered to match PCB protocols. The adducts used for each UHLPC-MS assay are summarised in Table 5.6. After filtering of the SyGMa generated BTP lists, predictions of BTPs with identical molecular formulae were combined and only chemical structures with SyGMa probability score > 0.01% were retained for each xenobiotic.

**Table 5.6** List of common ion forms used for generating SyGMa predictions of xenobiotics under study.

| **HILIC (+) and RP $C_{18}$ lipidomics (+)** | | **HILIC (-)** | | **RP $C_{18}$ lipidomics (-)** | |
|---|---|---|---|---|---|
| **Ion name** | **Ion mass (Da)** | **Ion name** | **Ion mass (Da)** | **Ion name** | **Ion mass (Da)** |
| [M+H]+ | M+1.007276432 | $[M-H]^-$ | M-1.007276432 | [M-H]- | M-1.007276432 |
| $[M+NH4]^+$ | M+ 18.03382553 | $[M+Cl]^-$ | M+34.96940128 | [M+Cl]- | M+ +34.96940128 |
| $[M+Na]^+$ | M+ 22.98922068 | $[M+Acetate]^-$ | M+59.01385294 | [M+Formate]- | M+ +44.99820287 |

Those SyGMa-generated lists of predicted biotransformation products were subsequently used as original inclusion lists in a DDA method for each xenobiotic in the PCB untargeted xenobiotic analytical workflow implemented on a QExactive Focus Orbitrap LC-MS/MS system (Thermo Fisher Scientific, Hemel Hempstead, UK) and in the AcquireX data acquisition workflow as described in Section 5.2.5.1.

### 5.2.7.2 Phenome Centre Birmingham xenobiotic processing workflow

Untargeted metabolomics datasets (full scan $MS^1$ data and $MS^n$ data) collected on a Q-Exactive Focus Orbitrap LC-MS/MS system (Thermo Fisher Scientific, Hemel Hempstead, UK) were subsequently processed by PCB using a novel workflow[6] aiming to extract, process and identify features corresponding to the xenobiotic parents and/or their biotransformation products (BTPs) in rat plasma extracts. The graphical representation of the xenobiotic workflow implemented by PCB is shown in Figure 5.3.

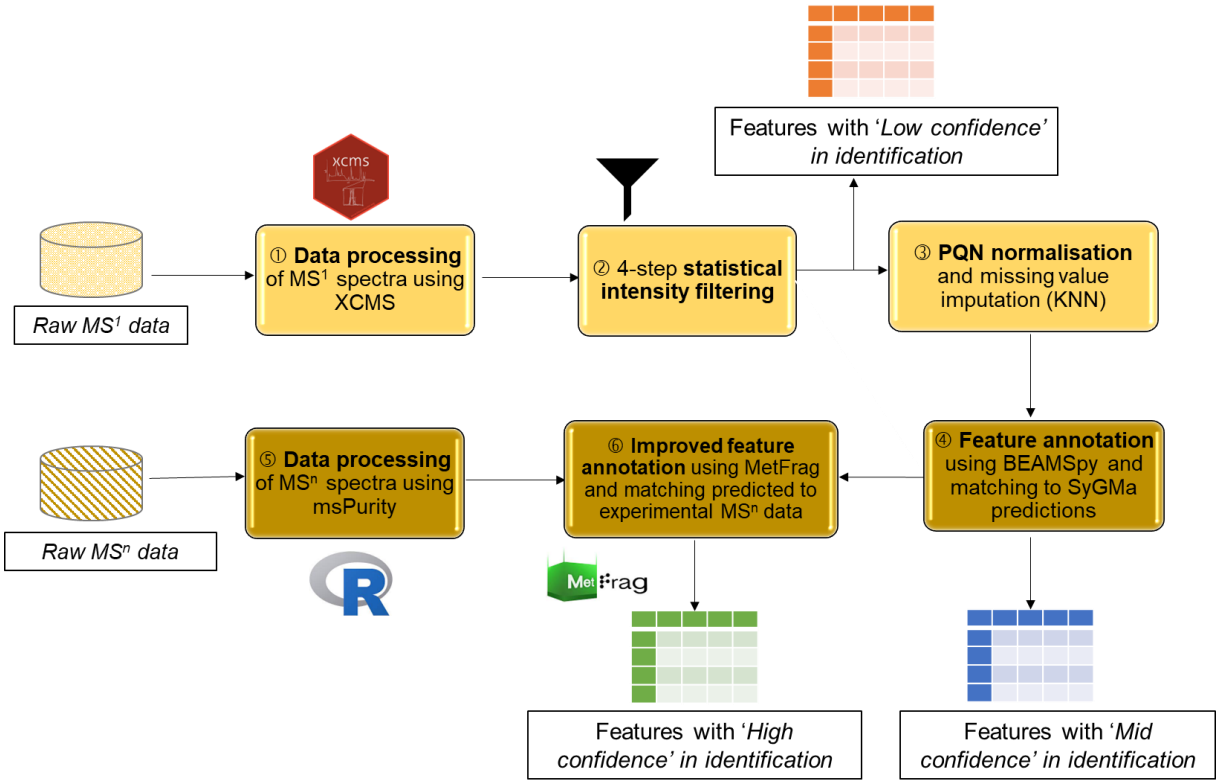


**Figure 5.3** Overview of the PCB xenobiotic data processing workflow (updated from Bowen *et al.*[6]). The initial four-step filtering of full scan $MS^1$ data yields *m/z* features with PCB '*low confidence*' in identification. Next, the *m/z* features are annotated using SyGMa and BEAMSPy to yield PCB '*mid confidence*' in identification. The final step is the inclusion of $MS^n$ data for PCB '*high confidence*' in identification using MetFrag.

The PCB xenobiotic data processing workflow incorporated six steps implemented to improve identification of xenobiotic-related *m/z* features using open-source packages. Briefly, full scan $MS^1$ data underwent processing and peak-picking using an open-source XCMS software (https://xcmsonline.scripps.edu/)[264]. Secondly, four-step feature intensity filters were applied to the resulting full scan $MS^1$ data matrix to extract putative xenobiotic-related features (referred to as with '*low confidence*' in identification by PCB). Next, the experimentally obtained full scan $MS^1$ data were compared with *in silico* SyGMa[255] predictions and annotated using the Python package, BEAMSPy

(v1.1.0; https://github.com/computational-metabolomics/beamspy) to yield xenobiotic-related features with PCB '*mid confidence*' in identification. Finally, $MS^n$ fragmentation data obtained for xenobiotic-related features in rat plasma were annotated using MetFrag *in silico* predicted $MS^n$ data (https://ipb-halle.github.io/MetFrag/projects/metfragweb/)[265,266]. These xenobiotic-related features were considered PCB '*high confidence*' in identification as the matches were based on accurate *m/z* full scan $MS^1$ and $MS^n$ data. In addition, the identity of xenobiotic parents was confirmed by comparison of experimental $MS^n$ data from obtained from rat plasma against experimental $MS^n$ data derived from the measurements of reference standards under the same analytical conditions.

All the above-described steps in the xenobiotic data processing workflow were conducted by PCB.

#### 5.2.7.2.1 DATA PROCESSING AND ANALYSIS USING COMPOUND DISCOVERER

Untargeted metabolomics datasets (full scan $MS^1$ data and $MS^n$ data) obtained on a Orbitrap ID-X Tribrid mass spectrometer LC-MS/MS system were imported into commercial software, Compound Discoverer (v3.3; Thermo Fisher Scientific, Hemel Hempstead, UK) to process, extract and identify xenobiotic-related features (specifically, parent chemicals and their biotransformation products) in rat plasma extracts. Compound Discoverer (CD) is an all-in-one toolbox for compound identification and structure elucidation[197,267,268].

#### 5.2.7.2.2 *IN SILICO* PREDICTION OF XENOBIOTIC METABOLISM

Raw UHPLC-MS/MS data files from all four assays were processed using an existing targeted CD workflow, namely 'Untargeted metabolomics using online databases, mzLogic, and Molecular Networks' implemented to find and identify differences between high dose treated and untreated control samples within ±5 ppm tolerance window. This automated workflow performs adaptive retention time alignment (using ChromAlign algorithm[269]), followed by unknown compound detection using mzCloud (from $ddMS^2$) and ChemSpider (based on a chemical formula or exact *m/z*), and feature grouping across all samples. It also predicts elemental compositions for all compounds, fills gaps across all samples and subtracts chemical background (using process or extraction blank samples). The mzLogic algorithm is subsequently applied to rank order ChemSpider results and Molecular Networks can be generated to reveal associations between compounds[197,267].

This existing CD workflow was further customised by the addition of the 'Generate Expected Compounds' and 'FISh Score' (Fragment ion search scoring algorithm) nodes, as shown in Figure 5.4. The 'Generate Expected Compounds' tool in CD was used to generate theoretical BTPs of the five xenobiotics under study. The standard CD software library was used, with default Phase I and Phase II modifications and a maximum of three dealkylation steps. A maximum number of Phase II steps and a maximum number of all steps were set to two and four, respectively. Mass error tolerance was set to ± 5 ppm and intensity tolerance to 30%. The detailed CD settings used for predicting the biotransformations of xenobiotics are summarised in Table 5.7.

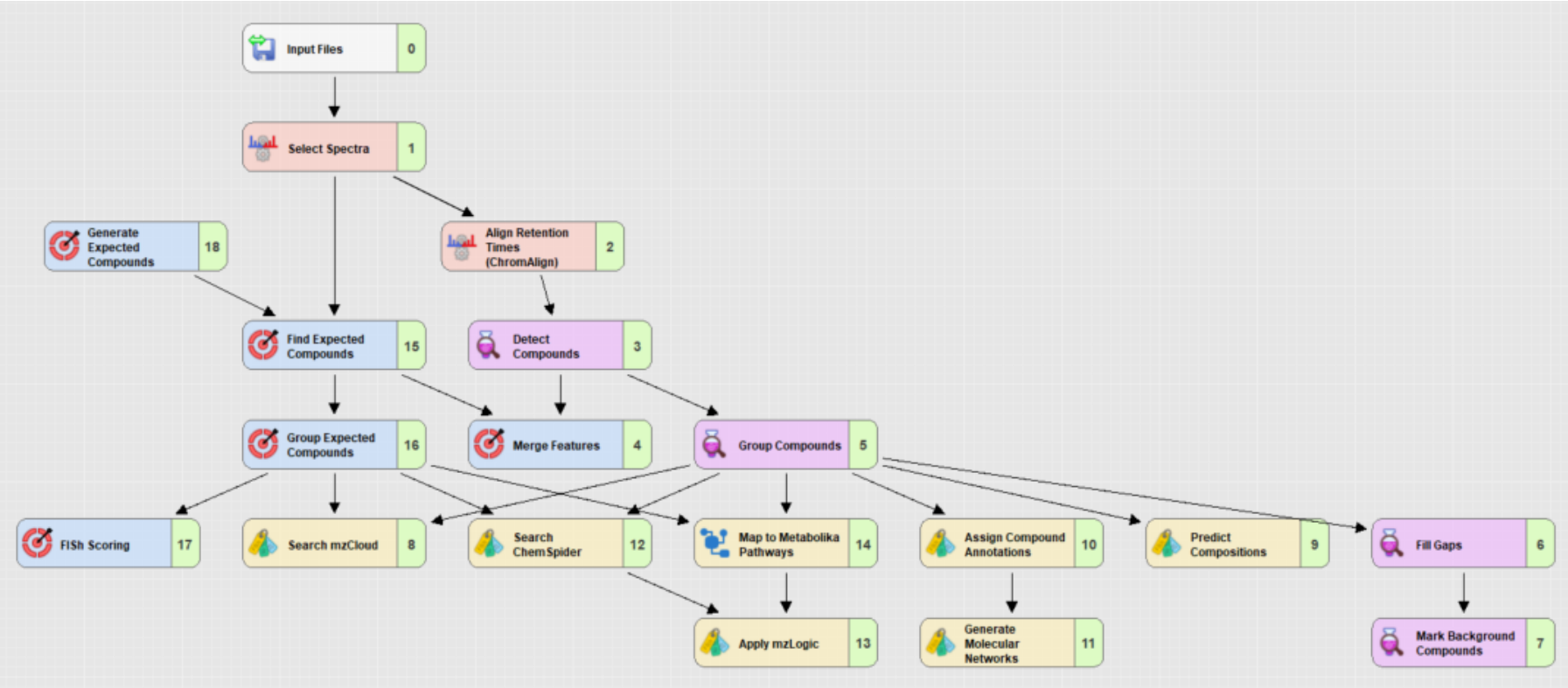


**Figure 5.4** Compound Discoverer workflow ('Untargeted metabolomics using online databases, mzLogic, and Molecular Networks') applied for the prediction, processing and identification of xenobiotic-related features in UHPLC-MS/MS datasets. *In silico* prediction of BTPs was performed using the 'Generate Expected Compounds' node. The 'FISh Scoring' node performs structural annotations of $MS^n$ spectra.

**Table 5.7** Summary of Compound Discoverer processing parameters applied for the prediction ('Generate Expected Compound' tool) and detection ('Find Expected Compounds' tool) of xenobiotic parents and BTPs.

| **'Generate Expected Compounds'** | |
|---|---|
| Dealkylation Max. # steps | 3 |
| Apply Dearylation | True |
| Min. mass (Da) | 200 |
| Phase I transformations (selected all) | Dehydration (H2 O → ); Desaturation (H2 → ); Hydration ( → H2 O); Nitro Reduction (O2 → H2); Oxidation ( → O); Oxidative Deamination to Alcohol (H2 N → H O); Oxidative Deamination to Ketone (H3 N → O); Oxidative Debromination (Br → H O); Oxidative Dechlorination (Cl → H O); Oxidative Defluorination (F → H O); Reduction ( → H2); Reductive Debromination (Br → H); Reductive Dechlorination (Cl → H); Reductive Defluorination (F → H); Thiourea to Urea (S → O) |
| Phase II transformations (selected all) | Acetylation (H → C2 H3 O); Arginine Conjugation (H O → C6 H13 N4 O2); Cysteine Conjugation 1 (H → C3 H6 N O2 S); Cysteine Conjugation 2 ( → C3 H7 N O2 S); Glucoside Conjugation (H → C6 H11 O5); Glucuronide Conjugation (H → C6 H9 O6); Glutamine Conjugation (H O → C5 H9 N2 O3); Glycine Conjugation (H O → C2 H4 N O2); GSH Conjugation (on Bromine) (Br → C10 H16 N3 O6 S); GSH Conjugation (on Chlorine) (Cl → C10 H16 N3 O6 S); GSH Conjugation (on Fluorine) (F → C10 H16 N3 O6 S); GSH Conjugation 1 ( → C10 H15 N3 O6 S); GSH Conjugation 2 ( → C10 H17 N3 O6 S); Methylation (H → C H3); Ornitine Conjugation (H O → C5 H11 N2 O2); Palmitoyl Conjugation (H → C16 H31 O); Stearyl Conjugation (H → C18 H35 O); Sulphation (H → H |

| | |
|---|---|
| **'Generate Expected Compounds'** | |
| | O3 S); Taurine Conjugation (H O → C2 H6 N O3 S) |
| Max. # phase II reactions | 2 |
| Max. # all steps | 4 |
| Ionisation (default settings for both ion modes) | [2M+ACN+H]+1; [2M+ACN+Na]+1; [2M+FA-H]-1; [2M+H]+1; [2M+K]+1; [2M+Na]+1; [2M+NH4]+1; [2M-H]-1; [2M-H+HAc]-1; [M+2H]+2; [M+3H]+3; [M+ACN+2H]+2; [M+ACN+H]+1; [M+ACN+Na]+1; [M+Cl]-1; [M+DMSO+H]+1; [M+FA-H]-1; [M+H]+1; [M+H+K]+2; [M+H+MeOH]+1; [M+H+Na]+2; [M+H+NH4]+2; [M+H-H2O]+1; [M+H-NH3]+1; [M+K]+1; [M+Na]+1; [M+NH4]+1; [M-2H]-2; [M-2H+K]-1; [M-H]-1; [M-H+HAc]-1; [M-H+TFA]-1; [M-H-H2O]-1 |
| **'Find Expected Compounds'** | |
| Mass tolerance | 5 ppm |
| Intensity tolerance (isotope search) (%) | 30 |
| Intensity threshold (%) | 0.1 |
| Use most intense isotope only | True |
| Min. peak intensity | 1e5 |
| **FISh Scoring (fragment prediction)** | |
| S/N ratio threshold | 3 |
| Min fragment m/z | 50 |
| High acc. mass tolerance | 2.5 mmu |
| High acc. mass tolerance | 0.5 Da |
| Max depth | 5 |
| Aromatic cleavage | True |
| Use libraries | True |

CD detected the chromatographic peaks in each dataset (containing both experimental $MS^1$ and $MS^n$ data) and compared the corresponding mass for each compound against

a list of predicted BTPs. The experimental fragmentation ($MS^2$ and $MS^3$) mass spectra were annotated, and a FISh Score Coverage value (ranging from 0% to 50% in UHPLC-MS/MS datasets) was subsequently assigned to each detected 'expected compound' to determine the percentage match between *in silico* predicted and experimental fragmentation spectra.

Fragment ion search scoring algorithm (FISh) can be used with any level of $MS^n$ data and applies Thermo Fisher Mass Frontier™ Fragmentation Libraries[270] to predict *in silico* fragments based on the structure of the parent compound or dealkylation[7,268]. A composite FISh Score (%) is determined by dividing the number of matched centroids by the number of used (i.e., matched and unmatched) centroids and multiplying by 100 using the formula below[197,267]:

**FISh Coverage Score** = ($\Sigma_{\text{per all scan per all scans}}$ number of matched centroids) / ( $\Sigma_{\text{per all scans}}$ number of centroids in the fragmentation scan that are above the S/N threshold) × 100%

#### 5.2.7.2.3 METABOLITE IDENTIFICATION

First, the CD-generated list of expected compounds corresponding to the five xenobiotic was filtered by the chromatographic peak area, the FISh Coverage Score (as recommended in the '*Compound Discoverer 3.3 SP1 Metabolism Tutorial*'[267]) and ± 5 ppm mass error. The filtering criteria applied to extract the initial lists of xenobiotic-related features (putative annotations) from each dataset, corresponding to an UHLPC-MS assay, are shown in Figure 5.5. Any low-intensity *m/z* features (Area (Max.) < 1e05) or features with FISh Score (< 10%) were deemed insignificant and

rejected from the dataset. Potential BTPs were considered based on exact mass, presence of $MS^n$ fragmentation data (any features with only $MS^1$ data available were excluded from further analysis), retention time (RT) and a visual inspection of the isotopic pattern in $MS^1$ data. Any *m/z* features present in blanks or control samples were regarded as false positives and, therefore, removed from the candidate list to ensure that a particular fragment was not a result of contamination.

Data-driven mass accuracy tolerance thresholds specific for each dataset were derived following the examination of the initial error distributions (within ± 5 ppm mass error). Histograms of mass errors were created using the R programming language.

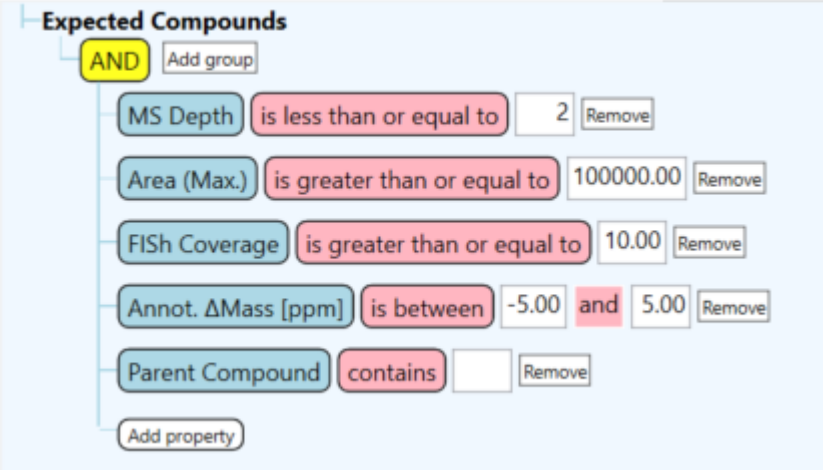


**Figure 5.5** Filtering criteria applied in Compound Discover to extract xenobiotic parents and biotransformation products (BTPs).

Different descriptors of confidence in annotation/identification have been proposed in the metabolomics community[10,11,184,271]. For the work described in this chapter, a series of specific criteria was derived to define confidence levels in identification (MetID) of xenobiotic parent and BTPs, as summarised in Figure 5.6 below. The general strategy

for identification of ‘high confidence’ *m/z* features in rat plasma extracts was by comparison with the analytical reference standard (available for the parent xenobiotics only) analysed under identical experimental UHPLC-MS/MS conditions. The chromatographic retention time, exact mass, the isotopic fragmentation pattern, and $MS^n$ fragmentation pattern in biological samples were compared against those obtained for the high purity standard. In the absence of $MS^n$ fragmentation data (or if *m/z* features were grouped incorrectly by Compound Discoverer) for the reference standards, a high confidence match to a mass spectral library entry (mzCloud or ChemSpider) was also considered to assign ‘high confidence’ in identification of the xenobiotic parents only as these five chemicals are in available in public databases (as confirmed by a manual search).

As reference standards are not available for the majority of BTPs and their analytical behaviour is not very predictable in terms of RT in relationship to parent[272], their identities were confirmed by annotating and explaining the accurate mass $MS^n$ fragments in the experimental data by applying FISh score. Only features with $MS^1$, RT information and $MS^n$ fragmentation data were considered. If multiple explanations were provided for the same *m/z* feature (i.e. identical MW × RT dimension) by CD, the preference was given to the features with the highest FISh Scoring and fewer reaction steps. This constitutes ‘medium confidence’ level in identification (for the purpose of this work).

‘Low confidence’ features did not pass the original filtering criteria (FISh Score ≥10 and ±1 ppm error threshold, only present in samples of interest, i.e. not detected in controls, blanks or any other biological samples) and were manually extracted from the dataset.

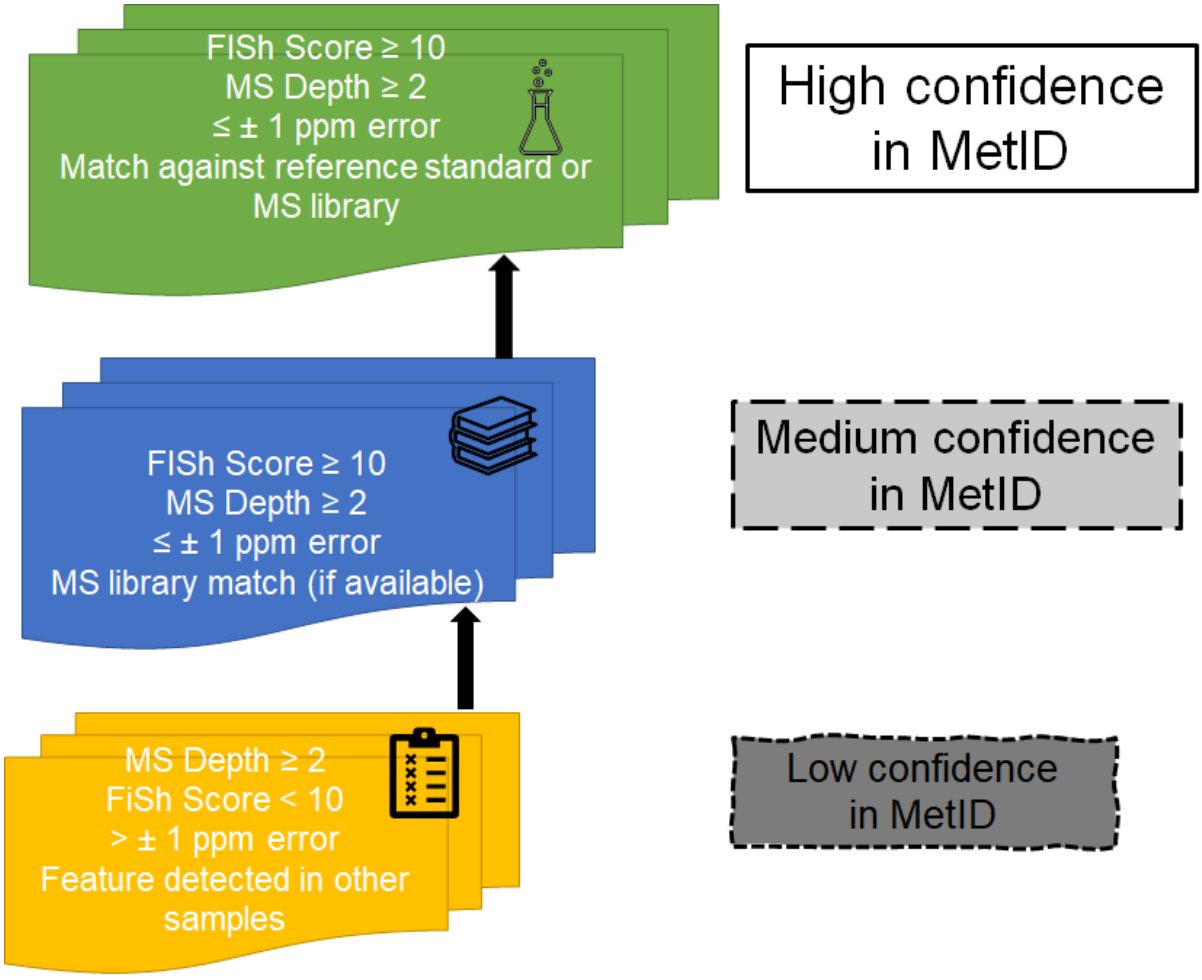


**Figure 5.6** Proposed levels of confidence in identification of xenobiotic-related *m/z* features in UHPLC-MS/MS datasets using Compound Discoverer for *m/z* features within approx. ± 1ppm mass error tolerance. Specific data-driven ppm error thresholds were derived for each assay based on ppm error distributions (as described later in section 5.3.3).

## 5.3 Results and discussion

### 5.3.1 ClassyFire taxonomic classification of xenobiotics

The five structures were submitted to ClassyFire (http://classyfire.wishartlab.com)[237], a web-based application for automated structural classification of chemical entities developed for the metabolomics community. Out of the five xenobiotics studied, four

are classified as benzenoids (BPAF, DEHP, TBBPA and TCS) and one (TCPP) belongs to organic acids and derivatives superclass (Table 5.8). These five structurally unrelated xenobiotics also represent four different subclasses suggesting that their biotransformation behaviour in rat may also be very different.

**Table 5.8** The ClassyFire taxonomic classification of the five xenobiotics.

| Name (abbr.) | Super class | Class | Subclass |
|---|---|---|---|
| **BPAF** | Benzenoids | Benzene and substituted derivatives | Diphenylmethanes |
| **DEHP** | Benzenoids | Benzene and substituted derivatives | Benzoic acid esters |
| **TBBPA** | Benzenoids | Benzene and substituted derivatives | Diphenylmethanes |
| **TCPP** | Organics acids and derivatives | Organic phosphoric acids and derivatives | Phosphate esters |
| **TCS** | Benzenoids | Benzene and substituted derivatives | Diphenylethers |

## 5.3.2. Published *in vivo* rat metabolism data for xenobiotics

Published literature was consulted to obtain and collate relevant information on metabolism and metabolic fate of the five xenobiotics in rat models in various sample types. The summary is provided in Table 5.9.

**Table 5.9** Biotransformation products formed by the five xenobiotics in *in vivo* and *in vitro* studies (only rat data was considered). Table adapted and updated from Skedlar et *al*, 2016[12].

| Name (abbr.) | Matrix | Major metabolites formed | References |
|---|---|---|---|
| **BPAF** | Rat bile, rat urine, rat plasma, hepatocytes | • BPAF glucuronide[a,b,c]<br>• BPAF diglucuronide[a,b]<br>• BPAF glucuronide dehydrated[b]<br>• BPAF sulphate[a,b]<br>• BPAF glucuronide sulphate[a] | Li et *al.*, 2013[273]; Li et *al*., 2016; Waidyanatha *et al*., 2015, Waidyanatha et al., 2019; Waidyanatha *et al*., 2020; Waidyanatha et *al*., 2021 |
| **DEHP** | Rat urine, rat liver microsomes | • Mono (2-ethylhexyl)phthalate (MEHP)<br>• 2-ethylhexanol (2-EH)<br>• mono(2-ethyl-5-hydroxyhexyl) phthalate (5-OH MEHP)<br>• mono(2-ethyl-5-oxohexyl) phthalate (5-Oxo MEHP)<br>• mono(2-ethyl-5-carboxypentyl) phthalate (5-carboxy MEPP)<br>• mono(2-carboxymethyl-hexyl) phthalate (2-carboxy MMHP)<br>• mono-(2-ethyl-5-oxohexyl) phthalate (MEOHP)<br>• mono-(2-ethyl-5-hydroxyhexyl) phthalate (MEHHP)<br>• mono-(2-ethyl-5-carboxypentyl) phthalate (MECPP)<br>• mono-*n*-butyl phthalate (MBP)<br>• di-*n*-butyl phthalate (DBP)<br>• o-phthalic acid (PA) | ATSDR, 2021; Choi *et al*., 2012 |

| Name (abbr.) | Matrix | Major metabolites formed | References |
|---|---|---|---|
| **TBBPA** | Rat bile | • TBBPA glucuronide<br>• TBBPA diglucuronide<br>• TBBPA glucuronide sulphate<br>• Tribromobisphenol A<br>• Tribromobisphenol A<br>• TBBPA sulphate<br>• TBBPA bisglucuronide<br>• TBBPA glucuronide, sulphate adduct | Hakk *et al*., 2000; Schauer *et al*., 2006; Knudsen *et al*., 2014; Knudsen *et al*., 2018 |
| **TCCP** | Rat urine, rat feaces | • 0,0-[bis(1-chloro-2-propyl)]-0-(2,propionic acid)phosphate<br>• bis(1-chloro-2-propyl) monophosphoric acid<br>• 1-chloro-2-propanol | Stauffer Chemical Co., 1984 (as cited in Health Canada, October 2020); Minegishi *et al*., 1998; ECHA 2008; |
| **TCS** | Rat urine | • Monohydroxylated TCS (OH-TCS)<br>• TCS glucuronide<br>• TCS sulphate<br>• TCS glucoside<br>• Hydroxylated TCS sulphate<br>• TCS cysteine conjugation<br>• TCS acetylcysteine conjugation<br>• TCS glucuronide, acetylcysteine conjugation<br>• 2,4-dichlorophenol<br>• 4-chlorocatechol | Wu *et al*., 2010; Fang *et al*., 2010 |

[a] Detected in rat bile, [b] in rat urine and/or in [c] rat plasma.

Published ADME/TK data for BPAF suggests a similar metabolic profile *in vivo* to its structural analogue, BPA[273]. Glucuronidation and sulphation are considered the major

metabolic pathways for BPAF and TBBPA, while oxidation is a minor detoxification mechanism[12,274].

DEHP ADME/TK properties have been widely studied with the majority of studies conducted in rat models[275,276]. DEHP is rapidly and extensively metabolised to >30 metabolites that are excreted in urine or bile primarily as glucuronide conjugates[275,276]. Urinary concentrations of four primary DEHP metabolites (MEHP, MEOHP, MEHHP and MECPP) are considered biomarkers for DEHP exposure and have been measured in the US CDC's (Centres for Disease and Control and Prevention) National Biomonitoring Programme (https://www.cdc.gov/biomonitoring/DEHP_BiomonitoringSummary.html).

While BPAF and DEHP metabolism in rodent models appears relatively extensively reported in literature, limited metabolism data exists for TCCP. To my knowledge, only one study to date has pertained to investigate TCCP metabolism in mammals (Stauffer Chemical Co, 1984, as cited in Health Canada, 2020 and EPA, 2012)[277,278]. According to this study, TCCP undergoes rapid metabolism in rats with a dose-dependent elimination pattern (89% of TCPP and its metabolites is eliminated by 72 h, primarily via urine), resulting in the formation of potentially stable BTPs. 0,0-[bis(1-chloro-2-propyl)]-0-(2,propionic acid)phosphate is the major TCCP metabolite and accounts for over half of the dose[277]. Rapid biotransformation rates may also suggest a low bioaccumulation potential for TCCP.

Wu *et al*. (2010) identified 12 triclosan biotransformation products using high-performance liquid chromatography-atmospheric pressure chemical ionisation ion trap mass spectrometry (HPLC-APCI-MS/MS). It predominantly undergoes hydroxylation

in phase I metabolism, while glucuronidation and sulphation are the main phase II metabolism modifications[279]. Triclosan can also be cleaved to form 2,4-dichlorophenol, and 4-chlorocatechol, detectable in rat urine and faeces[280].

### 5.3.2 Manual inspection of raw UHLPC-MS/MS data

Prior to the application of the automated targeted CD workflow to each dataset, the raw UHLPC-MS/MS files (specifically $MS^1$, retention time and $MS^n$ fragmentation data) in all four assays were examined manually to confirm the presence of the parent chemical for all five xenobiotics under study. Both analytical standard samples and experimental rat plasma samples were interrogated, and the initial findings are presented in Tables 5.10 and 5.11, respectively. Chromatographic peaks were detected for all five xenobiotic parents in the analytical standards. Molecular ions ($[M+H]^+$/$[M-H]^-$) were also detected for all xenobiotics in at least one assay in full scan $MS^1$ data in rat plasma. However, the shoulder peak for the parent was not intense enough to trigger an $MS^n$ scan so fragmentation data is often missing for the precursor ion of interest in rat plasma extracts.

**Table 5.10** Detection of parent chemicals in analytical standards by manual inspection of raw UHLPC-MS/MS data.

| Name (abbr.) | Experimental molecular ion[a] (*m/z*) | RT (min) | Parent chemical in analytical standard | |
|---|---|---|---|---|
| | | | Detected in raw LC-$MS^1$ data (assay) | Detected in LC-$MS^n$ data |
| **BPAF** | 335.0510<br>335.0511 | 0.44<br>0.82 | ✓ HILIC (-)<br>✓ $C_{18}$ Lipidomics (-) | ✓<br>✓ |
| **DEHP** | 391.2844<br>391.2842 | 0.44<br>5.0 | ✓ HILIC (+)<br>✓ $C_{18}$ Lipidomics (+) | ✓<br>✓ |
| **TBBPA** | 542.7458<br>542.7474 | 0.44<br>1.31 | ✓ HILIC (-)<br>✓ $C_{18}$ Lipidomics (-) | ✓<br>✓ |
| **TCPP** | 327.0082<br>327.0083<br>348.9901[b] | 0.46<br>0.88<br>0.88 | ✓ HILIC (+)<br>✓ $C_{18}$ Lipidomics (+)<br>✓ $C_{18}$ Lipidomics (+) | ✓<br>✓<br>✓ |
| **TCS** | 286.9440<br>286.9443 | 0.45<br>1.36 | ✓ HILIC (-)<br>✓ $C_{18}$ Lipidomics (-) | ✓<br>✓ |

[a] $[M+H]^+$ in positive ion mode and [M-H]- in negative ion mode

[b] $[M+Na]^+$

**Table 5.11** Detection of parent chemicals in rat plasma by manual inspection of raw UHPLC-MS/MS data.

| **Name (abbr.)** | **Experimental molecular ion[a] (*m/z*)** | **RT (min)** | **Parent chemical in treated biological sample** | |
|---|---|---|---|---|
| | | | **Detected in raw LC-MS$^1$ data (assay)** | **Detected in LC-MS$^n$ data** |
| **BPAF** | 335.0512<br>335.0510 | 0.45<br>0.80 | ✓ HILIC (-)<br>✓ $C_{18}$ Lipidomics (-) | ×<br>✓ |
| **DEHP** | 391.2844<br>391.2844 | 0.43<br>5.11 | ✓ HILIC (+)<br>✓ $C_{18}$ Lipidomics (+) | ×<br>× |
| **TBBPA** | 542.7457<br>- | 0.76<br>- | ✓ HILIC (-)<br>× $C_{18}$ Lipidomics (-) | ×<br>× |
| **TCPP** | -<br>327.0081 | -<br>0.86 | × HILIC (+)<br>✓ $C_{18}$ Lipidomics (+) | ×<br>× |
| **TCS** | 286.9439<br>286.9439 | 0.34<br>0.74 | ✓ HILIC (-)<br>✓ $C_{18}$ Lipidomics (-) | ✓<br>× |

[a]$[M+H]^+$ in positive ion mode and $[M-H]^-$ in negative ion mode

## 5.3.3 Defining mass ppm errors for each UHPLC-MS/MS dataset

Thermo Fisher Scientific technical guidance stipulates that the Orbitrap ID-X Tribrid mass spectrometer consistently achieves sub ±1 ppm mass measurement accuracy when using internal calibration[195,263]. In line with metabolomics best practices[3,281], the initial assessment of UHLPC-MS/MS data quality was performed by interrogating the ppm error distributions in each of the four datasets to derive mass error tolerance thresholds. Figure 5.7 shows histograms plotted for features retained after applying an

initial ±5 ppm mass error filter to each assay in Compound Discover (CD). This initial filter yielded a different number of putative xenobiotic-related features for each assay, as shown in Table 5.11. The optimal ppm error threshold was subsequently derived for each dataset (corresponding to the four UHPLC-MS/MS assays) in order to maximise the potential to gain insights into xenobiotic metabolism and metabolic fate in rat plasma. Using these optimised thresholds, the filtering of *m/z* features generated between 50 (HILIC positive) and 986 (positive RP $C_{18}$ lipidomics) putative annotations, summarised in Table 5.12. After examining the histograms of ppm error distributions (Figure 5.7), the $C_{18}$ lipidomics positive assay was considered problematic due to the relatively high ppm errors observed. However, it was still included in further analysis and, for consistency, a similar error threshold was applied to retain only the high-quality xenobiotic-related features in this dataset.

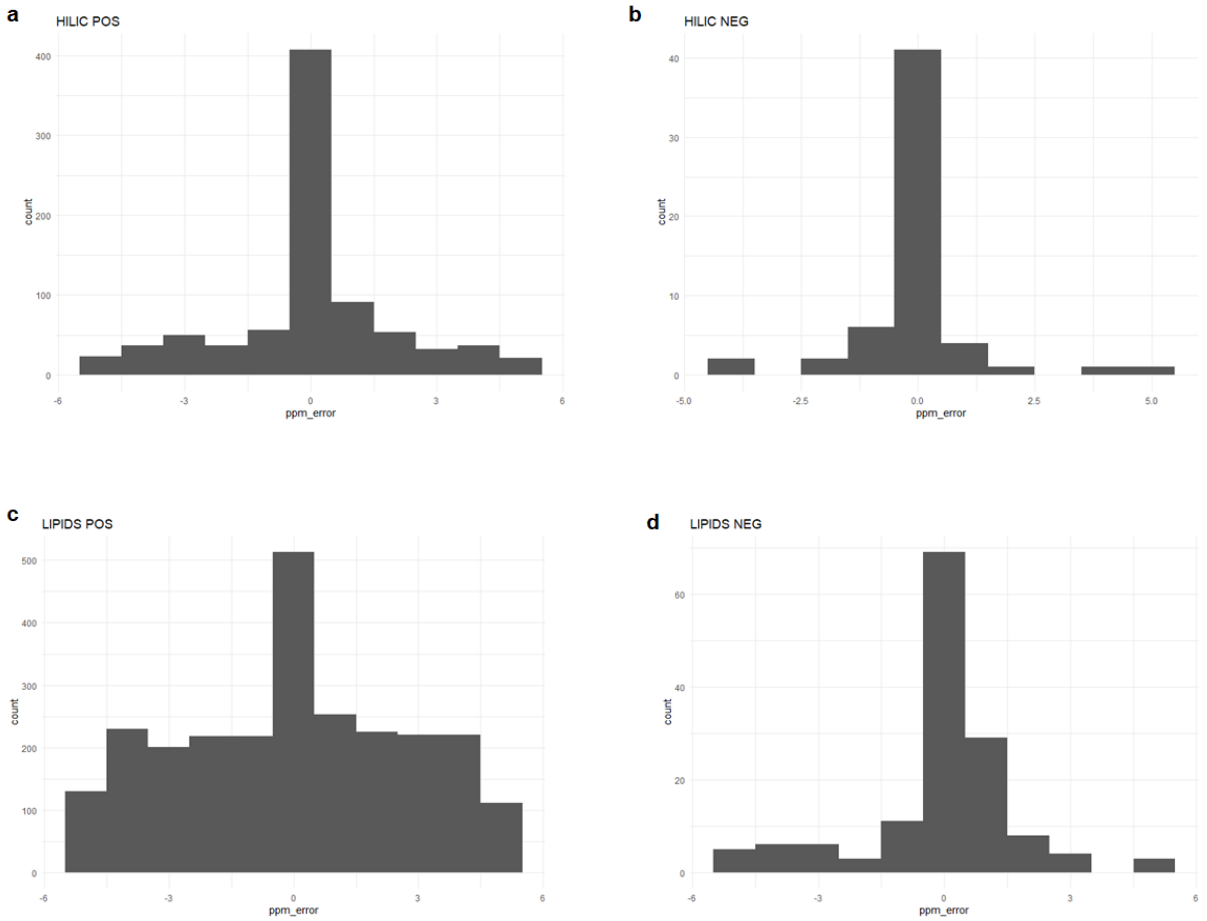


**Figure 5.7** Histograms summarising the m/z measurement error (ppm) across all xenobiotic-related features (putative annotations) detected in UHLPC-MS/MS assays: (**a**) HILIC (+) metabolomics, (**b**) HILIC (-) metabolomics, (**c**) RP $C_{18}$ (+) lipidomics and (**d**) RP $C_{18}$ (-) lipidomics. Abbreviations: (+) positive ion mode, (-) negative ion mode.

**Table 5.12**. Summary of xenobiotic features (putative annotations) retained in each UHLPC-MS/MS dataset after applying the optimised data-driven mass error thresholds in Compound Discoverer.

| Assay | Features within original ±5 ppm mass measurement error (putative annotations) | Selected mass accuracy threshold (ppm) derived from Figure 5.7 | Features retained after filtering by optimised ppm error tolerance |
|---|---|---|---|
| **HILIC (+)** | 844 | -1.25 to 1.25 | 528 |
| **HILIC (-)** | 58 | -1.25 to 1.25 | 50 |
| **Lipids (+)** | 2539 | -1.5 to 1.5 | 986 |
| **Lipids (-)** | 144 | -1.00 to 1.5 | 108 |

## 5.3.4 Parent chemicals and biotransformation products discovered by Compound Discoverer

The numbers of xenobiotic-related features (putative annotations) detected by Compound Discoverer per chemical, per assay, after applying the initial filtering parameters (i.e. MS depth ≥ 2, FISh Coverage ≥ 10%, peak Area (Max.) ≥ 1e5 and a ppm error threshold specific to each dataset, as shown in Table 5.12) are summarised in Table 5.13.

**Table 5.13** Summary of the number of biotransformation products (putative annotations) detected in each mass spectrometry assay after [1] applying the Compound Discoverer (CD) filtering parameters (i.e. ≥ $MS^2$, FISh Coverage ≥ 10%, peak area ≥ 1e5 and approx. ±1 ppm error threshold) followed by [2] manual inspection of the data (considering all adducts listed in CD).

| **Name (abbr.)** | **HILIC (+)** | | **HILIC (-)** | | **Lipids (+)** | | **Lipids (-)** | |
|---|---|---|---|---|---|---|---|---|
| | **[1]** | **[2]** | **[1]** | **[2]** | **[1]** | **[2]** | **[1]** | **[2]** |
| **BPAF** | 11 | 2 | 5 | 3 | 9 | 4 | 41 | 1 |
| **DEHP** | 371 | 30[a] | 30 | 10 | 65 | 12[a] | 626 | 28[a] |
| **TBBPA** | 2 | 0 | 2 | 2[a] | 1 | 1 | 0 | 0 |
| **TCPP** | 139 | 51[a] | 0 | 0 | 7 | 6[a] | 253 | 34[a] |
| **TCS** | 4 | 0 | 13 | 11 | 26 | 10 | 29 | 1 |
| **Total per assay** | 527 | 85 | 50 | 26 | 108 | 33 | 949 | 64 |

[a]Inclusive of parent chemical.

The highest number of biotransformation products was detected in the HILIC positive dataset and RP $C_{18}$ lipidomics negative dataset, which revealed between 85 and 64 putative xenobiotic-related features, respectively after manual examination of the chromatograms and mass spectra.

The sections below describe major xenobiotics parents and/or any biotransformation products (BTPs) discovered in rat plasma by applying the automated CD workflow to each assay and inspecting accurate mass $MS^1$, chromatographic peak retention time (RT) and $MS^n$ fragments for each *m/z* feature. The xenobiotic-related features revealed by the analysis were assigned a ‘high’, ‘medium’ or ‘low’ level of confidence based on the specific criteria defined in section 5.2.6.3.2 for this purpose.

### 5.3.5 BPAF

BPAF parent was detected in both analytical reference standard and rat plasma in the RP $C_{18}$ negative lipidomics dataset, eluting at 0.803 min. The injection and analysis of BPAF analytical standard (final concentration 10 µg $mL^{-1}$ in water: iso-2-propanol 1:3 v/v) under the same LC-HRMS conditions aimed to confirm the identity of parent in the biological sample, using accurate *m/z*, RT and $MS^2$ spectral match. This yields the highest level of confidence in identification, corresponding to Schymansky *et al*. (2014) confidence Level 1[11]. Figure 5.8 shows the comparison of RT and $MS^1$ in the biological sample and BPAF analytical standard. However, $MS^n$ fragmentation data were missing (or grouped incorrectly in the Compound Discoverer mass spectral tree) for the parent peak of interest in the reference standard, therefore a spectral match could not be ascertained for the biological sample. In the absence of $MS^n$ fragmentation data for both peaks, a high confidence match of the biological sample to the corresponding entries in the mzCloud (99.7%, within -0.51 ppm mass error) and ChemSpider library entries (within -0.50 ppm) was used to confirm the identity of BPAF parent in the RP $C_{18}$ negative lipidomics dataset, as shown in Figure 5.8. The fragments at 265 *m/z*, 315 *m/z* and 335 *m/z* represent the structural fragments of BPAF parent.

BPAF parent was also detected in analytical standard in the HILIC negative assay (not in rat plasma), but with a lower confidence in identification (FISh score: 3.70%) and automatically matched to the ChemSpider library (based on exact mass and chemical formula/elemental composition).

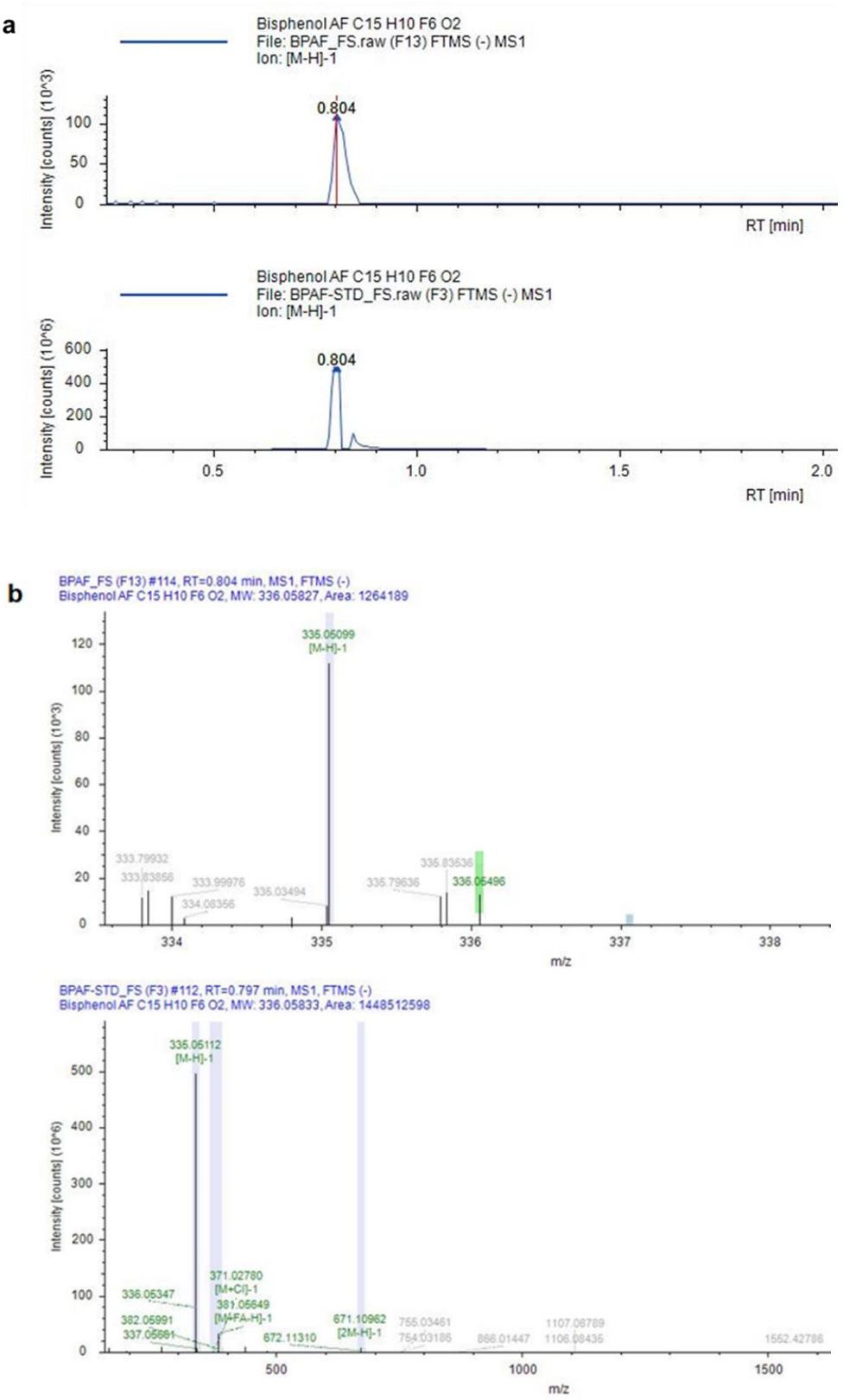


**Figure 5.8** Confirming BPAF parent identity in rat plasma $C_{18}$ negative lipidomics. (**a**) Extracted ion chromatograms of BPAF parent peak in rat plasma (top) and reference standard (bottom) from the RP $C_{18}$ lipidomics analysis. (**b**) Full scan $MS^1$ data showing the

isotope pattern fit for BPAF at $[M-H]^-$ 335.05099 *m/z* in rat plasma (top) and reference standard (bottom), shown on different *m/z* scales on the x-axis.

**a**

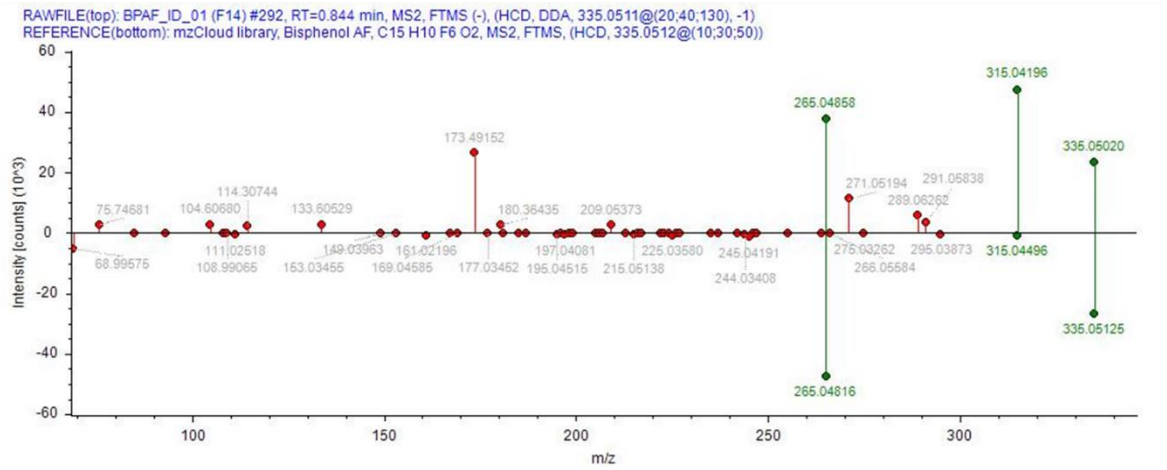


**b**

| Structure | Name | Formula | Molecular W | ΔMass [Da] | ΔMass [ppm] | Confidence | Match | Tree Match | Best Match | Best Sim. Match | Type |
|---|---|---|---|---|---|---|---|---|---|---|---|
| 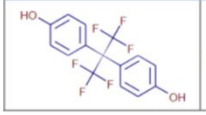 | Bisphenol AF | C15 H10 F6 O2 | 336.05850 | -0.00017 | -0.51 | 8.2 | 64.0 | 58.0 | 99.7 | 62.9 | Identity |

| Structure | Name | Formula | Molecular Weight | ΔMass [Da] | ΔMass [ppm] |
|---|---|---|---|---|---|
| 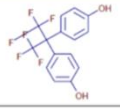 | Bisphenol AF | C15 H10 F6 O2 | 336.05850 | -0.00017 | -0.50 |

**Figure 5.9** BPAF parent identity match in rat plasma resulting from an $MS^2$ spectral match against the mzCloud library (**a**) Mirror plot of the $MS^n$ fragmentation spectrum in rat plasma (top) and match against the mzCloud reference spectrum (bottom). Three overlapping product ions are shown, including the precursor ion and lower molecular weight ions. (**b**) High confidence match for BPAF parent in mzCloud (top) and ChemSpider (bottom) libraries.

A total of five BTPs (M1 to M5) were identified for BPAF as listed by ascending RT in Table 5.14. Two of those BPAF-related features detected in the HILIC positive assay were assigned a 'medium level of confidence' in identification (M2, M5) (Table 5.14, Figure 5.10b and d, respectively).

**Table 5.14** BPAF metabolic biotransformation products identified in UHPLC-MS/MS datasets with assigned levels of confidence in identification: yellow – 'low confidence', blue – 'medium confidence', green – 'high confidence'. Abbreviations: FISh – Fragment ion search scoring, MW – molecular weight, RT – retention time.

| ID | Assay | Formula | Transformations | Composition Change | Annot. DeltaMass [ppm] | Calc. MW | m/z | RT [min] | FISh Coverage | Area (Max.) | mzCloud Best Match | Reference Ion |
|---|---|---|---|---|---|---|---|---|---|---|---|---|
| **M1** | HILIC neg | C15 H10 F6 O5 S | Sulphation | +(O3 S) | -0.61 | 416.01506 | 415.0078 | 0.354 | 8.57 | 4.01E+06 | | [M-H]-1 |
| **M2** | HILIC pos | C22 H23 F5 O10 | Hydration, Oxidative Defluorination, Glucuronide Conjugation, Methylation | -(F) +(C7 H13 O8) | 0.57 | 542.12145 | 543.1287 | 0.43 | 10.2 | 1.83E+05 | | [M+H]+1 |
| **M3** | C18 Lipidomics neg | C21 H18 F6 O8 | Glucuronide Conjugation | +(C6 H8 O6) | 0.47 | 512.09083 | 511.0835 | 0.602 | 5.56 | 2.82E+07 | 85.6 | [M-H]-1 |
| **M4** | C18 Lipidomics neg | C21 H16 F6 O7 | Dehydration, Glucuronide Conjugation | +(C6 H6 O5) | 1.81 | 494.08092 | 493.0736 | 0.644 | 22.22 | 4.11E+05 | | [M-H]-1 |

| ID | Assay | Formula | Transformations | Composition Change | Annot. DeltaMass [ppm] | Calc. MW | m/z | RT [min] | FISh Coverage | Area (Max.) | mzCloud Best Match | Reference Ion |
|---|---|---|---|---|---|---|---|---|---|---|---|---|
| P | C18 Lipidomics neg | C15 H10 F6 O2 | BPAF parent | | -0.5 | 336.05833 | 335.0511 | 0.803 | 11.11 | 1.34E+09 | 64 | [M-H]-1 |
| M3 | HILIC pos | C21 H18 F6 O8 | Glucuronide Conjugation | +(C6 H8 O6) | 0.07 | 512.09062 | 511.0833 | 5.258 | 7.69 | 2.69E+06 | 95.6 | [M-H]-1 |
| M5 | HILIC neg | C21 H18 F6 O11 S | Glucuronide Conjugation, Sulphation | +(C6 H8 O9 S) | -0.22 | 592.04727 | 591.0400 | 5.393 | 10.2 | 1.35E+06 | 97 | [M-H]-1 |

These *m/z* features ($[M+H]^+$ at 543.1287 *m/z* and $[M+H]^-$ 591.0400 *m/z*, respectively) represented phase I modifications observed in this dataset, specifically hydration and oxidative defluorination (M2), while phase II modifications were glucuronide conjugation (M2) followed by methylation (M2) or sulphation (M5). M2 resulted from several (five) phase I and phase II reactions. M5 (predicted by both SyGMa and Compound Discoverer) eluted at 5.393 min and was generated through glucuronide conjugation (+176 Da mass shift) at one of the phenolic hydroxyl groups followed by (phase II) sulphation of another hydroxyl group, as suggested by a +80 Da shift from BPAF parent. M5 fragmentation pattern contained four major product ion fragments of similar intensity (335 *m/z*, 415 *m/z*, 511 *m/z* and 591 *m/z*). In addition, this particular *m/z* feature was also automatically identified by mzCloud and ChemSpider libraries, based on accurate mass, chemical formula and observed fragmentation pattern (Figure 5.10d).

**a**

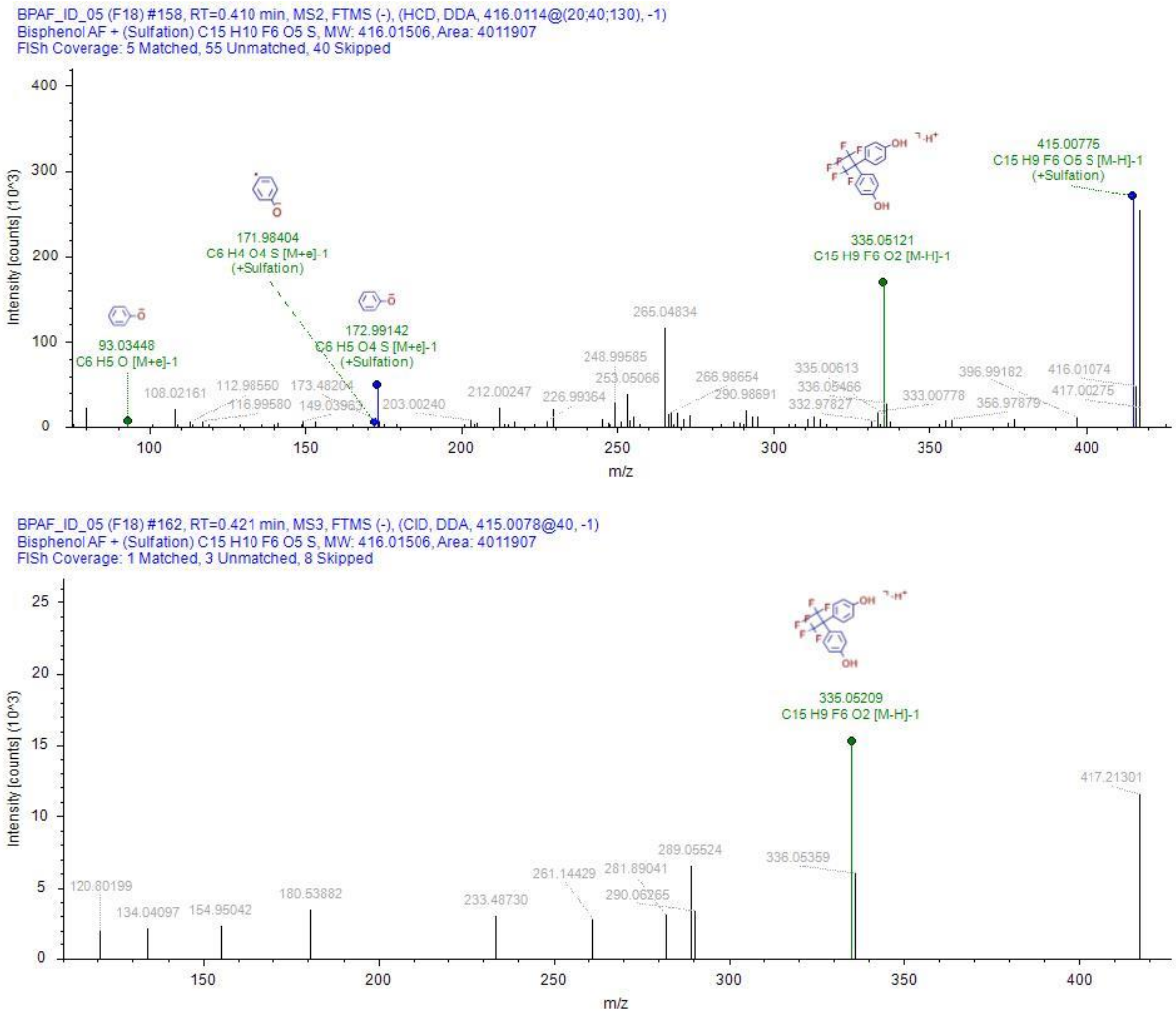
BPAF_ID_05 (F18) #158, RT=0.410 min, MS2, FTMS (-), (HCD, DDA, 416.0114@(20;40;130), -1)
Bisphenol AF + (Sulfation) C15 H10 F6 O5 S, MW: 416.01506, Area: 4011907
FISh Coverage: 5 Matched, 55 Unmatched, 40 Skipped
Intensity [counts] (10^3)
m/z
93.03448
C6 H5 O [M+e]-1
171.98404
C6 H4 O4 S [M+e]-1
(+Sulfation)
172.99142
C6 H5 O4 S [M+e]-1
(+Sulfation)
335.05121
C15 H9 F6 O2 [M-H]-1
415.00775
C15 H9 F6 O5 S [M-H]-1
(+Sulfation)
BPAF_ID_05 (F18) #162, RT=0.421 min, MS3, FTMS (-), (CID, DDA, 415.0078@40, -1)
Bisphenol AF + (Sulfation) C15 H10 F6 O5 S, MW: 416.01506, Area: 4011907
FISh Coverage: 1 Matched, 3 Unmatched, 8 Skipped
335.05209
C15 H9 F6 O2 [M-H]-1

**b**

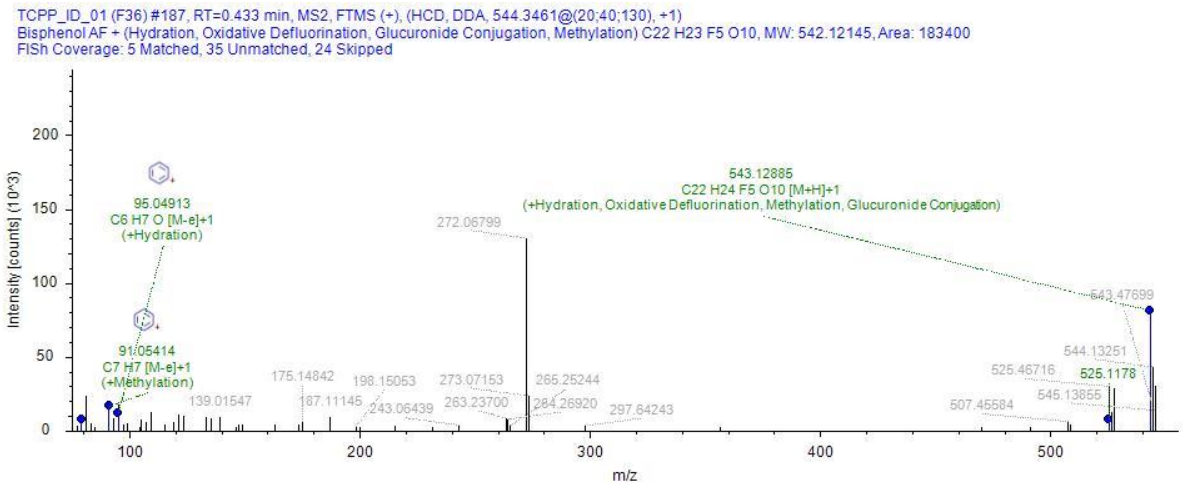
TCPP_ID_01 (F36) #187, RT=0.433 min, MS2, FTMS (+), (HCD, DDA, 544.3461@(20;40;130), +1)
Bisphenol AF + (Hydration, Oxidative Defluorination, Glucuronide Conjugation, Methylation) C22 H23 F5 O10, MW: 542.12145, Area: 183400
FISh Coverage: 5 Matched, 35 Unmatched, 24 Skipped
Intensity [counts] (10^3)
m/z
95.04913
C6 H7 O [M-e]+1
(+Hydration)
91.05414
C7 H7 [M-e]+1
(+Methylation)
543.12885
C22 H24 F5 O10 [M+H]+1
(+Hydration, Oxidative Defluorination, Methylation, Glucuronide Conjugation)

**c**

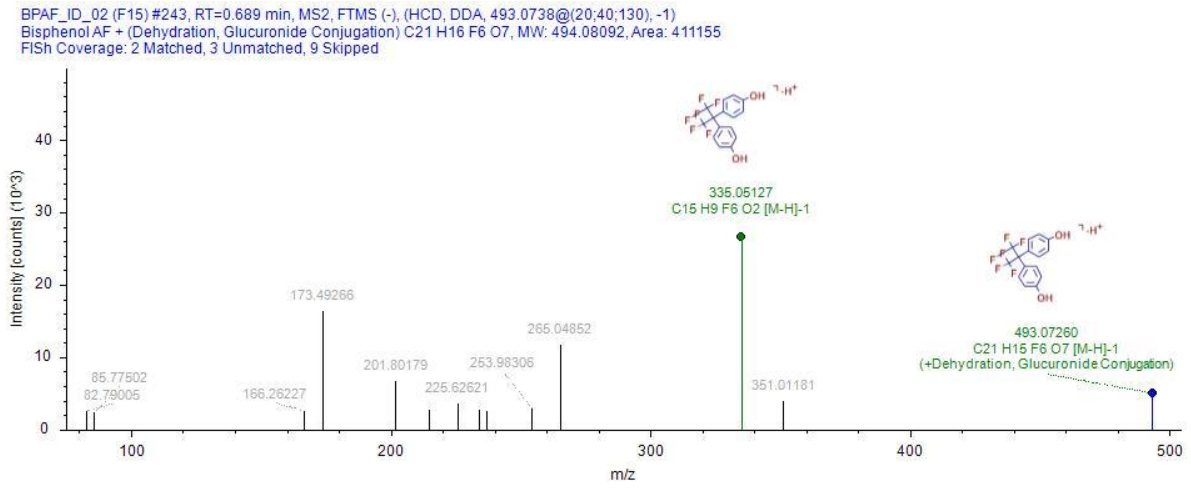


**d**

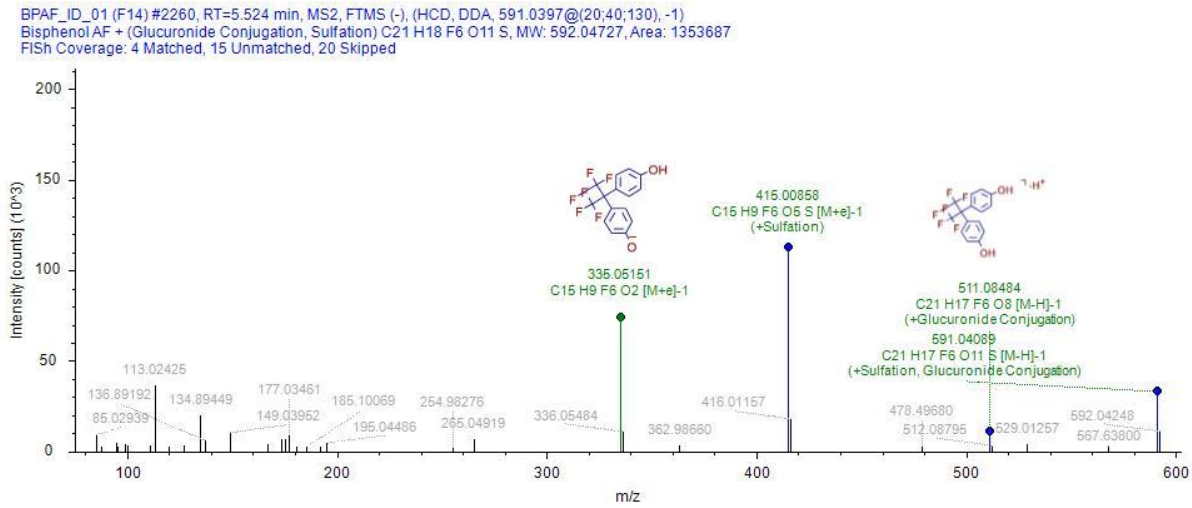


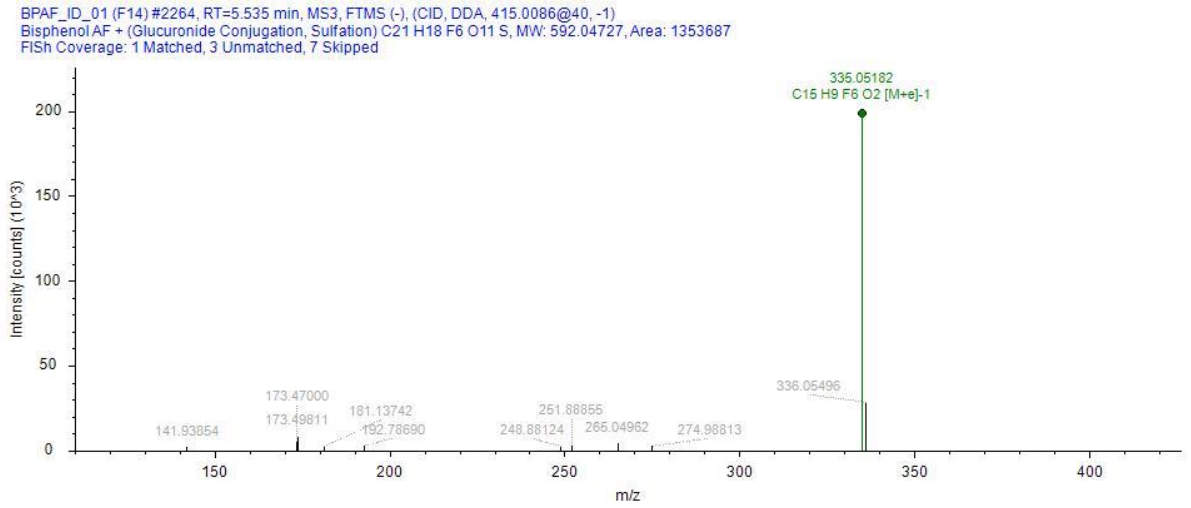


**Figure 5.10** Structure annotations from FISh scoring on MS$^n$ spectra of major BPAF

metabolites discovered in rat plasma: (**a**) M1, (**b**) M2, (**c**) M4 and (**d**) M5. Green – indicates direct match fragments, blue – transformation shifted fragments.

FISh scoring was used to define product ions by structural annotations for the detected BTPs. Specifically, FISh scoring algorithm was applied to the chemical structures of M2 and M5 and associated with the $MS^n$ fragmentation spectrum of the corresponding precursor masses at 543.1287 *m/z* and 591.0400 *m/z*. In the spectra, over 10 % of the possible product ions assessed can be structurally related to the BTPs of interest (Figures 5.10b and d, respectively).

One BPAF-related feature formed by dehydration followed by glucuronidation (M4, 494.08909 *m/z* eluting at 0.644 min in the negative RP $C_{18}$ lipidomics dataset, peak area: 4.11e5) was marked as 'low confidence' as it was outside the ppm error tolerance window of ±1 ppm (1.81 ppm). Figure 5.10c shows $MS^2$ fragmentation spectrum of M4 with structure annotations (from FISh scoring: 22.22%), two product ions were sufficiently matched to theoretical fragment ion masses. The site of transformation can be elucidated from $MS^3$ fragmentation.

Additionally, two 'low confidence' tentative BPAF metabolites discovered in rat plasma were predicted by both SyGMa and Compound Discoverer. Sulphation BTP (M1, 415.0079 *m/z* eluting at 0.354 min and peak area of 4.01e6) was detected in the HILIC negative assay with a lower FISh score value (8.57%) and sub ±1 ppm error (-0.61 ppm). Structure annotations of $MS^n$ mass spectra of the sulphated BTP (M1) are shown in Figure 5.10a.

BPAF glucuronide conjugates (M3) were discovered in two assays (HILIC positive and $C_{18}$ lipidomics negative) with a lower FISh score (7.69% and 5.56%, respectively), sub ±1 ppm error (0.07 ppm and 0.47 ppm, respectively) and automatically matched to the mzCloud spectral library with high confidence (95.6% and 85.6%, respectively). M1 (sulphated BPAF) and M3 (BPAF glucuronide) are also BPAF metabolites with the most intense signal in rat plasma, with a chromatographic peak area (4.01e6 and 2.69e6, respectively). These findings are consistent with published literature that reported BPAF glucuronide as the main BTP formed in *in vivo* studies[12,273,282–284], BPAF glucuronide sulphate was also detected *in vivo*[12,273].

No BTPs were discovered for BPAF in the positive RP $C_{18}$ lipidomics assay. The BTPs (M1 to M5) identified across the three UHPLC-MS/MS datasets (ranked in ascending RT order) are summarised in Table 5.14 above with levels of confidence assigned according to the criteria described in section 5.2.6.3.2.

Proposed biotransformation map for BPAF is shown in Figure 5.11. Chemical structures were generated from canonical SMILES using the ChemDraw Professional software (v22.0.0.22; PerkinElmer).

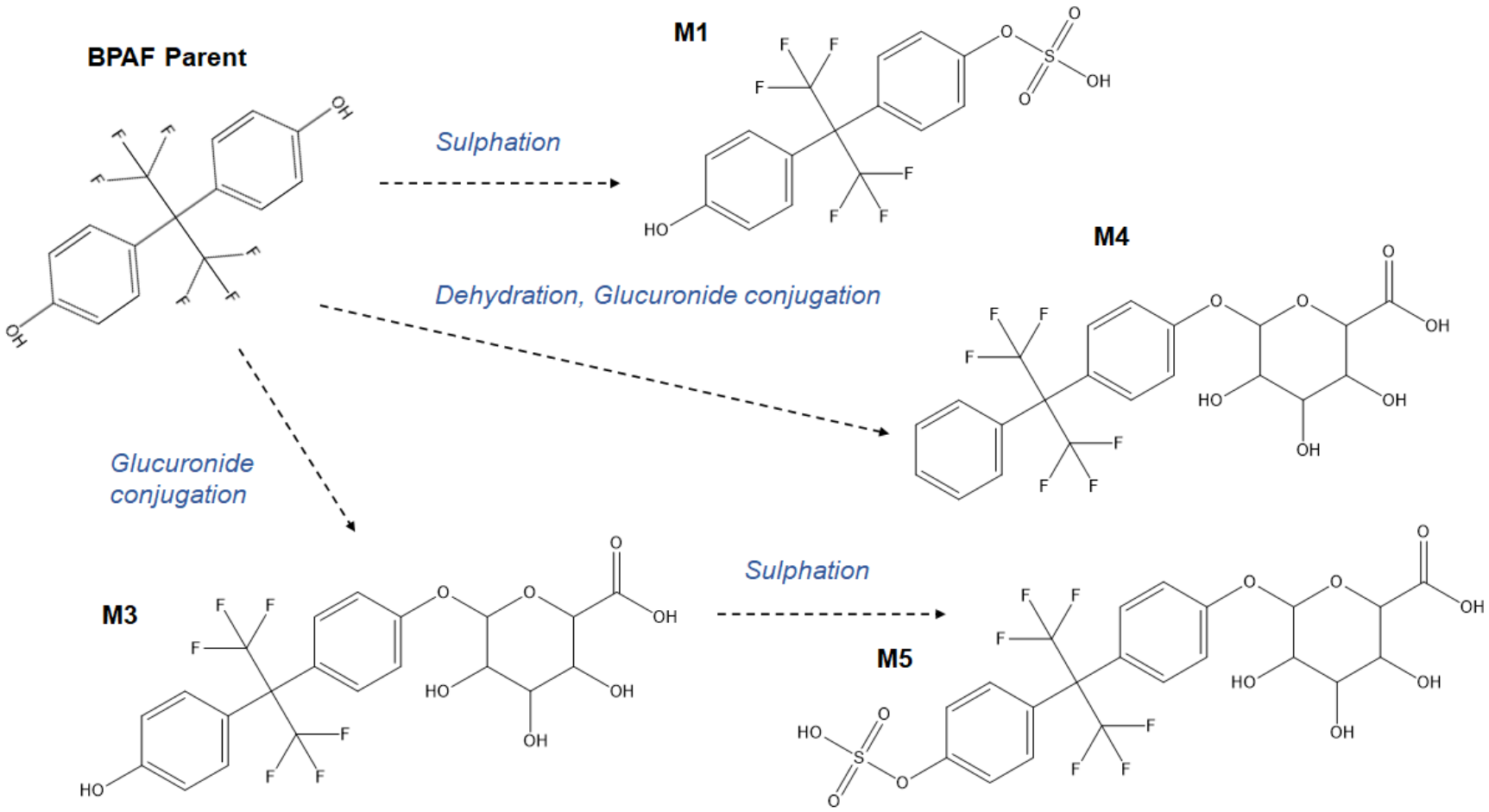


**Figure 5.11** BPAF suggested metabolic pathway for major BTPs discovered in the UHPLC-MS/MS datasets. Plain arrow – phase I reaction, dashed arrow – phase II reaction.

### 5.3.6 DEHP

DEHP parent was detected in both analytical reference standard sample and rat plasma in the HILIC positive dataset (391.2844 *m/z*, RT: 0.418 min). The injection and analysis of DEHP reference standard (10 µg $mL^{-1}$ in water:acetonitrile:methanol 1:1.5:1.5 v/v/v) under the same LC-HRMS conditions aimed to confirm the identity of parent, whereby the RT and MSn fragmentation pattern matched those observed in the biological sample (Figure 5.12). The $[M+H]^+$ was detected in both rat plasma and analytical standard. However, in the absence of $MS^n$ fragmentation data for the DEHP precursor ion in rat plasma possibly due to lower intensity of the shoulder peak (only $MS^n$ data for the reference standard are available), the highest confidence spectral match (equivalent to Schymansky *et al.* (2014) confidence Level 1) could not be performed, and the feature was annotated based on accurate mass (within 0.33 pm mass error), matching retention times (RTs) and high confidence match to the mzCloud spectral library (98.6%) (Figure 5.12d). The mirror plot of the $MS^n$ fragmentation spectrum in rat plasma and match against the mzCloud reference spectrum shows several overlapping product ions, including the precursor ion and lower molecular weight ions.

**a**

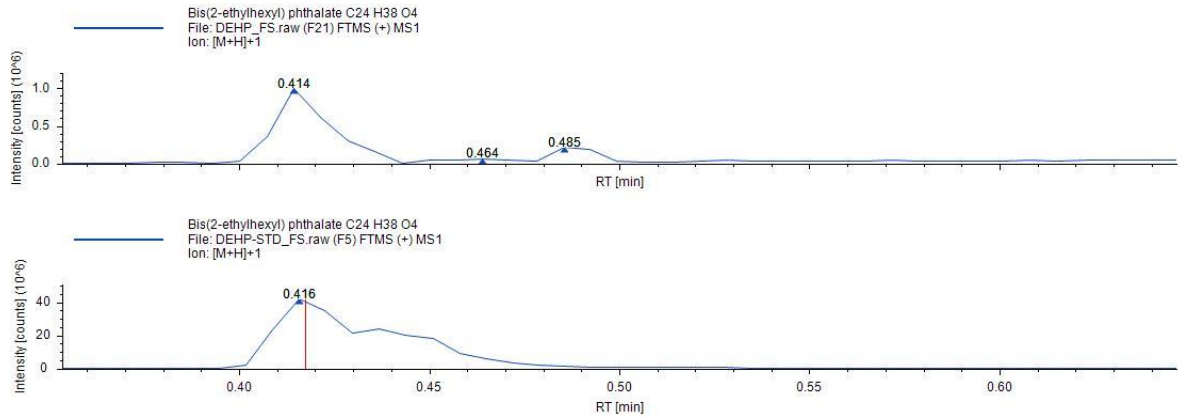


**b**

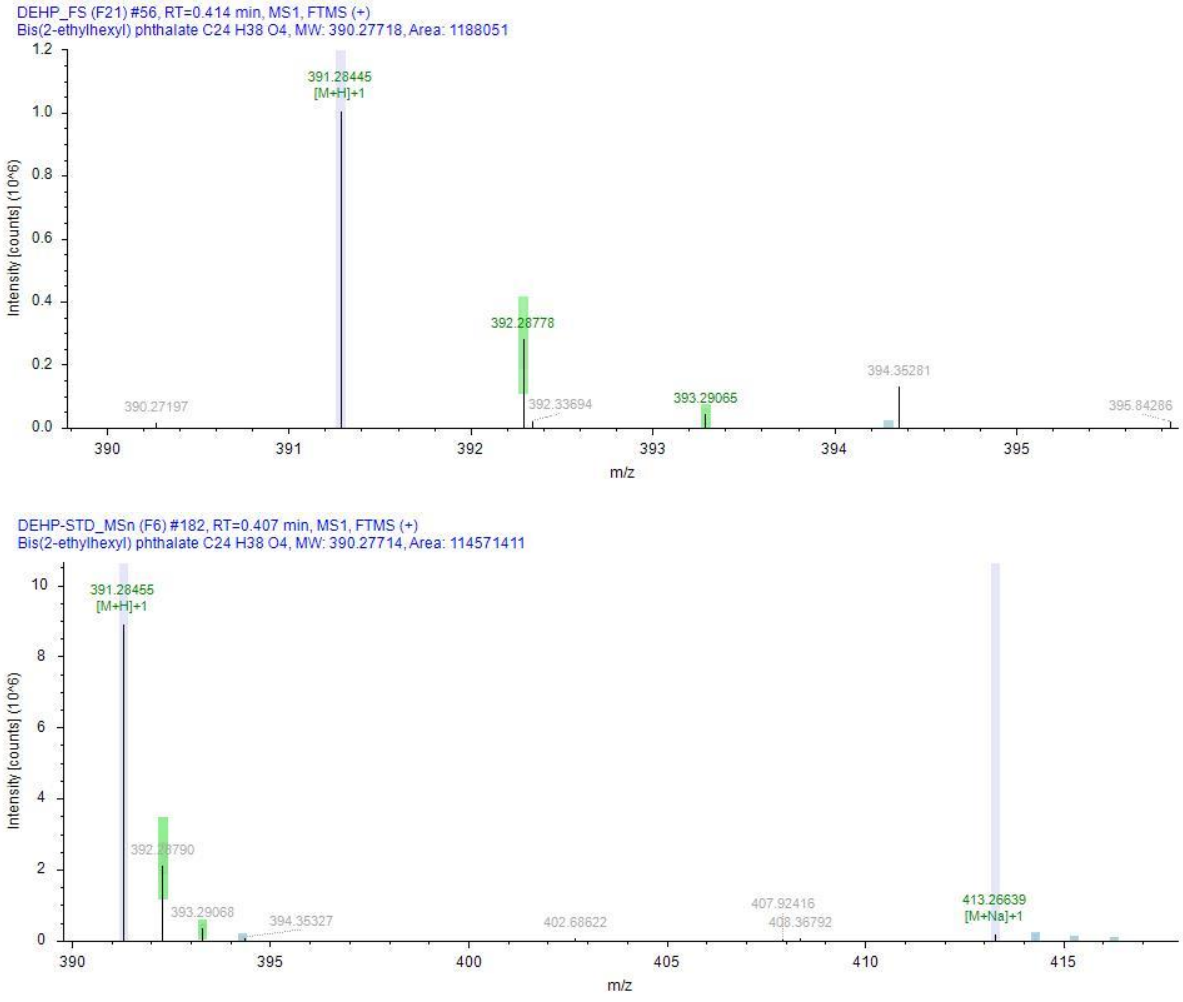


**c**

| Structure | Name | Formula | Molecular Weight | ΔMass [Da] | ΔMass [ppm] | CSID |
|---|---|---|---|---|---|---|
| 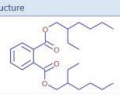 | Bis(2-ethylhexyl) phthalate | C24 H38 O4 | 390.27701 | 0.00013 | 0.33 | 21106505 |

**Figure 5.12** Confirming DEHP parent identity in rat plasma HILIC positive assay. (**a**) Extracted ion chromatograms of DEHP parent peak in rat plasma (top) and reference standard (bottom) from the HILIC positive analysis. (**b**) Full scan $MS^1$ data showing the isotope pattern fit (shown on different *m/z* scales on the x-axis) for DEHP at $[M+H]^-$ 391.2844 *m/z* in rat plasma (top) and reference standard (bottom). (**c**) High confidence match for DEHP parent in mzCloud library.

In addition, data processing and analysis using Compound Discoverer revealed 17 metabolic biotransformation products of DEHP in rat plasma extracts detected across all four assays. These BTPs (M1 to M17) are listed in Table 5.15 according to ascending RT. Four dealkylated BTPs resulting from desaturation (M8), glucuronidation (M9), oxidation followed by glucuronide conjugation (M5), and reduction followed by glycine conjugation (M3) were discovered across multiple UHPLC-MS/MS assays.

Major phase I metabolic modifications included dealkylation for 16 features (M3 to M10 and M12 to M17), desaturation (M1, M4, M5, M9, M11, M12, M13, M14) and oxidation (M4, M5, M6, M7, M11, M13, M16); reduction (M3) and nitro reduction (M17) were a minor phase I reactions. Four BTPs underwent glucuronide conjugation (M5, M6, M10, M14) while methylation (M17) was a minor phase II reaction. Metabolic transformations for DEHP (accurate *m/z*, elemental composition, RT and chromatographic peak areas) are summarised in Table 5.15. Dehydration reactions (M1, M2) previously reported in DEHP metabolism *in vivo* were generally infrequent with lower peak areas. Mass accuracy was below ±1 ppm error for DEHP-related features across all UHPLC-MS/MS assays, increasing confidence in these annotations.

The detection of various oxidation and glucuronide metabolites is consistent with literature findings postulating that DEHP is rapidly metabolised, MEHP and 2-ethyxanol (2-EH) *in vivo* followed by oxidation and/or glucuronide conjugation[275,285]. MEHP, 5-OH MEHP followed by 5-Oxo MEHP were also major metabolites produced *in vitro*[275,276]. A 279.1591 *m/z* feature eluting at 2.813 min and corresponding to mono(2-ethylhexyl) phthalate (MEHP, M15) was discovered in the HILIC positive dataset suggesting that DEHP was metabolised via hydrolytic cleavage to another phthalate ester, MEHP. This was also confirmed by a positive match to mzCloud (88.7%, within 0.07 ppm) and ChemSpider libraries. MEHP peak area was 9.35e6 in the HILIC positive assay, representing one of the most abundant DEHP-derived BTPs.

Three additional MEHP-derived hydrolytic metabolites were detected in UHPLC-MS/MS datasets. Mono(2-ethyl-5-carboxypentyl) phthalate (5-carboxy MEPP) was discovered in both RP $C_{18}$ negative lipidomics and HILIC negative assay following dealkylation, desaturation and double-oxidation (M13, 371.25812 m/z, RT: 0.824 min) and automatically matched to a ChemSpider library entry (within -0.09 ppm and -0.19 ppm, respectively). Over 40% (FISh score: 41.51%) of the possible product ions (seven matching major fragments including 159 *m/z* and 121 *m/z*) can be structurally related to the corresponding precursor ion in the $MS^2$ fragmentation data collected for M13 in the RP $C_{18}$ negative lipidomics dataset (Figure 5.13b). This is also the most abundant DEHP-related feature (peak area: 2.2e8) and showed higher signal intensity compared to the parent discovered in the other HILIC assay, thus increasing confidence in identification.

Mono(2-ethyl-5-hydroxyhexyl) phthalate (5-OH MEHP) following dealkylation and oxidation (M16, 295.15408 m/z, RT: 4.772 min) was confirmed by a ChemSpider match in the HILIC positive assay (within 0.26 ppm). Mono-(2-ethyl-5-oxohexyl) phthalate (5-Oxo MEHP) was identified in the HILIC positive assay (M4, $[M+Na]^+$ at 315.12036 m/z, RT: 0.562 min) following dealkylation, desaturation and oxidation. These features were assigned 'medium confidence' in identification (Table 5.15). Structural characterisation of the $MS^n$ patterns for these representative DEHP-derived features (using FISh scoring to define products ions) is shown in Figure 5.13. No further MEHP-derived metabolites reported in literature were detected in the UHPLC-MS/MS datasets, however.

Proposed biotransformation map for DEHP is shown in Figure 5.14. Chemical structures were generated from canonical SMILES using the ChemDraw Professional software (v22.0.0.22; PerkinElmer).

**a**

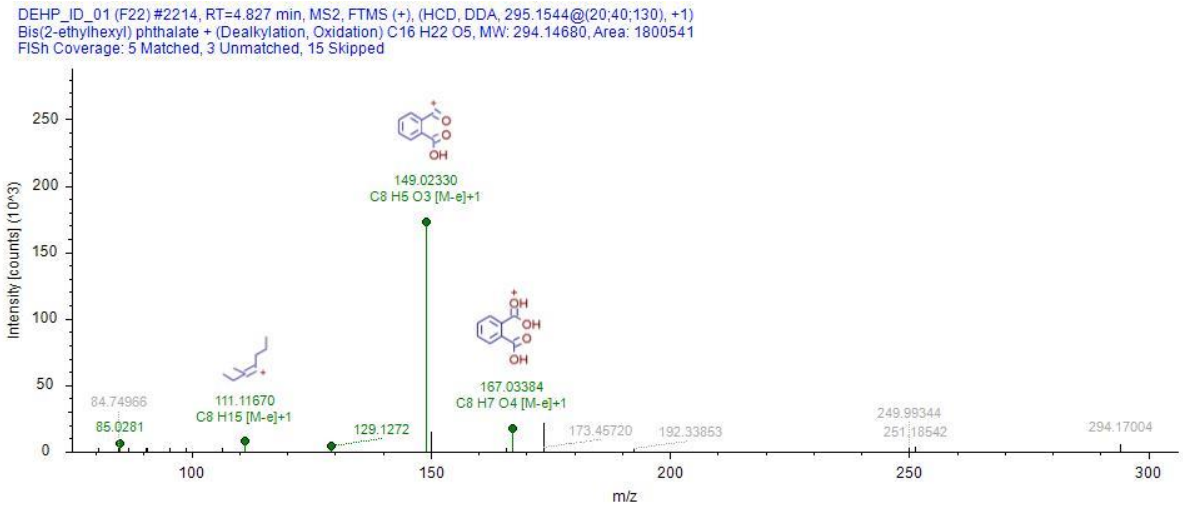
DEHP_ID_01 (F22) #2214, RT=4.827 min, MS2, FTMS (+), (HCD, DDA, 295.1544@(20;40;130), +1)
Bis(2-ethylhexyl) phthalate + (Dealkylation, Oxidation) C16 H22 O5, MW: 294.14680, Area: 1800541
FISh Coverage: 5 Matched, 3 Unmatched, 15 Skipped
149.02330
C8 H5 O3 [M-e]+1
111.11670
C8 H15 [M-e]+1
167.03384
C8 H7 O4 [M-e]+1
84.74966
85.0281
129.1272
173.45720
192.33853
249.99344
251.18542
294.17004
Intensity [counts] (10^3)
m/z

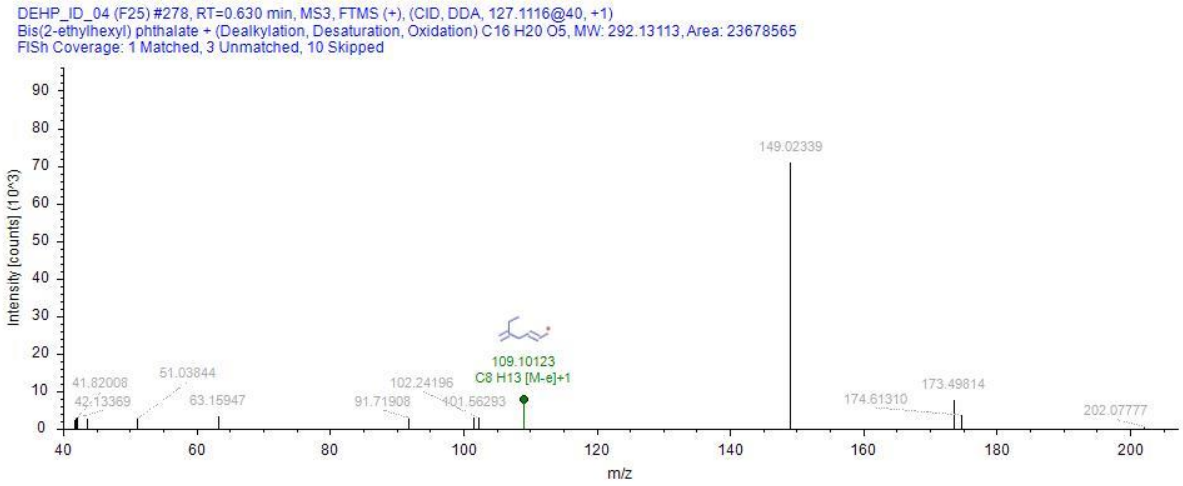
DEHP_ID_04 (F25) #278, RT=0.630 min, MS3, FTMS (+), (CID, DDA, 127.1116@40, +1)
Bis(2-ethylhexyl) phthalate + (Dealkylation, Desaturation, Oxidation) C16 H20 O5, MW: 292.13113, Area: 23678565
FISh Coverage: 1 Matched, 3 Unmatched, 10 Skipped
149.02339
109.10123
C8 H13 [M-e]+1
41.82008
42.13369
51.03844
63.15947
91.71908
102.24196
101.56293
174.61310
173.49814
202.07777
Intensity [counts] (10^3)
m/z

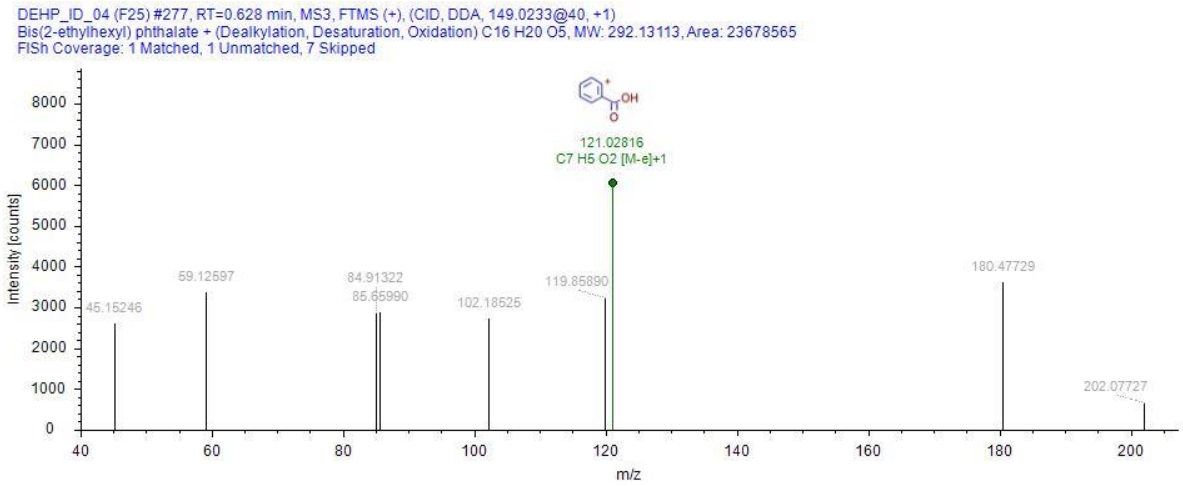
DEHP_ID_04 (F25) #277, RT=0.628 min, MS3, FTMS (+), (CID, DDA, 149.0233@40, +1)
Bis(2-ethylhexyl) phthalate + (Dealkylation, Desaturation, Oxidation) C16 H20 O5, MW: 292.13113, Area: 23678565
FISh Coverage: 1 Matched, 1 Unmatched, 7 Skipped
121.02816
C7 H5 O2 [M-e]+1
45.15246
59.12597
84.91322
85.65990
102.18525
119.85890
180.47729
202.07727
Intensity [counts]
m/z

**b**

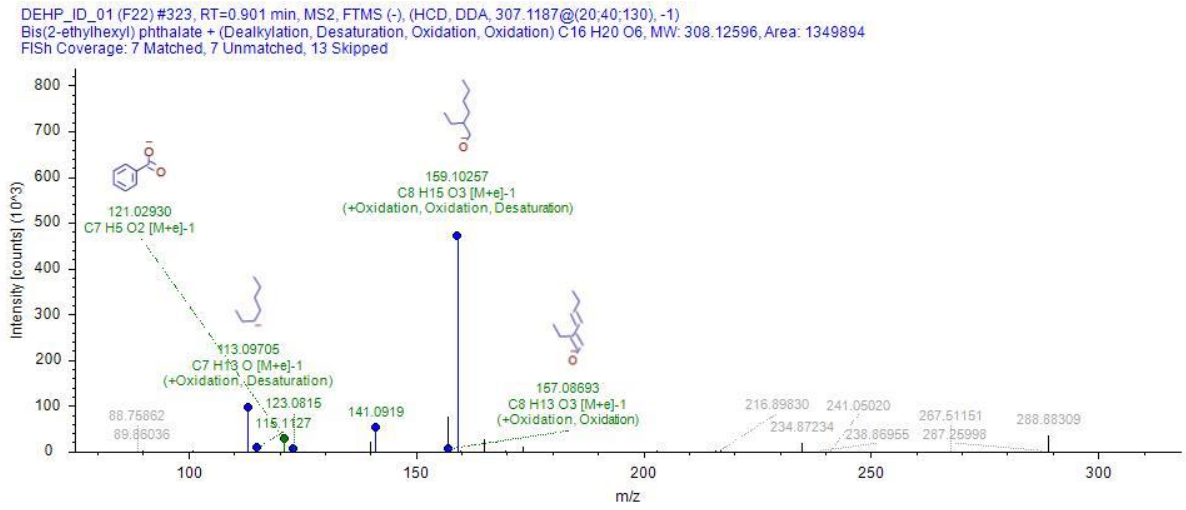
DEHP_ID_01 (F22) #323, RT=0.901 min, MS2, FTMS (-), (HCD, DDA, 307.1187@(20;40;130), -1)
Bis(2-ethylhexyl) phthalate + (Dealkylation, Desaturation, Oxidation, Oxidation) C16 H20 O6, MW: 308.12596, Area: 1349894
FISh Coverage: 7 Matched, 7 Unmatched, 13 Skipped
121.02930
C7 H5 O2 [M+e]-1
159.10257
C8 H15 O3 [M+e]-1
(+Oxidation, Oxidation, Desaturation)
113.09705
C7 H13 O [M+e]-1
(+Oxidation, Desaturation)
123.0815
115.1127
141.0919
157.08693
C8 H13 O3 [M+e]-1
(+Oxidation, Oxidation)
88.75862
89.86036
216.89830
234.87234
241.05020
238.86955
267.51151
287.25998
288.88309
Intensity [counts] (10^3)
m/z

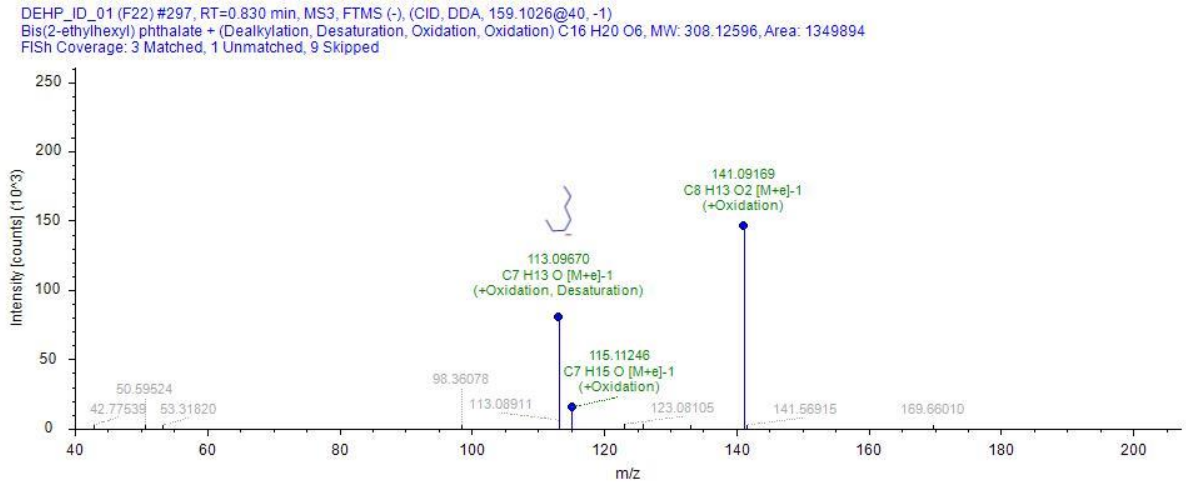
DEHP_ID_01 (F22) #297, RT=0.830 min, MS3, FTMS (-), (CID, DDA, 159.1026@40, -1)
Bis(2-ethylhexyl) phthalate + (Dealkylation, Desaturation, Oxidation, Oxidation) C16 H20 O6, MW: 308.12596, Area: 1349894
FISh Coverage: 3 Matched, 1 Unmatched, 9 Skipped
141.09169
C8 H13 O2 [M+e]-1
(+Oxidation)
113.09670
C7 H13 O [M+e]-1
(+Oxidation, Desaturation)
115.11246
C7 H15 O [M+e]-1
(+Oxidation)
50.59524
42.77539
53.31820
98.36078
113.08911
123.08105
141.56915
169.66010
Intensity [counts] (10^3)
m/z

**c**

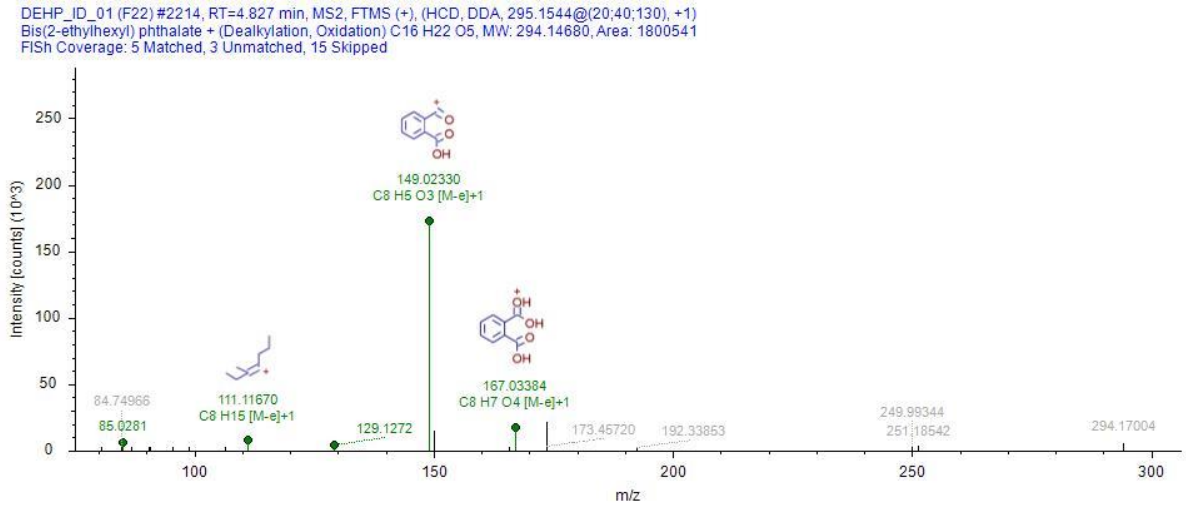
DEHP_ID_01 (F22) #2214, RT=4.827 min, MS2, FTMS (+), (HCD, DDA, 295.1544@(20;40;130), +1)
Bis(2-ethylhexyl) phthalate + (Dealkylation, Oxidation) C16 H22 O5, MW: 294.14680, Area: 1800541
FISh Coverage: 5 Matched, 3 Unmatched, 15 Skipped
149.02330
C8 H5 O3 [M-e]+1
111.11670
C8 H15 [M-e]+1
167.03384
C8 H7 O4 [M-e]+1
84.74966
85.0281
129.1272
173.45720
192.33853
249.99344
251.18542
294.17004
Intensity [counts] (10^3)
m/z

**Figure 5.13** Structure annotations from FISh scoring on $MS^n$ spectra of major DEHP metabolites discovered in rat plasma (**a**) M4, (**b**) M13, (**c**) M16. Green – indicates direct match fragments, blue – transformation shifted fragments.

**Table 5.15** DEHP metabolic biotransformation products identified in UHPLC-MS/MS datasets with assigned levels of confidence in identification: yellow – 'low confidence', blue – 'medium confidence', green – 'high confidence'. Abbreviations: FISh – Fragment ion search scoring, MW – molecular weight, RT – retention time.

| ID | Assay | Formula | Transformations | Composition Change | Annot. DeltaMass [ppm] | Calc. MW | m/z | RT [min] | FISh Coverage | Area (Max.) | mzCloud Best Match | Reference Ion |
|---|---|---|---|---|---|---|---|---|---|---|---|---|
| **P** | HILIC pos | C24 H38 O4 | | | 0.33 | 390.277 | 391.2844 | 0.418 | 47.37 | 1.15E+08 | 99.3 | [M+H]+1 |
| **M1** | HILIC pos | C24 H32 O2 | Dehydration, Dehydration, Desaturation | -(H6 O2) | 0.93 | 352.241 | 353.2478 | 0.491 | 23.08 | 1.09E+06 | | [M+H]+1 |
| **M2** | HILIC pos | C24 H34 O2 | Dehydration, Dehydration | -(H4 O2) | 0.33 | 354.256 | 355.2633 | 0.492 | 57.89 | 2.30E+05 | | [M+H]+1 |
| **M3** | HILIC pos | C18 H27 N O5 | Dealkylation, Reduction, Glycine Conjugation | -(C6 H11) +(N O) | 0.18 | 337.189 | 338.1963 | 0.558 | 41.67 | 3.35E+06 | | [M+H]+1 |
| **M4** | HILIC pos | C16 H20 O5 | Dealkylation, Desaturation, Oxidation | -(C8 H18) +(O) | 0.19 | 292.131 | 315.1204 | 0.562 | 43.48 | 2.37E+07 | 97.2 | [M+Na]+1 |

| ID | Assay | Formula | Transformations | Composition Change | Annot. DeltaMass [ppm] | Calc. MW | m/z | RT [min] | FISh Coverage | Area (Max.) | mzCloud Best Match | Reference Ion |
|---|---|---|---|---|---|---|---|---|---|---|---|---|
| **M5** | C18 Lipidomics neg | C22 H28 O11 | Dealkylation, Desaturation, Oxidation, Glucuronide Conjugation | -(C2 H10) +(O7) | 0.45 | 468.163 | 467.1561 | 0.594 | 28.57 | 4.91E+06 | | [M-H]-1 |
| **M6** | C18 Lipidomics neg | C22 H30 O11 | Dealkylation, Oxidation, Glucuronide Conjugation | -(C2 H8) +(O7) | 0.53 | 470.179 | 469.1718 | 0.597 | 23.08 | 2.29E+06 | | [M-H]-1 |
| **M7** | C18 Lipidomics neg | C16 H22 O6 | Dealkylation, Oxidation, Oxidation | -(C8 H16) +(O2) | 0.52 | 310.142 | 309.1345 | 0.643 | 19.05 | 2.90E+06 | | [M-H]-1 |
| **M8** | C18 Lipidomics pos | C18 H27 N O6 | Dealkylation, Hydration, Glycine Conjugation | -(C6 H11) +(N O2) | -0.04 | 353.184 | 354.1911 | 0.715 | 40 | 1.59E+07 | | [M+H]+1 |
| **M3** | C18 Lipidomics pos | C18 H27 N O5 | Dealkylation, Reduction, Glycine Conjugation | -(C6 H11) +(N O) | -0.28 | 337.189 | 338.1961 | 0.724 | 60 | 5.00E+07 | 90.6 | [M+H]+1 |

| ID | Assay | Formula | Transformations | Composition Change | Annot. DeltaMass [ppm] | Calc. MW | m/z | RT [min] | FISh Coverage | Area (Max.) | mzCloud Best Match | Reference Ion |
|---|---|---|---|---|---|---|---|---|---|---|---|---|
| **M9** | C18 Lipidomics pos | C16 H20 O4 | Dealkylation, Desaturation | -(C8 H18) | 0.13 | 276.136 | 277.1435 | 0.734 | 37.5 | 1.99E+06 | | [M+H]+1 |
| **M10** | C18 Lipidomics neg | C22 H30 O10 | Dealkylation, Glucuronide Conjugation | -(C2 H8) +(O6) | 0.1 | 454.184 | 453.1767 | 0.766 | 26.67 | 1.57E+07 | 57.9 | [M-H]-1 |
| **M11** | HILIC neg | C16 H20 O5 | Dealkylation, Desaturation, Oxidation | -(C8 H18) +(O) | 0.16 | 292.131 | 291.1238 | 0.775 | 17.19 | 7.92E+07 | 70 | [M-H]-1 |
| **M12** | C18 Lipidomics pos | C24 H34 O3 | Dehydration, Desaturation | -(H4 O) | 0.12 | 370.251 | 371.2581 | 0.824 | 23.33 | 3.83E+05 | 92.5 | [M+H]+1 |
| **M13** | C18 Lipidomics neg | C16 H20 O6 | Dealkylation, Desaturation, Oxidation, Oxidation | -(C8 H18) +(O2) | -0.09 | 308.126 | 307.1187 | 0.85 | 41.51 | 1.35E+06 | 81.3 | [M-H]-1 |
| **M14** | HILIC pos | C40 H62 O11 | Dealkylation, Desaturation, Glucuronide | +(C16 H24 O7) | -0.78 | 718.429 | 736.4625 | 0.859 | 34.55 | 1.85E+06 | 100 | [M+NH4]+1 |

| ID | Assay | Formula | Transformations | Composition Change | Annot. DeltaMass [ppm] | Calc. MW | m/z | RT [min] | FISh Coverage | Area (Max.) | mzCloud Best Match | Reference Ion |
|---|---|---|---|---|---|---|---|---|---|---|---|---|
| | | | Conjugation, Stearyl Conjugation | | | | | | | | | |
| **M7** | HILIC pos | C16 H22 O6 | Dealkylation, Oxidation, Oxidation | -(C8 H16) +(O2) | 0.36 | 310.142 | 333.1310 | 0.919 | 39.29 | 7.69E+06 | 99.4 | [M+Na]+1 |
| **M9** | C18 Lipidomics neg | C16 H20 O4 | Dealkylation, Desaturation | -(C8 H18) | -0.13 | 276.136 | 275.1289 | 1.001 | 20 | 6.23E+05 | | [M-H]-1 |
| **M15** | HILIC pos | C16 H22 O4 | Dealkylation | -(C8 H16) | 0.07 | 278.152 | 279.1591 | 2.813 | 16.67 | 9.35E+06 | 89.6 | [M+H]+1 |
| **M10** | HILIC neg | C22 H30 O10 | Dealkylation, Glucuronide Conjugation | -(C2 H8) +(O6) | -0.71 | 454.184 | 453.1763 | 3.749 | 17.74 | 4.66E+07 | 86.8 | [M-H]-1 |
| **M13** | HILIC neg | C16 H20 O6 | Dealkylation, Desaturation, Oxidation, Oxidation | -(C8 H18) +(O2) | -0.19 | 308.126 | 307.1187 | 4.412 | 23.26 | 2.02E+08 | 81.4 | [M-H]-1 |

| ID | Assay | Formula | Transformations | Composition Change | Annot. DeltaMass [ppm] | Calc. MW | m/z | RT [min] | FISh Coverage | Area (Max.) | mzCloud Best Match | Reference Ion |
|---|---|---|---|---|---|---|---|---|---|---|---|---|
| **M6** | HILIC pos | C22 H30 O11 | Dealkylation, Oxidation, Glucuronide Conjugation | -(C2 H8) +(O7) | 0.42 | 470.179 | 488.2128 | 4.771 | 35.9 | 4.05E+06 | 74.4 | [M+NH4]+1 |
| **M16** | HILIC pos | C16 H22 O5 | Dealkylation, Oxidation | -(C8 H16) +(O) | 0.26 | 294.147 | 295.1541 | 4.772 | 40 | 1.80E+06 | | [M+H]+1 |
| **M6** | HILIC neg | C22 H30 O11 | Dealkylation, Oxidation, Glucuronide Conjugation | -(C2 H8) +(O7) | 0.16 | 470.179 | 469.1716 | 5.008 | 19.54 | 3.37E+06 | | [M-H]-1 |
| **M17** | C18 Lipidomics pos | C17 H28 | Dealkylation, Nitro Reduction, Nitro Reduction, Methylation | -(C7 H10 O4) | -0.06 | 232.219 | 233.2264 | 9.39 | 25 | 3.80E+06 | | [M+H]+1 |

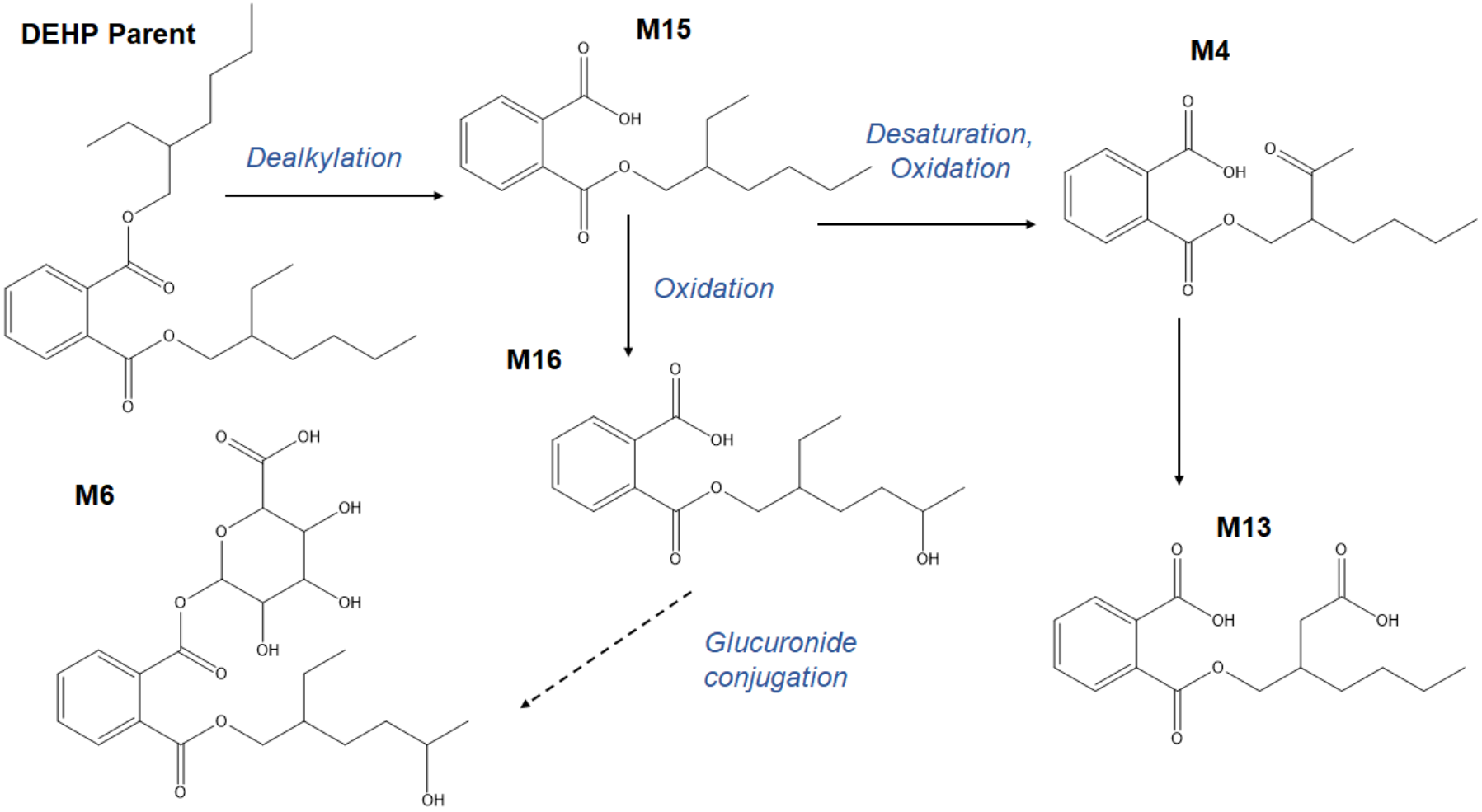


**Figure 5.14** DEHP suggested metabolic pathway for major BTPs discovered in the UHPLC-MS/MS datasets. Plain arrow – phase I reaction, dashed arrow – phase II reaction.

### 5.3.7 TBBPA

TBBPA parent chemical was detected in rat plasma extracts analysed in the HILIC negative assay ($[M-H]^-$ at 538.7501 *m/z*, RT: 0.460 min). The peak identity could not be confirmed by full spectral comparison with the reference standard for TBBPA (10 µg $mL^{-1}$ in water:acetonitrile:methanol 1:1.5:1.5 v/v/v), analysed using the same analytical method and identical instrument conditions due to the absence of $MS^n$ data for the biological sample. As a result, the comparison was based on chromatographic peak retention time (11 s shift compared to the standard), isotopic pattern, exact mass and a high confidence match to both mzCloud and ChemSpider libraries. TBBPA parent was also detected with 'lower confidence' in the chemical reference standard only in the RP $C_{18}$ lipidomics dataset (1.61 ppm error). In addition, TBBPA parent peak was automatically matched to the spectral libraries (mzCloud and ChemSpider) with high confidence (within 0.61 ppm).

**a**

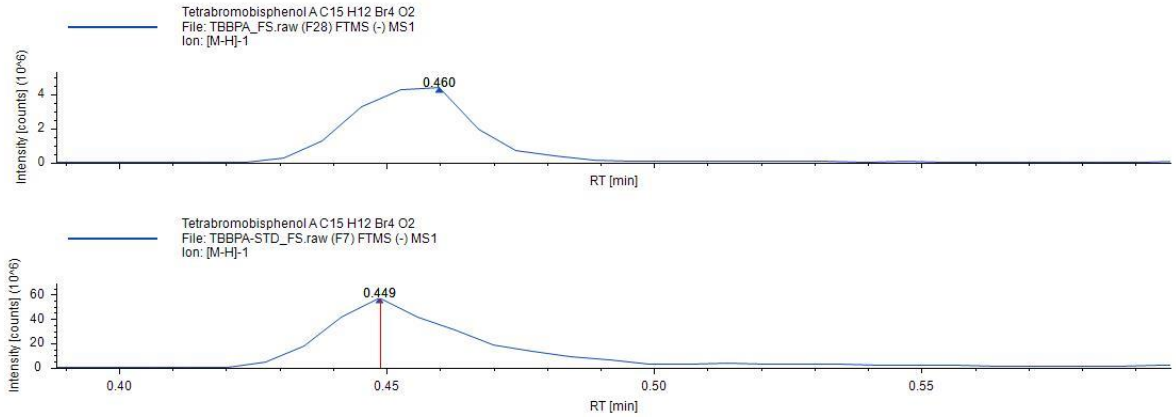


**b**

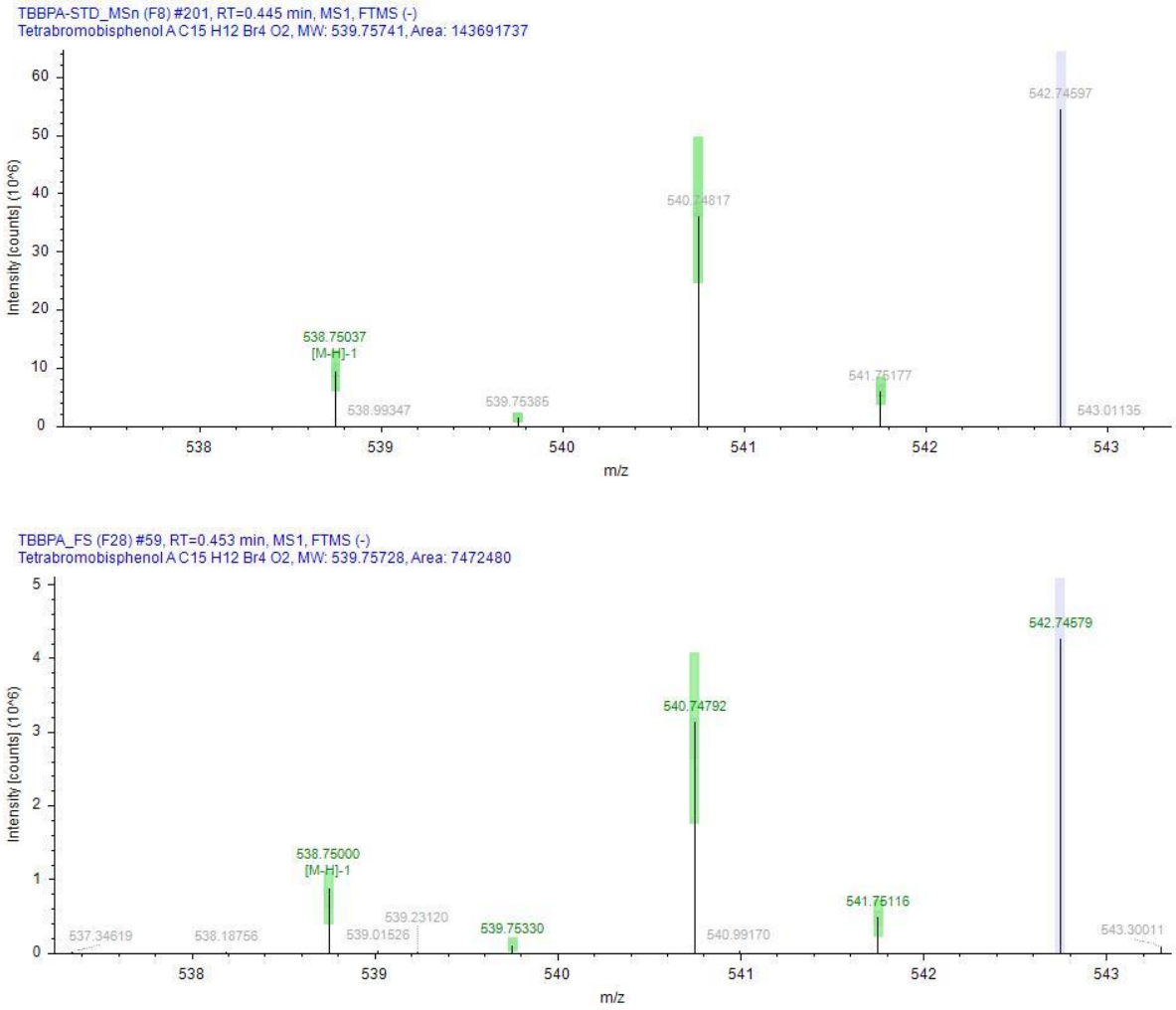


**Figure 5.15** Confirming TBBPA parent identity in rat plasma in the HILIC negative assay. (**a**) Extracted ion chromatograms of TBBPA parent peak in rat plasma (top) and reference

standard (bottom). (**b**) Full scan $MS^1$ data showing the isotope pattern fit for TBBPA at $[M-H]^-$ 538.7501 *m/z* in rat plasma (top) and reference standard (bottom).

Eight TBBPA metabolites were reported in literature from *in vivo* rat studies (specifically, detected in rat bile[274]), resulting from reductive or oxidative debromination (phase I) or glucuronidation (phase II). All of these earlier reported BTPs were also predicted by Compound Discoverer. However, no additional BTPs were discovered in the UHPLC-MS/MS datasets when applying the initial filtering, suggesting that TBBPA is either rapidly metabolised by rat or that rat plasma extracts are not suitable biomarkers of exposure for this xenobiotic. TBBPA sulphate (M1, $[M+H]^+$ at 618.7064 *m/z*, RT: 0.453 min) was also discovered in the HILIC negative dataset within -0.30 ppm error. However, it did not meet the initial filtering criteria (FISh score > 10.0%) and is, therefore, reported as a 'low confidence' in identification feature (FISh score: 7.14%). $MS^2$ and $MS^3$ fragmentation spectra of M1 with structure annotations resulting from applying FISh scoring are presented in Figure 5.16.

Proposed biotransformation map for TBBPA is shown in Figure 5.17. Chemical structures were generated from canonical SMILES using the ChemDraw Professional software (v22.0.0.22; PerkinElmer).

**Table 5.16** TBBPA metabolic biotransformation products identified in UHPLC-MS/MS datasets with assigned levels of confidence in identification: yellow – 'low confidence', blue – 'medium confidence', green – 'high confidence'. Abbreviations: FISh – Fragment ion search scoring, MW – molecular weight, RT – retention time.

| ID | Assay | Formula | Transformations | Composition Change | Annot. DeltaMass [ppm] | Calc. MW | m/z | RT [min] | FISh Coverage | Area (Max.) | mzCloud Best Match | Reference Ion |
|---|---|---|---|---|---|---|---|---|---|---|---|---|
| **M1** | HILIC neg | C15 H12 Br4 O5 S | Sulphation | +(O3 S) | -0.3 | 619.7137 | 618.706 | 0.359 | 7.14 | 1.78E+06 | | [M-H]-1 |
| **P** | HILIC neg | C15 H12 Br4 O2 | | | 0.61 | 539.7574 | 538.75 | 0.453 | 37.5 | 1.44E+08 | | [M-H]-1 |
| **P** | $C_{18}$ Lipidomics neg | C15 H12 Br4 O2 | | | 1.61 | 539.7580 | 538.751 | 1.294 | 53.85 | 2.46E+08 | 95.1 | [M-H]-1 |

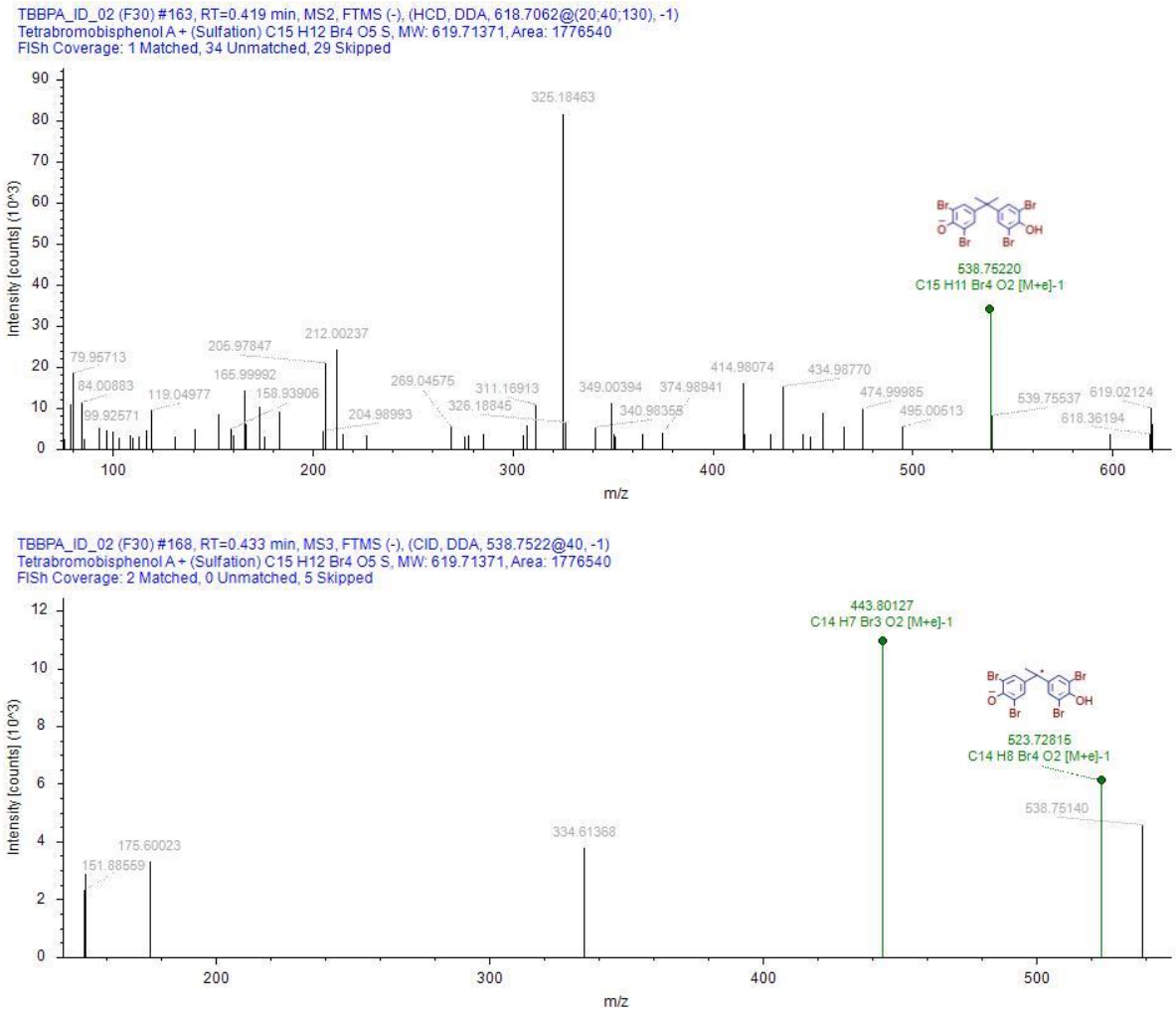


**Figure 5.16** Structure annotations from FISh scoring on $MS^n$ spectra of TBBPA sulphation metabolite (M1) discovered in rat plasma. Green – indicates direct match fragments, blue – transformation shifted fragments.

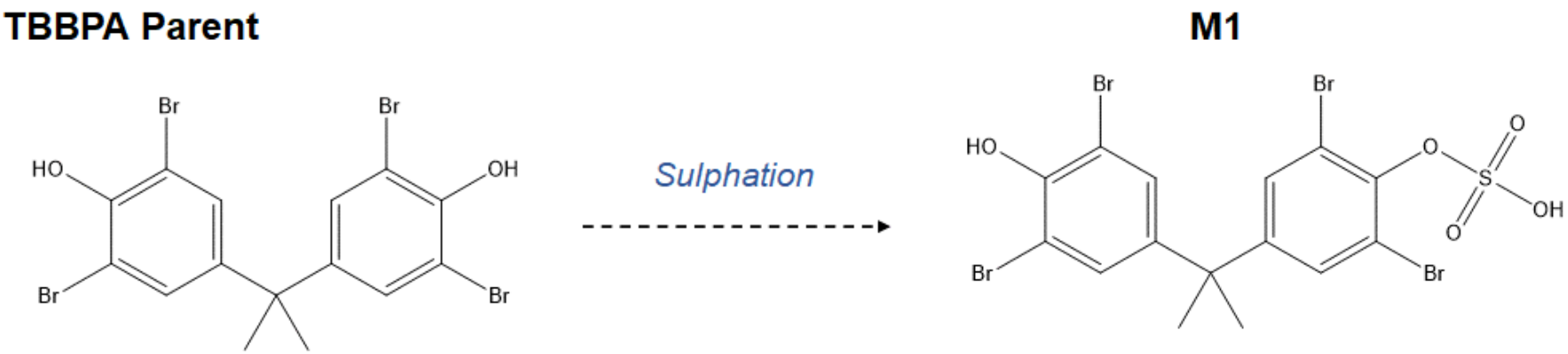


**Figure 5.17** TBBPA suggested metabolic pathway for major BTPs discovered in the UHPLC-MS/MS datasets. Plain arrow – phase I reaction, dashed arrow – phase II reaction.

### 5.3.8 TCPP

The identity of TCPP parent detected in the RP $C_{18}$ lipidomics positive assay ($[M+H]^+$ at 327.0083 m/z, RT: 0.843 min) could not be validated by a spectral match to the reference standard due the absence of $MS^n$ fragmentation data for the precursor ion detected in rat plasma. $MS^2$ scan was not triggered likely due to a lower shoulder peak intensity for TCPP parent. As a result, the identification ('high confidence') was based on accurate *m/z*, chromatographic retention time, and isotopic pattern in $MS^1$ data only with no ChemSpider library match, however. The peak corresponding to TCPP parent was also detected (with 'lower confidence' in identification) in the reference standard only analysed in the HILIC positive assay.

**a**

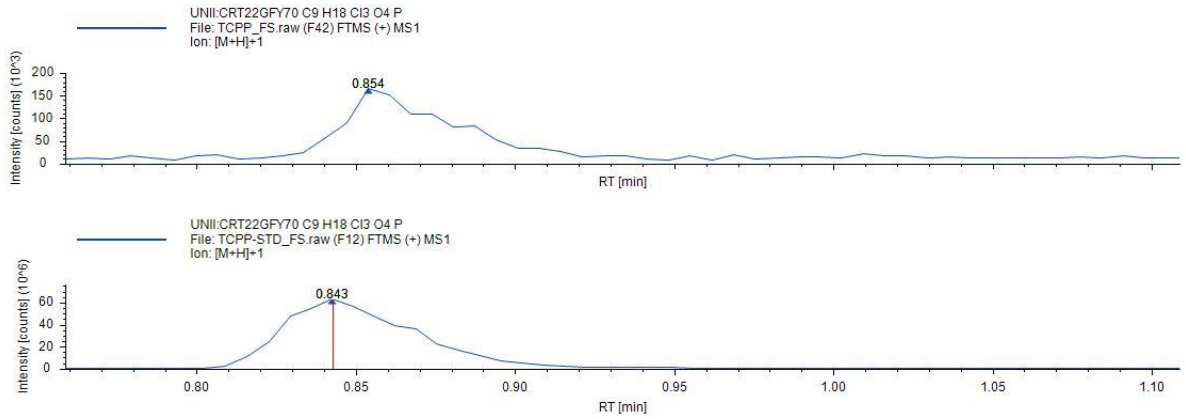


**b**

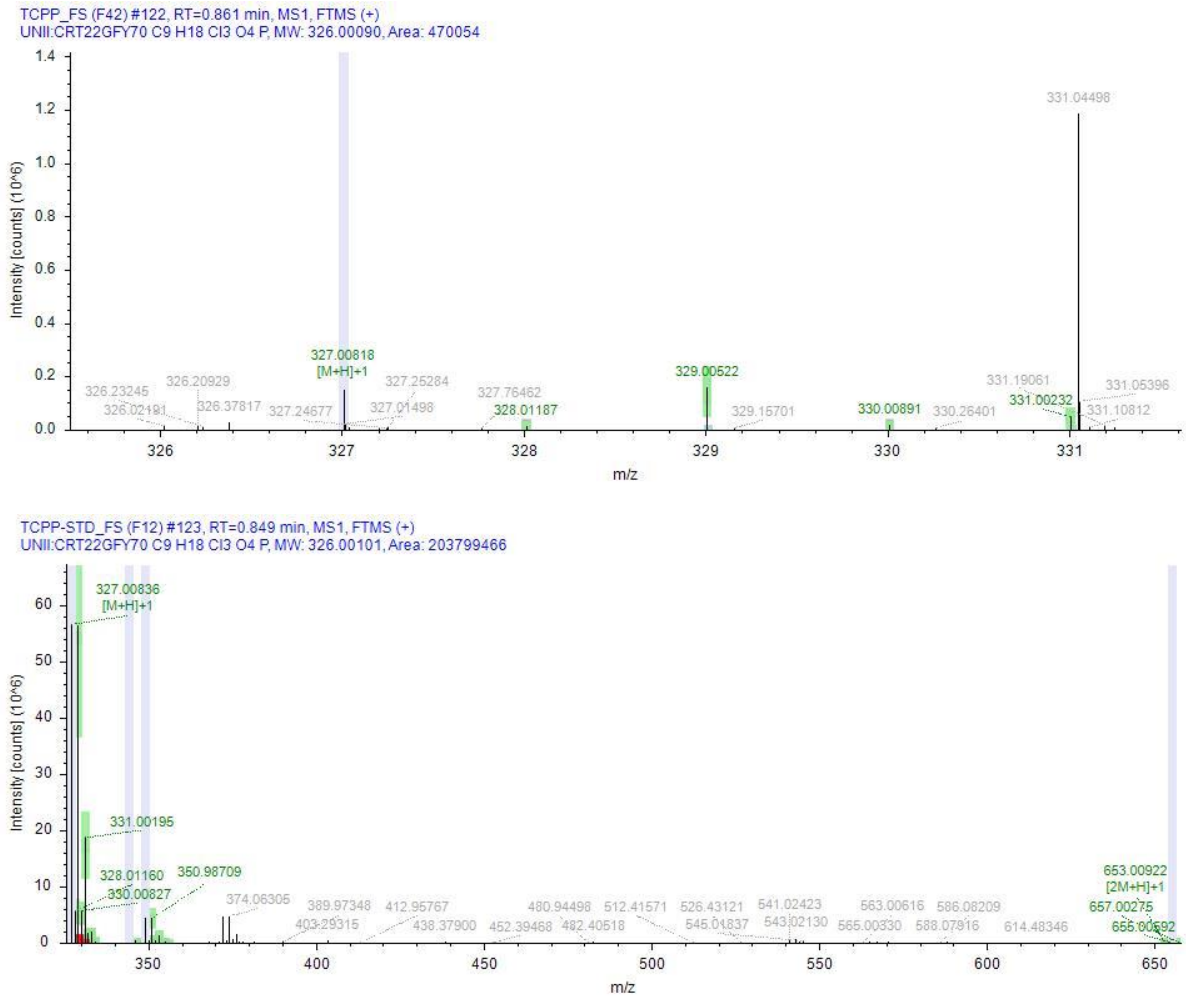


**Figure 5.18** Confirming TCCP parent identity in rat plasma RP $C_{18}$ positive lipidomics. (**a**) Extracted ion chromatograms of BPAF parent peak in rat plasma (top) and reference standard (bottom) from the RP $C_{18}$ lipidomics analysis. (**b**) Full scan $MS^1$ data showing the isotope

pattern fit for 327.0083 at $[M+H]^+$ 335.05099 *m/z* in rat plasma (top) and reference standard (bottom).

In addition, Compound Discoverer workflow revealed 22 metabolic biotransformation products for TCPP, the majority of them being detected in the HILIC positive assay, as summarised in Table 5.17. No BTPs were annotated within the HILIC negative dataset. Over half of the BTPs underwent oxidative dechlorination (M1, M4, M6, M10, M12, M13, M14, M16, M17, M18, M19, M20, M22). Other major phase I modifications were dealkylation (M3, M7, M8, M9, M11, M13, M16, M17, M21), oxidation (M1, M6, M9, M10, M18, M21), nitro reduction (M2, M3, M7), reductive dechlorination (M2, M15, M19) and desaturation (M1, M7, M10, M16, M18). The most prevalent phase II modifications were acetylation (M4, M6, M9, M13, M17, M17), methylation (M1, M4, M6, M9, M13, M17), glucuronide conjugation (M2, M20, M22), glucoside conjugation (M3, M7, M11, M19, M21) and glycine conjugation (M15, M19). Ornithine conjugation (M21) was a minor metabolic pathway of TCPP detoxification mechanism. One feature (M9) was consistently discovered across all three assays and six features were reported in two UHPLC-MS/MS assays (M3, M4, M10, M14, M15, M16), thus enhancing confidence in these annotations.

One TCPP biotransformation product of dealkylation followed by oxidation, acetylation and methylation (M9, $[M+H]^+$ at 323.0214 mz, RT: 0.489 min) was measured across multiple UHPLC-MS/MS assays with a high FISh score (50%) and a positive match to mzCloud library. Half of the possible product ions assessed in the $MS^2$ data collected for M9 in the HILIC positive and RP $C_{18}$ negative lipidomics datasets (five matching fragments including 98 *m/z*, 171 *m/z* and 124 *m/z* direct match fragments) can be

structurally related to the corresponding precursor ion, increasing confidence in identification of this TCPP-derived feature.

Another TCPP-related feature corresponding to dealkylation followed by dehydration, nitro reduction and glucosidation (M3, $[M+H]^+$ at 365.0684 *m/z*, RT:0.476) was revealed by examining the HILIC and RP $C_{18}$ lipidomics (positive ion mode) datasets (FISh score: 28.57% and 25.93%, respectively) with five matching *m/z* fragments. Extracted ion chromatograms, full scan $MS^1$ data and structural annotations of these BTPs (M3, M9) using FISh scoring are shown in Figures 5.18 and 5.19, respectively.

**a**

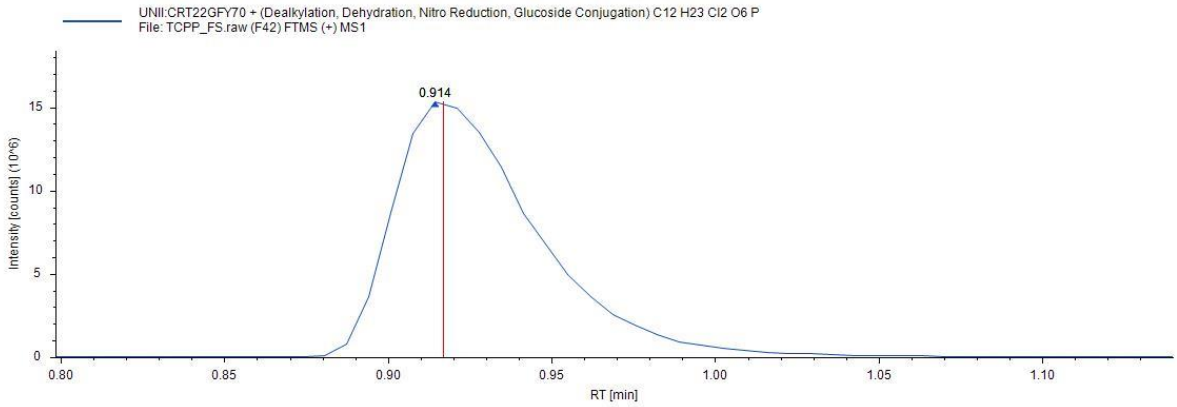
UNII:CRT22GFY70 + (Dealkylation, Dehydration, Nitro Reduction, Glucoside Conjugation) C12 H23 Cl2 O6 P
File: TCPP_FS.raw (F42) FTMS (+) MS1
0.914
Intensity [counts] (10^6)
RT [min]

**b**

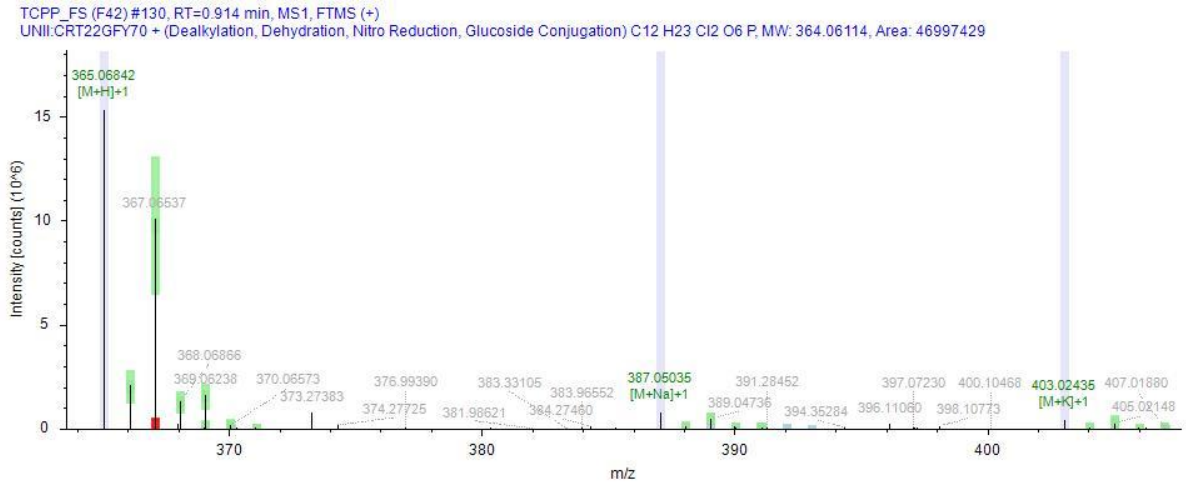
TCPP_FS (F42) #130, RT=0.914 min, MS1, FTMS (+)
UNII:CRT22GFY70 + (Dealkylation, Dehydration, Nitro Reduction, Glucoside Conjugation) C12 H23 Cl2 O6 P, MW: 364.06114, Area: 46997429
365.06842 [M+H]+1
387.05035 [M+Na]+1
403.02435 [M+K]+1
Intensity [counts] (10^6)
m/z

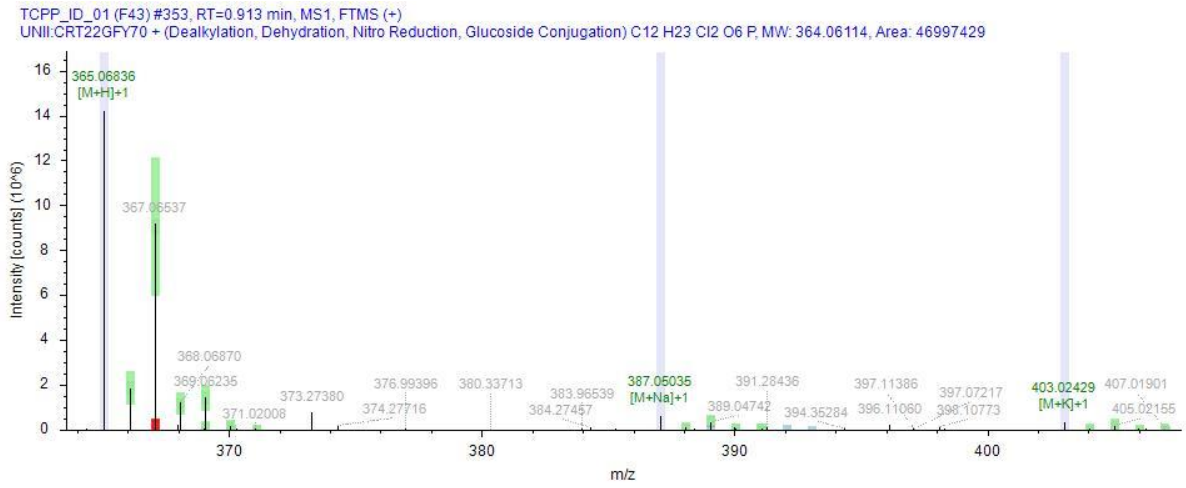
TCPP_ID_01 (F43) #353, RT=0.913 min, MS1, FTMS (+)
UNII:CRT22GFY70 + (Dealkylation, Dehydration, Nitro Reduction, Glucoside Conjugation) C12 H23 Cl2 O6 P, MW: 364.06114, Area: 46997429
365.06836 [M+H]+1
387.05035 [M+Na]+1
403.02429 [M+K]+1
Intensity [counts] (10^6)
m/z

**c**

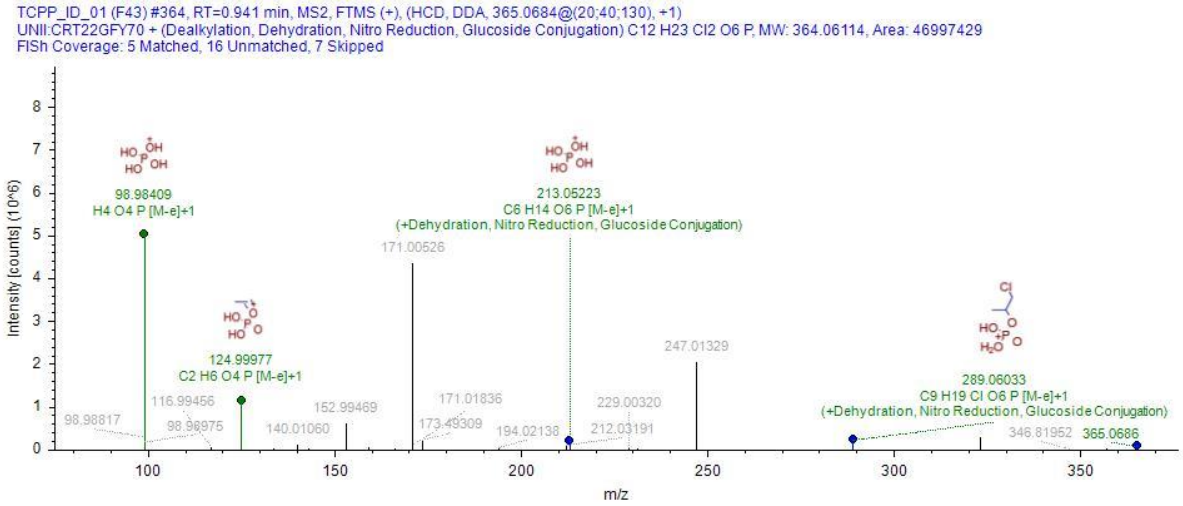


**d**

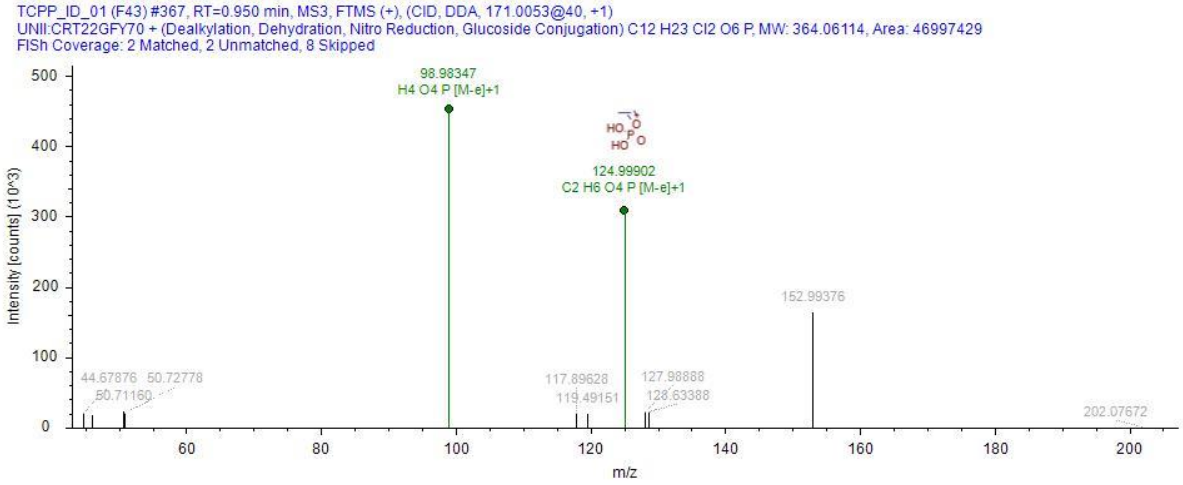


**Figure 5.19** Confirming identity of a major TCPP metabolite (M3) discovered in two UHPLC-MS/MS assays. (**a**) Extracted ion chromatogram of M3 [M+H]+ peak in rat plasma (**b**) Full scan $MS^1$ data showing the isotope pattern fit for M3 ion in rat plasma, (**c**) Structure annotations from FISh scoring on $MS^2$ spectrum. (**d**) Structure annotations from FISh scoring on $MS^3$ spectrum. Green – indicates direct match fragments, blue – transformation shifted fragments.

**a**

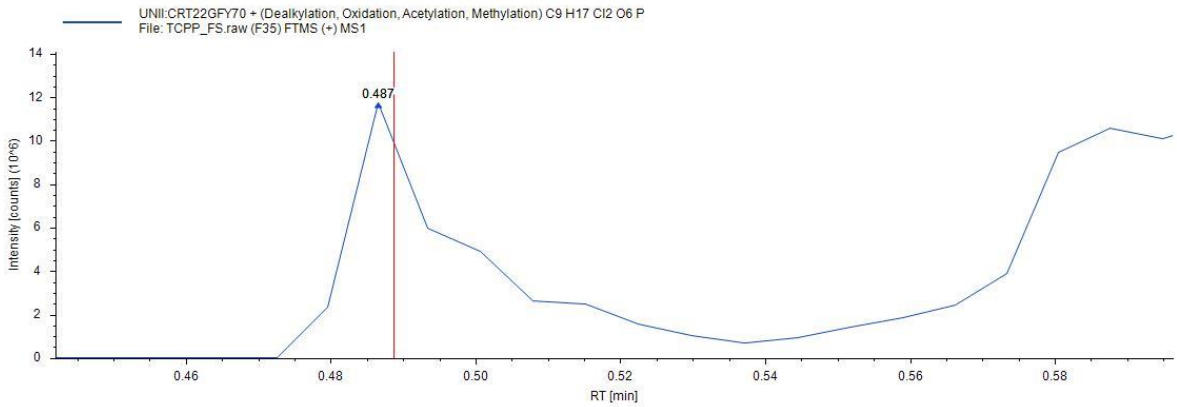
UNII:CRT22GFY70 + (Dealkylation, Oxidation, Acetylation, Methylation) C9 H17 Cl2 O6 P
File: TCPP_FS.raw (F35) FTMS (+) MS1
0.487
Intensity [counts] (10^6)
RT [min]

**b**

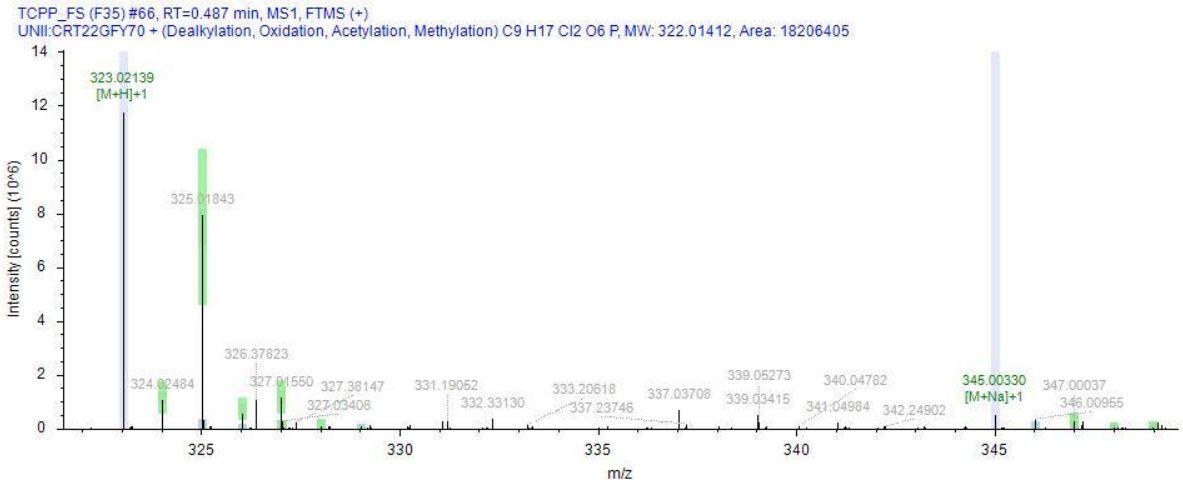
TCPP_FS (F35) #66, RT=0.487 min, MS1, FTMS (+)
UNII:CRT22GFY70 + (Dealkylation, Oxidation, Acetylation, Methylation) C9 H17 Cl2 O6 P, MW: 322.01412, Area: 18206405
323.02139
[M+H]+1
325.01843
345.00330
[M+Na]+1
Intensity [counts] (10^6)
m/z

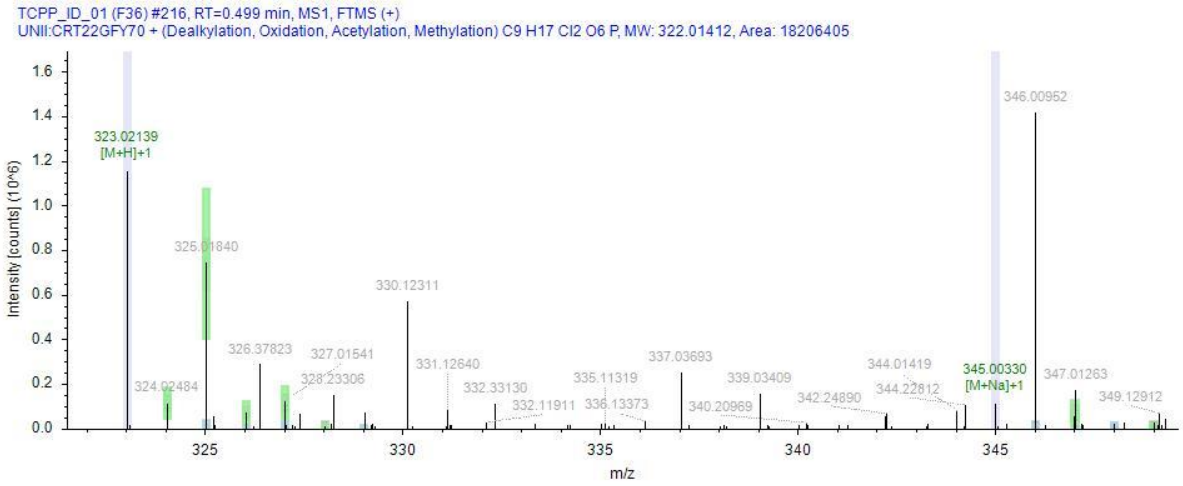
TCPP_ID_01 (F36) #216, RT=0.499 min, MS1, FTMS (+)
UNII:CRT22GFY70 + (Dealkylation, Oxidation, Acetylation, Methylation) C9 H17 Cl2 O6 P, MW: 322.01412, Area: 18206405
323.02139
[M+H]+1
346.00952
325.01840
330.12311
345.00330
[M+Na]+1
Intensity [counts] (10^6)
m/z

**c**

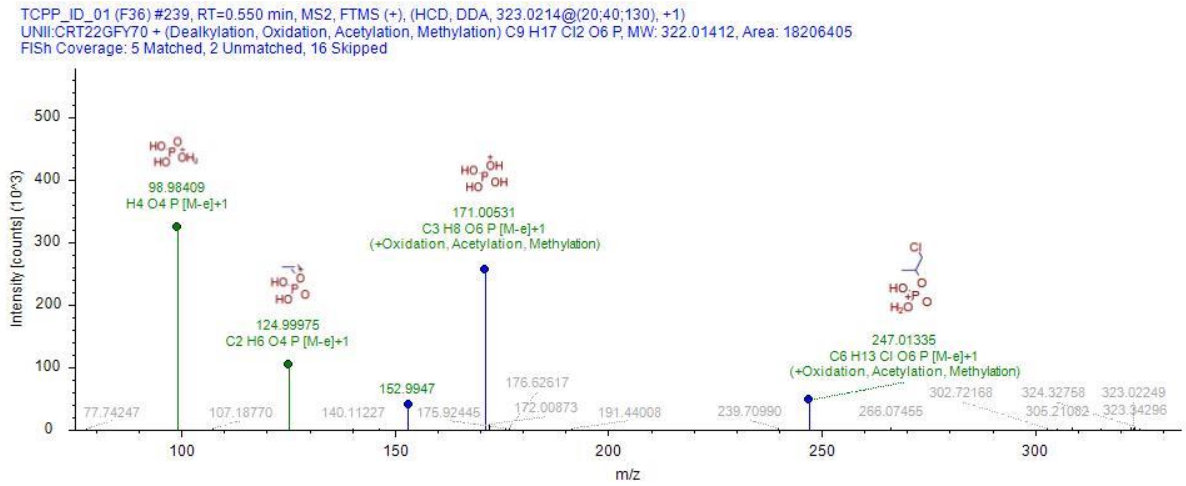


**d**

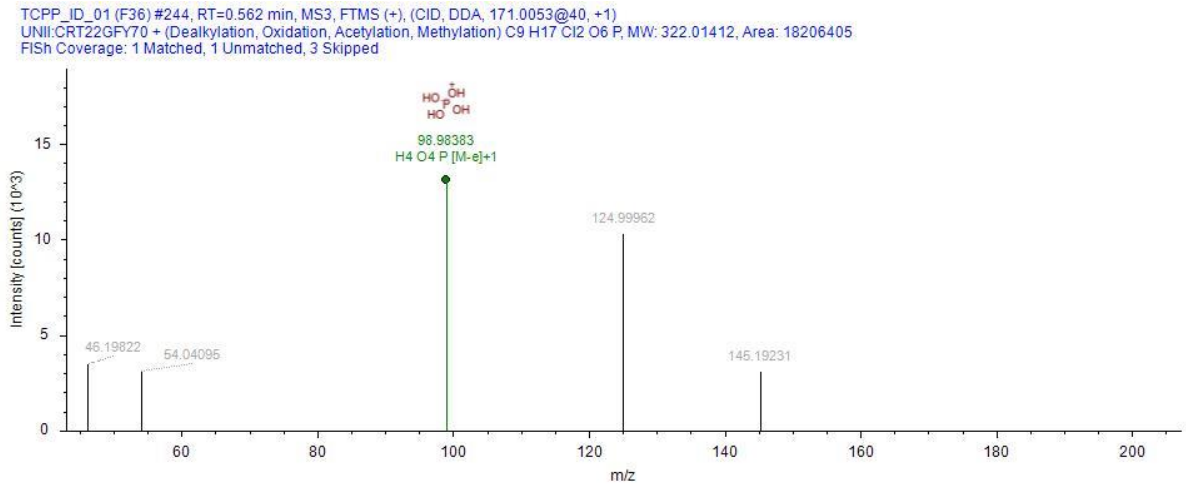


**Figure 5.20** Confirming identity of a major TCPP metabolite (M9) discovered in multiple UHPLC-MS/MS assays. (**a**) Extracted ion chromatogram of M9 [M+H]+ peak in rat plasma (**b**) Full scan $MS^1$ data showing the isotope pattern fit for M9 ion in rat plasma, (**c**) Structure annotations from FISh scoring on $MS^2$ spectrum. (**d**) Structure annotations from FISh scoring on $MS^3$ spectrum. Green – indicates direct match fragments, blue – transformation shifted fragments.

The major TCPP BTP reported in one study[277], namely bis(1-chloro-2-propyl) 1-hydroxy-2-propyl phosphate was not discovered in any of the datasets. However, a sodium adduct (M12, 313.05774 *m/z*, RT: 0.664 min) corresponding to tetraethyl pyrophosphate (TEPP) was also identified in the positive $C_{18}$ lipidomics dataset following double oxidative dechlorination, and matched to the mzCloud and ChemSpider libraries (within 0.4 ppm, 77.4%). The application of FISh scoring revealed major fragment peaks at 159 *m/z*, 174 *m/z* and 233 *m/z* representing substructures of TEPP, as shown in Figure 5.21.

**a**

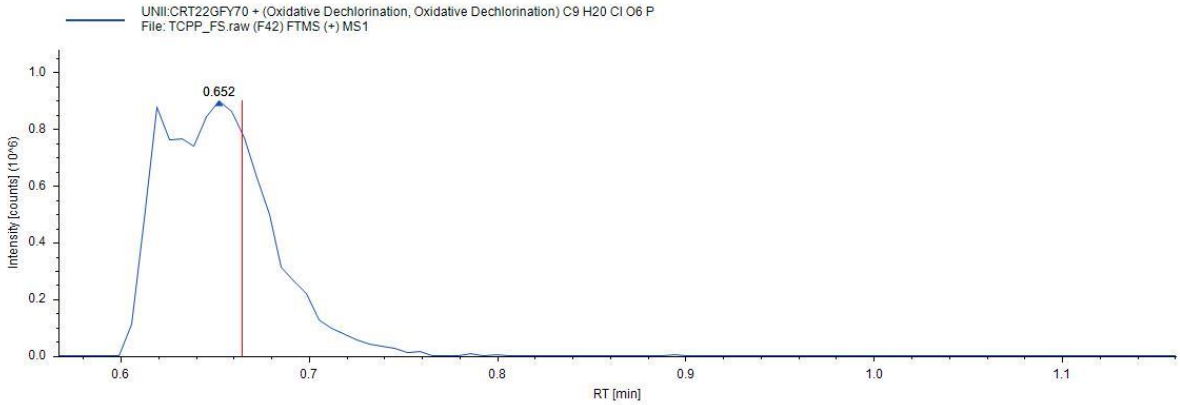
UNII:CRT22GFY70 + (Oxidative Dechlorination, Oxidative Dechlorination) C9 H20 Cl O6 P
File: TCPP_FS.raw (F42) FTMS (+) MS1
0.652
Intensity [counts] (10^6)
RT [min]

**b**

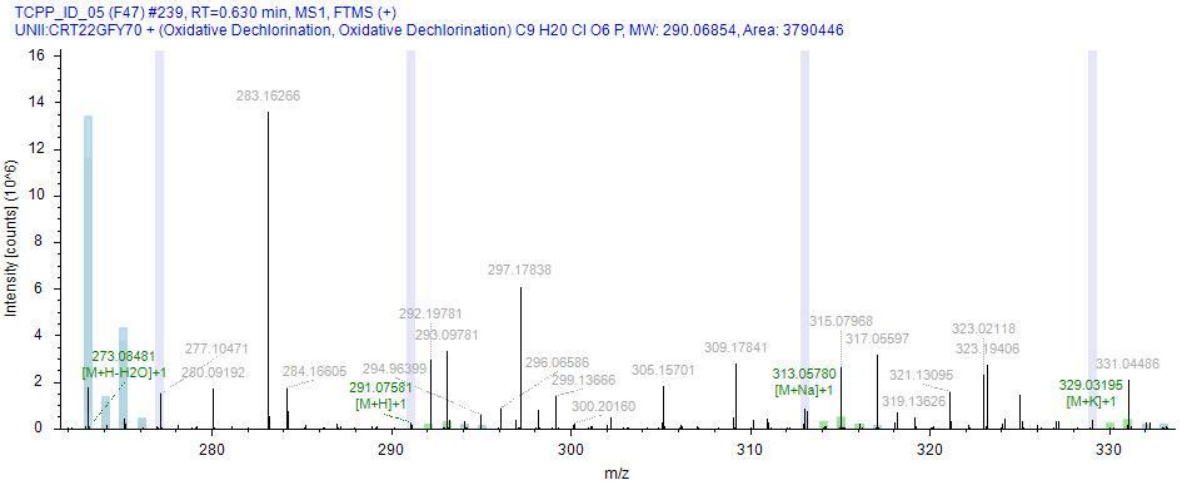
TCPP_ID_05 (F47) #239, RT=0.630 min, MS1, FTMS (+)
UNII:CRT22GFY70 + (Oxidative Dechlorination, Oxidative Dechlorination) C9 H20 Cl O6 P, MW: 290.06854, Area: 3790446
283.16266
297.17838
292.19781
293.09781
315.07968
317.05597
323.02118
323.19406
273.08481
[M+H-H2O]+1
277.10471
280.09192
284.16605
294.96399
291.07581
[M+H]+1
296.06586
299.13666
305.15701
309.17841
313.05780
[M+Na]+1
321.13095
319.13626
329.03195
[M+K]+1
331.04486
300.20160
Intensity [counts] (10^6)
m/z

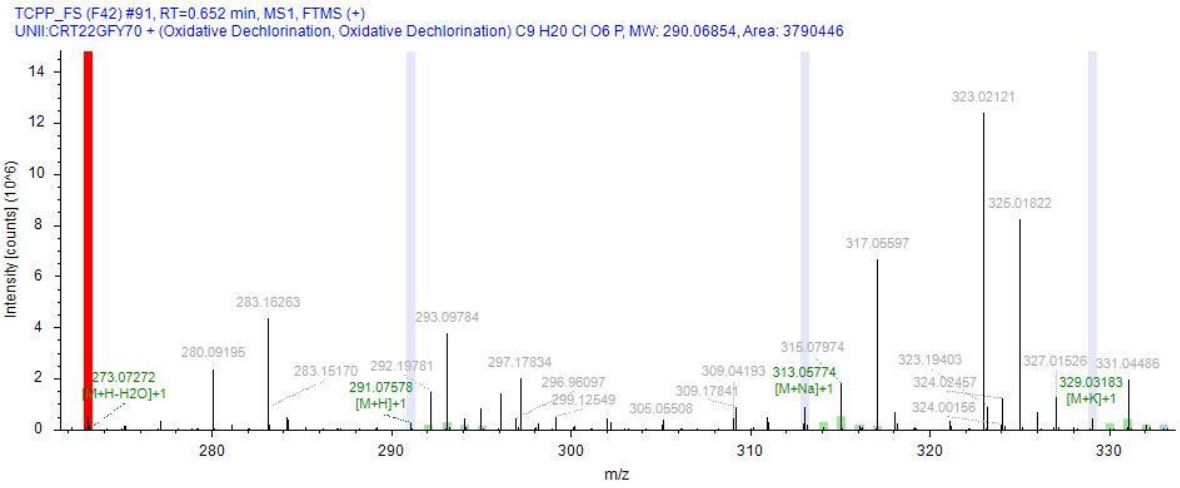
TCPP_FS (F42) #91, RT=0.652 min, MS1, FTMS (+)
UNII:CRT22GFY70 + (Oxidative Dechlorination, Oxidative Dechlorination) C9 H20 Cl O6 P, MW: 290.06854, Area: 3790446
323.02121
326.01822
317.05597
283.16263
293.09784
280.09195
315.07974
323.19403
327.01526
331.04486
273.07272
[M+H-H2O]+1
283.15170
292.19781
297.17834
291.07578
[M+H]+1
296.96097
299.12549
309.04193
313.05774
[M+Na]+1
309.17841
305.05508
324.02457
324.00156
329.03183
[M+K]+1
Intensity [counts] (10^6)
m/z

**c**

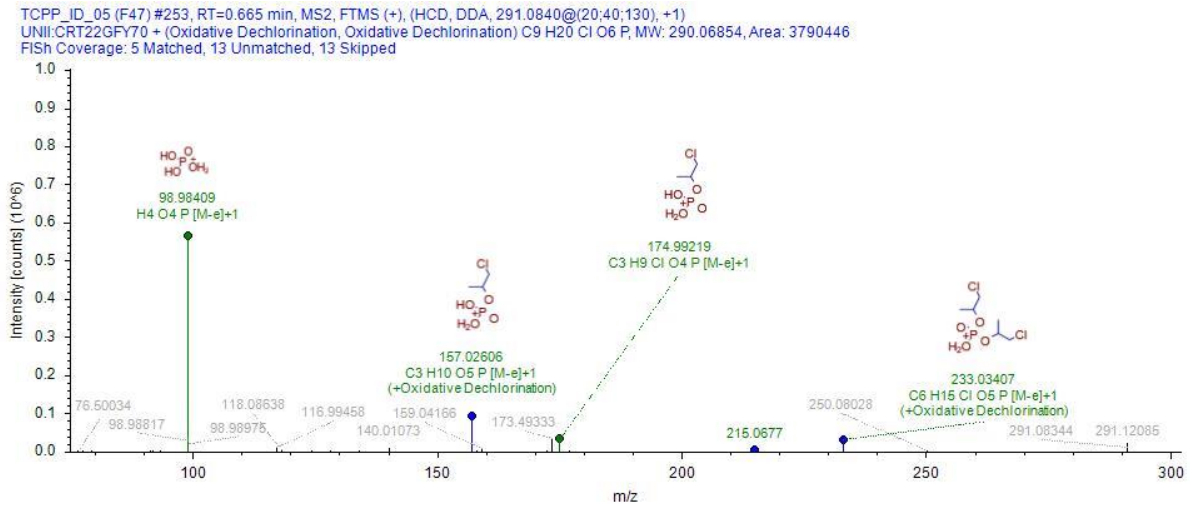


**d**

| Structure | Name | Formula | Molecular Weight | ΔMass [Da] | ΔMass [ppm] | CSID |
|---|---|---|---|---|---|---|
| 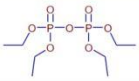 | Tetraethyl pyrophosphate | C8 H20 O7 P2 | 290.06843 | 0.00012 | 0.40 | 7585 |

| Structure | Name | Formula | Molecular Weight | ΔMass [Da] | ΔMass [ppm] | Confidence | Match | Tree Match | Best Match | Best Sim. Match | Type |
|---|---|---|---|---|---|---|---|---|---|---|---|
|  | Tetraethyl pyrophosphate (TEPP) | C8 H20 O7 P2 | 290.06843 | 0.00012 | 0.40 | 8.9 | 77.4 | 40.6 | 77.4 | | Identity |

**Figure 5.21** Confirming identity of a major TCPP metabolite (M12) discovered in multiple UHPLC-MS/MS assays. (**a**) Extracted ion chromatogram of M12 [M+H]+ peak in rat plasma (**b**) Full scan $MS^1$ data showing the isotope pattern fit for M9 ion in rat plasma, (**c**) Structure annotations from FISh scoring on $MS^2$ spectrum. Green – indicates direct match fragments, blue – transformation shifted fragments. (**d**) High confidence match for M12 in mzCloud (top) and ChemSpider (bottom) libraries.

A proposed biotransformation map for TCPP is shown in Figure 5.22. Many of these TCPP-related features revealed by UHPLC-MS/MS analyses of rat plasma extracts are the result of a several phase I and phase II modifications. Chemical structures were generated from canonical SMILES using the ChemDraw Professional software (v22.0.0.22; PerkinElmer).

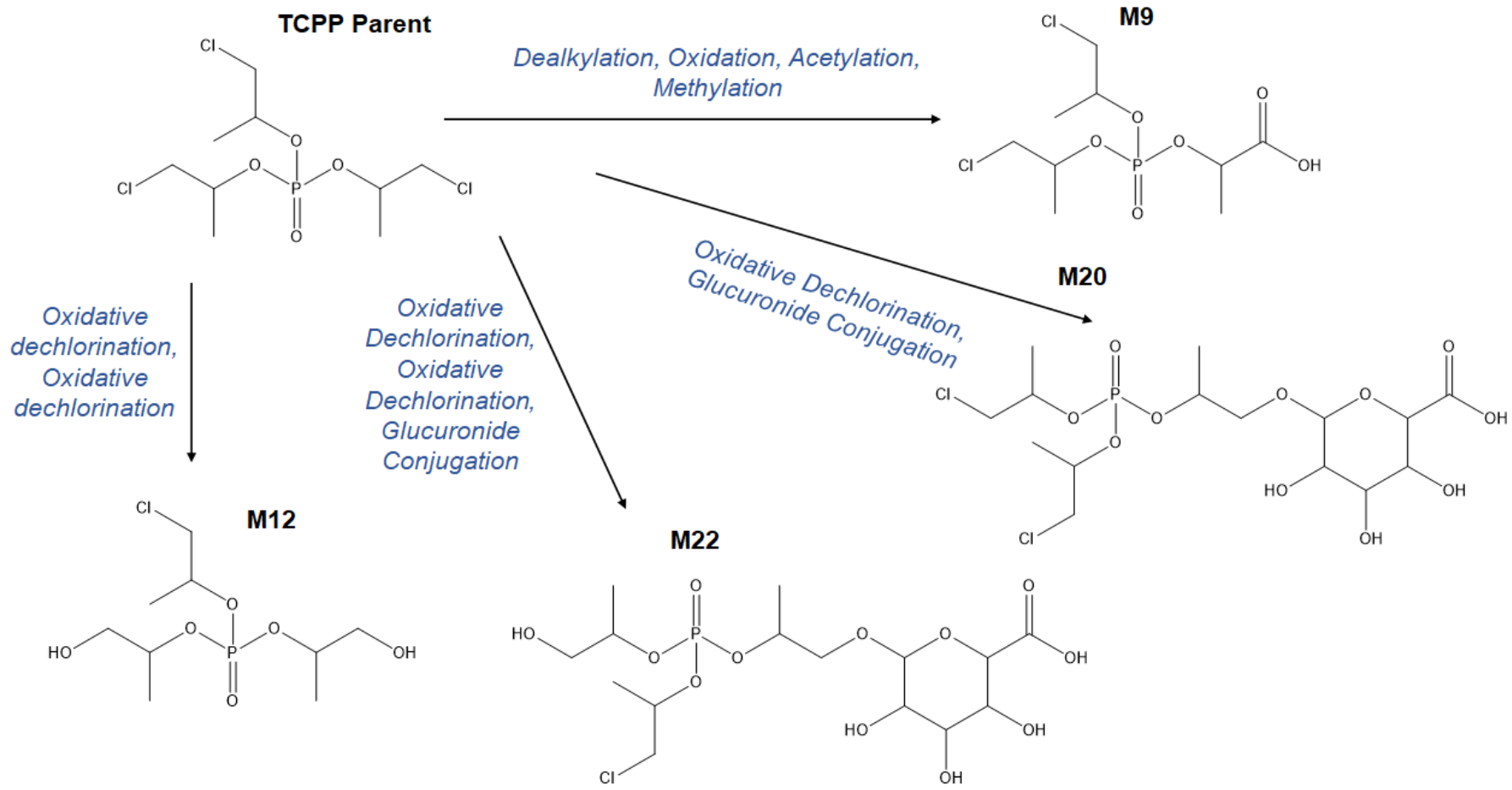


**Figure 5.22** TCPP suggested metabolic pathway for major BTPs discovered in the UHPLC-MS/MS datasets. Plain arrow – phase I reaction, dashed arrow – phase II reaction.

**Table 5.17** TCPP metabolic biotransformation products identified in UHPLC-MS/MS datasets with assigned levels of confidence in identification: yellow – 'low confidence', blue – 'medium confidence', green – 'high confidence'. Abbreviations: FISh – Fragment ion search scoring, MW – molecular weight, RT – retention time.

| ID | Assay | Formula | Transformations | Composition Change | Annot. DeltaMass [ppm] | Calc. MW | m/z | RT [min] | FISh Coverage | Area (Max.) | mzCloud Best Match | Reference Ion |
|---|---|---|---|---|---|---|---|---|---|---|---|---|
| **P** | HILIC pos | C9 H18 Cl3 O4 P | | | 0.32 | 326.0009 | 327.0082 | 0.431 | 36.36 | 4.54E+07 | 96.6 | [M+H]+1 |
| **M1** | HILIC pos | C10 H19 Cl2 O6 P | Desaturation, Oxidation, Oxidative Dechlorination, Methylation | -(Cl) +(C H O2) | 0.24 | 336.0297 | 337.0370 | 0.434 | 33.33 | 1.94E+08 | | [M+H]+1 |
| **M2** | HILIC pos | C15 H29 Cl2 O8 P | Nitro Reduction, Reductive Dechlorination, Glucuronide Conjugation | -(Cl) +(C6 H11 O4) | 0.34 | 438.0979 | 439.1051 | 0.467 | 15.00 | 3.27E+05 | 83.7 | [M+H]+1 |
| **M3** | HILIC pos | C12 H23 Cl2 O6 P | Dealkylation, Dehydration, Nitro Reduction, | -(Cl) +(C3 H5 O2) | 0.4 | 364.0611 | 365.0684 | 0.476 | 28.57 | 4.65E+05 | | [M+H]+1 |

| ID | Assay | Formula | Transformations | Composition Change | Annot. DeltaMass [ppm] | Calc. MW | m/z | RT [min] | FISh Coverage | Area (Max.) | mzCloud Best Match | Reference Ion |
|---|---|---|---|---|---|---|---|---|---|---|---|---|
| | | | Glucoside Conjugation | | | | | | | | | |
| **M4** | HILIC pos | C12 H23 Cl2 O6 P | Oxidative Dechlorination, Acetylation, Methylation | -(Cl) +(C3 H5 O2) | 0.4 | 364.0611 | 365.0684 | 0.476 | 28.57 | 4.65E+05 | | [M+H]+1 |
| **M7** | HILIC pos | C12 H23 Cl2 O7 P | Dealkylation, Desaturation, Nitro Reduction, Glucoside Conjugation | -(Cl) +(C3 H5 O3) | 0.21 | 380.0559 | 381.0632 | 0.477 | 12.50 | 4.17E+06 | | [M+H]+1 |
| **M6** | HILIC pos | C12 H23 Cl2 O7 P | Oxidation, Oxidative Dechlorination, Acetylation, Methylation | -(Cl) +(C3 H5 O3) | 0.21 | 380.0559 | 381.0632 | 0.477 | 31.25 | 4.17E+06 | | [M+H]+1 |
| **M8** | HILIC pos | C6 H13 Cl2 O4 P | Dealkylation | -(C3 H5 Cl) | 0.22 | 249.9929 | 251.0002 | 0.48 | 18.18 | 5.03E+05 | | [M+H]+1 |

| ID | Assay | Formula | Transformations | Composition Change | Annot. DeltaMass [ppm] | Calc. MW | m/z | RT [min] | FISh Coverage | Area (Max.) | mzCloud Best Match | Reference Ion |
|---|---|---|---|---|---|---|---|---|---|---|---|---|
| **M9** | HILIC pos | C9 H17 Cl2 O6 P | Dealkylation, Oxidation, Acetylation, Methylation | -(H Cl) +(O2) | 0.43 | 322.0141 | 323.0214 | 0.489 | 50.00 | 1.82E+07 | 82.2 | [M+H]+1 |
| **M10** | HILIC pos | C9 H17 Cl2 O6 P | Desaturation, Oxidation, Oxidative Dechlorination | -(H Cl) +(O2) | 0.43 | 322.0141 | 323.0214 | 0.489 | 57.14 | 1.82E+07 | 82.2 | [M+H]+1 |
| **M11** | C18 Lipidomics neg | C12 H25 Cl2 O10 P | Dealkylation, Hydration, Glucoside Conjugation | -(Cl) +(C3 H7 O6) | 0.61 | 430.0565 | 429.0492 | 0.623 | 11.11 | 2.49E+05 | | [M-H]-1 |
| **M9** | C18 Lipidomics neg | C9 H17 Cl2 O6 P | Dealkylation, Oxidation, Acetylation, Methylation | -(H Cl) +(O2) | 1.17 | 322.0144 | 321.0071 | 0.657 | 50.00 | 3.34E+06 | | [M-H]-1 |
| **M9** | C18 Lipidomics pos | C9 H17 Cl2 O6 P | Dealkylation, Oxidation, Acetylation, Methylation | -(H Cl) +(O2) | -0.17 | 322.0139 | 323.0212 | 0.663 | 30.00 | 5.61E+07 | 97.2 | [M+H]+1 |

| ID | Assay | Formula | Transformations | Composition Change | Annot. DeltaMass [ppm] | Calc. MW | m/z | RT [min] | FISh Coverage | Area (Max.) | mzCloud Best Match | Reference Ion |
|---|---|---|---|---|---|---|---|---|---|---|---|---|
| **M10** | C18 Lipidomics pos | C9 H17 Cl2 O6 P | Desaturation, Oxidation, Oxidative Dechlorination | -(H Cl) +(O2) | -0.17 | 322.0139 | 323.0212 | 0.663 | 33.33 | 5.61E+07 | 97.2 | [M+H]+1 |
| **M12** | C18 Lipidomics pos | C9 H20 Cl O6 P | Oxidative Dechlorination, Oxidative Dechlorination | -(Cl2) +(H2 O2) | -0.2 | 290.0685 | 313.0577 | 0.664 | 20.83 | 3.79E+06 | 77.4 | [M+Na]+1 |
| **M13** | C18 Lipidomics pos | C9 H19 Cl2 O5 P | Dealkylation, Reduction, Acetylation, Methylation | -(Cl) +(H O) | -0.11 | 308.0347 | 309.0420 | 0.683 | 36.36 | 4.09E+06 | | [M+H]+1 |
| **M14** | C18 Lipidomics pos | C9 H19 Cl2 O5 P | Oxidative Dechlorination | -(Cl) +(H O) | -0.11 | 308.0347 | 309.0420 | 0.683 | 36.36 | 4.09E+06 | | [M+H]+1 |
| **M15** | C18 Lipidomics pos | C11 H24 Cl2 N O6 P | Hydration, Reductive Dechlorination, Glycine Conjugation | -(Cl) +(C2 H6 N O2) | -0.09 | 367.0718 | 368.0791 | 0.698 | 13.79 | 2.18E+06 | | [M+H]+1 |

| ID | Assay | Formula | Transformations | Composition Change | Annot. DeltaMass [ppm] | Calc. MW | m/z | RT [min] | FISh Coverage | Area (Max.) | mzCloud Best Match | Reference Ion |
|---|---|---|---|---|---|---|---|---|---|---|---|---|
| **M15** | HILIC pos | C11 H24 Cl2 N O6 P | Hydration, Reductive Dechlorination, Glycine Conjugation | -(Cl) +(C2 H6 N O2) | 0.15 | 367.0719 | 368.0792 | 0.774 | 17.86 | 1.52E+06 | | [M+H]+1 |
| **P** | C18 Lipidomics pos | C9 H18 Cl3 O4 P | | | 0.55 | 326.0010 | 327.0083 | 0.843 | 27.27 | 1.85E+08 | 97.5 | [M+H]+1 |
| **M16** | C18 Lipidomics pos | C6 H12 Cl O6 P | Dealkylation, Desaturation, Oxidation, Oxidative Dechlorination | -(C3 H6 Cl2) +(O2) | 0.11 | 246.0060 | 247.0133 | 0.916 | 30.77 | 1.79E+06 | | [M+H]+1 |
| **M17** | C18 Lipidomics pos | C9 H18 Cl O6 P | Dealkylation, Oxidative Dechlorination, Acetylation, Methylation | -(Cl2) +(O2) | 0.15 | 288.0530 | 289.0603 | 0.916 | 23.08 | 2.49E+06 | | [M+H]+1 |

| ID | Assay | Formula | Transformations | Composition Change | Annot. DeltaMass [ppm] | Calc. MW | m/z | RT [min] | FISh Coverage | Area (Max.) | mzCloud Best Match | Reference Ion |
|---|---|---|---|---|---|---|---|---|---|---|---|---|
| **M18** | C18 Lipidomics pos | C9 H18 Cl O6 P | Desaturation, Oxidative Dechlorination, Oxidative Dechlorination | -(Cl2) +(O2) | 0.15 | 288.0530 | 289.0603 | 0.916 | 23.08 | 2.49E+06 | | [M+H]+1 |
| **M3** | C18 Lipidomics pos | C12 H23 Cl2 O6 P | Dealkylation, Dehydration, Nitro Reduction, Glucoside Conjugation | -(Cl) +(C3 H5 O2) | 0.59 | 364.0611 | 365.0684 | 0.917 | 25.93 | 4.70E+07 | | [M+H]+1 |
| **M4** | C18 Lipidomics pos | C12 H23 Cl2 O6 P | Oxidative Dechlorination, Acetylation, Methylation | -(Cl) +(C3 H5 O2) | 0.59 | 364.0611 | 365.0684 | 0.917 | 29.63 | 4.70E+07 | | [M+H]+1 |
| **M19** | HILIC pos | C17 H34 Cl2 N O11 P | Hydration, Reductive Dechlorination, Glucoside Conjugation, | -(Cl) +(C8 H16 N O7) | 0.09 | 529.1247 | 530.1320 | 4.929 | 32.91 | 1.01E+07 | 99.9 | [M+H]+1 |

| ID | Assay | Formula | Transformations | Composition Change | Annot. DeltaMass [ppm] | Calc. MW | m/z | RT [min] | FISh Coverage | Area (Max.) | mzCloud Best Match | Reference Ion |
|---|---|---|---|---|---|---|---|---|---|---|---|---|
| | | | Glycine Conjugation | | | | | | | | | |
| **M20** | HILIC pos | C15 H27 Cl2 O11 P | Oxidative Dechlorination, Glucuronide Conjugation | -(Cl) +(C6 H9 O7) | 0.4 | 484.0670 | 485.0743 | 5.011 | 24.14 | 3.60E+07 | 99.5 | [M+H]+1 |
| **M13** | HILIC pos | C9 H19 Cl2 O5 P | Dealkylation, Reduction, Acetylation, Methylation | -(Cl) +(H O) | 0.2 | 308.0348 | 309.0421 | 5.016 | 45.00 | 1.33E+07 | 100 | [M+H]+1 |
| **M14** | HILIC pos | C9 H19 Cl2 O5 P | Oxidative Dechlorination | -(Cl) +(H O) | 0.2 | 308.0348 | 309.0421 | 5.016 | 45.00 | 1.33E+07 | 100 | [M+H]+1 |
| **M21** | HILIC pos | C17 H33 Cl2 N2 O11 P | Dealkylation, Oxidation, Glucoside Conjugation, Ornitine Conjugation | -(Cl) +(C8 H15 N2 O7) | 0.37 | 542.1201 | 543.1274 | 5.274 | 19.05 | 1.46E+06 | | [M+H]+1 |

| ID | Assay | Formula | Transformations | Composition Change | Annot. DeltaMass [ppm] | Calc. MW | m/z | RT [min] | FISh Coverage | Area (Max.) | mzCloud Best Match | Reference Ion |
|---|---|---|---|---|---|---|---|---|---|---|---|---|
| **M22** | HILIC pos | C15 H28 Cl O12 P | Oxidative Dechlorination, Oxidative Dechlorination, Glucuronide Conjugation | -(Cl2) +(C6 H10 O8) | 0.21 | 466.1008 | 467.1081 | 6.088 | 45.83 | 1.26E+06 | | [M+H]+1 |

### 5.3.9 Triclosan

Triclosan parent was detected in rat plasma in the HILIC negative assay and manually matched against the reference standard in the same assay. The peak identity was also confirmed by a positive match to a mass spectral ChemSpider library entry (within -0.63 ppm). However, it was assigned 'low confidence' due to not passing the original filtering criteria in Compound Discoverer (FISh score: 2.6%) and in the absence of a positive mzCloud match for this feature. Triclosan parent was also annotated within the negative RP $C_{18}$ lipidomics dataset, in the reference standard only.

In addition, a total of 9 triclosan-related features were detected in the negative ionisation mode datasets, predominantly in the HILIC assay. The major phase I pathways identified were oxidation (M2, M3, M7) and desaturation (M4, M5). Oxidative dechlorination was a minor phase I modification (M4). The highest responses for phase II modifications were found for glucuronide conjugation (M6, M7) and sulphation (M1, M3, M5), with the highest peak areas (6.80e8 and 5.20e8, respectively) reported in the HILIC negative assay. This consistent with findings reported in literature[279]. Triclosan glucuronide is reported as a 'low confidence' feature due to FISh score < 10%, however.

Sulphated BTPs for triclosan were also detected in multiple UHPLC-MS/MS assay, thus increasing confidence in these annotations. No hydroxylated or dealkylated BTPs were annotated within any of the UHPLC-MS/MS assays. Figures 5.23 and 5.24 show extracted ion chromatograms, $MS^1$ data and annotated $MS^n$ spectra resulting from applying FISh scoring to the major triclosan BTPs (M1, M3; respectively). Fragment

ion at 366 *m/z* indicates sulphation (M1), which is consistent with a +80 Da shift from the parent $[M-H]^-$ ion at 286 *m/z* for triclosan. Sulphation followed by oxidation (M3) is evidenced by the presence of fragment ion at 382 *m/z* in $MS^2$ spectrum and this modification corresponds to a +96 Da mass shift from the parent.

**a**

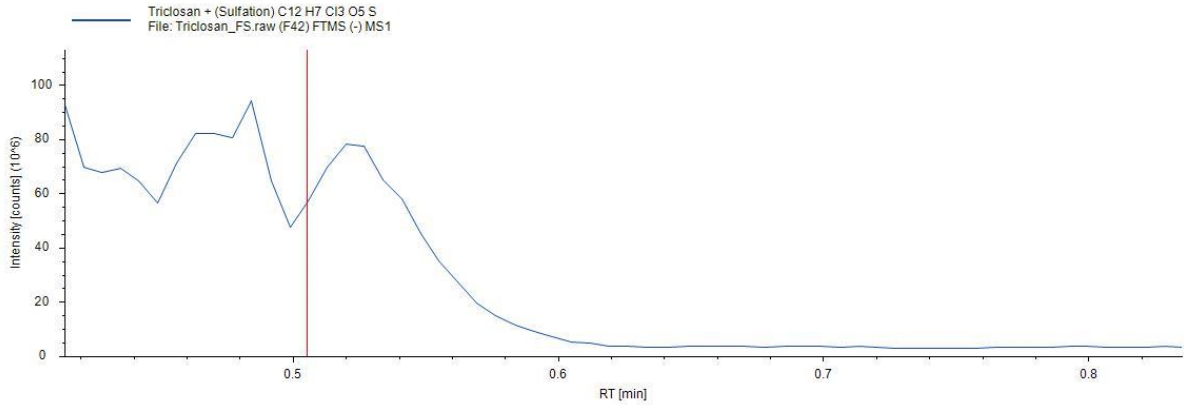


**b**

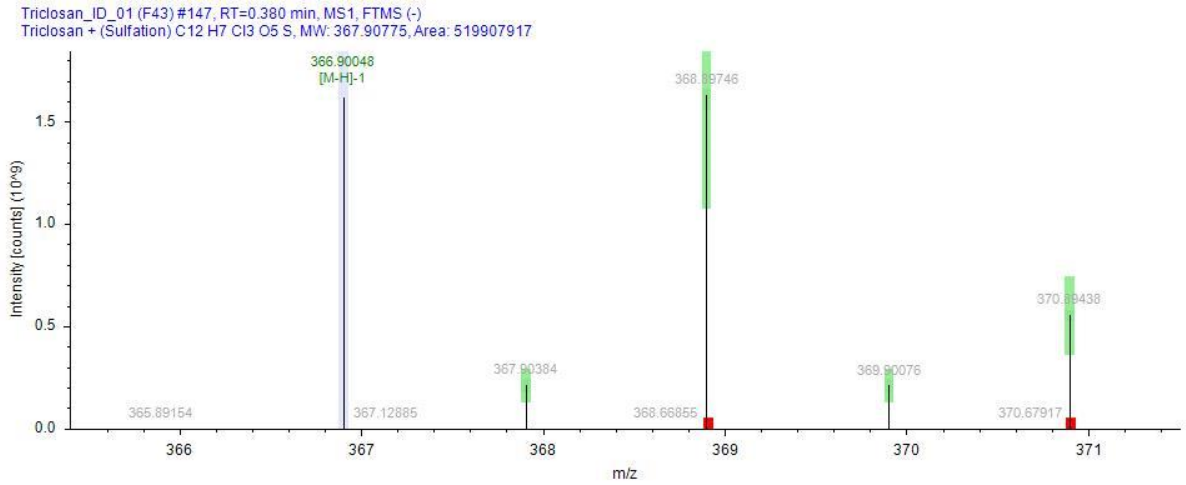


**c**

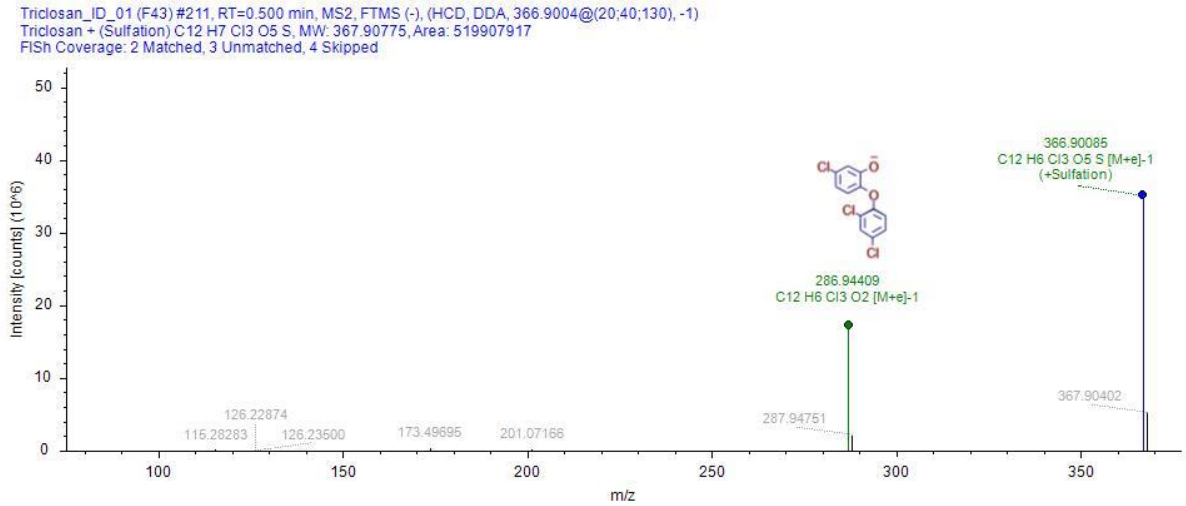


**Figure 5.23** Confirming identity of a major TCS metabolite (M1) discovered in the HILIC negative dataset. (**a**) Extracted ion chromatogram of M1 $[M-H]^-$ peak in rat plasma (**b**) Full scan $MS^1$ data showing the isotope pattern fit for M1 ion in rat plasma, (**b**) Structure annotations

from FISh scoring on $MS^2$ spectrum. Green – indicates direct match fragments, blue – transformation shifted fragments.

**a**

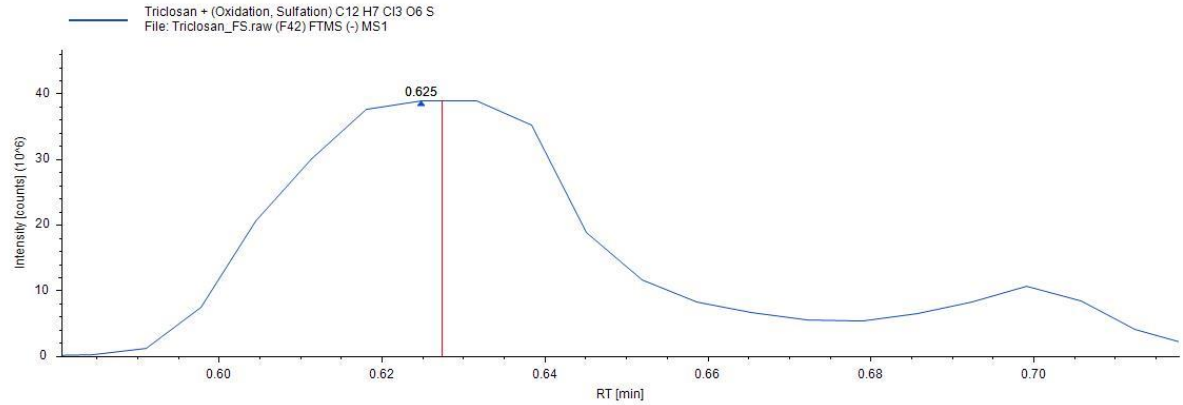


**b**

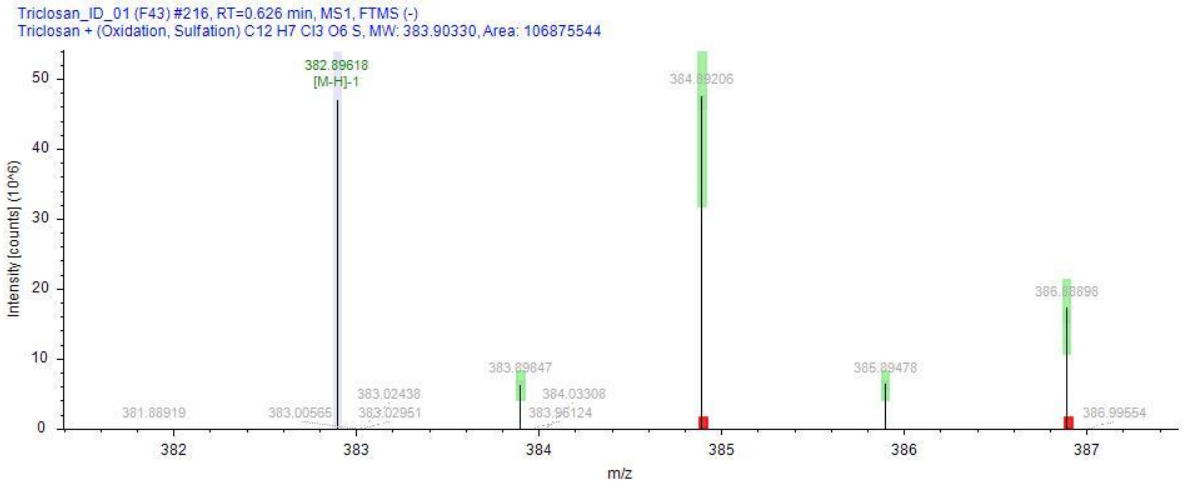


**c**

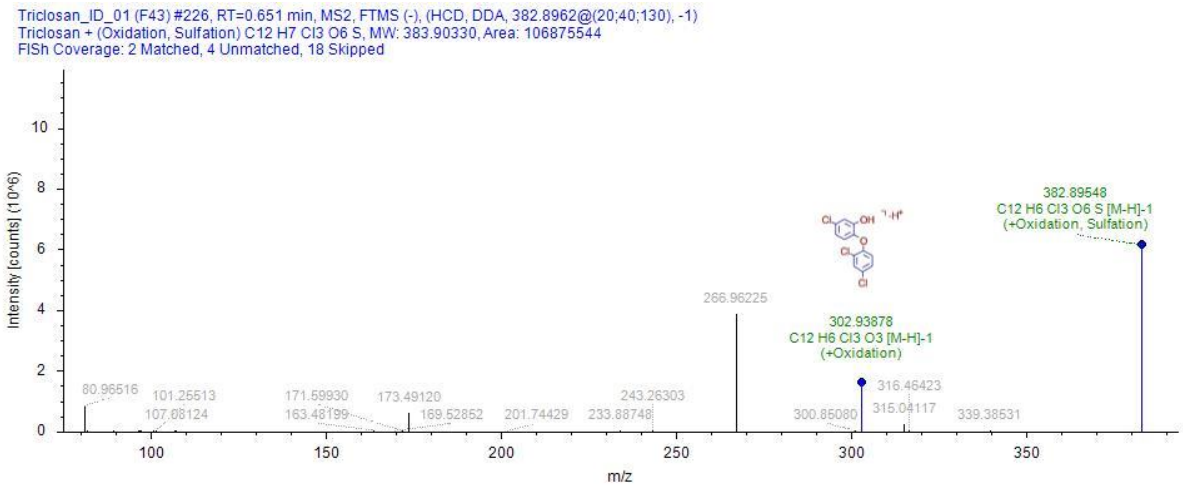


**Figure 5.24** Confirming identity of a major TCS metabolite (M3) discovered in negative $C_{18}$ lipidomics. (**a**) Extracted ion chromatogram of M3 $[M-H]^-$ peak in rat plasma (**b**) Full scan $MS^1$ data showing the isotope pattern fit for M3 ion in rat plasma, (**c**) Structure annotations from

FISh scoring on $MS^2$ spectrum. Green – indicates direct match fragments, blue – transformation shifted fragments.

In addition, a chlorine adduct corresponding to desaturation followed by sulphation was discovered in the RP $C_{18}$ lipidomics negative assay (M5, $[M+Cl]^-$ at 400.8616 m/z, RT: 0.855 min). Half of the *m/z* fragments in the mass spectra can be explained and annotated for this triclosan-related feature (FISh score: 50%; Figure 5.25).

Proposed biotransformation map for triclosan is shown in Figure 5.26. Chemical structures were generated from canonical SMILES using the ChemDraw Professional software (v22.0.0.22; PerkinElmer).

**a**

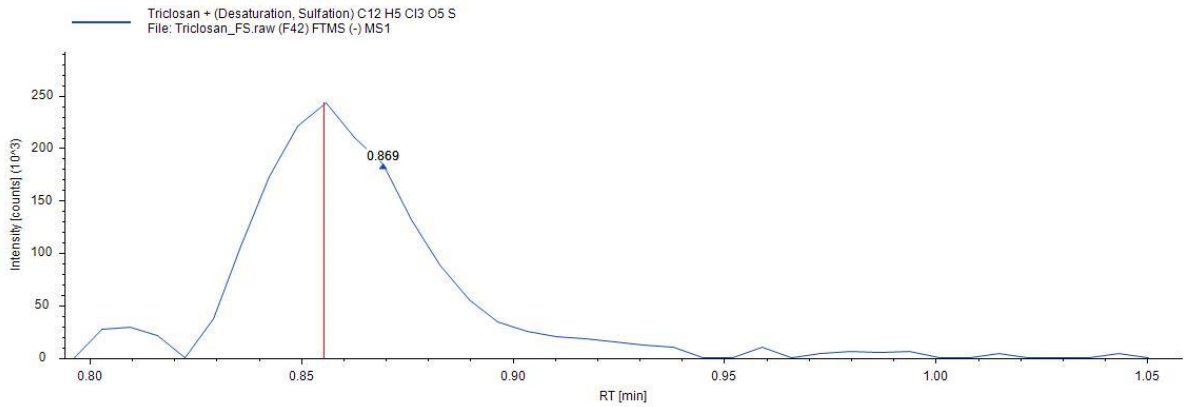


**b**

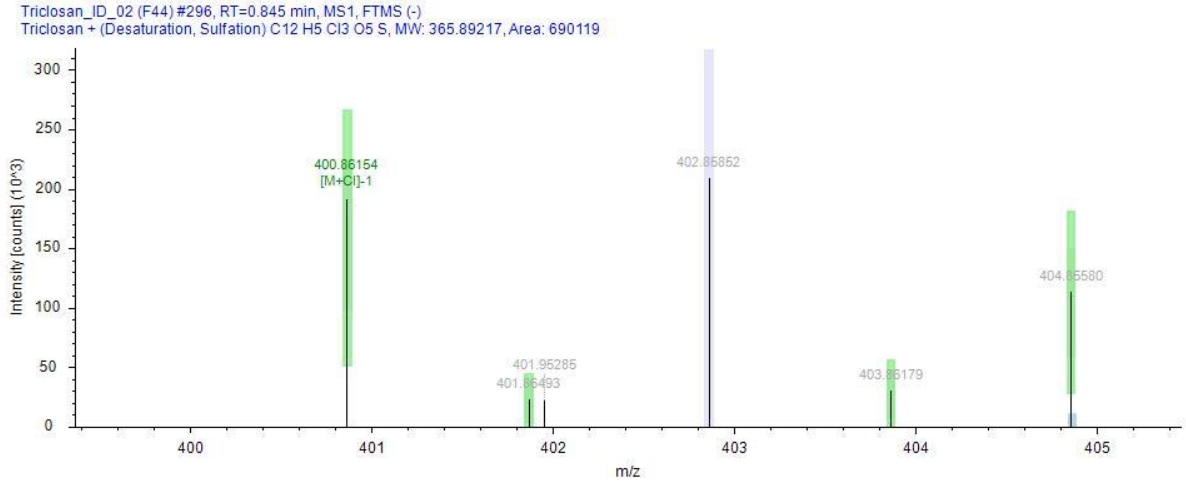


**c**

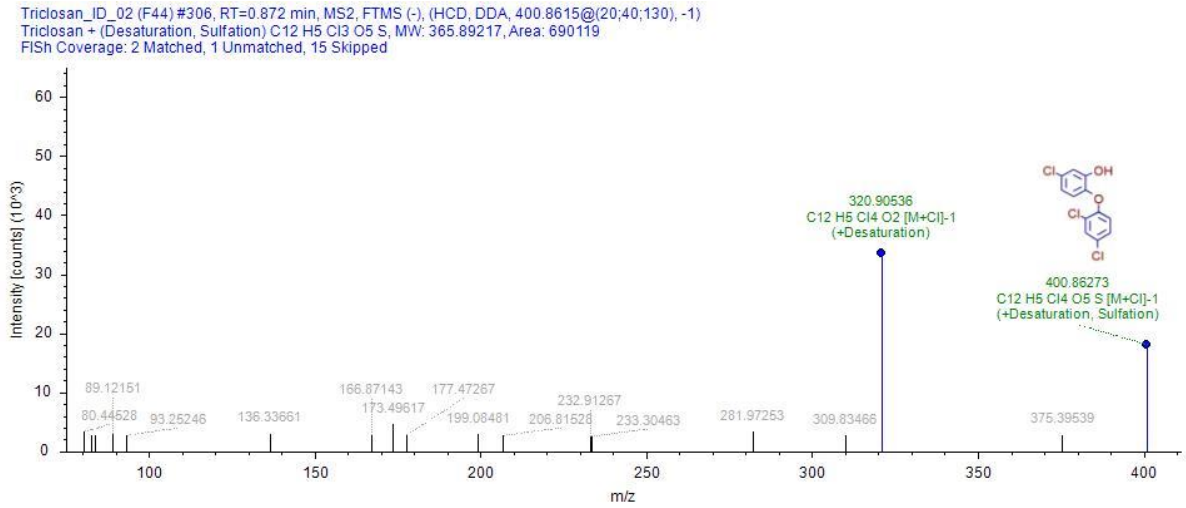


**Figure 5.25** Confirming identity of a major TCS metabolite (M5) discovered in negative $C_{18}$ lipidomics. (**a**) Extracted ion chromatogram of M5 $[M-H]^-$ peak in rat plasma (**b**) Full scan $MS^1$ data showing the isotope pattern fit for M5 ion in rat plasma, (**b**) Structure annotations from

FISh scoring on $MS^2$ spectrum. Green – indicates direct match fragments, blue – transformation shifted fragments.

**Table 5.18** Triclosan metabolic biotransformation products identified in UHPLC-MS/MS datasets with assigned levels of confidence in identification: yellow – 'low confidence', blue – 'medium confidence', green – 'high confidence'. Abbreviations: FISh – Fragment ion search scoring, MW – molecular weight.

| ID | Assay | Formula | Transformations | Composition Change | Annot. DeltaMass [ppm] | Calc. MW | m/z | RT [min] | FISh Coverage | Area (Max.) | Reference Ion |
|---|---|---|---|---|---|---|---|---|---|---|---|
| **P** | C18 Lipidomics neg | C12 H7 Cl3 O2 | | | 1.13 | 287.9515 | 286.9443 | 1.35 | 0.00 | 2.49E+08 | [M-H]-1 |
| **M3** | C18 Lipidomics neg | C12 H7 Cl3 O6 S | Oxidation, Sulphation | +(O4 S) | 1.07 | 383.9033 | 382.8960 | 0.627 | 20.00 | 1.07E+08 | [M-H]-1 |
| **M4** | C18 Lipidomics neg | C12 H6 Cl2 O6 S | Desaturation, Oxidative Dechlorination, Sulphation | -(H Cl) +(O4 S) | -0.04 | 347.9262 | 382.8956 | 0.699 | 30.00 | 1.84E+07 | [M+Cl]-1 |
| **M5** | C18 Lipidomics neg | C12 H5 Cl3 O5 S | Desaturation, Sulphation | -(H2) +(O3 S) | -0.43 | 365.8922 | 400.8616 | 0.855 | 50.00 | 6.90E+05 | [M+Cl]-1 |
| **M1** | C18 Lipidomics neg | C12 H7 Cl3 O5 S | Sulphation | +(O3 S) | -0.18 | 367.9079 | 366.9006 | 2.558 | 16.67 | 1.75E+05 | [M-H]-1 |

| | | | | | | | | | | | |
|---|---|---|---|---|---|---|---|---|---|---|---|
| **P** | HILIC neg | C12 H7 Cl3 O2 | | | 0.43 | 287.9513 | 286.9440 | 0.435 | 2.26 | 7.93E+08 | [M-H]-1 |
| **M6** | HILIC neg | C18 H15 Cl3 O8 | Glucuronide Conjugation | +(C6 H8 O6) | -0.32 | 463.9831 | 462.9758 | 3.129 | 6.21 | 6.80E+08 | [M-H]-1 |
| **M1** | HILIC neg | C12 H7 Cl3 O5 S | Sulphation | +(O3 S) | -0.63 | 367.9078 | 366.9005 | 0.505 | 16.67 | 5.20E+08 | [M-H]-1 |
| **M7** | HILIC neg | C18 H15 Cl3 O12 S | Oxidation, Glucuronide Conjugation, Sulphation | +(C6 H8 O10 S) | 0.17 | 559.9351 | 558.9278 | 5.416 | 16.84 | 1.14E+07 | [M-H]-1 |
| **M2** | HILIC neg | C18 H17 Cl3 O11 S | Oxidation, Glucoside Conjugation, Sulphation | +(C6 H10 O9 S) | -0.36 | 545.9555 | 544.9482 | 0.592 | 13.79 | 5.54E+05 | [M-H]-1 |

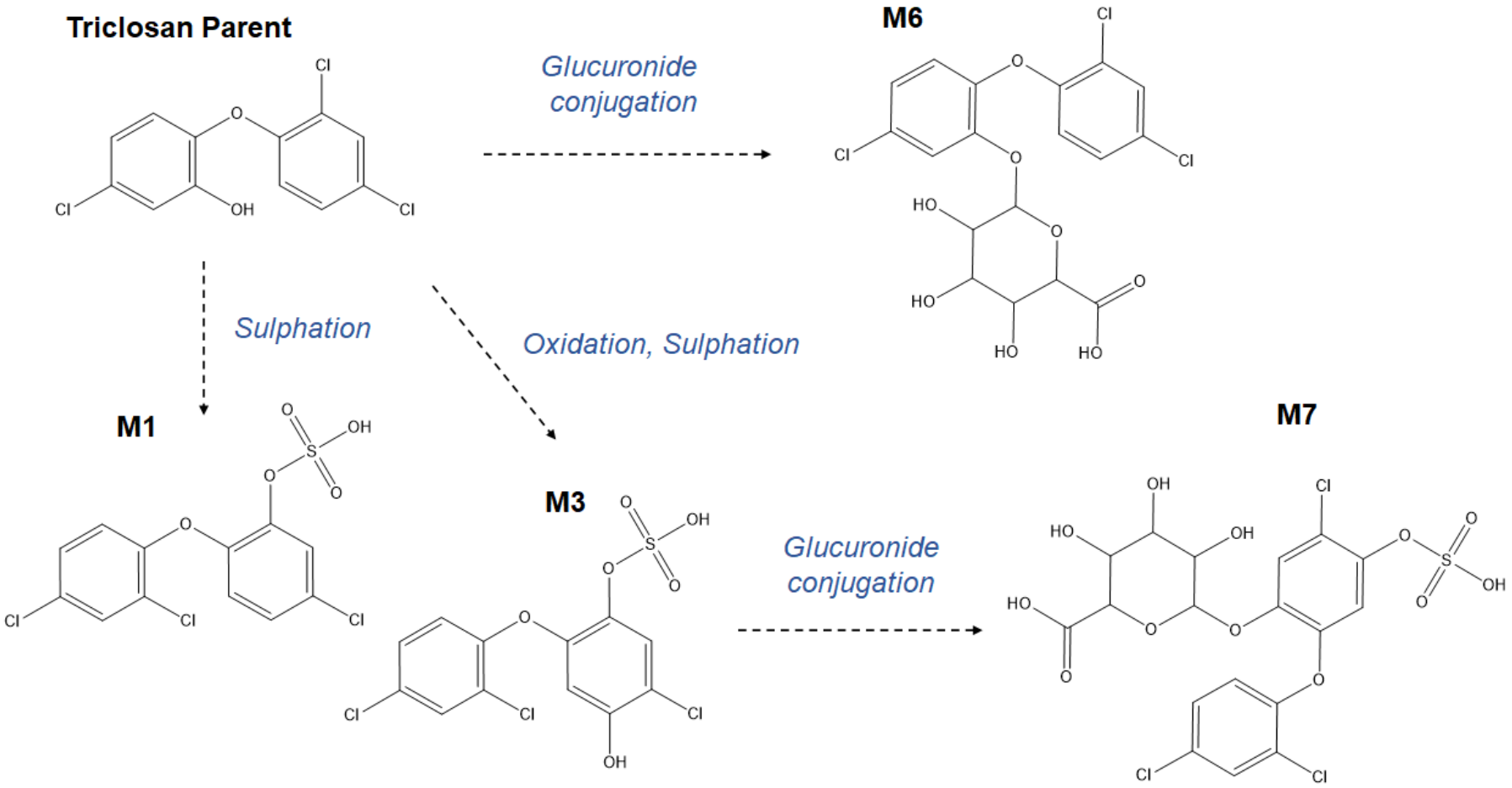


**Figure 5.26** Triclosan suggested metabolic pathway for major BTPs discovered in the UHPLC-MS/MS datasets. Plain arrow – phase I reaction, dashed arrow – phase II reaction.

## 5.4 Intra-laboratory comparison of xenobiotic metabolism predictions and findings with Phenome Centre Birmingham study

To appropriately address the third objective in this study, the results were compared with a parallel study conducted by Phenome Centre Birmingham (PCB). In my ADME/TK study, parent chemical was detected by Compound Discoverer in all reference standards (both $MS^1$ and $MS^n$ data) for all five xenobiotics in at least one UHPLC-MS/MS assay, with 'high confidence' in identification (Table 5.10). In addition, a molecular ion ($[M+H]^+$ or $[M+H]^-$) corresponding to the parent chemical was also detected in $MS^1$ data from rat plasma samples for each xenobiotic (Table 5.11). However, due to the absence of $MS^n$ data (for BPAF, DEHP, TBBPA and TCPP, possibly due to low peak intensity) or poor quality of $MS^2$ spectra (triclosan) full spectral match against reference standard could not be performed. Four xenobiotic parents (specifically, BPAF, DEHP, TBBPA and TCPP) were annotated as 'high confidence' in rat plasma extracts based on the $MS^1$ data and RT, and a positive spectral library match (to mzCloud or ChemSpider). Triclosan parent was assigned 'low confidence' in identification (FISh score: 2.6%, no library match).

In contrast, results from a parallel ADME/TK study using the PCB's in-house xenobiotic workflow[6] show that the parent chemical was also detected in rat plasma for four xenobiotics, but not for TCPP.

A comparison of the biotransformation products (BTPs) predicted by SyGMa, Compound Discoverer (CD) and detected in UHPLC-MS/MS datasets is shown in Table 5.19 below. Compared to SyGMa, Compound Discoverer predicted an

unexpectedly large number of theoretical metabolites (based on 15 phase I and 19 phase II reactions) indicating it is rather prone to significant overprediction. These *in silico* prediction tools use different sets of rules, but all the major metabolic pathways were predicted by both software packages. CD did not predict any hydroxylated BTPs, however. SyGMa was previously reported to have high coverage matching nearly 40% of predictions generated by other *in silico* liver metabolism tools to guide analogue selection for read-across[286].

**Table 5.19** Summary of biotransformation products in published literature (mainly from *in vivo* rat studies), predicted by SyGMa and Compound Discoverer (exclusive of parent).

| Name (abbr.) | Literature search | SyGMa predictions | CD predictions |
|---|---|---|---|
| **BPAF** | 5 | 57 | 4227 |
| **DEHP** | 30 | 156 | 3353 |
| **TBBPA** | 8 | 69 | 4227 |
| **TCCP** | 3 | 69 | 6243 |
| **TCS** | 14 | 42 | 4218 |

Untargeted UHPLC-MS/MS experiments revealed different metabolic behaviour for these five structurally different xenobiotics. While BPAF and triclosan are predominantly metabolised by phase II reactions (glucuronidation, sulphation and methylation), DEHP and TCPP mainly undergo dealkylation and oxidation (phase I). Glucuronide conjugation and sulphation are the most prevalent metabolic modifications discovered for all five xenobiotics, which is expected as these constitute two major phase II modifications in xenobiotic metabolism and are catalysed by UDP-glucuronic acid transferases (UGTs) and sulfotransferases (SULTs), respectively[287]. Glucuronide conjugation (low affinity-high capacity) and sulphation (high affinity-low

capacity) often compete for a mutual substrate. The balance between the two pathways is dose- and species-dependent, and is also affected by the availability of co-substrates and activation or inhibition of the respective transferases[288].

The majority of biotransformation products (BTPs) reported in the literature were also detected in rat plasma with ‘medium’ to ‘low confidence‘ in identification. The highest overall number of metabolites was discovered for TCPP (22) followed by DEHP (17). These findings are largely consistent with the PCB results, which showed a rich pattern of BTPs for these two compounds (Table 5.20). Overall, the CD-based workflow discovered over 50% more BTPs compared to the equivalent PCB workflow. This can be attributed to instrumental settings (i.e., using AcquireX versus more ‘traditional’ DDA methods on a Thermo Fisher Scientific Q -Exactive Focus Orbitrap UHPLC-MS/MS system), different *in silico* prediction tools used in each workflow (Compound Discoverer versus SyGMa, which both rely on different fragmentation rules to predict BTPs) as well as differences in the untargeted xenobiotic data processing and analysis (commercial software versus open-source packages typically used by the metabolomics community).

**Table 5.20** Summary of biotransformation products revealed by the Compound Discoverer (CD) xenobiotic data processing workflow (exclusive of parent) compared to the results from the equivalent workflow in Phenome Centre Birmingham.

| Name (abbr.) | BTPs discovered using ID-X mass spectrometer and Compound Discoverer workflow | BTPs reported by PCB from a parallel ADME/TK study (Q Exactive Focus mass spectrometer and open-source software |
|---|---|---|
| **BPAF** | 5 | 3 |
| **DEHP** | 17 | 10 |
| **TBBPA** | 1 | 1 |
| **TCCP** | 22 | 7 |
| **TCS** | 7 | 4 |
| **Total** | 52 | 25 |

## 5.5 Key findings and conclusions

The aim of the work presented in this chapter was to evaluate an untargeted UHPLC-MS/MS metabolomics workflow, using state-of-the-art Thermo Fisher Scientific hardware and software, to characterise the metabolism and metabolic fate of five industrial chemicals in rat plasma samples provided to PCB by the US NTP laboratory.

The first objective was to assess the capability of this new technology (specifically, a Thermo Fisher Scientific Orbitrap ID-X Tribrid mass spectrometer) and a commercial software package (Compound Discoverer version 3.3.1.111, Thermo Fisher Scientific, Hemel Hempstead, UK) to discover and confirm identities of parent chemicals in both analytical reference standards and rat plasma extracts. However, this objective was only partially achieved as, due to lack of high-quality $MS^n$ data for parent peaks in rat plasma, the highest level of identification (i.e. spectral match against corresponding reference standards) could not be achieved for these xenobiotics. The absence of parent $MS^n$ data for biological samples needs further investigation, but it may have been caused by low feature intensity, specific apex triggering and dynamic exclusion parameters in the UHPLC-MS/MS analytical method, or incorrect grouping of a mass spectral tree under another *m/z* feature in Compound Discoverer software (e.g. for triclosan).

The second objective was to interrogate the same untargeted UHPLC-MS/MS datasets to discover any biotransformation products (BTPs) for each of the five xenobiotics under study. The Thermo Fisher Scientific Compound Discoverer workflow provided insights into metabolism and metabolic fate of these xenobiotics in rat plasma by

revealing a rich pattern of BTPs for four out of five xenobiotics, whereby between five (for BPAF) and up to 22 (for TCPP) were detected and annotated. However, out of eight BTPs reported in the literature, only a single (sulphated) BTP was discovered for TBBPA. This is consistent with the parallel PCB findings (where a glucuronidation BTP was detected) and suggests that plasma samples are either not suitable biomarkers of exposure for this xenobiotic (predominantly rat bile metabolites were previously cited in literature, see Table 5.9) or that TBBPA is not fully metabolised by rat.

The third objective was to compare these results with the earlier PCB findings to evaluate the potential 'added value' of the newer approach. Overall, the two approaches generated comparable results and the majority of xenobiotic features reported by PCB were also detected by this alternative workflow (except for TCPP dephosphorylation and TBBPA glucuronidation BTPs). However, over 50% more BTPs were discovered using AcquireX 'Deep Scan' intelligent data acquisition and processing of the UHPLC-MS/MS data using Compound Discoverer. In addition, this workflow revealed several previously unreported by PCB BTPs resulting from combinations of multiple phase I and phase II reactions, particularly for TCPP. Further data analysis is required, however, to enable a closer comparison of the results obtained from both workflows, for example by visualising proposed structures for these xenobiotic features and building detailed biotransformation maps for the xenobiotics under study, including all the identified metabolites and those postulated as intermediates.

Compound Discoverer (CD) is a comprehensive commercial tool for automatic data processing and multiple studies have been published, mainly applying CD for the

elucidation of drug metabolism[272,289–292]. One considerable advantage is its ease of use compared to multi-step data processing using various publicly available software tools, which can be time-consuming and may require programming skills. However, CD offers less scope for optimisation of parameters compared with open-source packages routinely used by the metabolomics community. Also, the FISh (Fragment ion search) score feature facilities enable identification and structure elucidation of predicted BTPs in the same workflow, thereby considerably reducing data processing time. However, the FISh score may be affected by the quality of $MS^2$ (i.e. lower intensity scans are more likely to results in lower FISh score values based on the lower number of matched *m/z* fragments), which may require further optimisation of the peak apex triggering and dynamic exclusion parameters in the UHPLC-MS/MS analytical method[289].

Overall, the above-discussed findings successfully demonstrate the relatively unexplored potential of untargeted metabolomics (and the 'added value' of the state-of-the-art Thermo Fisher technology) to provide promising insights into xenobiotic metabolism, thereby addressing the current knowledge gap in ADME/TK characterisation of data-poor industrial chemicals.

# CHAPTER 6 – CONCLUSIONS AND FURTHER WORK

## 6.1 Untargeted metabolomics in chemical risk assessment

My thesis aimed to demonstrate the value of untargeted metabolomics in supporting regulatory toxicology applications for advancing chemical risk assessment, exploring both toxicodynamics (TD) and toxicokinetics (TK). The work presented here aligns with the paradigm shift in toxicity testing towards more relevant 'alternative' and mechanistically-based strategies (such as using omics, *in vitro* and *in silico* methods; NAMs) to improve precision and the rate at which safety assessment can be made of the ever-increasing number of chemicals in use. Omics are a useful tool for this purpose due to their ability to comprehensively measure xenobiotic perturbations' molecular effects in biological systems. Among all omics, metabolomics is particularly well placed in this regard, as it provides a unique biomolecular snapshot of a metabolic phenotype at any given time, which makes it the closest approach to the traditional toxicity testing principles based on observing adverse outcomes in experimental models[3,19].

It is now widely recognised that both toxicodynamics and ADME/TK (mainly metabolism) provide important information to support mechanistic/biological plausibility and aid the elucidation of toxicological modes of actions (MoA) and adverse outcome pathways (AOPs)[107,293] for improved chemical safety assessment. The novelty of the approach I employed in this thesis stems from having used untargeted metabolomics to simultaneously measure these two dimensions of toxicity –

biomolecular phenotyping and metabolic transformation of xenobiotics – within a single toxicity assay, ultimately further empowering chemical risk assessment strategies.

However, several limitations currently prevent the timely uptake of this technology in chemical safety science, despite its regular use in other related applications, such as drug discovery[294–296]. One challenge is the relative scarcity of relevant, solid case studies focused on the regulatory applications of toxicological metabolomics, ideally also integrated with other omics (e.g. transcriptomics) to increase the biological validity and interpretation of the findings. Another challenge is the lack of robust experimental ADME/TK data for most industrial chemicals on the market, which constraints the applications of this knowledge in regulatory scenarios. Indeed, insufficient evidence of xenobiotic metabolism and metabolic fate is often perceived as the most problematic component of the grouping hypothesis justification. Thus, it often hinders the implementation of read-across[103,108,212] and the use of ADME/TK reference data for predictive *in silico* modelling of toxicity[204,297].

The investigations described in chapters 3-5 were driven by the recognition of this promising use of mass spectrometry-based untargeted metabolomics in regulatory toxicology and chemical safety science, yet needing to demonstrate its capabilities at producing regulatory-relevant information on the toxicodynamics and ADME/TK of industrial chemicals. Each study appropriately addressed the three objectives set out at the beginning of the thesis, highlighting the work's contribution to knowledge and areas for further exploration that lie outside of the scope of this thesis.

## 6.2 Toxicological metabolomics in grouping and read-across

In chapter 3, my large multi-omics grouping study (G/RAx) on seven data-poor azo dyes successfully grouped these substances based on their molecular acute (48 h) toxicity responses in an invertebrate model for aquatic toxicology and an OECD test species, *Daphnia magna*. This novel G/RAx workflow demonstrated the capability of high-throughput (approx. 2,000 analyses) untargeted nESI-DIMS metabolomics (integrated with complementary reduced-representation transcriptomics data of equal size) to substantiate chemical grouping of the seven azo dyes (originally based on structure and physico-chemical properties) by incorporating molecular omics-derived data into the grouping workflow. Also, the successful integration of the two metabolomics data streams (i.e. polar metabolomics and lipidomics) with transcriptomics significantly increased confidence (94%) in the grouping pattern observed for S1, DY3 and SRG dyes (compared to the transcriptomics data stream alone, 63%), guiding the selection of a possible 'source' dye (S1) for subsequent read-across (for 'target' DY3). This observation emphasizes the importance of including mechanistic omics-derived evidence alongside traditional structure-based information for more robust category formation, based on evidence that the omics data are minimally indicative of shared modes of action among members of a category. Another important aspect highlighted by this work is the integration of untargeted metabolomics with complementary transcriptomics, which together may provide a deeper and more precise evaluation of azo dye toxicity in *D. magna* to enable elucidation of potential MoAs for these chemicals.

The azo dye case study indeed demonstrates the applicability of untargeted metabolomics for chemical grouping solely based on the similarity of biological responses (i.e. unidentified MSI Level 4 features) in *D. magna*, without the need for rigorous metabolite annotation[191]. The grouping pattern observed for S1, DY3 and SRG could be further validated by, for example, attempting to link annotated metabolites to relevant pathways perturbed by these dyes (e.g. by performing metabolite set enrichment analysis (MSEA) in MetaboAnalyst), thereby, potentially, providing a line of evidence to predict azo dye toxicity responses across species when such pathways are evolutionarily conserved[298]. However, the main limitation of this high-throughput untargeted metabolomics approach is that only putative annotations (MSI Level 3) can be achieved based on $MS^1$ nESI-DIMS data alone. Another extension of this work could be grouping the dyes using ToxPrint Chemotypes (i.e. structural fragments that can be correlated with biological functions, MoAs or AOPs)[299] and mapping it onto the omics-derived grouping to hypothesise structural fragments that are driving the toxicity for the three dyes of interest. Several proposed caveats and improvements for future research are discussed in more detail the following sections.

## 6.3 Toxicological metabolomics for ADME/TK characterisation

It is postulated that any *in vivo* toxicity studies should be complemented with relevant ADME/TK data to inform safety assessment, particularly with regard to low-level exposure chemicals (i.e. within ng/kg/ per day range)[300]. Conducting *in vivo* ADME/TK studies is often expensive and time-consuming and, therefore, this conventional

approach could benefit from the ability to simultaneously measure the biological effects (endogenous metabolome) and xenobiotic metabolism (ADME/TK) within the same toxicity assay. However, the challenges of metabolite identification and annotation (MetID) are now compounded by the same challenge for xenobiotics and their biotransformation products. In the absence of high-purity chemical standards and published open-source data on xenobiotic metabolism, identification must heavily rely on *in silico* predictions. This ability to comprehensively characterise both toxicodynamics and ADME/TK processes in a biological system could contribute to a greater understanding of chemical toxicity and bioaccumulation.

I addressed some of the above challenges in chapter 4 by further interrogating $MS^1$ nESI-DIMS metabolomics datasets from chapter 3. Here, the features normally discarded from metabolomics datasets were extracted and examined using a novel xenobiotic workflow[6] to provide insights into azo dye exposure and metabolism. Noteworthily, these investigations revealed the presence of the parent chemicals within the mass spectrometry data for the three dyes of interest (S1, DY3, SRG; as described in chapter 3) across multiple nESI-DIMS assays, thereby providing confirmation of the relative internal exposure of *D. magna* to each of these three azo dyes across the three dose groups (low, medium and high). In addition, up to five biotransformation products were discovered for each azo dye, providing further evidence for the uptake (beyond the passage through the *Daphnia* gut) and xenobiotic metabolism by the exposed animals. The discovery of a shared biotransformation product for S1 and SRG suggests some ADME/TK similarity between the two dyes.

Chapter 4 also explored TK properties among the dyes. Specifically, the comparison of relative intensity measurements over the duration of the 48 h toxicity study revealed some variability in TK processes for the three dyes of interest. For example, DY3 showed relatively rapid clearance and is most substantially metabolised by *Daphnia* (five BTPs detected), whereas S1 exhibited low clearance and showed the least amount of biotransformation (one BTP detected). This ADME/TK characterisation from the same mass spectrometry data produced for metabolomics substantially adds an independent element of certainty (weight of evidence support) in the azo dye grouping hypothesis discussed in chapter 3.

However, there are several limitations associated with this ADME/TK work. First, a more robust and potentially bespoke experimental design is required to fully characterise TK metabolic clearance; the nESI-DIMS datasets were not designed specifically for this purpose, but rather mined to provide additional insights into xenobiotic exposure and very crude estimation of TK rates. This issue could be further addressed by adopting a more rigorous systematic framework for the assessment of TK parameters in future studies, employing multiple time points, as proposed by Gouliarmau *et al*. (2018)[253]. Second, there is a high degree of uncertainty associated with putative annotations (MSI Level 3 or above) for these azo dye-related features due to the absence of orthogonal data from $MS^n$ measurements. Finally, while this project investigated azo dye metabolism by *D. magna*, it is largely unclear to what extent these dyes are metabolised specifically by the exposed animals (directly by host enzymes) or the gut microbiome, which has capacity to biotransform (chemically modify) xenobiotics[301,302]. Also, the magnitude of the impact of multiple complex physico-chemical and environmental factors present throughout the study warrants

further investigation. However, this work has convincingly demonstrated an ‘added value’ of untargeted metabolomics in supporting regulatory toxicology applications.

Chapter 5 further builds upon the azo dye case study by conducting a more scientifically rigorous and comprehensive ADME/TK characterisation of five xenobiotics (small but diverse group of industrial chemicals) using orthogonal data from $MS^n$ measurements taken from existing rat plasma samples, obtained from the US National Toxicology Program (NTP) and previously used to study endogenous molecular responses to these chemicals. Specifically, untargeted metabolomics UHPLC-MS/MS datasets were interrogated to detect (and annotate or identify) the parent chemicals and any biotransformation products (BTPs). This was achieved by employing relatively new state-of-the art analytical and computational technology (i.e. Thermo Fisher Scientific Orbitrap ID-X mass spectrometer with AcquireX intelligent data acquisition workflow, and commercial Compound Discoverer software, CD) and the findings were subsequently compared with the existing PCB workflow (using identical analytical methods) to evaluate the potential ‘added value’ of this novel approach. My UHPLC-MS/MS analyses revealed the presence of the parents for all five xenobiotics (in at least one analytical assay, with varied level of MetID confidence) in the rat plasma, including TCPP that was previously undetected by the PCB workflow. However, the highest level of identification (MSI Level 1 or Schymanski *et al*[11], Level 1) could not be achieved for these xenobiotics due to the absence (or incorrect grouping by Compound Discoverer) of *m/z* features resulting from $MS^n$ fragmentation of the precursor ion (an issue that warrants further investigation).

In addition, a rich metabolism pattern was revealed for four xenobiotics, where between five (BPAF) and up to 22 (TCPP) distinct BTPs were discovered (often resulting from a combination of multiple phase I and phase II reactions), frequently across multiple UHPLC-MS/MS assays, thus rendering further confidence in these annotations. The detection of a single BTP for TBBPA is also consistent with the earlier PCB findings, suggesting that this xenobiotic is either not extensively metabolised in rat or that rat plasma extracts are not suitable biomarkers to probe TBBPA metabolism which was previously characterised in rat bile[274,303–305].

In conclusion, the workflow employing a Thermo Fisher Orbitrap ID-X mass spectrometer (with AcquireX) and CD significantly increased BTP coverage from 25 BTPs reported with 'high confidence' (based on the presence of $MS^n$ fragmentation data) by PCB to 52 BTPs across all four UHPLC-MS/MS assays for these five industrial chemicals. Therefore, this study supported and extended knowledge of biotransformation for these xenobiotics, particularly with regard to TCPP, which lacks robust (both *in vivo* and *in vitro*) biotransformation data and phase II BTPs were previously not detected for this chemical[306,307]. However, as previously pointed out, high confidence metabolite annotation, particularly for xenobiotic-related features, which are often not present in public mass spectral libraries, remains an ongoing challenge.

## 6.4 Further work

To reiterate, knowledge of xenobiotic ADME/TK (when considered with TD properties) can contribute two important aspects for G/RAx cases: supporting

mechanistic/biological plausibility of the grouping hypothesis (including deriving chemical MoA/AOP) and reducing uncertainty[107,293,308]. A recent example of G/RAx that incorporated (*in vivo* and *in vitro)* ADME/TK data is a case study that predicted repeated-dose toxicity of simple aryl alcohol alkyl carboxylic esters[309]. In another study, the inclusion of high-throughput chemical disposition and TK (Tox21) experimental data was previously shown to improve the prediction of *in vivo* pathway responses for 221 data-poor chemicals in rats[310].

As extension of the work presented in chapter 5, another project, utilising human-relevant *in vitro* approaches, was proposed and designed with my PhD funding partner, Thermo Fisher Scientific. The overarching aim of this study was to employ state-of-the-art technology (specifically, Thermo Fisher Orbitrap ID-X mass spectrometer with AcquireX intelligent acquisition and Compound Discoverer software) to demonstrate the value of experimental untargeted metabolomics data for simultaneously characterising the metabolism of a group of industrial chemicals, and the molecular responses of primary human hepatocytes (PHHs) to these chemicals.

Primary human hepatocytes were proposed for these investigations as they are well established in the pharmaceutical industry and are considered the 'gold standard' for assessing human hepatic metabolism (phase I and phase II), toxicity of drugs and other xenobiotics[311]. A set of six structurally-related xenobiotics (bisphenols, i.e. bisphenol A and five BPA analogues) for which their toxicities are relatively well characterised in literature were selected for the study. Specifically, the six bisphenols can demonstrate one or both MoAs, depending on structure: 1) endocrine disrupting (ED) effects (via binding to the α and β estrogen receptors); 2) oxidative stress (via phase I modification

of the phenol group, producing free radicals, catechols and *ortho*-quinones that can generate reactive oxygen species, ROS)[12].

Through the above investigations, I planned to demonstrate how the measurement of ADME/TK (xenobiotic metabolism) can be used to directly rationalise modes of action (MoAs) for these xenobiotics. It was hypothesised that where the toxicity is dissimilar between two structurally-related compounds, untargeted metabolomics may reveal differences in metabolic fate that could account for the differences in toxicity among these chemicals. The project would address three key challenges in toxicological metabolomics, namely 1) application of high-throughput *in vitro* assays as an alternative to animal testing; 2) identification of xenobiotics; and 3) ADME/TK characterisation of structurally-similar chemicals that may enhance grouping of these chemicals by potentially revealing shared biotransformation products.

Regrettably, the above study could not be conducted due to Covid-19 restrictions and post-Covid implications on Thermo Fisher Scientific which withdrew from the project.

Overall, my workflows and results from the case studies presented in chapters 3-5 of this thesis highlight the power of untargeted metabolomics for improved regulatory relevant chemical risk assessment. The added value of this type of analysis is its unique capability to simultaneously profile both xenobiotic-triggered biochemical effects (TD) and xenobiotic metabolism (ADME/TK), which (when additionally combined with transcriptomics data) may produce greater certainty in the grouping of substances based on a mechanistic investigation of their toxicity.

# REFERENCES


1. OECD. *Global Material Resources Outlook to 2060: Economic Drivers and Environmental Consequences*. (Organisation for Economic Co-operation and Development, 2019).
2. Rodrigues, A., Ribeiro, A. & Antonio, C. Experimental design and sample preparation in forest tree metabolomics. *Metabolites* **9**, 285 (2019).
3. Viant, M. R. *et al.* Use cases, best practice and reporting standards for metabolomics in regulatory toxicology. *Nat Commun* **10**, 3041 (2019).
4. Chen, L., Zhong, F. & Zhu, J. Bridging targeted and untargeted mass spectrometry-based metabolomics via hybrid approaches. *Metabolites* **10**, 348 (2020).
5. EFSA Scientific Colloquium 24 – 'omics in risk assessment: state of the art and next steps | EFSA.
6. Bowen, T. J. *et al.* An extensive metabolomics workflow to discover cardiotoxin-induced molecular perturbations in microtissues. *Metabolites* **11**, 644 (2022).
7. Souza, Amanda, Ntai, Ioanna, & Tautenhahn, Ralf. Accelerated unknown compound annotation with confidence: from spectra to structure in untargeted metabolomics experiments. Thermo Fisher Scientic, APPLICATION NOTE 65362. (2018) doi:https://assets.thermofisher.com/TFS-Assets/CMD/Application-Notes/an-65362-ms-compound-annotation-an65362-en.pdf.
8. Southam, A. D., Weber, R. J. M., Engel, J., Jones, M. R. & Viant, M. R. A complete workflow for high-resolution spectral-stitching nanoelectrospray direct-infusion mass-spectrometry-based metabolomics and lipidomics. *Nat Protoc* **12**, 310–328 (2017).
9. Ren, J.-L., Zhang, A.-H., Kong, L. & Wang, X.-J. Advances in mass spectrometry-based metabolomics for investigation of metabolites. *RSC Adv.* **8**, 22335–22350 (2018).

10. Sumner, L. W. *et al.* Proposed minimum reporting standards for chemical analysis: Chemical Analysis Working Group (CAWG) Metabolomics Standards Initiative (MSI). *Metabolomics* **3**, 211–221 (2007).
11. Schymanski, E. L. *et al.* Identifying small molecules via high resolution mass spectrometry: Communicating Confidence. *Environ. Sci. Technol.* **48**, 2097–2098 (2014).
12. Gramec Skledar, D. & Peterlin Mašič, L. Bisphenol A and its analogs: do their metabolites have endocrine activity? *Environmental Toxicology and Pharmacology* **47**, 182–199 (2016).
13. ECHA. European Chemicals Agency. Registered substances database. https://echa.europa.eu/information-on-chemicals/registered-substances (2020).
14. Wang, Z., Walker, G. W., Muir, D. C. G. & Nagatani-Yoshida, K. Toward a Global Understanding of chemical pollution: a first comprehensive analysis of national and regional chemical inventories. *Environ. Sci. Technol.* **54**, 2575–2584 (2020).
15. Sauvé, S. & Desrosiers, M. A review of what is an emerging contaminant. *Chemistry Central Journal* **8**, 15 (2014).
16. Stuart, M., Lapworth, D., Crane, E. & Hart, A. Review of risk from potential emerging contaminants in UK groundwater. *Science of The Total Environment* **416**, 1–21 (2012).
17. Bergkamp, L. & Herbatschek, N. Regulating chemical substances under REACH: the choice between authorization and restriction and the case of dipolar aprotic solvents: regulating chemical substances under REACH. *Rev Euro Comp & Int Env Law* **23**, 221–245 (2014).
18. ECHA. European Chemicals Agency. Search for chemicals. Chemicals database. https://chemicalsinourlife.echa.europa.eu/search-for-chemicals (2020).
19. Bouhifd, M., Hartung, T., Hogberg, H. T., Kleensang, A. & Zhao, L. Review: Toxicometabolomics: Toxicometabolomics. *J. Appl. Toxicol.* **33**, 1365–1383 (2013).

20. NRC. *Toxicity testing in the 21st Century: a vision and a strategy. National Research Council*. (2007). doi:10.17226/11970.
21. Bhattacharya, S., Zhang, Q., Carmichael, P. L., Boekelheide, K. & Andersen, M. E. Toxicity testing in the 21 century: defining new risk assessment approaches based on perturbation of intracellular toxicity pathways. *PLoS One* **6**, e20887 (2011).
22. Ankley, G. T. *et al.* Adverse outcome pathways: A conceptual framework to support ecotoxicology research and risk assessment. *Environ Toxicol Chem* **29**, 730–741 (2010).
23. Ankley, G. T. & Edwards, S. W. The Adverse Outcome Pathway: a multifaceted framework supporting 21st century toxicology. *Curr Opin Toxicol* **9**, 1–7 (2018).
24. Hartung, T. *et al.* Systems toxicology: Real world applications and opportunities. *Chem. Res. Toxicol.* **30**, 870–882 (2017).
25. Thomas, R. S. *et al.* Incorporating new technologies into toxicity testing and risk assessment: moving from 21st century vision to a data-driven framework. *Toxicological Sciences* **136**, 4–18 (2013).
26. Brockmeier, E. K. *et al.* The role of omics in the application of adverse outcome pathways for chemical risk assessment. *Toxicol Sci* **158**, 252–262 (2017).
27. Krimsky, S. The unsteady state and inertia of chemical regulation under the US Toxic Substances Control Act. *PLOS Biology* **15**, e2002404 (2017).
28. Jeong, J., Kim, D. & Choi, J. Application of ToxCast/Tox21 data for toxicity mechanism-based evaluation and prioritization of environmental chemicals: Perspective and limitations. *Toxicol In Vitro* **84**, 105451 (2022).
29. ECHA. New approach methodologies in regulatory science. (2016) doi:https://echa.europa.eu/documents/10162/22816069/scientific_ws_proceedings_en.pdf.
30. Kavlock, R. J. *et al.* Accelerating the pace of chemical risk assessment. *Chem. Res. Toxicol.* **31**, 287–290 (2018).

31. Stucki, A. O. *et al.* Use of new approach methodologies (NAMs) to meet regulatory requirements for the assessment of industrial chemicals and pesticides for effects on human health. *Frontiers in Toxicology* **4**, (2022).
32. Alonso, A., Marsal, S. & Julià, A. Analytical methods in untargeted metabolomics: state of the art in 2015. *Frontiers in Bioengineering and Biotechnology* **3**, (2015).
33. Viant, P. M. Accelerating the impacts of metabolomics in regulatory toxicology – an academic view. (2017).
34. Wishart, D. S. *et al.* HMDB 5.0: the Human Metabolome Database for 2022. *Nucleic Acids Res* **50**, D622–D631 (2022).
35. Fernie, A. R. *et al.* Recommendations for reporting metabolite data. *Plant Cell* **23**, 2477–2482 (2011).
36. Tebani, A., Afonso, C. & Bekri, S. Advances in metabolome information retrieval: turning chemistry into biology. Part I: analytical chemistry of the metabolome. *J Inherit Metab Dis* **41**, 379–391 (2018).
37. Broadhurst, D. *et al.* Guidelines and considerations for the use of system suitability and quality control samples in mass spectrometry assays applied in untargeted clinical metabolomic studies. *Metabolomics* **14**, 72 (2018).
38. Johnson, C. H., Ivanisevic, J. & Siuzdak, G. Metabolomics: beyond biomarkers and towards mechanisms. *Nat Rev Mol Cell Biol* **17**, 451–459 (2016).
39. Dunn, W. B. & Lewis, M. R. The role of ultra-high performance liquid chromatography-mass spectrometry in metabolic phenotyping. in *The handbook of metabolic phenotyping* 97–136 (Elsevier, 2019). doi:10.1016/B978-0-12-812293-8.00003-7.
40. Ruan, X. *et al.* Evaluation of untargeted metabolomic strategy for the discovery of biomarker of breast cancer. *Front Pharmacol* **13**, 894099 (2022).
41. Billet, K. *et al.* Semi-targeted metabolomics to validate biomarkers of grape downy mildew infection under field conditions. *Plants* **9**, 1008 (2020).

42. Fiehn, O. Metabolomics--the link between genotypes and phenotypes. *Plant Mol Biol* **48**, 155–171 (2002).
43. Wishart, D. S. Emerging applications of metabolomics in drug discovery and precision medicine. *Nat Rev Drug Discov* **15**, 473–484 (2016).
44. Alarcon-Barrera, J. C., Kostidis, S., Ondo-Mendez, A. & Giera, M. Recent advances in metabolomics analysis for early drug development. *Drug Discovery Today* **27**, 1763–1773 (2022).
45. Athersuch, T. J. & Keun, H. C. Metabolic profiling in human exposome studies. *Mutagenesis* **30**, 755–762 (2015).
46. Escher, B. I. *et al.* From the exposome to mechanistic understanding of chemical-induced adverse effects. *Environment International* **99**, 97–106 (2017).
47. Wild, C. P. Complementing the genome with an ‘exposome’: the outstanding challenge of environmental exposure measurement in molecular epidemiology. *Cancer Epidemiol Biomarkers Prev* **14**, 1847–1850 (2005).
48. Walker, D. I. *et al.* The metabolome: A key measure for exposome research in epidemiology. *Curr Epidemiol Rep* **6**, 93–103 (2019).
49. Schymanski, E. L. & Bolton, E. E. FAIRifying the exposome journal: Templates for chemical structures and transformations. *Exposome* **2**, osab006 (2022).
50. Viant, M. R. Metabolomics of aquatic organisms: the new ‘omics’ on the block. *Marine Ecology Progress Series* **332**, 301–306 (2007).
51. Wishart, D. S. Metabolomics for investigating physiological and pathophysiological processes. *Physiological Reviews* **99**, 1819–1875 (2019).
52. Araújo, A. M., Carvalho, F., Guedes de Pinho, P. & Carvalho, M. Toxicometabolomics: small molecules to answer big toxicological questions. *Metabolites* **11**, 692 (2021).
53. Hernández-Mesa, M., Le Bizec, B. & Dervilly, G. Metabolomics in chemical risk analysis - a review. *Anal Chim Acta* **1154**, 338298 (2021).

54. Bundy, J. G., Davey, M. P. & Viant, M. R. Environmental metabolomics: a critical review and future perspectives. *Metabolomics* **5**, 3–21 (2009).

55. Krastanov, A. Metabolomics—the state of art. *Biotechnology & Biotechnological Equipment* **24**, 1537–1543 (2010).

56. Bedia, C. Metabolomics in environmental toxicology: applications and challenges. *Trends in Environmental Analytical Chemistry* **34**, e00161 (2022).

57. Taylor, N. S. *et al.* A new approach to toxicity testing in *Daphnia magna*: application of high throughput FT-ICR mass spectrometry metabolomics. *Metabolomics* **5**, 44–58 (2009).

58. Taylor, N. S., Gavin, A. & Viant, M. R. Metabolomics discovers early-response metabolic biomarkers that can predict chronic reproductive fitness in individual *Daphnia magna*. *Metabolites* **8**, 42 (2018).

59. Jeong, T.-Y. & Simpson, M. J. *Daphnia magna* metabolic profiling as a promising water quality parameter for the biological early warning system. *Water Research* **166**, 115033 (2019).

60. da Silva, K. M. *et al.* Mass Spectrometry-based zebrafish toxicometabolomics: a Review of analytical and data quality challenges. *Metabolites* **11**, 635 (2021).

61. Fu, J., Gong, Z. & Kelly, B. C. Metabolomic profiling of zebrafish (*Danio rerio*) embryos exposed to the antibacterial agent triclosan. *Enviro Toxic and Chemistry* **38**, 240–249 (2019).

62. Schade, S. *et al.* Improved algal toxicity test system for robust omics-driven mode-of-action discovery in *Chlamydomonas reinhardti*i. *Metabolites* **9**, 94 (2019).

63. Mo, J. *et al.* Metabolomic profiles in a green alga (*Raphidocelis subcapitata*) following erythromycin treatment: ABC transporters and energy metabolism. *J Environ Sci (China)* **124**, 591–601 (2023).

64. Hines, A. *et al.* Discovery of metabolic signatures for predicting whole organism toxicology. *Toxicological Sciences* **115**, 369–378 (2010).

65. Ramirez, G. *et al.* Early biological modulations resulting from 1-week Venlafaxine exposure of marine mussels *Mytilus galloprovincialis* determined by a metabolomic approach. *Metabolites* **12**, 197 (2022).
66. Southam, A. D. *et al.* Distinguishing between the metabolome and xenobiotic exposome in environmental field samples analysed by direct-infusion mass spectrometry based metabolomics and lipidomics. *Metabolomics* **10**, 1050–1058 (2014).
67. Campos, B. *et al.* How omics technologies can enhance chemical safety regulation: perspectives from academia, government, and industry. *Environmental Toxicology and Chemistry* **37**, 1252–1259 (2018).
68. OECD. Metabolomics Reporting Framework (MRF) Guidance Document. (2021) doi:https://www.oecd.org/chemicalsafety/testing/metabolomics-reporting-framework.pdf.
69. OECD. Transcriptomics Reporting Framework (TRF) Guidance Document. (2021) doi:https://www.oecd.org/chemicalsafety/testing/transcriptomic-reporting-framework.pdf.
70. Sostare, E. *et al.* Knowledge-driven approaches to create the MTox700+ Metabolite panel for predicting toxicity. *Toxicological Sciences* **186**, 208–220 (2022).
71. Jeong, J., Kim, J. & Choi, J. Identification of molecular initiating events (MIE) using chemical database analysis and nuclear receptor activity assays for screening potential inhalation toxicants. *Regulatory Toxicology and Pharmacology* **141**, 105391 (2023).
72. Lindon, J. C. *et al.* The Consortium for Metabonomic Toxicology (COMET): aims, activities and achievements. *Pharmacogenomics* **6**, 691–699 (2005).
73. Lindon, J. C. *et al.* Contemporary issues in toxicology the role of metabonomics in toxicology and its evaluation by the COMET project. *Toxicol Appl Pharmacol* **187**, 137–146 (2003).
74. Celander, M. C. *et al.* Species extrapolation for the 21st century. *Environmental Toxicology and Chemistry* **30**, 52–63 (2011).
75. SETAC. Cross-species extrapolation - Society of Environmental Toxicology and Chemistry. https://www.setac.org/page/scixspecies (2022).

76. Olesti, E., González-Ruiz, V., Wilks, M. F., Boccard, J. & Rudaz, S. Approaches in metabolomics for regulatory toxicology applications. *Analyst* **146**, 1820–1834 (2021).

77. Southam, A. D. *et al.* Metabolomics reveals target and off-target toxicities of a model organophosphate pesticide to roach (*Rutilus rutilus*): implications for biomonitoring. *Environ. Sci. Technol.* **45**, 3759–3767 (2011).

78. LaLone, C. A. *et al.* International consortium to advance cross-species extrapolation of the effects of chemicals in regulatory toxicology. *Enviro Toxic and Chemistry* **40**, 3226–3233 (2021).

79. OECD. Test No. 417: Toxicokinetics. (2010).

80. OECD. Guidance on grouping of chemicals, 2nd edition. (2014) doi:http://www.oecd.org/officialdocuments/publicdisplaydocumentpdf/?cote=env/jm/mono(2014)4&doclanguage=en.

81. Breen, M., Wambaugh, J. F., Bernstein, A., Sfeir, M. & Ring, C. L. Simulating toxicokinetic variability to identify susceptible and highly exposed populations. *J Expo Sci Environ Epidemiol* **32**, 855–863 (2022).

82. Harrill, J. A. *et al.* Progress towards an OECD reporting framework for transcriptomics and metabolomics in regulatory toxicology. *Regulatory Toxicology and Pharmacology* **125**, 105020 (2021).

83. OECD. Metabolomics Reporting Framework. (2021) doi:https://www.oecd.org/chemicalsafety/testing/metabolomics-reporting-framework.pdf.

84. Lowe, R., Shirley, N., Bleackley, M., Dolan, S. & Shafee, T. Transcriptomics technologies. *PLoS Comput Biol* **13**, e1005457 (2017).

85. Schirmer, K., Fischer, B. B., Madureira, D. J. & Pillai, S. Transcriptomics in ecotoxicology. *Anal Bioanal Chem* **397**, 917–923 (2010).

86. Moffat, I. *et al.* Comparison of toxicogenomics and traditional approaches to inform mode of action and points of departure in human health risk assessment of benzo[*a*]pyrene in drinking water. *Critical Reviews in Toxicology* **45**, 1–43 (2015).

87. Hawliczek-Ignarski, A., Cenijn, P., Legler, J., Segner, H. & Legradi, J. Mode of action assignment of chemicals using toxicogenomics: a case study with oxidative uncouplers. *Front. Environ. Sci.* **5**, 80 (2017).
88. Nakagawa, S., Okamoto, M., Nukada, Y. & Morita, O. Comparison of the potential mechanisms for hepatotoxicity of p-dialkoxy chlorobenzenes in rat primary hepatocytes for read-across. *Regulatory Toxicology and Pharmacology* **113**, 104617 (2020).
89. Reilly, K. *et al. Daphnia* as a model organism to probe biological responses to nanomaterials—from individual to population effects via adverse outcome pathways. *Frontiers in Toxicology* **5**, (2023).
90. Tkaczyk, A., Bownik, A., Dudka, J., Kowal, K. & Ślaska, B. *Daphnia magna* model in the toxicity assessment of pharmaceuticals: A review. *Science of The Total Environment* **763**, 143038 (2021).
91. OECD. Test No. 202: *Daphnia* sp., acute immobilisation test. (2004).
92. OECD. Test No. 211: *Daphnia magna* reproduction test. (2012).
93. Colbourne, J. K. *et al.* The ecoresponsive genome of *Daphnia pulex*. *Science* **331**, 555–561 (2011).
94. Lee, B.-Y. *et al.* The genome of the freshwater water flea *Daphnia magna*: a potential use for freshwater molecular ecotoxicology. *Aquat Toxicol* **210**, 69–84 (2019).
95. Konkel, L. A Closer Look at obesogens: lipid Homeostasis disruption in *Daphnia*. *Environ Health Perspect* **123**, A219 (2015).
96. King-Herbert, A. & Vasbinder, M. A. Chapter 22 - Toxicology. in *The Laboratory rat (Third Edition)* (eds. Suckow, M. A., Hankenson, F. C., Wilson, R. P. & Foley, P. L.) 849–862 (Academic Press, 2020). doi:10.1016/B978-0-12-814338-4.00022-2.
97. OECD. Test No. 407: Repeated dose 28-day oral toxicity study in rodents. (2008).
98. OECD. Test No. 408: Repeated dose 90-day oral toxicity study in rodents.
99. ECHA. Read-Across Assessment Framework (RAAF). (2017) doi:https://echa.europa.eu/documents/10162/13628/raaf_en.pdf.

100. Batke, M. *et al.* Innovative Strategies to develop chemical categories using a combination of structural and toxicological properties. *Front. Pharmacol.* **7**, (2016).
101. Low, Y. *et al.* Integrative chemical–biological read-across approach for chemical hazard classification. *Chem. Res. Toxicol.* **26**, 1199–1208 (2013).
102. Patlewicz, G., Helman, G., Pradeep, P. & Shah, I. Navigating through the minefield of read-across tools: A review of in silico tools for grouping. *Computational Toxicology* **3**, 1–18 (2017).
103. Ball, N. *et al.* Key read across framework components and biology based improvements. *Mutation Research/Genetic Toxicology and Environmental Mutagenesis* **853**, 503172 (2020).
104. Patlewicz, G. *et al.* Use of category approaches, read-across and (Q)SAR: General considerations. *Regulatory Toxicology and Pharmacology* **67**, 1–12 (2013).
105. ECHA. The Use of alternatives to testing on animals for the REACH Regulation Second report under Article 117(3) of the REACH Regulation. (2014).
106. ECHA. The use of alternatives to testing on animals for the REACH Regulation Fourth report under Article 117(3) of the REACH Regulation. (2020).
107. Schultz, T. W. *et al.* A strategy for structuring and reporting a read-across prediction of toxicity. *Regulatory Toxicology and Pharmacology* **72**, 586–601 (2015).
108. Schultz, T. W., Richarz, A.-N. & Cronin, M. T. D. Assessing uncertainty in read-across: questions to evaluate toxicity predictions based on knowledge gained from case studies. *Computational Toxicology* **9**, 1–11 (2019).
109. Escher, S. E. *et al.* Towards grouping concepts based on new approach methodologies in chemical hazard assessment: the read-across approach of the EU-ToxRisk project. *Arch Toxicol* **93**, 3643–3667 (2019).
110. Rovida, C. Internationalization of read-across as a validated new approach method (NAM) for regulatory toxicology. *ALTEX* (2020) doi:10.14573/altex.1912181.

111. van Ravenzwaay, B. *et al.* Metabolomics as read-across tool: a case study with phenoxy herbicides. *Regulatory Toxicology and Pharmacology* **81**, 288–304 (2016).
112. van Ravenzwaay, B. *et al.* Metabolomics: a tool for early detection of toxicological effects and an opportunity for biology based grouping of chemicals—From QSAR to QBAR. *Mutation Research/Genetic Toxicology and Environmental Mutagenesis* **746**, 144–150 (2012).
113. Sperber, S. *et al.* Metabolomics as read-across tool: an example with 3-aminopropanol and 2-aminoethanol. *Regulatory Toxicology and Pharmacology* **108**, 104442 (2019).
114. Rooseboom, M. *et al.* P21-06 Approaches to support read-across for UVCB substances. Abstract. *Toxicology Letters* **368**, S259 (2022).
115. Aretz, I. & Meierhofer, D. Advantages and pitfalls of mass spectrometry-based metabolome profiling in systems biology. *International Journal of Molecular Sciences* **17**, 632 (2016).
116. Gertsman, I. & Barshop, B. A. Promises and pitfalls of untargeted metabolomics. *Journal of Inherited Metabolic Disease* **41**, 355–366 (2018).
117. Garreta-Lara, E. *et al.* Combined targeted/untargeted analytical and chemometric approaches in the characterization of *Daphnia magna* metabolomic changes under bisphenol A exposure. *Microchemical Journal* **165**, 106150 (2021).
118. Moseley, H. N. B. Error analysis and propagation in metabolomics data analysis. *Computational and Structural Biotechnology Journal* **4**, e201301006 (2013).
119. Burger, B., Vaudel, M. & Barsnes, H. Importance of block randomization when designing proteomics experiments. *J Proteome Res* **20**, 122–128 (2021).
120. Southam, A. D. *et al.* Assessment of human plasma and urine sample preparation for reproducible and high-throughput UHPLC-MS clinical metabolic phenotyping. *Analyst* **145**, 6511–6523 (2020).
121. Southam, A. D. *et al.* Characterization of monophasic solvent-based tissue extractions for the detection of polar metabolites and lipids applying ultrahigh-performance liquid

chromatography–mass spectrometry clinical metabolic phenotyping assays. *J. Proteome Res.* **20**, 831–840 (2021).

122. Sostare, J. *et al.* Comparison of modified Matyash method to conventional solvent systems for polar metabolite and lipid extractions. *Analytica Chimica Acta* **1037**, 301–315 (2018).
123. Evans, A. M. *et al.* Dissemination and analysis of the quality assurance (QA) and quality control (QC) practices of LC–MS based untargeted metabolomics practitioners. *Metabolomics* **16**, 113 (2020).
124. Ho, C. *et al.* Electrospray ionisation mass spectrometry: principles and clinical applications. *Clin Biochem Rev* **24**, 3–12 (2003).
125. Banerjee, S. & Mazumdar, S. Electrospray ionization mass spectrometry: a technique to access the information beyond the molecular weight of the analyte. *International Journal of Analytical Chemistry* **2012**, e282574 (2012).
126. Lei, Z., Huhman, D. V. & Sumner, L. W. Mass spectrometry strategies in metabolomics *. *Journal of Biological Chemistry* **286**, 25435–25442 (2011).
127. Commisso, M., Anesi, A., Dal Santo, S. & Guzzo, F. Performance comparison of electrospray ionization and atmospheric pressure chemical ionization in untargeted and targeted liquid chromatography/mass spectrometry based metabolomics analysis of grapeberry metabolites. *Rapid Communications in Mass Spectrometry* **31**, 292–300 (2017).
128. El-Faramawy, A., Siu, K. W. M. & Thomson, B. A. Efficiency of nano-electrospray ionization. *J. Am. Soc. Mass Spectrom.* **16**, 1702–1707 (2005).
129. Rahman, M. M. & Chingin, K. Stable and reproducible nano-electrospray ionization of aqueous solutions and untreated biological samples using ion current limitation combined with polarity reversing. *Anal. Methods* **11**, 205–212 (2019).

130. Kempa, E. E., Hollywood, K. A., Smith, C. A. & Barran, P. E. High throughput screening of complex biological samples with mass spectrometry – from bulk measurements to single cell analysis. *Analyst* **144**, 872–891 (2019).
131. Gaudin, M. *et al.* Atmospheric pressure photoionization as a powerful tool for large-scale lipidomic studies. *J Am Soc Mass Spectrom* **23**, 869–879 (2012).
132. He, M. J. *et al.* Comparing DESI-MSI and MALDI-MSI mediated spatial metabolomics and their applications in cancer studies. *Frontiers in Oncology* **12**, (2022).
133. Alexandrov, T. Spatial metabolomics and imaging mass spectrometry in the age of artificial intelligence. *Annu Rev Biomed Data Sci* **3**, 61–87 (2020).
134. Nadler, W. M. *et al.* MALDI versus ESI: the impact of the ion source on peptide identification. *J Proteome Res* **16**, 1207–1215 (2017).
135. Trimpin, S., Inutan, E. D., Herath, T. N. & McEwen, C. N. Laserspray ionization, a new atmospheric pressure MALDI method for producing highly charged gas-phase ions of peptides and proteins directly from solid solutions. *Mol Cell Proteomics* **9**, 362–367 (2010).
136. Emmanuelle Claude, Emrys A. Jones, & Steven D. Pringle. DESI mass spectrometry imaging (MSI). (2017).
137. G. Marshall, A. *et al.* Mass resolution and mass accuracy: how much is enough? *Mass Spectrom (Tokyo)* **2**, S0009 (2013).
138. Kerstin Strupat, Olaf Scheibner, and Maciej Bromirski. High-resolution, accurate-mass Orbitrap mass spectrometry – definitions, opportunities, and advantages. *Thermo Fisher Technical Note 64287* (2016) doi:https://assets.thermofisher.com/TFS-Assets/CMD/Technical-Notes/tn-64287-hram-orbitrap-ms-tn64287-en.pdf.
139. Murray, K. K. Resolution and resolving power in mass spectrometry. *J. Am. Soc. Mass Spectrom.* **33**, 2342–2347 (2022).

140. Allen, D. R. & McWhinney, B. C. Quadrupole time-of-flight mass spectrometry: a paradigm shift in toxicology screening applications. *Clin Biochem Rev* **40**, 135–146 (2019).

141. Spraggins, J. M. *et al.* High-Performance Molecular imaging with MALDI trapped ion-mobility time-of-flight (timsTOF) mass spectrometry. *Anal. Chem.* **91**, 14552–14560 (2019).

142. Zubarev, R. A. & Makarov, A. Orbitrap mass spectrometry. *Anal. Chem.* **85**, 5288–5296 (2013).

143. García-Reyes, J. F., Moreno-González, D., Nortes-Méndez, R., Gilbert-López, B. & Molina Díaz, A. HRMS. in *Applications in High Resolution Mass Spectrometry* 15–57 (Elsevier, 2017). doi:10.1016/B978-0-12-809464-8.00002-6.

144. Hendrickson, C. L. *et al.* 21 Tesla Fourier transform ion cyclotron resonance mass spectrometer: a national resource for ultrahigh resolution mass analysis. *J. Am. Soc. Mass Spectrom.* **26**, 1626–1632 (2015).

145. Shaw, J. B. *et al.* 21 Tesla Fourier transform ion cyclotron resonance mass spectrometer greatly expands mass spectrometry toolbox. *J. Am. Soc. Mass Spectrom.* **27**, 1929–1936 (2016).

146. Bromirski, M. First choice in high resolution mass spectrometry with Orbitrap mass analyzer technology for screening, confirmative and quantitative Analyses. *Thermo Fisher Scientific White Paper 65146* (2018) doi:https://assets.thermofisher.com/TFS-Assets/CMD/Reference-Materials/wp-65146-ms-orbitrap-high-resolution-wp65146-en.pdf.

147. Schwaiger-Haber, M. *et al.* A Workflow to perform targeted metabolomics at the untargeted scale on a triple quadrupole mass spectrometer. *ACS Meas Sci Au* **1**, 35–45 (2021).

148. Bonte, R. *et al.* Untargeted metabolomics-based screening method for inborn errors of metabolism using semi-automatic sample preparation with an UHPLC- Orbitrap-MS platform. *Metabolites* **9**, 289 (2019).
149. Stettin, D., Poulin, R. X. & Pohnert, G. Metabolomics benefits from Orbitrap GC–MS—comparison of low- and high-resolution GC–MS. *Metabolites* **10**, 143 (2020).
150. Kirwan, J. A., Weber, R. J. M., Broadhurst, D. I. & Viant, M. R. Direct infusion mass spectrometry metabolomics dataset: a benchmark for data processing and quality control. *Sci Data* **1**, 140012 (2014).
151. Dieterle, F., Ross, A., Schlotterbeck, G. & Senn, H. Probabilistic quotient normalization as robust method to account for dilution of complex biological mixtures. Application in 1H NMR metabonomics. *Anal Chem* **78**, 4281–4290 (2006).
152. Di Guida, R. *et al.* Non-targeted UHPLC-MS metabolomic data processing methods: a comparative investigation of normalisation, missing value imputation, transformation and scaling. *Metabolomics* **12**, 93 (2016).
153. Hrydziuszko, O. & Viant, M. R. Missing values in mass spectrometry based metabolomics: an undervalued step in the data processing pipeline. *Metabolomics* **8**, 161–174 (2012).
154. Li, B. *et al.* Performance evaluation and online realization of data-driven normalization methods used in LC/MS based untargeted metabolomics analysis. *Sci Rep* **6**, 38881 (2016).
155. Misra, B. B. Data normalization strategies in metabolomics: current challenges, approaches, and tools. *Eur J Mass Spectrom (Chichester)* **26**, 165–174 (2020).
156. Waaijenborg, S. *et al.* Fusing metabolomics data sets with heterogeneous measurement errors. *PLoS One* **13**, e0195939 (2018).
157. Percival, B., Gibson, M., Leenders, J., Wilson, P. B. & Grootveld, M. Chapter 1 Univariate and multivariate statistical approaches to the analysis and interpretation of

NMR-based metabolomics datasets of increasing complexity. 1–40 (2020) doi:10.1039/9781788015882-00001.

158. Saccenti, E., Hoefsloot, H. C. J., Smilde, A. K., Westerhuis, J. A. & Hendriks, M. M. W. B. Reflections on univariate and multivariate analysis of metabolomics data. *Metabolomics* **10**, 361–374 (2014).
159. Vinaixa, M. *et al.* A guideline to univariate statistical analysis for LC/MS-Based untargeted metabolomics-derived data. *Metabolites* **2**, 775–795 (2012).
160. Benjamini, Y. & Hochberg, Y. Controlling the false discovery rate: a practical and powerful approach to multiple testing. *Journal of the Royal Statistical Society: Series B (Methodological)* **57**, 289–300 (1995).
161. Antonelli, J. *et al.* Statistical workflow for feature selection in human metabolomics data. *Metabolites* **9**, 143 (2019).
162. Peluso, A., Glen, R. & Ebbels, T. M. D. Multiple-testing correction in metabolome-wide association studies. *BMC Bioinformatics* **22**, 67 (2021).
163. Ruiz-Perez, D., Guan, H., Madhivanan, P., Mathee, K. & Narasimhan, G. So you think you can PLS-DA? *BMC Bioinformatics* **21**, 2 (2020).
164. Szymańska, E., Saccenti, E., Smilde, A. K. & Westerhuis, J. A. Double-check: validation of diagnostic statistics for PLS-DA models in metabolomics studies. *Metabolomics* **8**, 3–16 (2012).
165. Westerhuis, J. A. *et al.* Assessment of PLSDA cross validation. *Metabolomics* **4**, 81–89 (2008).
166. Tarazona, S., Arzalluz-Luque, A. & Conesa, A. Undisclosed, unmet and neglected challenges in multi-omics studies. *Nat Comput Sci* **1**, 395–402 (2021).
167. Picard, M., Scott-Boyer, M.-P., Bodein, A., Périn, O. & Droit, A. Integration strategies of multi-omics data for machine learning analysis. *Computational and Structural Biotechnology Journal* **19**, 3735–3746 (2021).

168. Wieder, C. *et al.* Pathway analysis in metabolomics: recommendations for the use of over-representation analysis. *PLoS Comput Biol* **17**, e1009105 (2021).

169. Chicco, D. & Agapito, G. Nine quick tips for pathway enrichment analysis. *PLoS Comput Biol* **18**, e1010348 (2022).

170. Karp, P. D., Midford, P. E., Caspi, R. & Khodursky, A. Pathway size matters: the influence of pathway granularity on over-representation (enrichment analysis) statistics. *BMC Genomics* **22**, 191 (2021).

171. Wieder, C., Lai, R. P. & Ebbels, T. Single sample pathway analysis in metabolomics: performance evaluation and application.

172. Karnovsky, A. & Li, S. Pathway analysis for targeted and untargeted metabolomics. in *Computational Methods and Data Analysis for Metabolomics* (ed. Li, S.) 387–400 (Springer US, 2020). doi:10.1007/978-1-0716-0239-3_19.

173. Fraisier-Vannier, O. *et al.* MS-CleanR: a feature-filtering workflow for untargeted LC–MS based metabolomics. *Anal. Chem.* **92**, 9971–9981 (2020).

174. Kohler, I., Verhoeven, M., Haselberg, R. & Gargano, A. F. G. Hydrophilic interaction chromatography – mass spectrometry for metabolomics and proteomics: state-of-the-art and current trends. *Microchemical Journal* **175**, 106986 (2022).

175. Davies, V. *et al.* Rapid development of improved data-dependent acquisition strategies. *Anal. Chem.* **93**, 5676–5683 (2021).

176. Jankevics, A., Jenkins, A., Dunn, W. B. & Najdekr, L. An improved strategy for analysis of lipid molecules utilising a reversed phase C30 UHPLC column and scheduled MS/MS acquisition. *Talanta* **229**, 122262 (2021).

177. Pezzatti, J., González-Ruiz, V., Boccard, J., Guillarme, D. & Rudaz, S. Evaluation of different tandem MS acquisition modes to support metabolite annotation in human plasma using ultra high-performance liquid chromatography high-resolution mass spectrometry for untargeted metabolomics. *Metabolites* **10**, 464 (2020).

178. Jones, M.R., Lawson, T.N., Weber, R.J.M, Dunn, W.B., & Viant, M.R. Deep Metabolome annotation of the model organism *Daphnia magna*. Unpublished work. 2018.
179. Azad, R. K. & Shulaev, V. Metabolomics technology and bioinformatics for precision medicine. *Brief Bioinform* **20**, 1957–1971 (2018).
180. Meier, R., Ruttkies, C., Treutler, H. & Neumann, S. Bioinformatics can boost metabolomics research. *Journal of Biotechnology* **261**, 137–141 (2017).
181. Gauglitz, J. M. *et al.* Enhancing untargeted metabolomics using metadata-based source annotation. *Nat Biotechnol* **40**, 1774–1779 (2022).
182. Blaženović, I., Kind, T., Ji, J. & Fiehn, O. Software tools and approaches for compound identification of LC-MS/MS data in metabolomics. *Metabolites* **8**, 31 (2018).
183. Nash, W. J. & Dunn, W. B. From mass to metabolite in human untargeted metabolomics: recent advances in annotation of metabolites applying liquid chromatography-mass spectrometry data. *TrAC Trends in Analytical Chemistry* **120**, 115324 (2019).
184. Dunn, W. B. *et al.* Mass appeal: metabolite identification in mass spectrometry-focused untargeted metabolomics. *Metabolomics* **9**, 44–66 (2013).
185. Rochat, B. Proposed confidence scale and ID score in the identification of known-unknown compounds using high resolution MS data. *J. Am. Soc. Mass Spectrom.* **28**, 709–723 (2017).
186. Camunas-Alberca, S. M. *et al.* Integrating the potential of ion mobility spectrometry-mass spectrometry in the separation and structural characterisation of lipid isomers. *Frontiers in Molecular Biosciences* **10**, (2023).
187. Creek, D. J. *et al.* Metabolite identification: are you sure? And how do your peers gauge your confidence? *Metabolomics* **10**, 350–353 (2014).

188. Ichou, F. *et al.* Comparison of the activation time effects and the internal energy distributions for the CID, PQD and HCD excitation modes. *Journal of Mass Spectrometry* **49**, 498–508 (2014).
189. Vaniya, A. & Fiehn, O. Using fragmentation trees and mass spectral trees for identifying unknown compounds in metabolomics. *Trends Analyt Chem* **69**, 52–61 (2015).
190. Edison, A. S. *et al.* The time Is right to focus on model organism metabolomes. *Metabolites* **6**, 8 (2016).
191. Malinowska, J. M. & Viant, M. R. Confidence in metabolite identification dictates the applicability of metabolomics to regulatory toxicology. *Current Opinion in Toxicology* **16**, 32–38 (2019).
192. Scheubert, K. *et al.* Significance estimation for large scale metabolomics annotations by spectral matching. *Nat Commun* **8**, 1494 (2017).
193. Witting, M. & Böcker, S. Current status of retention time prediction in metabolite identification. *Journal of Separation Science* **43**, 1746–1754 (2020).
194. Kasper, P. T. *et al.* Fragmentation trees for the structural characterisation of metabolites. *Rapid Communications in Mass Spectrometry* **26**, 2275–2286 (2012).
195. Thermo Fisher Scientific. Orbitrap ID-X Tribrid mass spectrometer. Transforming small molecule identification and structure elucidation. Product specifications. (2018) doi:https://assets.thermofisher.com/TFS-Assets/CMD/Specification-Sheets/ps-65188-orbitrap-id-x-tribrid-ms-ps65188-en.pdf.
196. Thermo Fisher Scientific. AcquireX Intelligent Data Acquisition Technology. Smart note. (2019) doi:https://assets.thermofisher.com/TFS-Assets/CMD/brochures/sn-65392-ms-acquirex-intelligent-data-acquisition-sn65392-en.pdf.
197. Thermo Fisher Scientific. Compound Discoverer user guide for LC Studies. Software Version 3.3 SP1. Revision B. XCALI-98478. (2022).
198. Jendoubi, T. Approaches to integrating metabolomics and multi-omics data: a primer. *Metabolites* **11**, 184 (2021).

199. Canzler, S. *et al.* Prospects and challenges of multi-omics data integration in toxicology. *Arch Toxicol* **94**, 371–388 (2020).

200. Misra, B. B., Langefeld, C., Olivier, M. & Cox, L. A. Integrated omics: tools, advances and future approaches. *Journal of Molecular Endocrinology* **62**, R21–R45 (2019).

201. Di Minno, A. *et al.* Challenges in metabolomics-based tests, biomarkers revealed by metabolomic analysis, and the promise of the application of metabolomics in precision medicine. *Int J Mol Sci* **23**, 5213 (2022).

202. Guo, J., Yu, H., Xing, S. & Huan, T. Addressing big data challenges in mass spectrometry-based metabolomics. *Chem. Commun.* **58**, 9979–9990 (2022).

203. Zulfiqar, M., Gadelha, L., Steinbeck, C., Sorokina, M. & Peters, K. MAW: the reproducible Metabolome Annotation Workflow for untargeted tandem mass spectrometry. *Journal of Cheminformatics* **15**, 32 (2023).

204. Spjuth, O., Rydberg, P., Willighagen, E. L., Evelo, C. T. & Jeliazkova, N. XMetDB: an open access database for xenobiotic metabolism. *Journal of Cheminformatics* **8**, 47 (2016).

205. Penner, N., Xu, L. & Prakash, C. Radiolabeled absorption, distribution, metabolism, and excretion studies in drug development: why, when, and how? *Chem. Res. Toxicol.* **25**, 513–531 (2012).

206. National Toxicology Promgramme. US Department of Health and Human Services. Chemical disposition & toxicokinetics. https://ntp.niehs.nih.gov/whatwestudy/testpgm/chemdisp/index.html.

207. Dixit, R., Riviere, J., Krishnan, K. & Andersen, M. Toxicokinetics and physiologically based toxicokinetics in toxicology and risk assessment. *Journal of Toxicology and Environmental Health, Part B* **6**, 1–40 (2003).

208. Creton, S. *et al.* Use of toxicokinetics to support chemical evaluation: Informing high dose selection and study interpretation. *Regulatory Toxicology and Pharmacology* **62**, 241–247 (2012).

209. Reichard, J. F. *et al.* Toxicokinetic and toxicodynamic considerations when deriving health-based exposure limits for pharmaceuticals. *Regulatory Toxicology and Pharmacology* **79**, S67–S78 (2016).
210. Mielke, H. & Gundert-Remy, U. Physiologically based toxicokinetic modelling as a tool to support risk assessment: Three case studies. *Journal of Toxicology* **2012**, e359471 (2012).
211. Leist, M. *et al.* Adverse outcome pathways: opportunities, limitations and open questions. *Arch Toxicol* **91**, 3477–3505 (2017).
212. Laroche, C. *et al.* Finding synergies for 3Rs – Toxicokinetics and read-across: report from an EPAA partners' Forum. *Regulatory Toxicology and Pharmacology* **99**, 5–21 (2018).
213. Öztürk, A. & Abdullah, M. I. Toxicological effect of indole and its azo dye derivatives on some microorganisms under aerobic conditions. *Science of The Total Environment* **358**, 137–142 (2006).
214. Krebs, A. *et al.* The EU-ToxRisk method documentation, data processing and chemical testing pipeline for the regulatory use of new approach methods. *Arch Toxicol* **94**, 2435–2461 (2020).
215. Paules, R. Phenotypic anchoring: linking cause and effect. *Environmental Health Perspectives* **111**, (2003).
216. Bugel, S. M., Wehmas, L. C., La Du, J. K. & Tanguay, R. L. Phenotype anchoring in zebrafish reveals a potential role for matrix metalloproteinases (MMPs) in tamoxifen's effects on skin epithelium. *Toxicology and Applied Pharmacology* **296**, 31–41 (2016).
217. Taylor, N. S., Weber, R. J. M., White, T. A. & Viant, M. R. Discriminating between Different acute chemical toxicities via changes in the daphnid metabolome. *Toxicological Sciences* **118**, 307–317 (2010).
218. Love, M. I., Huber, W. & Anders, S. Moderated estimation of fold change and dispersion for RNA-seq data with DESeq2. *Genome Biol* **15**, 550 (2014).

219. Suzuki, R. & Shimodaira, H. Pvclust: an R package for assessing the uncertainty in hierarchical clustering. *Bioinformatics* **22**, 1540–1542 (2006).

220. Hageman, J. A., van den Berg, R. A., Westerhuis, J. A., van der Werf, M. J. & Smilde, A. K. Genetic algorithm based two-mode clustering of metabolomics data. *Metabolomics* **4**, 141–149 (2008).

221. Heinemann, J. Cluster Analysis of untargeted metabolomic experiments. in *Microbial Metabolomics: Methods and Protocols* (ed. Baidoo, E. E. K.) 275–285 (Springer, 2019). doi:10.1007/978-1-4939-8757-3_16.

222. Murtagh, F. & Legendre, P. Ward's hierarchical agglomerative clustering method: which algorithms implement Ward's criterion? *J Classif* **31**, 274–295 (2014).

223. Patlewicz, G. Read-across approaches - misconceptions, promises and challenges ahead. *ALTEX* **31**, 387–396 (2014).

224. Langsch, A. *et al.* Hexamoll® DINCH: lack of in vivo evidence for obesogenic properties. *Toxicology Letters* **288**, 99–110 (2018).

225. Benkhaya, S., M'rabet, S. & El Harfi, A. Classifications, properties, recent synthesis and applications of azo dyes. *Heliyon* **6**, e03271 (2020).

226. Appendix 8: Entry 43 - Azocolourants - List of aromatic amines - ECHA. https://echa.europa.eu/appendix-8-list-of-aromatic-amines.

227. Brüschweiler, B. J. & Merlot, C. Azo dyes in clothing textiles can be cleaved into a series of mutagenic aromatic amines which are not regulated yet. *Regulatory Toxicology and Pharmacology* **88**, 214–226 (2017).

228. European Directorate for the Quality of Medicines & HealthCare (EDQM). Safer tattooing. Overview of current knowledge and challenges of toxicological assessment. Consumer Health Protection Committee (CD-P-SC). (2017).

229. IMAP Group Assessment Report. Azo Dyes that cleave to aromatic amines of potential toxicological concern: human health tier II assessment. Accelerated Assessment of Industrial Chemicals in Australia. (2016).

230. Health Canada. Screening assessment. Aromatic azo and benzidine-based substance grouping. Certain azo solvent dyes. (2016).
231. Hashemi, S. H. & Kaykhaii, M. Azo dyes: Sources, occurrence, toxicity, sampling, analysis, and their removal methods. in *Emerging Freshwater Pollutants* 267–287 (Elsevier, 2022). doi:10.1016/B978-0-12-822850-0.00013-2.
232. Croce, R. *et al.* Aquatic toxicity of several textile dye formulations: Acute and chronic assays with Daphnia magna and Raphidocelis subcapitata. *Ecotoxicology and Environmental Safety* **144**, 79–87 (2017).
233. Abe, F. R., Soares, A. M. V. M., Oliveira, D. P. de & Gravato, C. Toxicity of dyes to zebrafish at the biochemical level: Cellular energy allocation and neurotoxicity. *Environmental Pollution* **235**, 255–262 (2018).
234. Bienstock, R. J., Perera, L. & Pasquinelli, M. A. Molecular Modeling Study of the Genotoxicity of the sudan I and sudan II azo dyes and their metabolites. *Front. Chem.* **10**, 880782 (2022).
235. Zini Moreira Silva, E., Sehr, A., Grummt, T., Palma de Oliveira, D. & Morais Leme, D. The evaluation of reactive textile dyes regarding their potential to cause organ-specific cyto- and geno-toxicity. *EEC* **17**, 60–66 (2022).
236. Ramos-Souza, C., Bandoni, D. H., Bragotto, A. P. A. & De Rosso, V. V. Risk assessment of azo dyes as food additives: revision and discussion of data gaps toward their improvement. *Comprehensive Reviews in Food Science and Food Safety* **n/a**,.
237. Djoumbou Feunang, Y. *et al.* ClassyFire: automated chemical classification with a comprehensive, computable taxonomy. *J Cheminform* **8**, 61 (2016).
238. Benfenati, E., Chaudhry, Q., Gini, G. & Dorne, J. L. Integrating *in silico* models and read-across methods for predicting toxicity of chemicals: a step-wise strategy. *Environment International* **131**, 105060 (2019).

239. Melnikov, F., Kostal, J., Voutchkova-Kostal, A., Zimmerman, J. B. & T. Anastas, P. Assessment of predictive models for estimating the acute aquatic toxicity of organic chemicals. *Green Chem.* **18**, 4432–4445 (2016).

240. Lambert, F. N., Vivian, D. N., Raimondo, S., Tebes-Stevens, C. T. & Barron, M. G. Relationships between aquatic toxicity, chemical hydrophobicity, and mode of action: Log Kow revisited. *Arch Environ Contam Toxicol* **83**, 326–338 (2022).

241. Langfelder, P., Zhang, B. & Horvath, S. Dynamic tree cut: in-depth description, tests and applications.

242. Gil, M. *et al.* Discrimination of rosé wines using shotgun metabolomics with a genetic algorithm and MS ion intensity ratios. *Sci Rep* **10**, 1170 (2020).

243. Zou, W. & Tolstikov, V. V. Pattern recognition and pathway analysis with genetic algorithms in mass spectrometry-based metabolomics. *Algorithms* **2**, 638–666 (2009).

244. Lisitsyna, A. *et al.* Feature selection pipelines with classification for non-targeted metabolomics combining the neural network and genetic algorithm. *Anal. Chem.* **94**, 5474–5482 (2022).

245. Askr, H. *et al.* Deep learning in drug discovery: an integrative review and future challenges. *Artif Intell Rev* **56**, 5975–6037 (2023).

246. Patterson, E. A., Whelan, M. P. & Worth, A. P. The role of validation in establishing the scientific credibility of predictive toxicology approaches intended for regulatory application. *Computational Toxicology* **17**, 100144 (2021).

247. Parish, S. T. *et al.* An evaluation framework for new approach methodologies (NAMs) for human health safety assessment. *Regulatory Toxicology and Pharmacology* **112**, 104592 (2020).

248. ECHA. Guidance on information requirements and chemical safety assessment. Chapter R.7C: Endpoint specific guidance. Version 3.0. (2017) doi:https://echa.europa.eu/documents/10162/17224/information_requirements_r7c_en.pdf/e2e23a98-adb2-4573-b450-cc0dfa7988e5?t=1498476107907.

249. Perkins, E. J. *et al.* Building and applying quantitative adverse outcome pathway models for chemical hazard and risk assessment. *Enviro Toxic and Chemistry* **38**, 1850–1865 (2019).

250. Bessems, J. G. M. & Geraets, L. Proper knowledge on toxicokinetics improves human hazard testing and subsequent health risk characterisation. A case study approach. *Regulatory Toxicology and Pharmacology* **67**, 325–334 (2013).

251. EFSA. Modern methodologies and tools for human hazard assessment of chemicals. (2014) doi:https://efsa.onlinelibrary.wiley.com/doi/epdf/10.2903/j.efsa.2014.3638.

252. Yordanova, D. G., Schultz, T. W., Kuseva, C. D. & Mekenyan, O. G. Assessing metabolic similarity for read-across predictions. *Computational Toxicology* **18**, 100160 (2021).

253. Gouliarmou, V. *et al.* Establishing a systematic framework to characterise in vitro methods for human hepatic metabolic clearance. *Toxicology in Vitro* **53**, 233–244 (2018).

254. Browne, P., Delrue, N. & Gourmelon, A. Regulatory use and acceptance of alternative methods for chemical hazard identification. *Current Opinion in Toxicology* **15**, 18–25 (2019).

255. Ridder, L. & Wagener, M. SyGMa: Combining expert knowledge and empirical scoring in the prediction of metabolites. *ChemMedChem* **3**, 821–832 (2008).

256. Kovács, P., Botka, G. & Figyelmesi, Á. Automatic generation of Markush structures from specific compounds. *World Patent Information* **57**, 59–69 (2019).

257. Ken Webb, Tony Bristow, Mike Sargent, & Bridget Stein. Methodology for accurate mass measurement of small molecules. Best practice guide. Ken Webb*, Tony Bristow*, Mike Sargent* and Bridget Stein#. (2004).

258. Health Canada. Certain azo disperse dyes - information sheet. (2020) doi:https://www.canada.ca/en/health-canada/services/chemical-substances/fact-sheets/chemicals-glance/certain-azo-disperse-dyes.html.

259. Canada, H. Dyes of the aromatic azo and benzidine-based substance grouping. https://www.canada.ca/en/health-canada/services/chemical-substances/substance-groupings-initiative/aromatic-azo-benzidine-based/dyes.html (2013).

260. Environment and Climate Change Canada. Release guidelines for disperse yellow 3 and 25 other azo disperse dyes in the textile sector. doi:https://www.canada.ca/en/environment-climate-change/services/canadian-environmental-protection-act-registry/guidelines-objectives-codes-practice/release-guidelines-disperse-yellow-3.html.

261. Gwinn, W. M. *et al.* Evaluation of 5-day i*n vivo* rat liver and kidney with high-throughput transcriptomics for estimating benchmark doses of apical outcomes. *Toxicological Sciences* **176**, 343–354 (2020).

262. D'Elia, R. V. *et al.* Multiple metabolic pathways are predictive of ricin intoxication in a rat model. *Metabolomics* **15**, 102 (2019).

263. Thermo Fisher Scientific. EASY-ETD and EASY-IC ion sources. User guide for the Orbitrap Tribrid series mass spectrometer. (2018) doi:https://assets.thermofisher.com/TFS-Assets/CMD/manuals/man-80000-97515-easy-etd-ic-ion-sources-user-man8000097515-en.pdf.

264. Smith, C. A., Want, E. J., O'Maille, G., Abagyan, R. & Siuzdak, G. XCMS: Processing mass spectrometry data for metabolite profiling using nonlinear peak alignment, matching, and identification. *Anal. Chem.* **78**, 779–787 (2006).

265. Ruttkies, C., Neumann, S. & Posch, S. Improving MetFrag with statistical learning of fragment annotations. *BMC Bioinformatics* **20**, 376 (2019).

266. Ruttkies, C., Schymanski, E. L., Wolf, S., Hollender, J. & Neumann, S. MetFrag relaunched: incorporating strategies beyond in silico fragmentation. *J Cheminform* **8**, 3 (2016).

267. Thermo Fisher Scientific. Compound Discoverer 3.3 SP1 Metabolism tutorial, Revision B. XCALI-98473. (2022).

268. Caroline Ding1, Tim Stratton1, Martin Strohalm, Hans Grensemann, Ji Ma. Detection and identification of labelled compounds from high resolution tandem mass spectrometry. Poster Note 64747.

269. Sadygov, R. G., Martin Maroto, F. & Hühmer, A. F. R. ChromAlign: A two-step algorithmic procedure for time alignment of three-dimensional LC−MS chromatographic surfaces. *Anal. Chem.* **78**, 8207–8217 (2006).

270. Ding, Caroline, Comstock, Kate, Sharma, Seema, Sanders, Mark, & Raab, Michal. Building curated and annotated HRAM MSn spectral libraries to aid in unknown structure elucidation. Thermo Fisher Scientific. Technical note No. 65602. (2019) doi:https://www.thermofisher.com/document-connect/document-connect.html?url=https://assets.thermofisher.com/TFS-Assets%2FCMD%2FTechnical-Notes%2Ftn-65602-hram-ms-spectral-libraries-tn65602-en.pdf.

271. Alseekh, S. *et al.* Mass spectrometry-based metabolomics: a guide for annotation, quantification and best reporting practices. *Nat Methods* **18**, 747–756 (2021).

272. Picardo, M., Núñez, O. & Farré, M. A data independent acquisition all ion fragmentation mode tool for the suspect screening of natural toxins in surface water. *MethodsX* **8**, 101286 (2021).

273. Li, M. *et al.* Biotransformation of bisphenol AF to its major glucuronide metabolite reduces estrogenic activity. *PLoS ONE* **8**, e83170 (2013).

274. Knudsen, G. A., Hall, S. M., Richards, A. C. & Birnbaum, L. S. TBBPA disposition and kinetics in pregnant and nursing Wistar Han IGS rats. *Chemosphere* **192**, 5–13 (2018).

275. Choi, K. *et al.* In vitro metabolism of di(2-ethylhexyl) phthalate (DEHP) by various tissues and cytochrome P450s of human and rat. *Toxicology in Vitro* **26**, 315–322 (2012).

276. Di(2-Ethylhexyl)Phthalate (DEHP) | Toxicological Profile | ATSDR. *ATSDR US. Agency for Toxic Substances and Disease Registry. Toxic Substances Portal.* https://wwwn.cdc.gov/TSP/ToxProfiles/ToxProfiles.aspx?id=684&tid=65.

277. Health Canada. Updated draft screening assessment. Certain organic flame retardants. Substance grouping 2-Propanol, 1-chloro-, phosphate (3:1) (TCPP). Chemical Abstracts. Service Registry Number 13674-84-5 2-Propanol, 1,3-dichloro-, phosphate (3:1) (TDCPP) Chemical Abstracts Service Registry Number 13674-87-8. Environment and Climate Change Canada Health Canada. (2020) doi:https://www.canada.ca/content/dam/eccc/documents/pdf/pded/ofr-tcpp-tdcpp/Draft-screening-assessment-tcpp-tdcpp.pdf.

278. EPA. Provisional peer-reviewed toxicity values for Tris(1-chloro-2-propyl)phosphate (CASRN 13674-84-5). Superfund Health Risk Technical Support Center. National Center for Environmental Assessment. Office of Research and Development U.S. Environmental Protection Agency. (2012) doi:https://cfpub.epa.gov/ncea/pprtv/documents/Tris1chloro2propylphosphate.pdf.

279. Wu, J., Liu, J. & Cai, Z. Determination of triclosan metabolites by using in-source fragmentation from high-performance liquid chromatography/negative atmospheric pressure chemical ionization ion trap mass spectrometry. *Rapid Communications in Mass Spectrometry* **24**, 1828–1834 (2010).

280. Zhu, L. *et al.* Electrochemical simulation of triclosan metabolism and toxicological evaluation. *Science of The Total Environment* **622–623**, 1193–1201 (2018).

281. Kirwan, J. A. *et al.* Quality assurance and quality control reporting in untargeted metabolic phenotyping: mQACC recommendations for analytical quality management. *Metabolomics* **18**, 70 (2022).

282. Waidyanatha, S. *et al.* Disposition of bisphenol AF, a bisphenol A analogue, in hepatocytes *in vitro* and in male and female Harlan Sprague-Dawley rats and B6C3F1/N mice following oral and intravenous administration. *Xenobiotica* **45**, 811–819 (2015).

283. Waidyanatha, S. *et al.* Toxicokinetics and bioavailability of bisphenol AF following oral administration in rodents: A dose, species, and sex comparison. *Toxicology and Applied Pharmacology* **373**, 39–47 (2019).

284. Waidyanatha, S. *et al.* An investigation of systemic exposure to bisphenol AF during critical periods of development in the rat. *Toxicology and Applied Pharmacology* **411**, 115369 (2021).

285. Lhuguenot, J.-C., Mitchell, A. M., Milner, G., Lock, E. A. & Elcombe, C. R. The metabolism of di(2-ethylhexyl) phthalate (DEHP) and mono-(2-ethylhexyl) phthalate (MEHP) in rats: In vivo and in vitro dose and time dependency of metabolism. *Toxicology and Applied Pharmacology* **80**, 11–22 (1985).

286. Cronin, M. T. D. *et al. In Silico* prediction of organ level toxicity: linking chemistry to adverse effects. *ToxicolRes* **33**, 173–182 (2017).

287. Wu, B. *et al.* Regioselective sulfation and glucuronidation of phenolics: insights into the structural basis of conjugation. *Curr Drug Metab* **12**, 900–916 (2011).

288. Pan, L. *et al.* Sulfation predominates the pharmacokinetics, metabolism, and excretion of forsythin in humans: major enzymes and transporters identified. *Acta Pharmacologica Sinica* **42**, 311 (2021).

289. Swortwood, M. J. *et al. In vitro*, *in vivo* and *in silico* metabolic profiling of α-pyrrolidinopentiothiophenone, a novel thiophene stimulant. *Bioanalysis* **8**, 65–82 (2016).

290. Guo, N. *et al.* Pharmacokinetic, metabolic profiling and elimination of brusatol in rats. *Biomedical Chromatography* **32**, e4358 (2018).

291. Wang, X. *et al.* An integrated approach to characterize intestinal metabolites of four phenylethanoid glycosides and intestinal microbe-mediated antioxidant activity evaluation in vitro using UHPLC-Q-Exactive high-resolution mass spectrometry and a 1,1-diphenyl-2-picrylhydrazyl-based Assay. *Front. Pharmacol.* **10**, 826 (2019).

292. Di Trana, A. *et al. In silico* prediction, LC-HRMS/MS analysis, and targeted/untargeted data-mining workflow for the profiling of phenylfentanyl in vitro metabolites. *Talanta* **235**, 122740 (2021).

293. Przybylak, K. R. *et al.* Read-across of 90-day rat oral repeated-dose toxicity: A case study for selected β-olefinic alcohols. *Computational Toxicology* **1**, 22–32 (2017).

294. Chen, C., Gonzalez, F. J. & Idle, J. R. LC-MS-based metabolomics in drug metabolism. *Drug Metab Rev* **39**, 581–597 (2007).

295. Vrbanac, J. & Slauter, R. Chapter 3 - ADME in drug discovery. in *A Comprehensive Guide to Toxicology in Nonclinical Drug Development (Second Edition)* (ed. Faqi, A. S.) 39–67 (Academic Press, 2017). doi:10.1016/B978-0-12-803620-4.00003-7.

296. Cuperlovic-Culf, M. & Culf, A. S. Applied metabolomics in drug discovery. *Expert Opin Drug Discov* **11**, 759–770 (2016).

297. Fagerholm, U., Spjuth, O. & Hellberg, S. The impact of reference data selection for the prediction accuracy of intrinsic hepatic metabolic clearance. *Journal of Pharmaceutical Sciences* **111**, 2645–2649 (2022).

298. Colbourne, J. K. *et al.* Toxicity by descent: A comparative approach for chemical hazard assessment. *Environmental Advances* **9**, 100287 (2022).

299. Yang, C. *et al.* New publicly available chemical query language, CSRML, To support chemotype representations for application to data mining and modelling. *J. Chem. Inf. Model.* **55**, 510–528 (2015).

300. Claire, T. & Sean, H. Integrating toxicokinetics into toxicology studies and the human health risk assessment process for chemicals: Reduced uncertainty, better health protection. *Regulatory Toxicology and Pharmacology* **128**, 105092 (2022).

301. Koppel, N., Rekdal, V. M. & Balskus, E. P. Chemical transformation of xenobiotics by the human gut microbiota. *Science (New York, N.y.)* **356**, (2018).

302. Das, A., Srinivasan, M., Ghosh, T. S. & Mande, S. S. Xenobiotic metabolism and gut microbiomes. *PLoS ONE* **11**, (2016).

303. Hakk, H., Larsen, G., Bergman, Å. & Örn, U. Metabolism, excretion and distribution of the flame retardant tetrabromobisphenol-A in conventional and bile-duct cannulated rats. *Xenobiotica* **30**, 881–890 (2000).

304. Knudsen, G. A., Sanders, J. M., Sadik, A. M. & Birnbaum, L. S. Disposition and kinetics of tetrabromobisphenol A in female Wistar Han rats. *Toxicology Reports* **1**, 214–223 (2014).

305. Schauer, U. M. D., Völkel, W. & Dekant, W. Toxicokinetics of tetrabromobisphenol A in humans and rats after oral administration. *Toxicological Sciences* **91**, 49–58 (2006).

306. Van den Eede, N., Maho, W., Erratico, C., Neels, H. & Covaci, A. First insights in the metabolism of phosphate flame retardants and plasticizers using human liver fractions. *Toxicology Letters* **223**, 9–15 (2013).

307. National Toxicology Program (NTP). NTP Developmental and reproductive toxicity technical report on the prenatal development studies of tris(chloropropyl) phosphate (CASRN 13674-84-5) in Sprague Dawley. https://ntp.niehs.nih.gov/go/dart01abs (2020) doi:10.22427/NTP-DART-01.

308. Schultz, T. W. & Cronin, M. T. D. Lessons learned from read-across case studies for repeated-dose toxicity. *Regulatory Toxicology and Pharmacology* **88**, 185–191 (2017).

309. OECD. A case study on the use of integrated approaches for testing and assessment for sub-chronic repeated-dose toxicity of simple aryl alcohol alkyl carboxylic esters: read-across. Organisation for Economic Co-operation and Development. **ENV/JM/MONO(2018)29**, (2018).

310. Ring, C. *et al.* Predictive modeling of biological responses in the rat liver using in vitro Tox21 bioactivity: Benefits from high-throughput toxicokinetics. *Computational Toxicology* **18**, 100166 (2021).

311. *Hepatocytes: Methods and Protocols*. vol. 640 (Humana Press, 2010).

# APPENDIX A

**Table A-1** Putatively annotated features which were found to be significantly changing (*q*-value < 0.1) in the nESI-DIMS lipidomics datasets for S1, DY3 and SRG azo dyes.

| Feature ID | *m/z* | Intensity | Molecular formula | Adduct | Compound name | Lipid class | Ppm error |
|---|---|---|---|---|---|---|---|
| **M61** | 693.4465 | 6992.929017 | P\|\|C37H67O8P\|\|C37H67 | [M+Na]+ | sn-glycero-3-phosphate(2- | PA | 0.11 |
| **M62** | 695.4629 | 18032.0542 | P\|\|C37H69O8P\|\|C37H69 | [M+Na]+ | glycero-3-phosphate\|\|1-octadecanoyl-2-(9Z)-hexadecenoyl-sn-glycero-3-phosphate(2-)\|\|1-oleoyl-2-palmitoyl-sn- | PA | -0.98 |
| **M71** | 723.4938 | 11147.68368 | P\|\|C39H73O8P\|\|C39H73 | [M+Na]+ | glycero-3-phosphate\|\|1-oleoyl-2-(6Z)-octadecenoyl-sn-glycero-3-phosphate\|\|1-oleoyl-2-stearoyl-sn-glycero-3- | PA | -0.42 |
| **M74** | 730.5386 | 273425.4688 | O8P\|\|C40H76NO8P\|\|C4 | [M+H]+ | tetradecanoyl-2-[(9Z,12Z)-octadecadienoyl]-sn-glycero-3- | PC | -0.57 |
| **M65** | 706.5388 | 27372.01685 | O8P\|\|C38H76NO8P\|\|C3 | [M+H]+ | octadecanoyl-2-dodecanoyl-sn-glycero-3-phosphocholine\|\|1-palmitoyl-2-myristoyl-sn-glycero-3-phosphocholine\|\|1- | PC | -1.01 |
| **M68** | 718.5386 | 69731.57813 | O8P\|\|C39H76NO8P\|\|C3 | [M+H]+ | glycero-3-phosphoethanolamine\|\|1-hexadecanoyl-2-(9Z-octadecenoyl)-sn-glycero-3-phosphoethanolamine\|\|1- | PC | -0.64 |
| **M37** | 520.3405 | 110958.2109 | O7P\|\|C26H50NO7P\|\|C2 | [M+H]+ | phosphocholine\|\|LysoPC(18:2(9Z,12Z))\|\|PC(18:2(2E,4E)/0:0)\|\|PC(18:2(9Z,12Z)/0:0)\|\|linoleoyl-sn-glycero-3- | PC | -1.47 |
| **M86** | 746.5698 | 155839.7637 | O8P\|\|C41H80NO8P\|\|C4 | [M+H]+ | zwitterion\|\|1-palmitoyl-2-(9Z-heptadecenoyl)-sn-glycero-3-phosphocholine\|\|1-pentadecanoyl-2-oleoyl-sn-glycero-3- | PC | -0.46 |
| **M158** | 1042.529 | 1357.77164 | C52H83N3O13P2 | [M+Na]+ | CDP-2,3-bis-O-(geranylgeranyl)-sn-glycerol(2-) | | 0.54 |
| **M98** | 798.669 | 29259.7168 | C15H10I4NO4 | [M+Na]+ | L-thyroxine(1-) | | -1.17 |
| **M58** | 673.1014 | 13064.82935 | 8 | [M+Na]+ | Methyl 2,3,6-tri-O-galloyl-beta-D-glucopyranoside\|\|Methyl 3,4,6-tri-O-galloyl-beta-D-glucopyranoside | | -0.46 |
| **M76** | 731.6068 | 60635.64844 | N2O6P\|\|C41H83N2O6P\|\| | [M+H]+ | phosphocholine\|\|N-octadecenoylsphinganine-1-phosphocholine\|\|N-oleoylsphinganine-1-phosphocholine\|\|N- | PE / SM | -0.84 |
| **M67** | 717.591 | 32684.88477 | N2O6P\|\|C40H81N2O6P\|\| | [M+H]+ | phosphocholine\|\|N-octadecanoyl-15-methylhexadecasphingosine-1-phosphocholine\|\|PE-Cer(d14:1(4E)/24:0)\|\|PE- | PE / SM | -0.73 |
| **M85** | 745.6229 | 14126.49048 | N2O6P\|\|C42H85N2O6P\|\| | [M+H]+ | Cer(d14:1(4E)/26:0)\|\|PE-Cer(d16:1(4E)/24:0)\|\|SM(d18:1/19:0)\|\|SM(d19:1/18:0)\|\|sphingomyelin 37:1\|\|20:0 | PE / SM | -1.45 |
| **M23** | 431.3802 | 11162.98706 | C29H51P\|\|C20H46N8O2 | [M+H]+ | None | | -0.26 |
| **M47** | 593.4544 | 15197.71619 | \|\|C34H66O5\|\|C34H66O5 | [M+H]+\|\|[M+K]+ | 21:0/0:0)\|\|DG(10:0/i-21:0/0:0)\|\|DG(12:0/0:0/19:0)\|\|DG(12:0/0:0/i- | DG | -0.64 |
| **M91** | 792.4792 | 7457.976563 | NO10P\|\|C41H72NO10P\|\| | [M+Na]+ | 1Z,14Z,17Z))\|\|PS(15:1(9Z)/20:3(8Z,11Z,14Z))\|\|PS(17:0/18:4(6Z,9Z,12Z,15Z))\|\|PS(17:1(9Z)/18:3(6Z,9Z,12Z))\|\|PS(1 | PS | -0.78 |
| **M111** | 833.6629 | 14014.61401 | C52H90O6\|\|C52H90O6\|\| | [M+Na]+ | 5Z,8Z,11Z,14Z,17Z))[iso6]\|\|TG(12:0/17:1(9Z)/20:4(5Z,8Z,11Z,14Z))[iso6]\|\|TG(12:0/17:2(9Z,12Z)/20:3(8Z,11Z,14Z)) | TG | 0.02 |
| **M110** | 831.6475 | 20497.39233 | C52H88O6\|\|C52H88O6\|\| | [M+Na]+ | 1(9Z)/20:5(5Z,8Z,11Z,14Z,17Z))[iso6]\|\|TG(12:0/17:2(9Z,12Z)/20:4(5Z,8Z,11Z,14Z))[iso6]\|\|TG(13:0/14:0/22:6(4Z,7Z, | TG | -0.25 |
| **M125** | 861.6943 | 14108.47192 | C54H94O6\|\|C54H94O6\|\| | [M+Na]+ | Z)/22:3(10Z,13Z,16Z))[iso6]\|\|TG(12:0/19:0/20:5(5Z,8Z,11Z,14Z,17Z))[iso6]\|\|TG(12:0/19:1(9Z)/20:4(5Z,8Z,11Z,14Z)) | TG | -0.05 |

# APPENDIX B

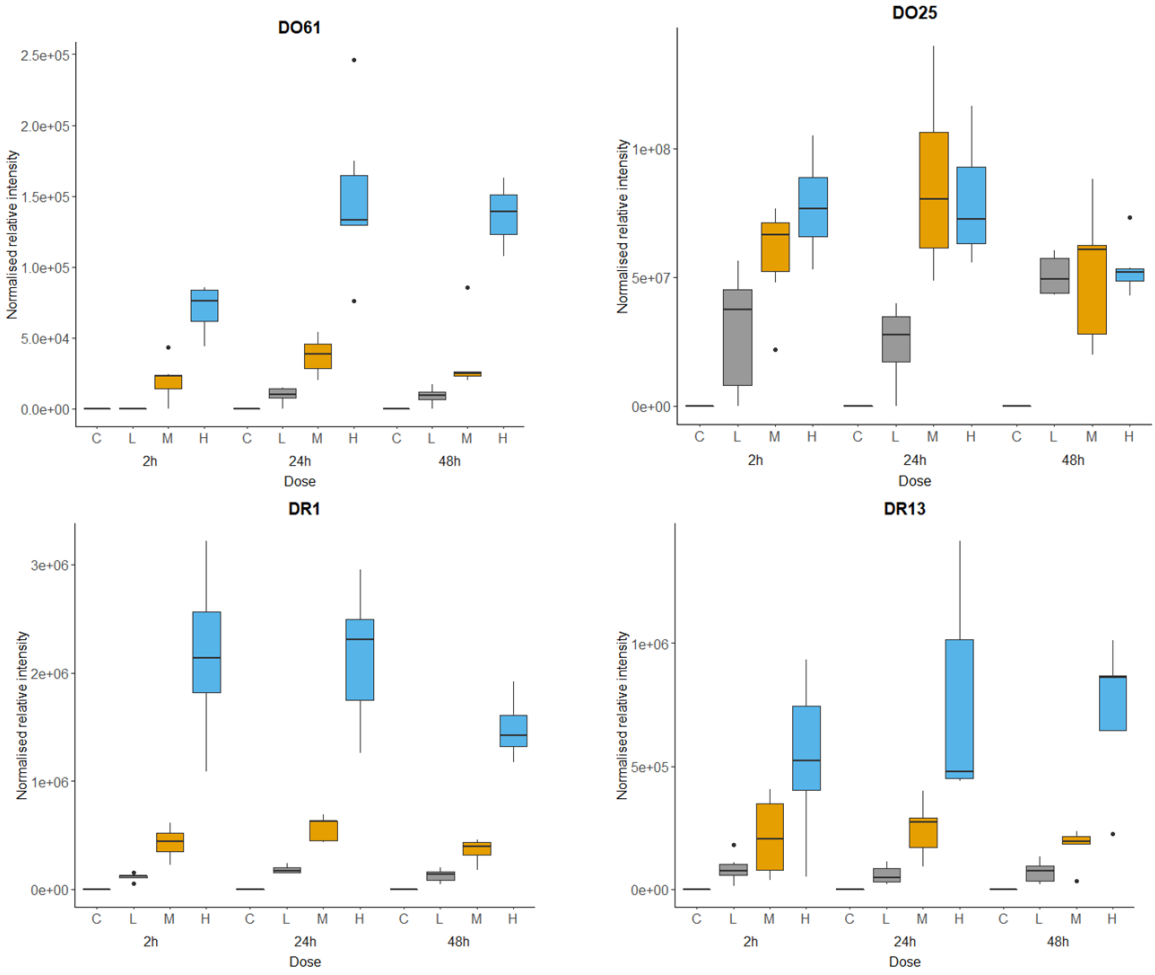


**Figure B-1** Normalised peak intensities (relative internal concentrations) of the azo dye parent chemicals measured across the three treatment doses (L – low, M – medium and H – high) and three sampling time points (2 h, 24 h, 48 h) in the nESI-DIMS lipidomics dataset.

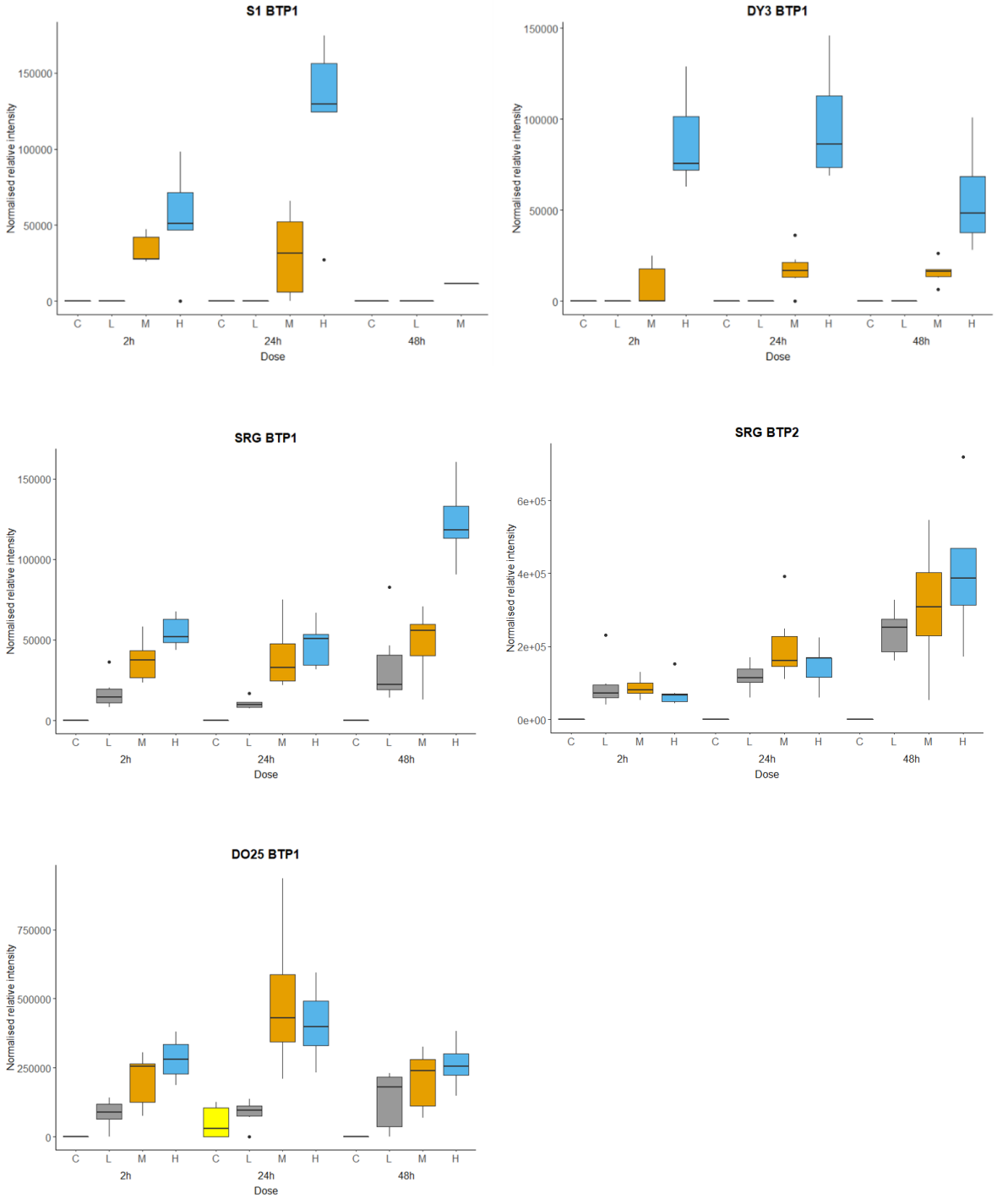


**Figure B-2** Normalised peak intensities (relative internal concentrations) of the azo dye biotransformation products (BTPs) measured across the three treatment doses (L – low, M – medium and H – high) and three sampling time points (2 h, 24 h, 48 h) in the nESI-DIMS polar lipidomics dataset. High dose group at 48 h is missing for S1 BTP1.

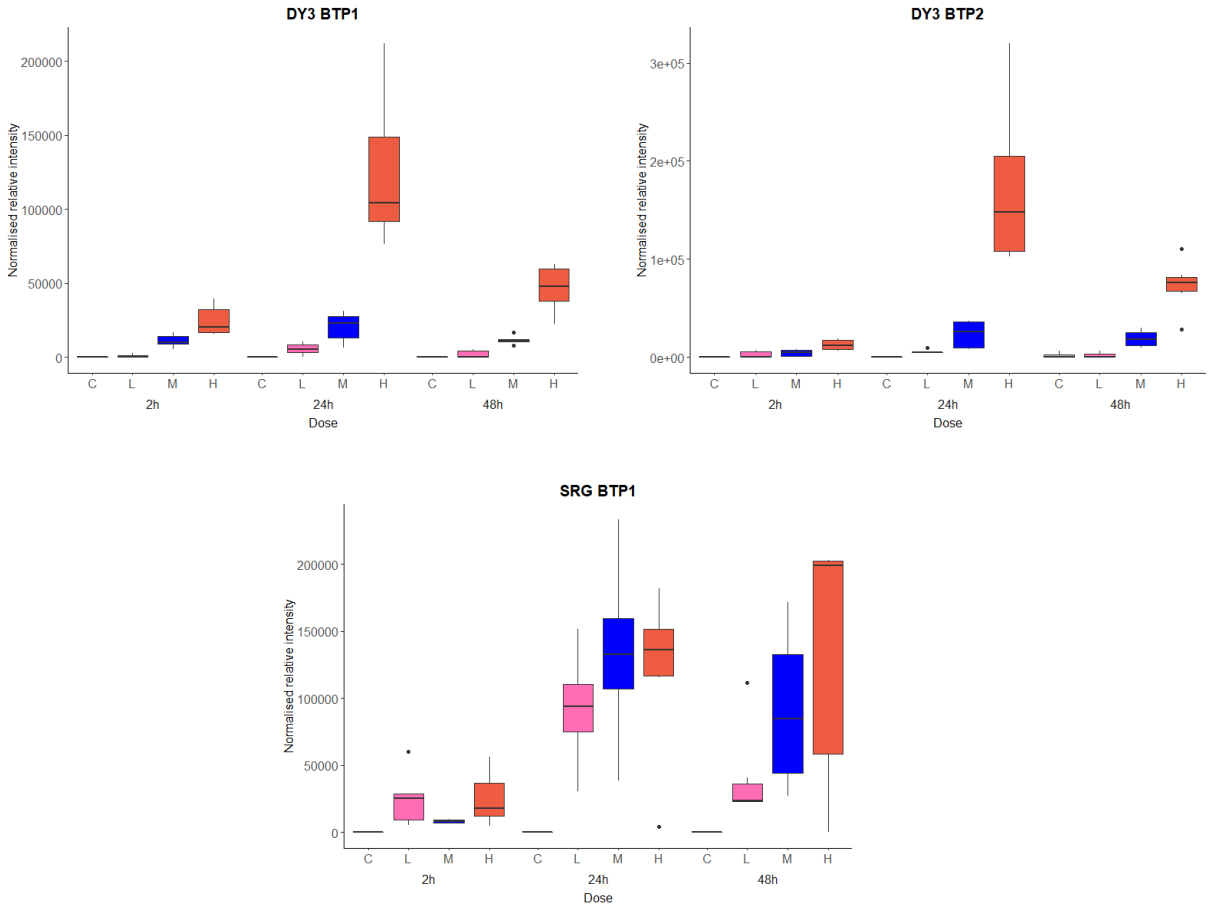


**Figure B-3** Normalised peak intensities (relative internal concentrations) of the azo dye biotransformation products (BTPs) measured across the three treatment doses (L – low, M – medium and H – high) and three sampling time points (2 h, 24 h, 48 h) in the nESI-DIMS polar positive metabolomics dataset. High dose group at 48 h is missing for S1.

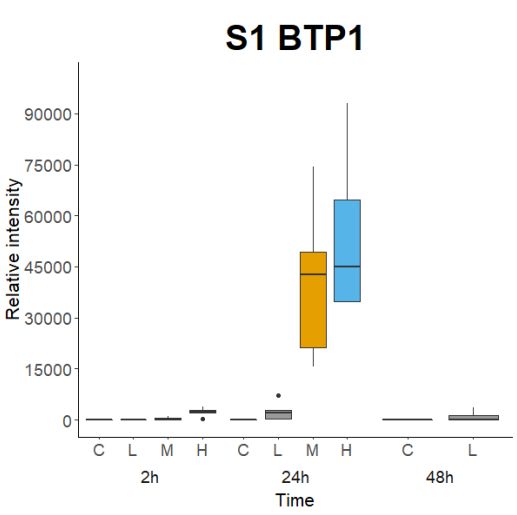
S1 BTP1
Relative intensity
90000
75000
60000
45000
30000
15000
0
C L M H C L M H C L
2h
24h
48h
Time

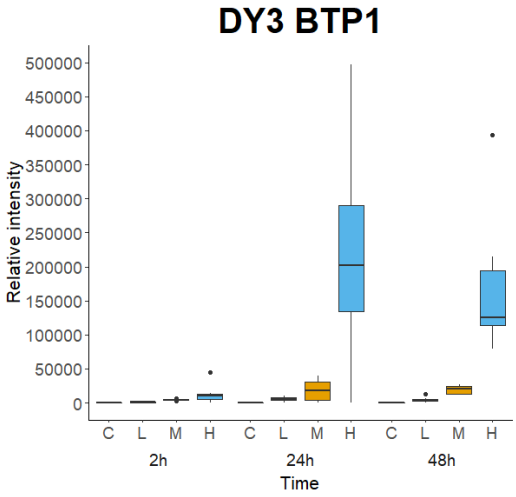
DY3 BTP1
Relative intensity
500000
450000
400000
350000
300000
250000
200000
150000
100000
50000
0
C L M H C L M H C L M H
2h
24h
48h
Time

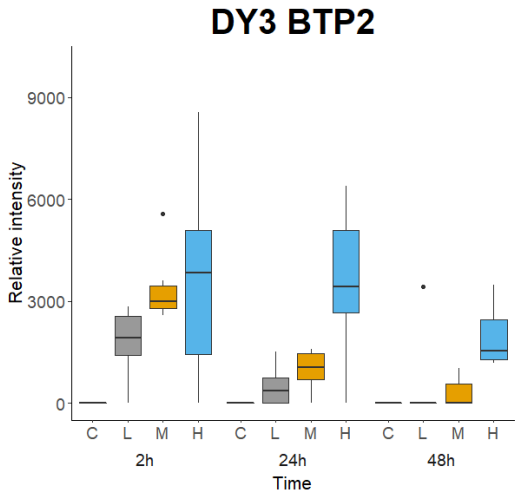
DY3 BTP2
Relative intensity
9000
6000
3000
0
C L M H C L M H C L M H
2h
24h
48h
Time

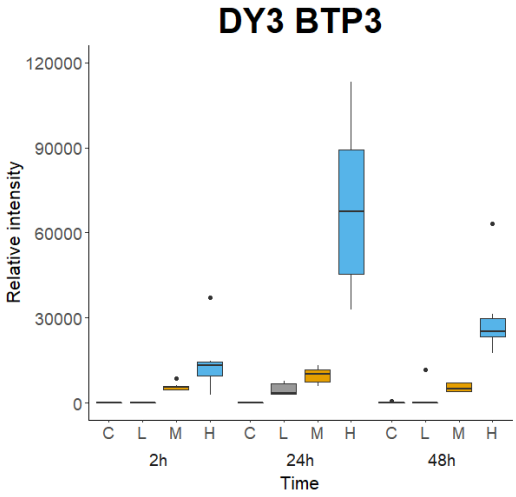
DY3 BTP3
Relative intensity
120000
90000
60000
30000
0
C L M H C L M H C L M H
2h
24h
48h
Time

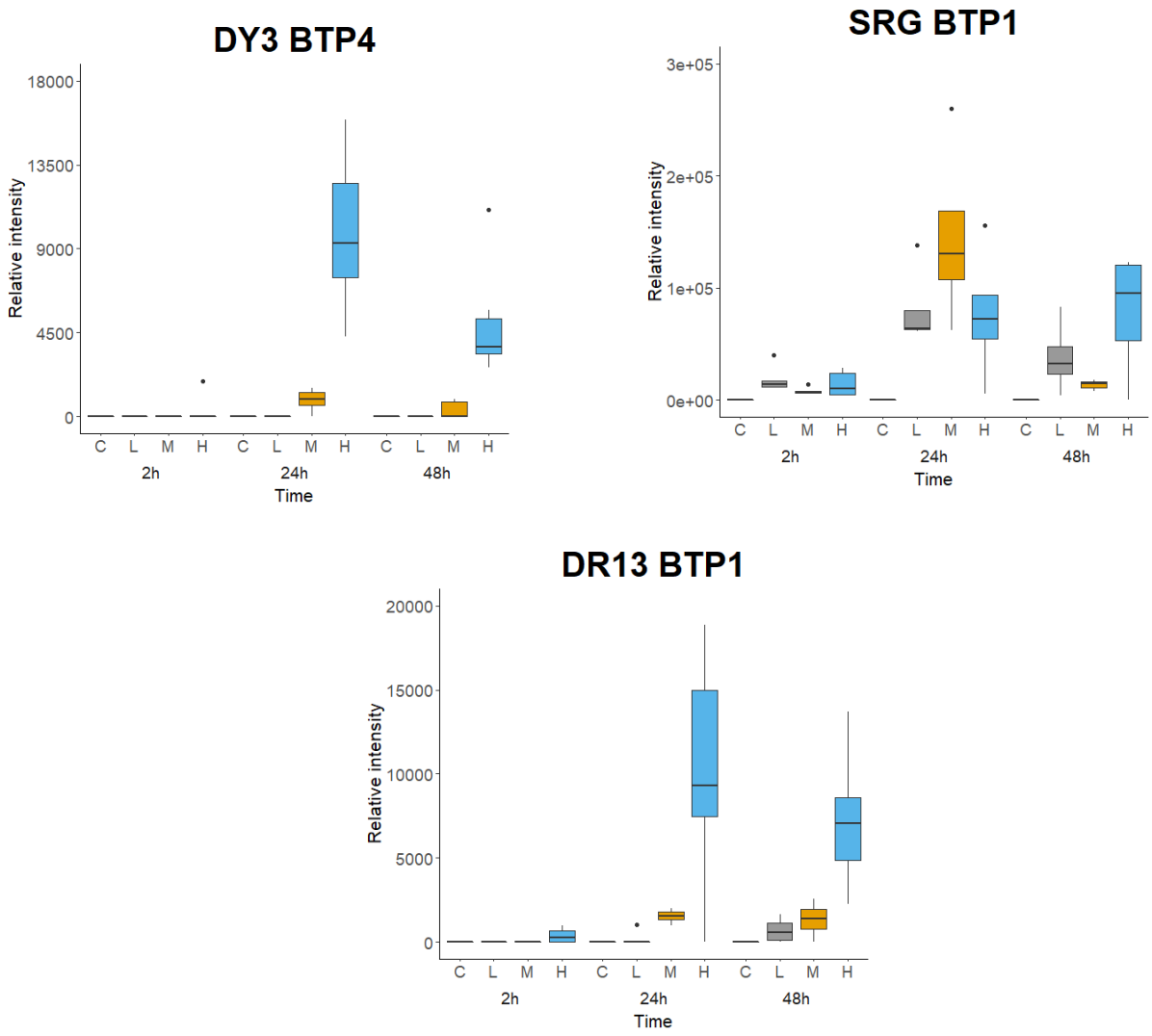


**Figure B-4** Normalised peak intensities (relative internal concentrations) of the azo dye biotransformation products (BTPs) measured across the three treatment doses (L – low, M – medium and H – high) and three sampling time points (2 h, 24 h, 48 h) in the nESI-DIMS polar negative metabolomics dataset.

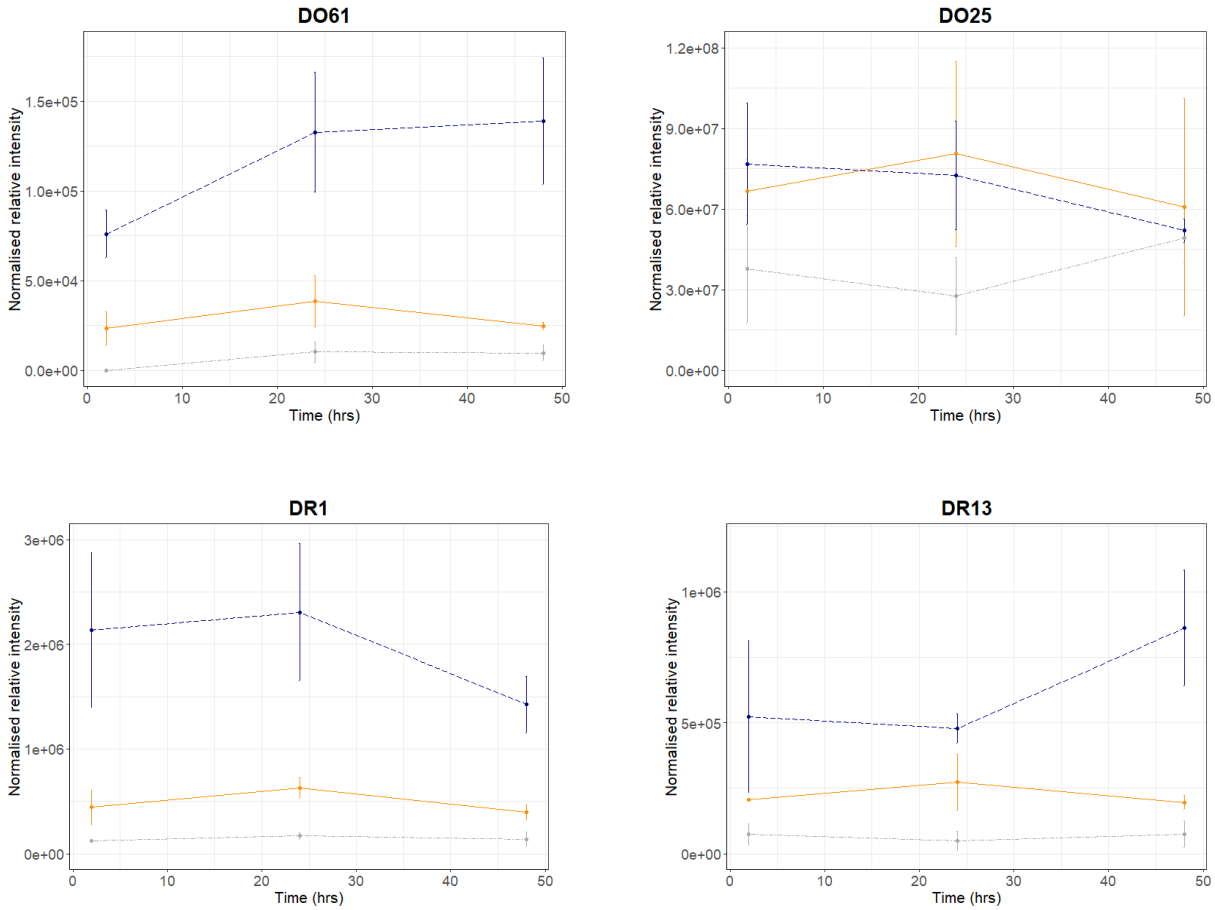


**Figure B-5** Visualisation of azo dye TK rates. Median relative intensities (relative internal concentrations) of the azo dye parent chemicals (DO61, DO25, DR1, DR13) measured over the duration of the 48-h study for the three treatment doses (L – low, M – medium and H – high) in the nESI-DIMS lipidomics dataset.

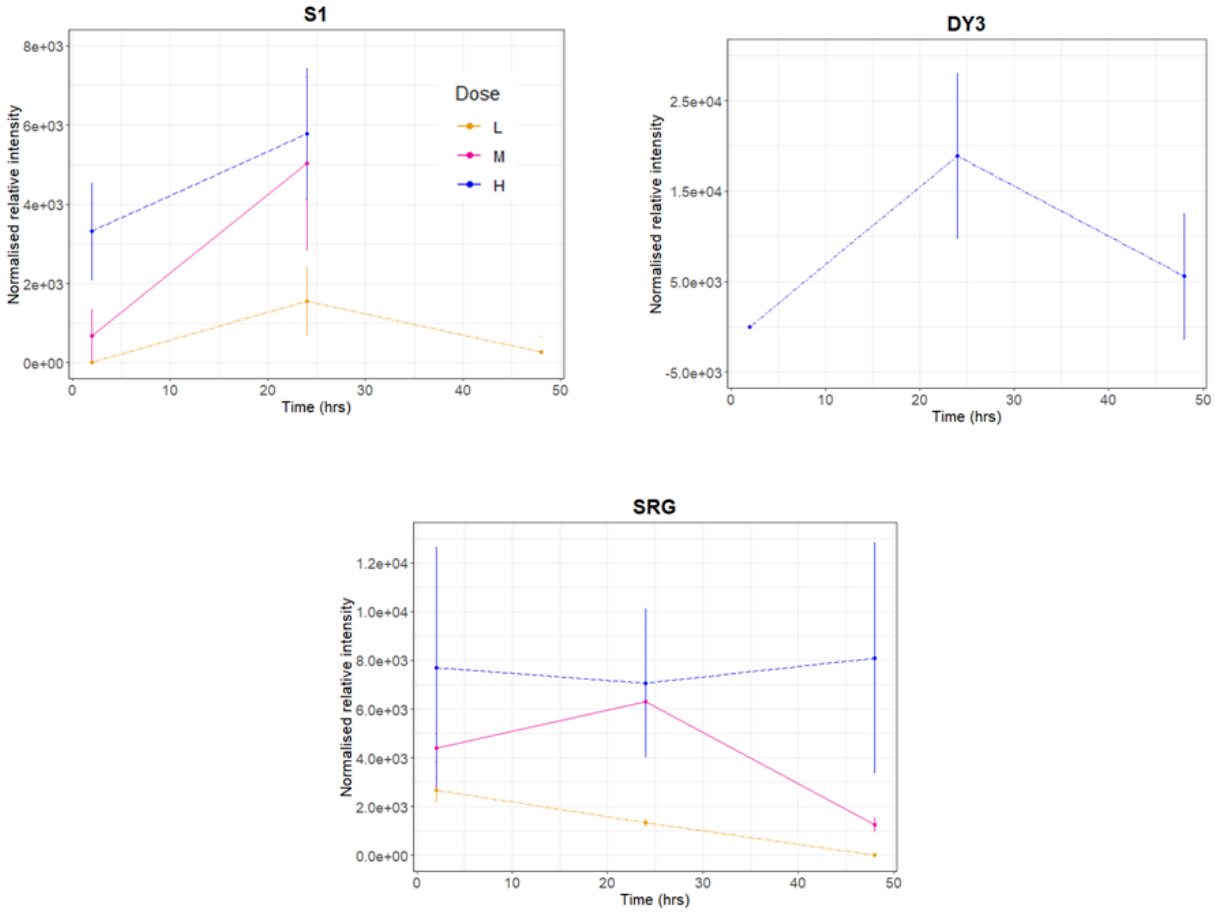


**Figure B-6** Visualisation of azo dye TK rates. Median relative intensities (relative internal concentrations) of the azo dye parent chemicals (DO61, DO25, DR1, DR13) measured over the duration of the 48-h study for the three treatment doses (L – low, M – medium and H – high) in the nESI-DIMS polar negative metabolomics dataset.